THE UNIVERSITY *of* EDINBURGH

Investigating the role of orphan GPR50 in normal brain function and mental illness

Ellen Grünewald

BSc Psychobiology, Universiteit van Amsterdam, 2006

MSc Neuroscience by Research, University of Edinburgh, 2007

A thesis submitted for the degree of Doctor of Philosophy

The University of Edinburgh, 2011

Declaration

I declare that, except for where noted, all work contained in this thesis was performed and composed by myself. Where others have contributed to elements of the work, this is stated clearly in the text. No element of this work has been submitted for any other degree or professional qualification, unless where clearly stated.

Ellen Grünewald

Acknowledgements

There are a few people without whos help I couldn't have done the work or written this thesis. First of all I would like to thank my supervisors, Pippa Thomson and David Porteous for their support and guidance. Especially Pippa has been a great supervisor throughout the project. She was critical when needed and was always there to help out if I had any questions. This is not only the case for me as she has time for everybody else in the lab too, which is abmirable. I am grateful to Janice Bramham, Elisabeth Blackburn, Martin Wear and especially Dinesh Soares for helping me out with the structural and biophysical past of this thesis. I would also like to thank the University of Edinburgh College of Medicine and Veterinary Medicine for providing me with a PhD studentship.

Secondly, I am grateful to Shaun Mackie, Fumiaki Ogawa, Christoph Grünewald, Dinesh Soares, Nick Bradshaw and Sheila Christie for transferring their knowledge and lab skills. Even though I wasn't officially part of the DISC1 group it did feel this way, and it has always been a great craic too! But I wouldn't want to miss out anyone else from the MMC and Medgen, especially the MMC social committee: Andy, Abby, Keith, Aisha, Helen, Gillian, Kamna, Amanda, Rhona, Jennifer and Lowri. I hope the Karaoke Challenge will be a staple of the Christmas party for many years.

A special thank you also to the 'girls' in the office: Rosemary, Heather, Susan and Helen, and of course Sharon. It is thanks to you that everything is so well organised in Medgen and that visiting students/researchers feel welcome.

Thanks also to the other (PhD) students past and present: Lorna, Andrea, Helen, Nick, Becky, Sarah, Manu, Wanting, Elise, Gareth, Rosie. It is sad to (have) see(n) you go but alas, such is science. I hope you stay well and we keep in touch. Good luck to Qian and Nneka, I'm sure you'll do great!

Thank you to my friends here. My cousin, Joyce, for introducing me to Edinburgh and making me feel at home here. I hope Neal will grow up to have your warm personality. Michael, my interdisciplinarity-partner-in-crime, thanks for the good discussions. To my friends at the Hillwalking club, thanks for keeping me company and experience with me how truly wonderful Scotland is. I couldn't have worked so hard if it wasn't for all the weekends away. 143 Munros and counting!

The warmest thank you goes to Gerben for being there for me, and to move over to Edinburgh and settle here with me. Thank you for still being cheerful (to the point of jumping up and down) to see me everytime I come home from work late, with dinner warm and ready, and despite my many grumpy and thankless moments, especially towards the end of the PhD. For loving me.

Last but not least I would like to thank the people 'back home': my mum, dad, brother and my friends all over the globe. Although we may not see each other as much as we want, you are always in my thoughts. This thesis is dedicated to you.

Table of Contents

List of Figures

List of Tables

List of abbreviations

5-HT	5-hydroxytryptamine, serotonin
7TM	Seven transmembrane
ABCA1	ATP-binding cassette sub-family A member 1
ABCA2	ATP-binding cassette sub-family A member 2
ACN	Acetonitrile
Ala	Alanine
AD	Alzheimer's disease
BACE1	Beta-site amyloid precursor protein cleaving enzyme 1, Beta-secretase
BCF	Biophysical characterisation facility
BSA	Bovine serum albumin
CA1/2/3	Cornu ammonis 1/2/3
Ca^{2+}	Calcium
cAMP	Cyclic Adenosine monophosphate
CDH8	Cadherin 8
CTD	C-terminal domain
CNS	Central nervous system
Co-IP	Co-immunoprecipitation
CTCB	Centre for translational and chemical biology
DBH	Dopamine beta hydroxylase
ddH_2O	Double distilled water
dH_2O	Distilled water
DG	Dentate gyrus
DMEM	Dulbecco's modified eagle medium
DIV	Days-in-vitro
DLS	Dynamic light scattering
DTT	Dithiothreitol
EDTA	Ethylenediaminetetraacetic acid
EPPF	Edinburgh protein production facility
ER	Endoplasmic reticulum
ESI/MS	Electrospray ionization mass spectrometry

FBS	Fetal bovine serum
FGF	Fibroblast Growth Factor
FGFR	Fibroblast Growth Factor receptor
GPCR	G protein-coupled receptor
GPR50	G protein-coupled receptor 50
HBSS	Hank's buffered salt solution
HDL	High density lipoprotein
HEK	Human embryonic kidney cells
His	Histidine
HRP	Horseradish peroxidase
ICC	Immunocytochemistry
IHC	Immunohistochemistry
IMAC	Immobilised metal affinity chromatography
LC	Locus coeruleus
LD	Linkage Disequilibrium
MAG	Myelin associated glycoprotein
MALDI	Matrix-assisted laser desorption/ionization
Mel1c	Melatonin receptor 1C
MS	Mass spectrometry
MT1	Melatonin receptor 1/1A
MT2	Melatonin receptor 2/1B
NGF	Nerve growth factor
NgBR	Nogo-B receptor
Ni^{2+}	Nickel
NRMSD	Normalised root-mean-square deviation
NgR	Nogo receptor
NRG1	Neuregulin-1
NS-1	Neuroscreen-1 cells
OMgp	Oligodendrocyte myelin glycoprotein
PCR	Polymerase chain reaction
PDE4B	Phosphodiesterase 4B
PDZ	Postsynaptic density/Disc-large/ZO1

PBS	Phosphate buffered saline
PBS-T	PBS-Tween 20
PPII	Polyproline type II helix
PS1	Presenilin-1
PSD	Postsynaptic density
RHD	Reticulon homology domain
RIPA	Radio-Immunoprecipitation Assay buffer
RPMI-1640	Roswell Park Memorial Institute 1640 medium
RTN	Reticulon protein
Rt-PCR	Reverse transcriptase polymerase chain reaction
SDS	Sodium dodecyl sulfate
SE	Standard error
SH2/3	Src homology 2/3
SREBP/F2	Sterol regulatory element-binding protein/factor 2
TBS	Tris buffered saline
TBS-T	TBS-Tween
TEV	Tobacco etch virus
TOF	Time-of-flight spectrometer
TH	Tyrosine Hydroxylase
Thr	Threonine
UCSC	University of California Santa Cruz
Y2H	Yeast two-hybrid

Units

ºC	Degrees centigrade
Da	Dalton
D_h	Hydrodynamic diameter/radius
g	Gram
k	Kilo
l	Litre
µ	Micro
m	Milli
M	Molar
min	minute
Mw	Molecular weight
m/z	Mass-to-charge ratio
n	Nano
p	Pico
Pd	Polydispersity
Psi	Pound per square inch
rpm	Revolutions per minute
s	Seconds
V	Volt

List of solutions and buffers

1. Cloning and bacterial culture

2xTY medium

16 g	Tryptone (Sigma)
10 g	Yeast Extract (Sigma)
5 g	Sodium Chloride (Fisher)

Make up to 1 litre with dH_2O, adjust the pH to 7.0. Store at 4°C

Alkaline Phosphatase (AP) buffer

100 mM	Tris pH 9.5
100 mM	NaCl
50 mM	$MgCl_2$

in dH_2O

Auto induction medium

60 g	TB Overnight Express (Merck)
10 ml	glycerol

Make up to 1 litre with dH_2O
Heat in microwave, cool

L-Broth

50 g	Tryptone
25 g	Yeast Extract
25 g	Sodium chloride

L-Agar

50 g	Tryptone
25 g	Yeast Extract
50 g	Sodium Chloride

Make up to 5 litres with dH_2O, adjust pH to 7.2. Pour into a bottle and add 75 g of Agar. Store at 4°C until use. Microwave to melt prior to use.
Make up to 5 litres with dH_2O, pH to 7.2. Store at 4°C.

Orange G loading dye

3 g	Ficoll 400 (Sigma)
50 µl	20% SDS (Fisher)
800 µl	0.5M EDTA (Sigma)
25 µg	Orange G (Sigma)

Make up to 1 litre with dH_2O and store at room temperature.

TBE Buffer (5x)

54 g	Tris (hydroxymethyl) aminomethane (Sigma)
27.5 g	Boric Acid (Sigma)
20 ml	0.5M EDTA (Sigma)

Make up to 1 litre with dH_2O. Store at 4^oC.
Dilute to 0.5x for preparing and running agarose gels.

TE buffer

10mM	Tris-HCl, pH 7.5
1 mM	EDTA
in dH_2O	

2. Neuronal cell culture

Borate buffer

50 mM Boric Acid (Sigma)
in dH_2O, adjust pH to 8.0

Poly D-Lysine solution

25 ml	0.3M Borate buffer (Sigma)
2.5 ml	500 µg/ml Poly D-Lysine (Sigma)
22.5 ml	dH_2O

Dissection buffer (for primary neuronal culture)

500 ml	HBSS (with $CaCl_2$ and $MgCl_2$)
5 ml	L-Glutamate
3.5 ml	HEPES (cell culture standard, pH7.3-7.5)

For trypsinisation of dissected brain tissue, 20mls of Tryple Express (Invitrogen) is added to 30mls dissection buffer.

Neurobasal Medium

All reagents are from Gibco (Invitrogen).

500 ml	Neurobasal medium
10 ml	B27 supplement

5 ml	GlutaMAX-1 supplement
2.5 ml	Penicillin/Streptomycin solution

3. Protein purification and biochemistry

Citrate buffer

2.1 g	Citric Acid (Sigma)

Make up to 1 litre dH_2O, adjust pH to 6.0

Guanidine Hydrochloride solution

6 M Gndn-HCl (Sigma)
50 mM Tris-HCl, pH 7.5
in dH_2O

IMAC 'buffer A'

25 mM	Na_2HPO_4
500 mM	NaCl
20 mM	Imidazole

in ddH_2O, adjust pH to 7.4

IMAC 'buffer B'

25 mM	Na_2HPO_4
500 mM	NaCl
500 mM	Imidazole

in ddH_2O, adjust pH to 7.4

Laemmli protein sample buffer

100mM	Tris-HCl pH 6.8 (Fisher)
20% v/v	Glycerol (Promega)
4% w/v	SDS (Fisher)

in dH_2O

Add bromophenol blue (Sigma) to colour. Store at room temperature. Before use Dithiothreitol (DTT, from 1M stock) is added at 100 mM final concentration.

MOPS-SDS-Tris running buffer

62.8 g	MOPS
72.6 g	Tris Base

10 g	SDS
6.5 g	Na Bisulfite

Make up to 10 litres dH_2O. Store at room temperature

Mowiol/Dapi mounting solution

7.5 g	Mowiol (Sigma)
10 ml	Glycerol (Promega)
25 ml	dH_2O

Solution is left overnight at room temperature.
Add 50 ml 200 mM Tris-HCl pH 8.5 (Fisher).
Heat the solution in 100 ^oC water bath for 20 minutes and leave to cool.
Add 1.75 g DABCO (Sigma).
Mowiol can be stored at -20 ^oC. Dapi is added at a final concentration of 50 µg/ml and can be stored at 4 ^oC.

Phosphate buffered saline (PBS), pH 7.3-7.5

From tablets (Invitrogen) containing:

10 mM	Phosphate
150mM	NaCl

Ponceau S stain

1 g	Ponceau S (Sigma)
4 ml	Acetic Acid (Fisher)

Make up to 200 ml with dH_2O. Store at room temperature.

RIPA Lysis Buffer

50mM	Tris-HCL pH 7.5 (Fisher)
150 mM	NaCl (Fisher)
1% v/v	IGEPAL/NP-40 (Sigma)
0.5% w/v	Sodium Deoxicholate (Fisher)
0.1% v/v	SDS (Fisher)

in dH_2O, store at -20 or 4°C.

Before use add protease inhibitor cocktail tablets (Roche) at a concentration of 1 tablet per 50ml of solution.

Semi-dry transfer buffer

48 mM	Tris (5.82 g)
39 mM	glycine (2.93 g)
20% v/v	methanol (200 ml)

Make up to 1 litre with ddH_2O

Size Exclusion Buffer

1x PBS tablets (Invitrogen) in 1 litre ddH_2O
10% v/v glycerol

Sodium Phosphate (20 mM) with NaF (100 mM) pH 7.0

(Circular Dichroism buffer)
16 mM Na_2HPO_4
4 mM NaH_2PO_4
100 mM NaF
in dH_2O

Tris Buffered Saline (TBS)

50 mM Tris (hydroxymethyl) aminomethane (Fisher)
150 mM NaCl

in dH_2O, adjust pH to 7.5 with HCl. Store at room temperature

4. Mass spectrometry sample preparation buffers

500mM ABC [NH_4HCO_3]

988 mg NH_4HCO_3 (Ammonium bicarbonate)
25 ml dH_2O

200mM ABC / 50% ACN (v/v, Acetonitrile)

6 ml 500 mM ABC
1.5 ml dH_2O
7. 5ml Acetonitrile

20mM DTT / 200mM ABC / 50% ACN v/v

300 µl 1 M DTT
1.2 ml 500 mM ABC
1.5 ml Acetonitrile

50mM IAA / 200mM ABC / 50% ACN v/v

100 µl 500 mM IAA (Iodoacetamide)
400 µl 500 mM ABC
500 µl Acetonitrile

20mM ABC / 50% ACN (v/v, enough for 6-8 bands)

600 µl	500 mM ABC	x 18 = 10.8 ml
5.4 µl	dH_2O	x 18 = 97.2 µl
7.5 µl	Acetonitrile	x 18 = 135 µl

50mM ABC

50 µl	500 mM ABC	x 10 = 500 µl
450 µl	dH_2O	x 10 = 4.5 ml

Sinapinic acid (3,5-Dimethoxy-4-hydroxycinnamic acid) matrix for MALDI mass spectrometry

(10 mg/ml)
Mix 10 mg Sinapinic acid with 400 µl dH_2O
Add 100 µl 3% v/v trifluoroactetic acid (TFA) in dH_2O
Add 500 µl acetonitrile (ACN) and mix.

Ammonium Acetate buffer for ESI MS

10 mM Ammonium acetate in dH_2O
Adjust pH to 6.7 using ammonium hydroxide and acetic acid

Abstract

G protein-coupled receptors (GPCRs) form a link between the cell and their environment when signaling pathways are activated upon ligand binding. However, the ligands and functions for many GPCRs remain to be determined. G protein-coupled receptor 50 (GPR50) is one such orphan, and its exact role is yet unknown. There is however emerging functional and genetic evidence suggesting a function for GPR50 in psychiatric illness and lipid metabolism. It was hypothesised that investigating GPR50's protein-protein interactions would lead to a greater understanding of the role of GPR50 in normal brain functioning and in mental illness. Putative protein interactors were initially isolated by a yeast two-hybid study and were further tested here. To address GPR50's links to mental illness, the $GPR50^{\Delta 502\text{-}505}$ deletion variant associated with mood disorders was also investigated. To test this hypothesis I sought to confirm some of the key yeast two-hybrid interactions. Using co-immunoprecipitation and immunocytochemistry the interaction of GPR50 with reticulon family members Nogo-A, Nogo-C and RTN3, and with cell-cell adhesion molecule CDH8 and lipid-associated protein ABCA2 were validated.

In order to identify the location of interactions, subcellular fractionation of mouse brain and rt-PCR and immunohistochemistry in developing and adult mouse brain were performed. GPR50 and several interactors were found to be enriched at the synapse by subcellular fractionation of whole adult brain, and at embryonic day 18 (E18) and 5 weeks by rt-PCR. Colocalisation of GPR50 and interactors was found in the amygdala, hypothalamus, cortex and specific brain stem nuclei by immunohistochemistry. The discovery of GPR50 expression in noradrenergic, serotonergic and dopaminergic nuclei in the adult brain stem suggests a further role for GPR50 in neurotransmitter signaling and stress.

To investigate the function of GPR50 two assays were performed that measure processes which are known to be affected by Nogo and RTN3: The first assay was a neurite outgrowth assay in Neuroscreen-1 cells, a PC12 cell clone. A significant increase in neurite length was detected after transient overexpression of GPR50 and this effect was increased in the $GPR50^{\Delta 502\text{-}505/T532A}$ variant. Additionally GPR50-

overexpression resulted in an increase in filopodia formation suggesting a role in actin dynamics. As a second functional assay *in vitro* BACE1 activity assays were performed in HEK293 cells. GPR50 but not GPR50$^{\Delta 502\text{-}505/T532A}$ overexpression resulted in a significant increase in BACE1 activity.

Lastly a final series of pilot experiments were performed to gain insight into the secondary structure of the C-terminal domain and the effects of the polymorphisms on structure. The 35kDa GPR50 C-terminal domain was purified and Circular Dichroism studies indicated a predominantly unstructured protein with increased α-helical content in the GPR50$^{\Delta 502\text{-}505}$ variant.

The results in this thesis indicate a role for GPR50 in neuronal development and synaptic functioning. The results also strengthen an association with major mental illness, with links to several disease mechanisms.

Chapter 1

Introduction

1 Chapter One: Introduction

1.1 Mental illness

Psychiatric disorders are a major health problem in the world today. One in four people are affected by mental disorders during their lives, according to the World Health Report 2001 (WHO, 2001). The cost of major mental illness to society is enormous. In 2006 mental disorders were joint 3rd (with cancer) in total expenditures for medical conditions in the United States (US), after heart conditions and trauma-related disorders (AHRQ/NIMH, 2006). It is difficult to place an exact number on the total cost as it does not only involve direct healthcare costs but also loss of earnings, income support, homelessness and even inprisonment. The total economic burden in the US in 2002 was estimated as greater than $317 billion, or an equivalent of $1000 per individual in the US that year (Insel, 2008; Kessler et al., 2008). Three of the most common major psychiatric disorders are bipolar disorder, major depressive disorder and schizophrenia. Bipolar disorder and major depressive disorder are affective (mood) disorders whilst schizophrenia is a psychotic disorder.

Bipolar affective disorder (BP) (formerly termed manic depressive disorder) is characterised by repeated episodes of mania and depression. Episodes of mania consist of elevated mood and increased energy, activity and productivity, and unpredictable behaviour. Depressive episodes feature lowered mood and decreased energy, activity and productivity. Feelings of hopelessness, worthlessness and suicidal thoughts are common during depressive episodes (WHO, 1992). The DSM-IV (Diagnostic and Statistical Manual of Mental Disorders) (American Psychiatric Association, 1994) and the ICD-10 (International Classification of Diseases of the World Health Organisation (WHO, 1992)) recognise several subtypes of bipolar disorders: bipolar I, which includes one or more manic episodes; bipolar II, which involves one or more hypomanic epicodes and one or more depressive episodes; cyclothymia, which is a milder form of bipolar disorder and includes episodes of

hypomania with periods of depression that do not meet the criteria for major depressive disorder; and bipolar disorder not otherwise specified (NOS), which includes all other forms of the disease (APA, 2000). Bipolar disorder can be rapid cycling, meaning at least four separate episodes over a 12-month period (Dunner and Fieve, 1974). Approximately 13-20% of bipolar patients experience rapid cycling (Mackin and Young, 2004).

Major depressive disorder (MDD), or unipolar depression, is characterised by the depressive symptoms present in bipolar disorder, without the manic episodes.

Schizophrenia (SCZ) on the other hand is characterised by 'positive' symptoms such as hallucinations, delusions, thought disorder, and 'negative' symptoms such as social withdrawal, blunted affect and lack of motivation (WHO, 1992; APA, 2000). Although not included in the diagnostic criteria of DSM-IV (TR), cognitive symptoms such as working memory deficits and impaired executive functions are common to schizophrenia, and are more severe than in affective disorders (Keefe and Fenton, 2007).

Major depressive disorder has a lifetime prevalence (ie the proportion of people having at least one episode during their lives) of 20% (men) to 30% (women) (Kruijshaar et al., 2005), although the 12-month risk is substantially lower at approximately 7% overall (Kessler et al., 2003). Both bipolar disorder and schizophrenia are believed to affect 1-2% of the population, and both cause severe disability. General onset of symptoms of schizophrenia and bipolar disorder is in adolescence and early adulthood. Bipolar disorder affects both men and women equally, although 70% or more of rapid cycling bipolar patients are women (Mackin and Young, 2004). There is no sex difference in prevalence of schizophrenia, although the age of onset is lower in men (Saha et al., 2005) and other differences have also been found, for instance in substance abuse, brain and cognitive abnormalities and responsiveness to antipsychotics (Leung and Chue, 2000).

These prevalence percentages are however dependent on the diagnostic criteria used and recognition of various subtypes of these illnesses. A recent study, using DSM-IV criteria, estimated the lifetime prevalence of schizophrenia at 0.87%, but estimated the risk for combined psychotic disorders (including schizophrenia, schizoaffective disorder, schizophreniform disorder, delusional disorder, bipolar I disorder, major depressive disorder with psychotic features, substance-induced psychotic disorders, psychotic disorders due to a general medical condition) to be 3% (Perala et al., 2007). Another recent study estimated the 12-month prevalence of bipolar disorder at 2.6% (Kessler et al., 2005). The next version of the diagnostic and statistical manual, DSM-5, which is due in May 2013, is expected to change the number of subtypes (reduced in the case of schizophrenia) and the lifetime risk may therefore change. It is important to note that none of the diagnostic manuals to date are based on solid biological criteria for distinguishing between diseases. The DSM-5 will not change this (Hyman, 2007).

A reason for this lack of biological criteria is that the aetiology of psychiatric illnesses is still poorly understood. These are regarded as complex disorders, with a multitude of genetic, epigenetic and environmental factors playing a role in the development of disease. Patients with bipolar disorder are treated with mood stabilizers such as lithium, but up to 50% remain unresponsive to monotherapy (Sachs, 1996; Gershon and Soares, 1997). Strategies using combinations of Lithium with antipsychotics and antidepressants are common but are far from satisfactory as side effects are common (Solomon et al., 1998; Nemeroff et al., 2001; Sachs et al., 2007). Individual differences and needs of patients have so far been poorly accounted for in the development of drugs. A better understanding of the biology of mental illness will increase the likelihood of improving diagnostics, therapeutic interventions and quality of life of people with psychiatric illness.

There is a strong genetic component to psychiatric illness, as is clear from family, twin and adoption studies (Kinney and Matthysse, 1978). However, as it turns out, this high heritibility does not mean causative gene variants for mental illness are easily found. Research in the last decades has focused on finding candidate genes for

major mental disorders using methods to detect cytogenetic abnormalities, by linkage and association analyses, and through copy number variation (CNV) studies.

An example of a cytogenetic abnormality is a chromosomal translocation. This is caused by the rearrangement of nonhomologous chromosomes, resulting in possible disruption of genes at the breakpoints of the chromosomes. Chromosomal abnormalities have been found to cosegregate with mental illness in a number of cases (MacIntyre et al., 2003). Linkage analysis searches for genetic loci or alleles that are inherited together with disease markers, usually in large pedigrees or sets of sib-pairs or parent-offspring trios (Kruglyak et al., 1996). Case-control association studies are either hypothesis-driven candidate gene studies with a limited number of markers (variants) or hypothesis-free genome-wide association studies (GWAS), where markers cover the entire genome (>100.000 single nucleotide polymorphisms, SNPs) (Manolio, 2010). In both types of association the frequency of variants is compared between case and control populations of unrelated individuals. In association studies it is of importance that the control population has similar characteristics to the cases in order to control for selection bias and population stratification (differences that are due to differences in ethnic origin rather than the risk variant).

Despite high hopes GWAS has not lead to the enormous increase in the number of gene associations with major mental illness, as was the case for other common illnesses such as diabetes (WTCCC, Scott et al., 2007; 2007), obesity (Frayling et al., 2007) and inflammatory bowel disease (Duerr et al., 2006; WTCCC, 2007). Only a limited number of variants have been identified, each of which appears to carry a small effect (Ferreira et al., 2008; Sullivan et al., 2008; Cichon et al., 2011). Some large studies found no association at all (Belmonte Mahon et al., 2011). When psychiatric illness is as much as 89% heritable (McGuffin et al., 2003) this raises the question of the ‘missing heritability’ and the genetic absolution of those disorders (Maher, 2008).

The main theory behind GWAS is the 'common disease-common variant' hypothesis, which states that common illness is caused by (multiple) disease alleles/loci that are present in all human populations (at relatively high frequencies) (Reich and Lander, 2001). These variants are not necessarily causative but have different frequencies in the diseased population. In the last couple of years the common disease, common variant hypothesis has gradually lost its shine and been replaced with the idea that multiple rare variants may better explain the genetics of common complex mental disorders (Gershon et al., 2011). Perhaps the answer lies in copy number variations (CNVs, which refer to deletions, duplications or rearrangements of large regions of the genome (1 kilobase to several megabases), that are either inherited or the result of *de novo* mutations. They are very common from of variation in the human genome (Sebat et al., 2004). Several rare CNVs have recently been found to be associated with mental illness (Sebat et al., 2007; Cook and Scherer, 2008; Vacic et al., 2011).

The picture that emerges from these studies is a complex pattern of inheritance with common gene mutations of small effect and rare mutations with large effects (Sullivan, 2005). Epigenetic and gene-environment interactions will need to be added into the equation. Detailed ('deep') and costly sequencing efforts of candidate genes will be necessary to identify all the rare variants that may be associated with disease. A strong candidate gene will not only need to stand up to replication studies using various methods but will also need a strong biological and functional body of evidence in order to convince the critics (Crow, 2007).

Despite these difficulties some promising candidate genes were identified through multiple methods and substantial effort has been put into strengthening their functional links to illness (Craddock et al., 2005). Disrupted in Schizophrenia-1 (*DISC1*) (Millar et al., 2000), Dysbindin (*DTNBP1*) (Straub et al., 2002) and Neuregulin 1 (*NRG1*) (Stefansson et al., 2002) are some of the most commonly studied, and although there is a lack of consistency in the specific variants involved (Sullivan, 2005), recent functional biological evidence is encouraging (Stefansson et al., 2004; Clapcote et al., 2007; Duan et al., 2007; Mao et al., 2009). *DISC1* and

NRG1 are primarily candidate genes for schizophrenia but are also associated with bipolar disorder and other mental illnesses (Craddock et al., 2005).

It seems that bipolar disorder is somewhat lagging behind in the number of candidate genes identified and researched. This may be due to a limited research effort compared to some of the schizophrenia genes (Craddock et al., 2005). Some of the recently identified and replicated bipolar loci are present in D-amino acid oxidase activator *DAOA(G72)/G30* (Hattori et al., 2003; Chen et al., 2004a), brain derived neurotrophic factor *BDNF* (Neves-Pereira et al., 2002; Sklar et al., 2002; Geller et al., 2004) and Ankyrin 3 (*ANK3*) (Ferreira et al., 2008; Smith et al., 2009; Takata et al., 2011), although more genetic and functional evidence is needed. No doubt their time will come.

Interestingly several of these candidate genes have not been associated with a single illness but were shown to associated with schizophrenia, bipolar disorder, major depression, autism, and also with neurodegenerative disorders such as Alzheimer's disease (AD) (Kilpinen et al., 2008; Morgan et al., 2008; Di Maria et al., 2009; Hennah et al., 2009; Voineskos et al., 2011). This points to converging biological pathways and may indicate a role in common mental illness 'phenotypes' such as reduced grey/white matter in the brain, abnormalities in brain development, mania/psychosis and social and cognitive deficits. Candidate genes are commonly 'validated' by providing functional evidence for a role in brain development, pathology and behaviour that links back to these phenotypic abnormalities.

Recently, G protein-coupled receptor 50 (*GPR50*) was identified as a risk gene for major mental illness in women through case-control association (Thomson et al., 2005; Macintyre et al., 2010). In this thesis I will focus on GPR50 and its possible role in brain functioning and mental disorders.

1.2 GPR50 Structure and function

1.2.1 G protein-coupled receptors

GPR50 belongs to the 7-transmembrane (7TM) G protein-coupled receptor (GPCR) superfamily of over 1000 members. GPCRs form a link between the cell and its environment, moderating 80% of intracellular molecular signalling, by triggering several, highly interconnected, secondary messenger pathways in response to ligand binding (Marinissen and Gutkind, 2001; Lundstrom, 2006) (Figure 1.1). Secondary messenger systems are activated through the interaction with heterotrimeric G proteins (consisting of α, β and γ-subunits, Fig 1.1). Upon activation by a ligand, the GPCR associates with the G protein complex resulting in exchange of GDP into GTP-bound Gα. Gα is then dissociated from the Gβγ complex and from the receptor. The various types of Gα then bind to effector molecules, such as adenylyl cyclases and phospholipase C, resulting in the inhibition or activation of classic second messengers such as cAMP, diacyl glycerol (DAG) and phosphoinositides like Phosphatidylinositol 3,4,5-trisphosphate (PIP3). This can then lead to the opening of Ca^{2+} or K^{+} channels activation of further secondary messenger pathways (Flower, 1999; Marinissen and Gutkind, 2001). Ultimately this results in gene expression changes and the regulation of diverse functions such as neurotransmitter release, cell growth, apoptosis, chemotaxis and physiological responses (Harmar et al., 2009) (Fig 1.1). However, not all cellular responses are mediated by G proteins, nor does activation of a specific receptor lead to a single biochemical route, creating a multitude of intricate and interconnected pathways that lead to a biological response (Marinissen and Gutkind, 2001).

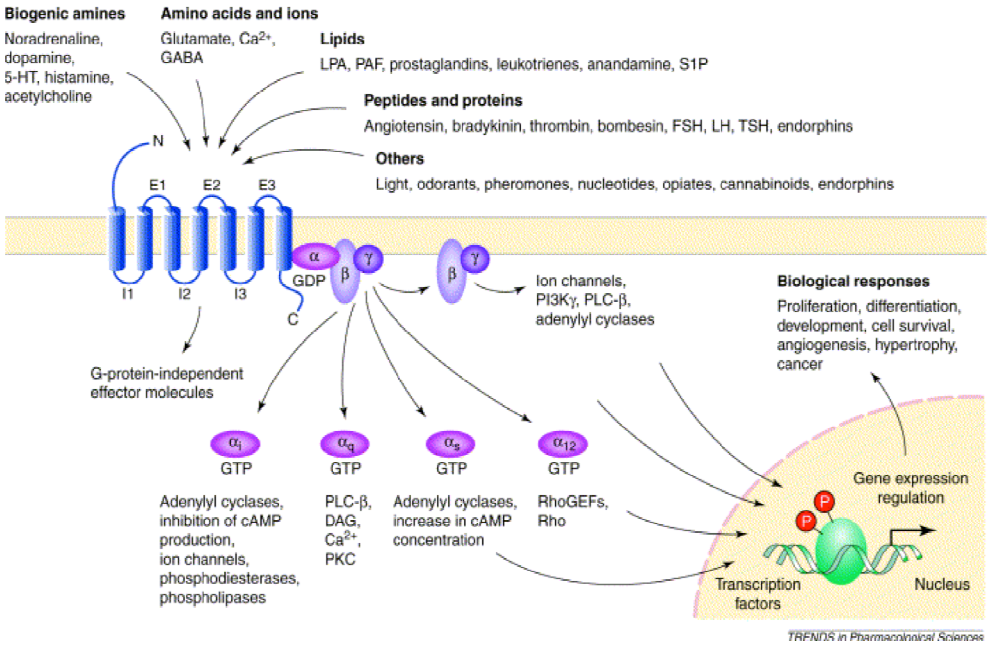

Figure 1.1. *GPCRs control a wide variety of signalling networks. GPCRs can be activated by binding various ligands, including biogenic amines, amino acids, ions, lipids, peptides and proteins, light and odorants. Through heterotrimeric G protein-dependent and –independent pathways effector molecules can be activated, resulting in diverse biological responses such as proliferation, differentiation, cell survival and cancer. Abbreviations: DAG, diacylglycerol; FSH, follicle-stimulating hormone; GEF, guanine nucleotide exchange factor; LH, leuteinizing hormone; LPA, lysophosphatidic acid; PAF, platelet-activating factor; PI3K, phosphoinositide 3-kinase; PKC, protein kinase C; PLC, phospholipase C; S1P, sphingosine-1-phosphate; TSH, thyroid-stimulating hormone. Figure published in Marinissen and Gutkind, 2001. Trends in Pharmacological Sciences. Copyright 2001, Elsevier Science Ltd. (Note: G-proteins bind 3rd intracellular loop of GPCR and not TM region as suggested here).*

G protein-coupled receptors are interesting candidates for psychiatric disorders as they are involved in many disease pathways and are considered important targets for therapeutic interventions. G protein-coupled receptor signaling is believed to play an important role in the aetiology and treatment of major mental illness. Of the drugs currently in development or on the market 25-30% target GPCRs, which represent 15% of the 'druggable genome' (Hopkins and Groom, 2002). Examples of drugs targeting GPCRs and GPCR signaling networks are Fluoxetine (Prozac, a 5-HT reuptake inhibitor or transporter blocker), Haloperidol and other typical antipsychotics (Dopamine D2 receptor antagonist), Clozapine and other atypical antipsychotics (Dopamine and 5-HT receptor antagonists) and inositol signalling (eg. Lithium, Carbamazepine and Valproic acid) (Harwood, 2003).

In humans, 354 non-sensory GPCRs have been identified, of which 214 have a known (endogenous) ligand (Harmar et al., 2009). The rest, which are classed 'orphans', have been resistant to current deorphanisation strategies by industry and academia. Their signaling mechanism and function remains to be identified. Although most of the functions of GPCRs are attributed to signaling in response to ligand binding and G protein-coupling, ligand-independent functions of GPCRs have also been proposed (Levoye et al., 2006).

GPR50 was originally cloned from cDNA of the human pituitary (Reppert et al., 1996), suggesting a role in neuroendocrine function. The GPR50 protein is 45% identical in amino acid sequence to members of the melatonin receptor family, hence it is also known as the melatonin-related receptor (Fig 1.2). Despite this homology it does not bind melatonin or any other known ligand and therefore remains an orphan G protein-coupled receptor (Reppert et al., 1996).

1.2.2 Melatonin and melatonin receptors

Melatonin is a neurohormone released by the pineal gland which has a regulatory role in seasonal and circadian rhythms and other physiological processes (Arendt, 1998; Dawson and van den Heuvel, 1998; Zawilska et al., 2009). It is rhythmically

secreted with peak expression during the night. Besides a function as circadian pacemaker it controls the hypothalamus-pituitary-adrenal (HPA)-axis and has role in energy metabolism, circulating lipid levels, growth and differentiation, stress responses and cell protection and cell survival (Dawson and van den Heuvel, 1998; Morgan et al., 1998; Hardeland, 2009; Luchetti et al., 2010).

Several melatonin receptor subtypes have been cloned: MT1 (Mel1A) and MT2 (Mel1B) from mammals, and Mel1c, which is expressed in non-mammalian vertebrates (birds, amphibians, fishes) (Ebisawa et al., 1994; Reppert et al., 1994; Reppert et al., 1995b; Reppert et al., 1995a). A third melatonin binding site has been identified, MT3, otherwise known as ML-2 or quinone reductase (QR) (Jockers et al., 2008), which has low affinity for melatonin (Duncan et al., 1988) (5-50 times less than MT1 and MT2) but has a specific ligand called 5-methoxycarbonylamino-N- acetyltryptamine (MCA-NAT) (Molinari et al., 1996).

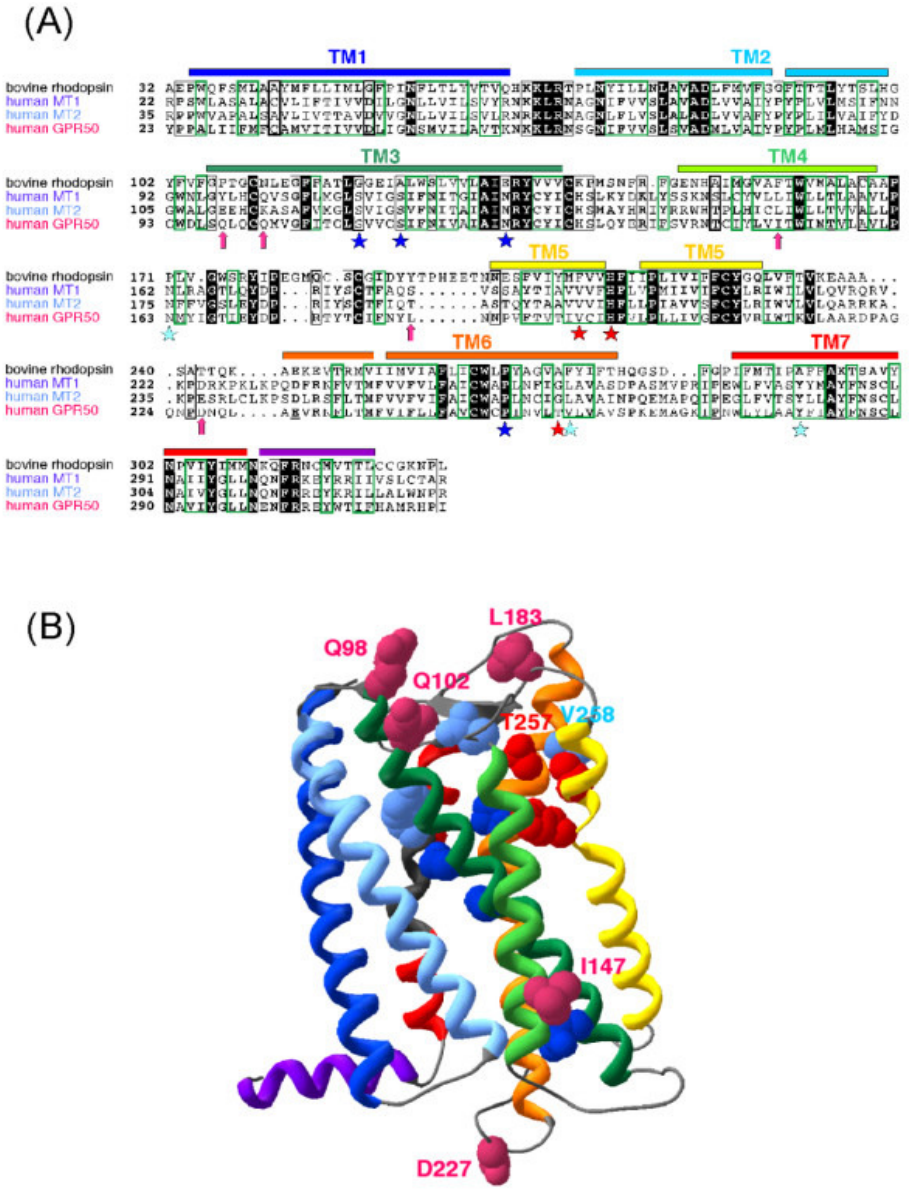

Figure 1.2 *Sequence alignment of human MT1, MT2 and GPR50 with bovine rhodopsin (transmembrane domains only). Sequence identities are reported white on a black background, whereas sequence similarities are boxed (A). The positions of the transmembrane helices, as observed in the bovine rhodopsin structure, are reported above its sequence. Arrows indicate the positions of the amino acids that, in GPR50, evolved under positive selection. Stars indicate amino acids, which have been shown to play a key role for melatonin binding in MT1 (dark blue), MT2 (light blue) or both (red) (Conway et al., 1997, 2000; Gubitz & Reppert., 2000; Mazna et al., 2004). A ribbon representation of the GPR50 3D structure model is represented (B), with transmembrane helices coloured according to the sequence alignment. Amino acids evolving under positive selection and amino acids important for melatonin binding in MT1/MT2 are shown according to the colours reported in the sequence alignment. From Dufourny et al., (2008), BMC Evolutionary Biology. Copyright 2008, BioMed Central Ltd.*

Human MT1 and MT2 show 55% homology at the amino acid level with 70% in the transmembrane domains only (reviewed in Jockers et al., 2008). The melatonin receptors form a specific receptor cluster within the rhodopsin family of GPCRs (Vassilatis et al., 2003). Although ubiquitously expressed in non-mammalian vertebrates, MT1 receptor distribution is restricted to low density in the pars tuberalis of the anterior pituitary, the suprachiasmatic nucleus (SCN), and also in the hippocampus, cortex, thalamus cerebellum and eye. MT2 expression was detected in the SCN, retina, hippocampus and cerebellum (reviewed in Zawilska et al., 2009). MT1 and MT2 preferentially couple through G_i, but also through G_{q11} proteins, thereby inhibiting cAMP, PKA and phosphorylation of cAMP, but stimulating MEK1, MEK2, ERK1, ERK2 and JNK phosphorylation (reviewed in Jockers et al., 2008).

Like many GPCRs, the melatonin receptors can homo- and heterodimerise, and bind non-G proteins to their C-terminal domain, expanding the possible signaling pathways, functional effects and therapeutic interventions (Jockers et al., 2008). Melatonin receptor density decreases with aging (van Coevorden et al., 1991; Savaskan et al., 2005; Savaskan et al., 2007; Wu et al., 2007) and further decreased MT1 and MT2 expression was found in the postmortem brain of Alzheimer's disease patients (Savaskan et al., 2005; Savaskan et al., 2007; Wu et al., 2007).

GPR50 is the mammalian ortholog of Mel1c (Dufourny et al., 2008), although it does not bind 2-[^{125}I] iodomelatonin or [^{3}H] melatonin (Reppert et al., 1996; Levoye et al., 2006). A study using MT1/GPR50 chimeric receptors indicated transmembrane domains (TM) 4 and 6 of MT1 are necessary for 2-[^{125}I] iodomelatonin binding and modulation of cAMP levels. Chimeric GPR50 including TM4 and 6 of MT1 did result in melatonin binding, albeit with low affinity (Conway et al., 2000; Gubitz and Reppert, 2000). Site directed mutagenesis pointed to the critical importance of non-conserved residue Gly258 in TM6 in melatonin binding (Fig, 1.2, Conway et al., 2000; Gubitz and Reppert., 2000; Dufourny et al, 2008). This residue may be

necessary for maintaining the structure of the ligand binding pocket, and the hydroxyl-containing sidechain of Thr257 in GPR50 may disrupt this (Conway, 2000; Gubitz and Reppert., 2000). Something similar may be the case for MT2 residue Leu272 which has been replaced for Val258 in GPR50 (Fig 1.2) (Mazna et al., 2004). Other residues that have been shown to be important for MT ligand binding are however conserved in GPR50 (Fig 1.2) (Conway et al., 1997; Kokkola et al., 1998; Dufourny et al., 2008). Dufourny et al. (2008) modelled sites of positive selection in GPR50 (Fig 1.2). Although these sites were not previously shown to be important for ligand binding, they are in close proximity to such sites in a 3D model (Fig 1.2B). In addition several are found at the top of the ligand binding pocket and may therefore interfere with ligand binding (Fig 1.2B).

1.2.3 GPR50 interacts with MT1 and MT2

GPR50 has been shown to interact with the melatonin receptors in a ligand-independent way under overexpressed conditions. GPR50 can homodimerize, and form heterodimers with melatonin receptors MT_1 and MT_2 (Levoye et al., 2006). This formation of GPR50/MT_1 heterodimers disrupts ligand binding to MT_1, moreover, the presence of GPR50 prevents further G protein signalling through MT_1, by inhibiting G_i protein coupling and β-arrestin binding (Levoye et al., 2006; See Fig 1.3). However under basal conditions (no melatonin), the binding between MT1 with β-arrestin was increased in the presence of GPR50, indicating possible constitutive activity of the MT1/GPR50 heterodimer (Levoye et al., 2006). This effect of GPR50 on MT_1 function seems to be dependent on the presence of the C-terminal domain (CTD) of GPR50, possibly through steric hindrance of the relatively long CTD. This interaction is intruiging and opens up the possibility for ligand-independent functions for GPR50. It is however important to note that endogenous interactions between GPR50 and MT1 have not been investigated or described, although GPR50 and MT1 are both found to be expressed in the pituitary and hypothalamus (Reppert et al., 1996; Wu et al., 2006), indicating a possible functional site of interaction.

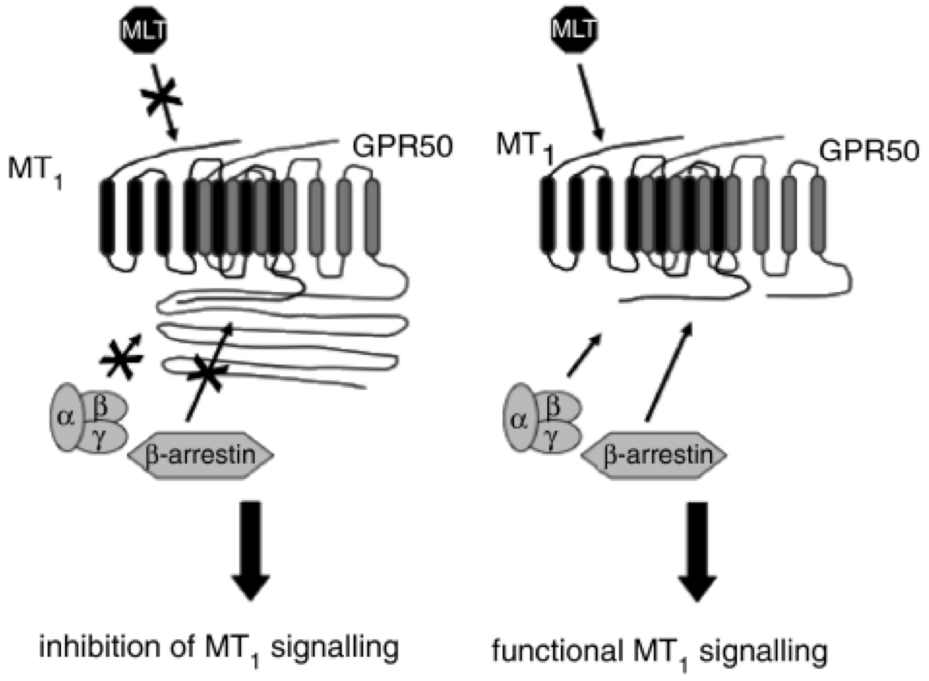

Figure 1.3 *GPR50-MT1 heterodimers. GPR50-MT1 heterodimerisation inhibits melatonin (agonist) binding, G-protein-coupling and β-arrestin binding, only in the presence of the GPR50 C-terminal domain. Image by Jockers et al., 2008. British Journal of Pharmacology. Copyright 2008, British Pharmacological Society.*

1.2.4 GPR50 expression

GPR50 is most highly expressed in the brain, but is also found in the adrenal glands, testes, ovary, eye, lung, kidney, intestines and heart of the rat and mouse by rt-PCR (Drew et al., 2001; Izzo et al., 2010), and in retina and retinal pigment epithelium of the sheep (Drew et al., 1998). Within the brain GPR50 was found to be mainly expressed in the pituitary and hypothalamic regions in the adult human, mouse, rat, hamster and sheep by *in situ* hybridization and immunohistochemistry (Reppert et al., 1996; Drew et al., 1998; Drew et al., 2001; Vassilatis et al., 2003; Barrett et al., 2006; Sidibe et al., 2010), and is therefore possibly involved in lipid metabolism and body weight control, circadian rhythms, and mood (Reppert et al., 1981; McAllister-Williams et al., 1998). By immunocytochemistry overexpressed GPR50 was detected on the plasma membrane of HEK293 cells (Hamouda et al., 2007). Western blotting revealed a monomeric form of GPR50 at 66 kDa and a dimeric form at 130 kDa

(Hamouda et al., 2007). The authors also detected an increase in GPR50-immunoreactivity in cells showing degenerative changes in patients with Alzheimer's disease (AD) as compared to healthy controls (Hamouda et al., 2007), which although tentative, may suggest a role for GPR50 in neurodegenerative disorders.

1.2.5 GPR50 and psychiatric illness

The *GPR50* gene is located on Xq28 (Gubitz and Reppert, 1999), a region implicated in several linkage and association studies in bipolar disorder (Massat et al., 2002). GPR50 consists of two exons separated by a single intron, generating a single GPR50 splice variant of 617 amino acids (Fig 1.4, GenBank accession number GI:73909216). Three GPR50 common variants were identified as putative functional polymorphisms in bipolar disorder and major depression, all located within the CTD: a 12-bp in-frame deletion, which results in the loss of four amino acids from the protein sequence (Δ502-505), and two single nucleotide polymorphisms (SNPs) that result in amino acid substitutions, T532A (rs561077) and V606I (rs13440581) (Figure 1.4, Thomson et al., 2005). T532A is in complete linkage disequilibrium with the deletion polymorphism. Two intronic SNPs were studied in *GPR50*, C-16X2GPR50T (rs1202874) and rs2072621 (Thomson et al., 2005; Bhattacharyya et al., 2006). Recently rare variant S493N (rs62620754) was identified in a Swedish population (Jonsson et al., 2010) (Fig 1.4).

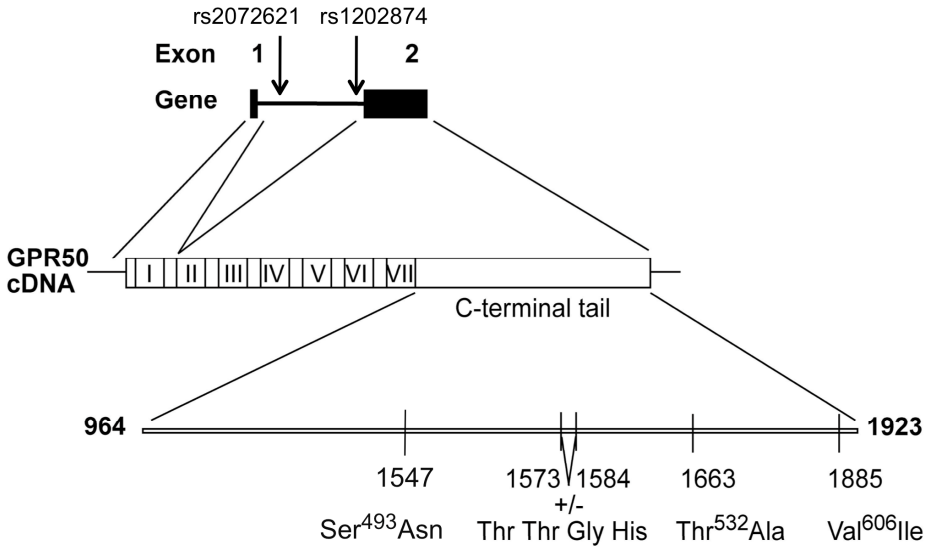

Figure 1.4 *GPR50 gene structure and the positions of the polymorphisms. Figure adapted from Thomson et al., 2005. Molecular Psychiatry. Copyright 2005, Nature Publishing Group.*

In a case-control association study of 264 subjects with bipolar disorder (BPD), 226 with major depressive disorder (MDD), 263 with schizophrenia (SCZ) and 562 matched controls the Δ502-505 deletion was found to be significantly associated with both BPD and MDD (global p-values 0.007 and 0.011 respectively, Thomson et al., 2005).). These associations were seen in females only, where the allele frequency of the Δ502-505 polymorphism was 51.0% in BP and 47.7% in MDD compared to 37.6% in controls (p-values 0.00023 and 0.0064 respectively). In addition intronic SNP rs2072621 was found to be significantly associated with the female schizophrenic sample (p=0.0014) only (Thomson et al., 2005). There is no reported gender bias in bipolar disorder or schizophrenia, but major depression is twice as common in females as in males, where the condition can be triggered by a postpartum episode (Sharma and Mazmanian, 2003). This sex difference is intriguing and suggests that hormones such as estrogen may mediate the risk of GPR50 in mental illness.

The association of GPR50 with mood disorders failed to replicate in a Hungarian sample of children and adolescents with childhood–onset mood disorders (girls: 215 boys: 253) (Feng et al., 2007) or Swedish cohort (Alaerts et al., 2006). The failure to replicate may be due to genetic heterogeneity of the populations, a smaller cohort (Alaerts et al., 2006), grouping of BPD and MDD together (Feng et al., 2007), or an example of the 'winner's curse'. This effect is common to association studies and means that the genetic effect size of the original finding is overestimated, resulting in the subsequent studies being underpowered (smaller sample size) and therefore not be able to reach the same significance (Lohmueller et al., 2003; Zollner and Pritchard, 2007; Xiao and Boehnke, 2009; Macintyre et al., 2010).

The association of variants within the GPR50 locus with bipolar disorder was however recently replicated using an expanded Scottish population sample of 338 patients with BD, 359 patients with major depressive disorder (MDD) and 913 control individuals (Macintyre et al., 2010). Significant association was found between BPD and women with intronic SNP rs1202874 ($p=0.0035$). Although initially no association was found with Δ502-505, when this sample was combined with a previous sample (Thomson et al., 2005) significant association was detected in females only ($p=0.0006$). In this study the clinical phenotype and treatment response was also investigated in a subgroup of 56 patients with early-onset MDD. In this subgroup association was found between Δ502-505 and age of onset, number of episodes, manic symptoms and initial thinking time in women and age of onset in men (Macintyre et al., 2010).

Studying a small French Caucasian sample (106 patients, 80 females, 26 males; 120 controls) intronic SNP rs2072621 was recently found to be associated with seasonal affective disorder (SAD) in women only ($p=0.049$) (Delavest et al., 2011). However, no multiple testing correction was performed on this p-value. Although the male sample is very small this result may reflect the higher incidence of SAD in women compared to men (3.5:1) (Lee and Chan, 1998).

GPR50 rare variant S493N was not found to be associated with autism in a study using a cohort of 109 Swedish people with autistic spectrum disorders (ASD) and 118 controls, although the control group was not age- and gender matched (Jonsson et al., 2010). In a larger mixed-ethnic cohort of 295 cases and 362 controls common variants in GPR50 were investigated (Chaste et al., 2010). The frequency of Δ502-505 and T532A was significantly decreased in ASD males only, although this did not withstand Bonferroni's multiple testing correction (Chaste et al., 2010). No significant associations were found in females although the frequency of Δ502-505 and T532A appeared to be higher in female ASD cases than controls, suggesting a possible difference between sexes. This needs to be further investigated however possibly using a bigger cohort.

1.2.6 GPR50 and lipid metabolism

Studying an English Caucasian population of 500 and 585 individuals, (Bhattacharyya et al., 2006) report an association between GPR50 variants Δ502-505, T532A, V606I and intronic SNP rs1202874 and elevated circulating fasting triglyceride levels. Rs1202874 was also associated with lower circulating HDL (High Density Lipoprotein, 'good' cholesterol) levels. No association was found between GPR50 variants and obesity (body mass index) (Bhattacharyya et al., 2006). In agreement with a role in lipid metabolism, Ivanova et al. (2007) report that the GPR50 knockout mice have an altered metabolism, with apparent resistance to obesity when kept on a high-energy diet.

A link of GPR50 to lipids would be interesting as cholesterol is a major component of the brain and myelin, and differences in cholesterol levels could therefore influence the development and cytoarchitecture of the brain (Dietschy and Turley, 2001; Puglielli et al., 2003). Cholesterol, glycolipids and sphingolipids are often organized into lipid rafts domains in the cell membrane, which are important in cell signalling, also in relation to psychiatric illness (Allen et al., 2007). Interestingly, cholesterol metabolism has also been linked to AD pathology (Puglielli et al., 2003).

1.2.7 GPR50 loss-of-function models

Several GPR50 knockout mouse models have been developed, by Astra Zeneca and Organon/Schering Plough/Merck, and recently stemcells were made available for generating mouse lines from the knockout mouse model repository (KOMP). However, only the Astra Zeneca mouse has so far been described in the literature (Barrett et al., 2006; Ivanova et al., 2008). The mice are viable and have a metabolic phenotype as they display attenuated weight gain and reduced body fat on a high-energy diet as compared to wild-type animals. Moreover, on comparison, GPR50 knockout mice displayed hyperactive behaviour and a heightened metabolic rate. To my knowledge none of these mice have been tested for major mental illness phenotypes.

1.2.8 The GPR50 C-terminal domain

The GPR50 C-terminal domain (CTD), which is over 300 amino acids long, is large compared to that of the melatonin receptors and its non-mammalian ortholog Mel1c (Dufourny et al., 2008) (Fig 1.5, see also snake-like diagram in Fig 1.3), which suggests it is important for its function. This is reflected by recent functional and genetic findings. The inhibitory effect of GPR50 on MT_1 signalling appears to be dependent on the presence of the GPR50 CTD. Genetic variants associated with BPD, MDD and elevated triglycerides are found in the CTD (Thomson et al., 2005; Bhattacharyya et al., 2006; Macintyre et al., 2010). The C-terminal region is likely to be involved in protein binding and the activation of downstream signalling pathways. The GPR50 CTD has high homology to the RNA polymerase II CTD (Dufourny et al., 2008) where the CTD has been shown to be key to protein binding and functioning. The GPR50 CTD is a proline-rich region, which may indicate binding to PDZ, SH2 or SH3 domain-containing proteins (Marinissen and Gutkind, 2001). Understanding protein interactions with the CTD might therefore give insight into GPR50 functioning.

Figure 1.5 *Multiple sequence alignment of the human Melatonin receptor 1 (MT1), 2 (MT2), the zebrafish (Danio rerio) Melatonin 1c receptor (Mel1c) and human GPR50, indicating the long C-terminal domain (residues 297-617) of GPR50 compared to its gene family members. The alignment was created using ClustalW. "*" indicates the residues in that column are identical in all sequences in the alignment; ":" indicates conserved substitutions have been observed; "." means that semi-conserved substitutions are observed. Sequences used: MT1: GI:60498974; MT2: GI:69122993; Mel1c: GI:238814399; GPR50: GI:73909216.*

1.2.9 Approaches to identifying GPCR function

GPCRs cannot be easily be purified and crystallised and therefore rational drug design, as applied in drug discovery of soluble enzymes is difficult. Functional cell-based assays have therefore been developed in order to identify GPCR ligands. Generally this involves overexpression of the GPCR in immortalized cell lines and performing high-throughput screening methods. Traditionally these are automated, methods, where a change in intracellular second messengers such as cAMP (for GPCRs coupled to $G\alpha_S$ or $G\alpha_i$), IP3 or Ca^{2+} ($G\alpha_o$ or $G\alpha_q$) is measured in response to the addition of ligand libraries, or tissue extracts.

Another method is to measure GTPγS binding to the receptor, in response to ligand binding, using either radiolabelled or non-radiolabelled GTP-analogues. An advantage of this method is that it is independent of the type of G protein or second messenger involved, which is likely to be unknown in the case of an orphan (Eglen et al., 2007). However, there are indications that GPR50 may couple to $G\alpha_i$ and $G\alpha_q$ (Levoye et al., 2006), and may therefore inhibit cAMP or activate PKC and IP3. It is known that the mitogen-activated protein kinase (MAPK) system is regulated by the activation of most (all) types of G proteins (Marinissen and Gutkind, 2001), and an assay where extracellular regulated kinase (ERK) MAPK activity is measured could therefore be used for the ligand screening of all types of GPCR (Eglen et al., 2007). One such assay is called AlphaScreen SureFire™ (Perkin Elmer).

Another universal method utilises β-arrestin translocation to the C-terminal domain of the receptor upon agonist stimulation. The interaction of the receptor to β-arrestin can then be measured by FRET (Förster (fluorescence) resonance energy transfer) or BRET (bioluminescence resonance energy transfer) techniques (Eglen et al., 2007). More sensitive techniques, using β-galactosidase enzyme complementation assays to measure β-arrestin translocation or receptor internalisation have also been developed (O'Dowd et al., 2005; Wehrman et al., 2005; Eglen et al., 2007)

Exogenous GPR50 has been shown to homodimerise and heterdimerise with the melatonin MT_1 and MT_2 receptors (Levoye et al., 2006). It is possible that GPR50 only binds its ligand in the presence of MT receptors. An example of this mechanism is GABA receptor signaling, where the $GABA_{B1}$ receptor has ligand-binding properties but does not couple to G proteins or adenylyl cyclase (AC) whereas the $GABA_{B2}$ receptor couples to G proteins and AC but does not bind GABA on its own (reviewed in Eglen et al., 2007). Although an endogenous system of GPR50/$MT_{1/2}$ heterodimerisation has yet to be identified, an approach whereby GPR50/$MT_{1/2}$ heterodimers are used in a cell-based screen may nevertheless be useful in identifying a ligand.

As GPR50 is a GPCR located within a linkage region with bipolar disorder, interest was raised by the pharmaceutical industry. Attempts to deorphanise GPR50 were undertaken (a least by Organon to my knowledge). Nothing however appears to have been found as no papers or patents have been published. One can however only speculate as to what methods were attempted and it is unclear whether GPR50 is still being investigated.

When it was clear deorphanisation experiments were being undertaken by industry it was decided to adopt a different strategy to investigate the function of GPR50. As it is known that GPCRs can bind many different proteins to their C-terminal domain (Marinissen and Gutkind, 2001), and given that the GPR50 CTD is relatively large compared to similar receptors, it was decided to identify interacting proteins with the GPR50 CTD. These interactions may provide clues to the function of GPR50. The initial method that was used was a yeast two-hybrid screen. This work was performed prior to the start of my PhD.

1.3 Identifying possible GPR50 interactors

1.3.1 Yeast two-hybrid

Apart from G proteins, many other intracellular proteins may interact with the C-terminal tail and trigger or alter downstream signaling (Marinissen and Gutkind, 2001). To investigate the possible interactors of GPR50, a yeast-two-hybrid screen was performed by Hybrigenics (S.A., Paris, France, http://www.hybrigenics-services.com) (Grünewald et al., 2009), prior to the start of this PhD. The screen was performed using both 'insertion' and 'deletion' forms of the GPR50 CTD as bait. The insertion form corresponded to the coding sequence for amino acids 292-617 of human GPR50 (GenBank accession number GI:73909216), presenting the mutation S320P. The deletion form corresponded to the same coding sequence of human GPR50, deleted for amino acids 502-505 and presenting the mutation T532A (Grünewald et al., 2009). The baits were screened against a human adult brain cDNA library using both LexA- and Gal4-based systems (Grünewald et al., 2009). To each of the 'prey' interactors a confidence score was attributed, Global PBS (Predicted Biological Score) A-E, indicating the likelihood of it being a true interactor. A, B and C are high confidence interactions identified through two or more overlapping fragments. PBS D corresponds to protein interactions with moderate confidence. The letter E indicates proteins that are considered 'sticky', i.e. that have been identified as prey in 6 or more independent Y2H screens (Grünewald et al., 2009).

1.3.2 GO analysis

Gene Ontology Tree Machine analysis (Zhang et al., 2004) was performed of the genes isolated in the screens with PBS scores A-E (Grünewald et al., 2009), prior to the start of this PhD. Two broad classes of biological processes enriched in the putative interactors were identified (Fig 1.6): neuron development/differentiation (neuron development p=0.004) and sterol/cholesterol metabolism (steroid metabolism p=0.001) (Grünewald et al., 2009). The identification of functional

classes of putative interactors involved in aspects of lipid metabolism and neurodevelopment is entirely compatible with the biological processes implicated in previous genetic association studies (Thomson et al., 2005; Bhattacharyya et al., 2006). However, these results should be interpreted with caution until the interactions between these genes and GPR50 have been confirmed in a relevant cell system.

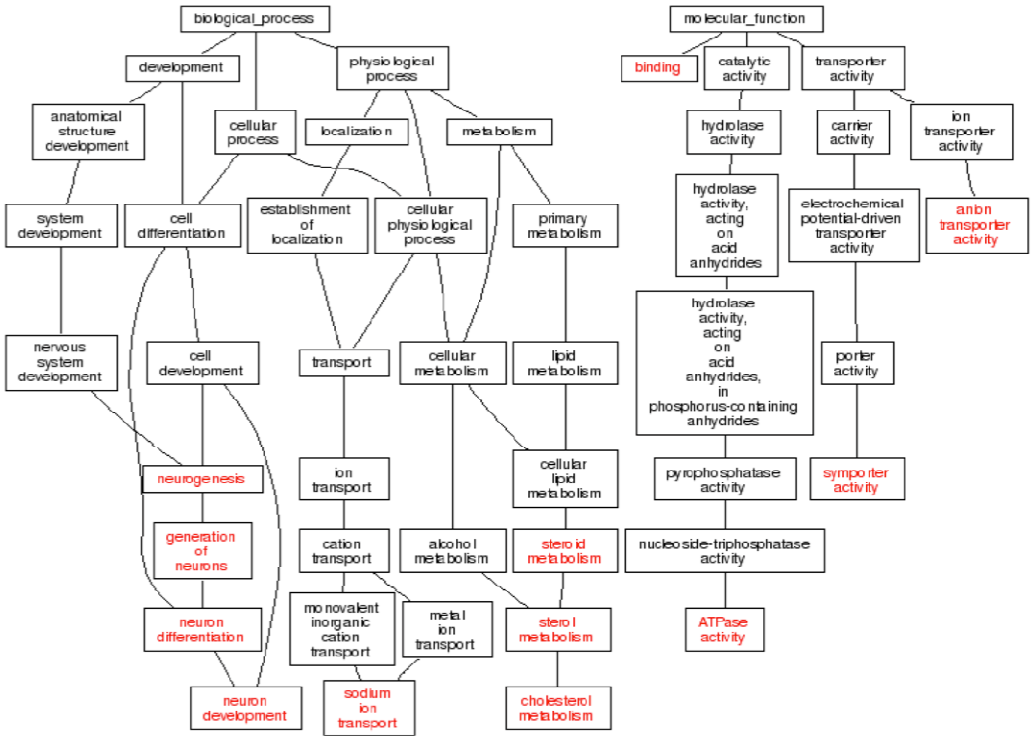

Figure 1.6 *Directed Acyclic Graph (DAG) produced using the Gene Ontology Tree Machine (GOTM). Visualised in red are significantly enriched GO categories of GPR50 Y2H interactors. Analysis included interactors with PBS of A-E only. Performed by Pippa Thomson. Figure published as supplementary material in Grünewald et al., 2009. Molecular and Cellular Neuroscience. Copyright 2009, Elsevier Science Ltd.*

1.3.3 Yeast two-hybid interactors

In the screen 23 putative protein interactors of the GPR50 CTD were identified. They are listed in Table 1 according to their PBS score. Proteins in several areas of interest were identified: neurodevelopment (ABCA2, CDH8, PCDH9, PAX6, RTN3, RTN4, SHOT1), stress response and apoptosis (SATB1, RTN3, RTN4, ST13, MADD), lipid and glucose metabolism (ABCA2, OSBP2, SREBP2, SATB1, MADD), and regulation of NMDA receptors and GABA transmission (PICK1, SLC12A5/ KCC2, MADD) (Grünewald et al., 2009). In terms of mechanisms several proteins appear to be involved in intracellular transport and sorting or molecules (SNX5, SNX6, CNST, RTN3, RTN4, ABCA2, OSBP2, KCC2) and actin and cytoskeletal remodeling (RTN4, SHOT1, PICK1, SPTAN1). The melatonin receptors, MT1 or MT2, were not identified in our yeast two-hybrid screen. The study by Levoye and colleagues (2006) indicates that GPR50 heterodimerises with these proteins through the transmembrane region of GPR50, which was not included in the bait sequence.

In this thesis the interaction with some of these proteins will be further investigated. Past research on some of the key interactors and their functions, relevant to this study, is briefly summarised below.

Symbol	Gene	Variant	Ins	Del	Global PBS
RTN4	reticulon 4	variant 5	5	2	A
CDH8	cadherin 8	variant 2		2	C
FLJ14752 fis	cDNA FLJ14752 fis, clone NT2RP3003071, C6orf111			1	C
ABCA2	ATP-binding cassette, sub-family A (ABC1), member 2	variant 2	1	2	D
RTN4	reticulon 4	variant 3	2		D
RTN3	reticulon 3	variant 2		4	D
SHOT1	Shootin-1		4	1	D
OSBP2	oxysterol binding protein 2	variant 1		2	D
PCDH9	protocadherin 9	variant 2	1		D
SNX6	sorting nexin 6	variant 2	1		D
MADD	MAP-kinase activating death domain	variant 4		1	D
PSMA1	proteasome (prosome, macropain) subunit, alpha type, 1	variant 1		1	D
SATB1	special AT-rich sequence binding protein 1		1		D
KCC2	potassium-chloride cotransporter		1		D
SLC4A10	solute carrier family 4, sodium bicarbonate transporter-like, member 10		1		D
FLJ34306	FLJ34306		2		D
PSMA1	proteasome (prosome, macropain) subunit, alpha type, 1	variant 1		1	D
SREBF2	sterol regulatory element binding transcription factor 2		4	10	E
SNX5	sorting nexin 5	variant 2	4	6	E
PICK1	protein interacting with PRKCA 1	variant 1		1	E
SPTAN1	spectrin, alpha, non-erythrocytic 1			2	E
ST13/HIP	suppression of tumorigenicity 13 / HSP70-interacting protein			3	E
CNST	consortin			2	E
PAX6	paired box gene 6 (aniridia, keratitis)	variant 2	2	1	E
DDX24	DEAD (Asp-Glu-Ala-Asp) box polypeptide 24		4	1	E
KIF5C	kinesin family member 5C	variant 15		1	N/A
PTPN5	protein tyrosine phosphatase, non-receptor type 5	variant 2	1		N/A
LOC653086	similar to RAN-binding protein 2-like 1 isoform 2	variant 12	1		N/A
GID: 1339887	EPB41L2 ? erythrocyte membrane protein 4.1-like 2				N/A

Table 1.1 *GPR50 Yeast-two-Hybrid (Y2H) screen hits, as performed by Hybrigenics. Shown are: symbol, full gene name and splice variant number, followed by the number of times each variant was captured by either the insertion (Ins), or the deletion (Δ502-505/T532A, Del) form of the GPR50 C-terminal tail.*

1.3.3.1 RTN3 and RTN4 (Nogo)

Reticulon family (RTN1-4) member RTN4, also known as Nogo (Schwab, 2010), scored highest in the yeast two-hybrid GPR50 interaction screen (Table 1.1). Nogo was identified as a putative partner in screens for both naturally occurring forms of GPR50: C-terminal GPR50 and GPR50$^{\Delta 502\text{-}505/T532A}$, but only considered as an interactor with the highest confidence in the GPR50 screen (PBS=A). A total of 7 Nogo variant 5 clones and 2 Nogo-C (variant 3) clones were identified in the screens (Grünewald et al., 2009).

Three main isoforms of Nogo are generated as a result of alternative splicing and promoter use (Oertle et al., 2003a): Nogo-A (RTN4 variant 1; 1192 amino acids, aa), -B (variant 2; lacking aa 186-1004) and -C (variant 3; lacks aa 186-1004 and has a

smaller N-terminal domain (Chen et al., 2000; GrandPre et al., 2000)) (Fig 1.7). Nogo variant 5 is a short form of Nogo-A, which lacks the first 206 aa. The isoforms share a C-terminal domain of 188 residues, the reticulon homology domain (RHD), found in all members of the reticulon family (Oertle and Schwab, 2003) (Fig 1.7) (Grünewald et al., 2009).

In addition, four RTN3 variant 2 clones were identified in the screen of the C-terminal GPR50$^{\Delta 502\text{-}505/T532A}$ form (Grünewald et al., 2009). RTN3 has multiple isoforms that are differentially expressed in tissues (Di Scala et al., 2005). The nomenclature of the RTN3 isoforms is confusing and varies according to the source used. The isoform identified in the yeast two-hybrid screen (gi: 41393607) corresponds to RTN3A3b (Di Scala et al., 2005), RTN3 variant 2 (ncbi) or RTN3-202 (Ensembl), contains 8 exons (including the large exon 3 and the common RHD, but not exon 2), and is 1013aa long with a predicted molecular weight of 110kDa (Fig 1.7). However according to Di Scala et al. (2005) this isoform is not expressed in any of the tissues investigated and their data suggests that exon 2 and 3 are only spliced together, yielding isoform RTN3A4b with a detected mass of 100kDa. Tissue distribution studies indicate that RTN3A1, RTN3A2 and RTN3A4b are more highly expressed in the CNS than in other tissues, especially in the cortex (Di Scala et al., 2005) and more in gray (neurons) than white (oligodendrocytes) matter (He et al., 2004).

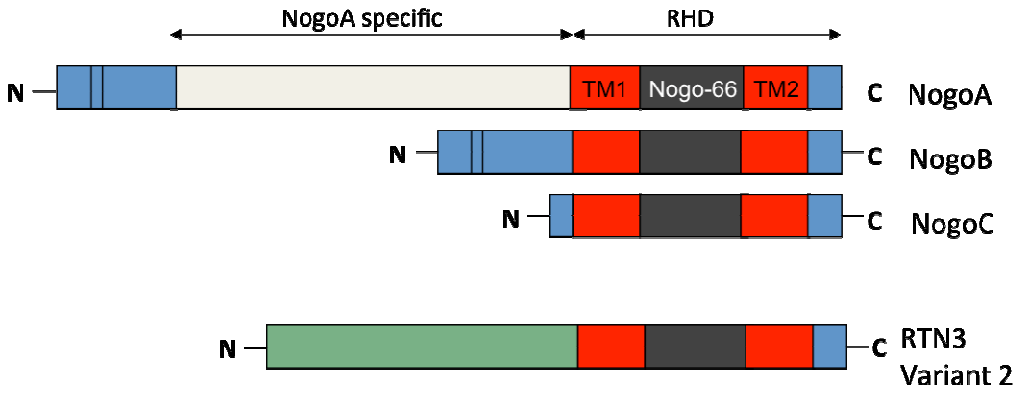

Figure 1.7 *RTN4/Nogo isoforms Nogo-A, Nogo-B and Nogo-C, and RTN3 variant 2. All reticulons share a C-terminal domain of 188 residues, the reticulon homology domain (RHD), consisting of the Nogo-66 domain flanked by two large transmembrane domains. They differ in the N-terminus.*

Reticulons play an important part under ER stress conditions and apoptosis (Teng and Tang, 2008). Overexpression of RTNs results in "ER overload response", ER calcium depletion and activation of apoptotic pathways such as the JNK-c-Jun pathway and Caspase 12 (Qu et al., 2002; Kuang et al., 2005; Chen et al., 2006; Xiang et al., 2006; Zhu et al., 2007; Lee et al., 2009). The majority of studies however indicate an important role for reticulon/Nogo proteins in neuronal regeneration, degenerative disorders and at the synapse (Chang et al., 2010; Schwab, 2010).

Of the three Nogo isoforms, Nogo-A has been the most extensively studied, and it is a potent inhibitor of neurite outgrowth *in vitro* and *in vivo* (Caroni and Schwab, 1988; Oertle et al., 2003b; Schwab, 2010). Neuronal receptors to Nogo-66 has been identified: Nogo-receptor (NgR) (Fournier et al., 2001), and recently Paired Immunoglobulin-like receptor B (PirB) (Atwal et al., 2008). This receptor also binds other outgrowth inhibitors, present in CNS myelin: Myelin-Associated Glycoprotein (MAG) (Liu et al., 2002) and Oligodendrocyte-Myelin glycoprotein (OMgp) (Wang et al., 2002). Through this receptor, signalling pathways are activated which lead to neurite outgrowth inhibition via regulation of the actin cytoskeleton (Niederost et al.,

2002; Montani et al., 2009; Schwab, 2010). Recently a role for neuronal Nogo-A and other myelin-associated inhibitors has been suggested as a negative regulator of functional and structural plasticity in the hippocampus (Raiker et al., 2010; Delekate et al., 2011) and in limiting ocular dominance plasticity by modifying the critical period (McGee et al., 2005), linking experience driven, activity dependent and injury induced plasticity (Akbik et al., 2011). The beneficial effects of Nogo-inhibition after spinal cord injury are currently being investigated (Gonzenbach et al., 2010; Schwab, 2010).

In relation to psychiatric illness, a significant increase in *Nogo-C* mRNA expression was found in the postmortem frontal cortex of individuals with schizophrenia as compared to age- and sex matched non-neurological controls (Novak and Tallerico, 2006). Additionally, there was a non-significant increase in expression in *Nogo-A* in schizophrenia, whereas *Nogo-B* was significantly reduced in the frontal cortex of major depressive patients (Novak and Tallerico, 2006). An insertion/deletion polymorphism in the 3' UTR of Nogo has shown association to schizophrenia in some, but not all studies (Novak et al., 2002; Tan et al., 2005). Mice lacking Nogo-A or the NgR showed behavioural changes that mimic symptoms of schizophrenia (Budel et al., 2008; Willi et al., 2009; Willi et al., 2010).

Reticulon proteins have also been implicated in Alzheimer's disease (AD). The expression of the NgR is increased in the CA1 and CA2 regions of the hippocampus in AD and is co-expressed with hyperphosphorylated Tau (Zhu et al., 2007). Recently it was shown that the NgR can regulate amyloid deposition by interacting with APP (Zhou et al., 2011). Further, Nogo-B/C and RTN3 were shown to inhibit BACE1-activity (beta-site amyloid precursor protein-cleaving enzyme 1, also known as β-secretase), thereby reducing the conversion of amyloid precursor protein (APP) to β-amyloid (He et al., 2006). RTN3 was also found to accumulate in dystrophic neurites and senile plaques in AD, and in neurofibrillary tangles and lewy bodies (Hu et al., 2007; Heath et al., 2010; Prior et al., 2010). Abnormal accumulation of β-amyloid and hyperphosphorylated Tau ('plaques and tangles') are believed to contribute to the onset of Alzheimer's disease (Bancher et al., 1989; Tanzi and

Bertram, 2005). Nogo has also been shown to modulate axonal sprouting in AD models in a mechanism seemingly distingt from the regulation of BACE1 activity and APP processing as seen with RTN3 and NgR (Masliah et al., 2010). The identification of reticulon proteins as cellular modulators of BACE1 (Hu et al., 2006) makes them possible targets for therapeutic interactions. Interestingly, BACE1 has many other substrates among which are NRG1 type III, Cadherins, Semaphorins and Ephrins (Lichtenthaler et al., 2003; Hu et al., 2006; Willem et al., 2006; Kim et al., 2007; Hemming et al., 2009). BACE1 and reticulon proteins are therefore implicated in myelination, cell adhesion, contact-dependent intercellular communication and cognitive functions.

1.3.3.2 CDH8

Cadherins are calcium-dependent, single-pass transmembrane, cell-cell adhesion molecules. They play a role in embryonic development and brain regionalisation, by establishing cell polarity and cell sorting according to their tissue type (Wheelock and Johnson, 2003). Cell types with different fates are found to express different types of cadherins (Inoue et al., 2001; Taniguchi et al., 2006) and a cell expressing a certain cadherin will almost exclusively adhere to another expressing the same type (homophilic binding specificity). Cadherins are highly expressed in the central nervous system, different cadherins by distinct neuronal groups (Suzuki et al., 1997; Gil et al., 2002; Saarimaki-Vire et al., 2011).

There is increasing evidence for the involvement of cadherins in neuronal functioning, most of which is based on research on N-Cadherin. In addition to brain regionalization, they are believed to play a role in CNS synaptic transmission and synapse formation (Togashi et al., 2002). Furthermore, it is thought that cadherins mediate the lock-and key mechanism (chemoaffinity hypothesis, (Sperry, 1963), which could account for the specificity of synaptic partners (Shapiro and Colman, 1999).

The cell-cell adhesion/dissociation mechanism of N-cadherin is mediated by Presenilin-1 (PS1) through a high molecular weight complex with γ-secretase (Parisiadou et al., 2004). Mutations in PS1 are linked to familial Alzheimer's disease (FAD) and γ-secretase performs the second cleavage of APP to liberate Aβ into the extracellular space. These mutations in PS1 are found to disrupt the normal cleavage of cadherins and thereby impair subsequent downregulation of CREB-mediated transcription (Parisiadou et al., 2004). In this model, alterations in the transcription mechanism could contribute to the pathogenesis of AD through interfering with cadherin signalling.

Cadherin 8 (CDH8, Table 1.1) is expressed in the dorsal horn of the spinal cord and in the dorsal root ganglia (DRG), and was found to play a role in synaptic transmission of cold sensation (Suzuki et al., 2007). CDH8 is also found in the thalamocortical afferents from medial posterior nucleus of the thalamus (POm) to the rat barrel cortex, and in the mouse somatosensory cortex, where it is expressed in a distinct laminar pattern (Gil et al., 2002; Krishna et al., 2011). CDH8 may be involved in radial migration of neurons during development in rhombomere 6 (Garel et al., 2000). In relation to mental illness, a recent genetic study indicated a role for CDH8 in the susceptibility of autism and learning disabilities (Pagnamenta et al., 2011). CDH8 is also one of two genes, the other being Phosphodiesterase 4B (PDE4B), that is disrupted in a balanced t(1;16)(p31.2;q21) translocation detected in a proband with schizophrenia, and a cousin with psychosis, carrying the translocation (Millar et al., 2005).

1.3.3.3 ABCA2

ATP-binding cassette sub-family A member 2 (ABCA2) is a multispan transmembrane protein primarily found to be expressed in the endolysosomal compartment of the cell. It is found to be highly expressed in the brain, most notably in the subventricular zone of the lateral ventricle and the dentate gyrus, regions important in adult neurogenesis (Broccardo et al., 2006). It is expressed by oligodendrocytes and by a subset of GABAergic and glutamatergic neurons in the

CNS (Broccardo et al., 2006) and by Schwann cells in the PNS (Saito et al., 2007). ABCA2 shares the highest homology with the HDL cholesterol transporter ABCA1 and may also influence cholesterol transport (Kaminski et al., 2001) and homeostasis (Davis, 2011) and sphingolipid metabolism (Sakai et al., 2007; Mack et al., 2011). Furthermore, ABCA2 regulates the expression of the LDL-cholesterol receptor and modulates the mobilisation of plasma membrane (but not lipid raft) cholesterol to apolipoprotein receptors and the trafficking of plasma membrane cholesterol to the ER for esterification (Davis et al., 2004; Davis, 2011). With respect to brain function, cholesterol is a key constituent of myelin and a function for ABCA2 in myelination of spinal cord and PNS is also indicated (Zhou et al., 2002).

Like RTN3, RTN4 and CDH8, ABCA2 has been implicated in Alzheimer's disease. Mace et al., (2005) identified a SNP in exon 14 (rs908832, C2037T) associated with early onset AD in a French Caucasian sample. However this association may be population dependent. The result was replicated in a Western European population (Wollmer et al., 2006), but not in a Southern European population (Wollmer et al., 2006). In the Japanese population on the other hand the T allele was not found (Wollmer et al., 2006). The T allele was also associated with heightened cholesterol levels in the cerebrospinal fluid (CSF) (Wollmer et al., 2006). In a Caucasian American sample no significant association was found between this SNP and early or late onset AD (Minster et al., 2009). In further support of a role in AD, ABCA2 colocalizes with APP and Aβ, and overexpression of ABCA2 results in an increase in intracellular protein levels of APP and Aβ (Chen et al., 2004b). ABCA2 expression was also linked to the oxidative stress response, oxidative damage being another pathological characteristic of AD (Chen et al., 2004). Finally, cholesterol is believed to play a distinct role in the pathogenesis of Alzheimer's disease as it is indicated to regulate β-amyloid generation and deposition (Puglielli et al., 2003).

Abca2 knockout mice display 'skittish behaviour' of hyperactivity, tremor and reduced body weight, perhaps reflective of changes in myelin ultrastructure or sphyngolipid composition (Mack et al., 2007). This behaviour was most notable in females as compared to males, suggesting the involvement of hormonal pathways.

Contrary to findings in *Nogo*-knockout mice (Woolf, 2003), *Abca2*-knockouts showed abnormal myelin structure in the CNS as compared to wild type littermates (Mack et al., 2007). Another study of *Abca2*-null mice however does not report this difference (Sakai et al., 2007).

1.3.3.4 SREBP2/SREBF2

Sterol regulatory element binding transcription protein 2 (SREBP2), or sterol regulatory element binding transcription factor 2 (SREBF2), is a ubiquitously expressed transcription factor that controls cholesterol homeostasis by stimulating transcription of sterol-regulated genes. When low cholesterol levels are detected in the ER SREBP2 precursor protein is sequestered/chaperoned to Golgi where it is cleaved by 2 proteases, releasing the transcriptionally active N-terminal domain. (Briggs et al., 1993; Goldstein et al., 2006). It is subsequently transported to the nucleus where it regulates the transcription of genes involved in lipid biosynthesis. At high sterol concentrations, SREBF2 disappears from the nuclear fraction, but not the (ER) membrane (Wong et al., 2006). SREBF/P2 expression has been researched mainly in the liver and not much is known about its activity in the CNS. As cholesterol is synthesised *de novo* in the brain, there could be a major role for SREBFs in processing fatty acids necessary for key processes such as myelination. In the adult mouse brain *Srebf2* mRNA expression is high in the cortex, olfactory bulb and hippocampal formation as measured by *in situ* hybridisation (Allen Brain Atlas, Lein et al., 2006).

SREBF2 has been studied in relation to AD. Variants in SREBF2 are potential candidates for CSF biomarkers in AD (Kim et al., 2011) and SREBF2 may also be a risk factor in vascular dementia (Kim et al., 2005). Transgenic mice overexpressing SREBP2 showed accumulation of mitochondrial cholesterol and increased neuronal death in response to Aβ1-42 compared to controls (Fernandez et al., 2009).

An association in the German and Scandinavian population between several SNPs in SREBF2 and schizophrenia was reported (Le Hellard et al., 2008). Drug related

metabolic effects in schizophrenic patients (weight gain) were also found to be associated with INSIG2, a gene involved in the SREBF2 pathway of activation of cholesterol and fatty acids production (Le Hellard et al., 2009). Interestingly, a functional SREBF2 pathway is required for ABCA1 transcription (Wong et al., 2006).

To briefly summarise, putative interactors RTN3, RTN4, CDH8, ABCA2 and SREBF2 are involved in neuronal development and plasticity and lipid metabolism. Interestingly each of them has been independently linked with psychiatric illness and neurodegenerative diseases. Investigating these interactions in more detail might give insight into the function of GPR50 and its association with mental disorders.

1.4 Aims of this thesis

The aim of my PhD was to gain more insight into the function of orphan GPR50.

This was subdivided into four objectives:

1. Verify a subset of putative interactors of GPR50 as identified by the yeast two-hybrid screen
2. Investigate the developmental expression pattern of Gpr50 and the confirmed interactors.
3. Investigate the functional consequence of GPR50s protein-protein interactions
4. Investigate the significance of the GPR50 C-terminal domain and the polymorphisms.

In Chapter Two, the physical interaction between GPR50 and RTN3, Nogo-A, Nogo-C, CDH8 and ABCA2 was further investigated by performing *in vitro* binding assays and colocalisation studies.

In Chapter Three, the developmental expression of Gpr50, Nogo, Cdh8, Abca2 and Srebf2 in the mouse brain was investigated by subcellular fractionation, rt-PCR and immunohistochemistry.

In Chapter Four, two functional assays relating to the function of the reticulon proteins were performed: neurite outgrowth and BACE1 activity.

In Chapter Five, the secondary structure of the GPR50 C-terminal domain was further investigated using biochemical and biophysical techniques.

Chapter 2

Validation of GPR50's interactions

2 Chapter Two: Validation of GPR50's interactions

2.1 Introduction

The first aim of this thesis was to confirm the interaction of GPR50 with some of its interactors. As several members of the reticulon family of proteins were identified in the yeast-two-hybrid (Y2H) screen, the interaction of GPR50 with Nogo-A, Nogo-C and RTN3 was further investigated. Additionally the interaction with cell-cell adhesion molecule CDH8 and lipid-associated protein ABCA2 was investigated because of the known role of cadherins in the development of the CNS and the links in the literature of GPR50 with lipid metabolism respectively. Initially, the interaction with C-terminal only GPR50 was investigated and later full-length GPR50 and the full-length GPR50$^{\Delta 502\text{-}505/T532A}$ variant associated with mood disorders (Thomson et al., 2005; Macintyre et al., 2010) were tested.

2.1.1 GPR50's interactors and mental illness

From previous findings it appears that the putative interactors of GPR50 are related to neuronal development, lipid metabolism and stress responses. Interestingly, several have also been associated with neurodegenerative and psychiatric disorders. GPR50, Nogo, CDH8 and ABCA2 may all have distinct roles in the pathology of Alzheimer's disease: though affecting BACE1 and Aβ (Nogo, He et al, 2004), lipid metabolism (ABCA2 and GPR50, Macé et al., 2005), or the interaction with Presenilin1 (cadherins, Parisiadou et al, 2004). Therefore, confirmation of these interactions would perhaps tell us more about the relationship between GPR50 and mental illness.

In this introduction to Chapter two past research on the cellular expression of GPR50 and the putative interactors that are investigated in this thesis is briefly summarised.

Developmental expression will be investigated and discussed in the next chapter (Chapter 3).

2.1.2 GPR50 expression

As is expected of a GPCR, overexpressed GPR50 is present at the cell surface of HEK293 cells (Levoye et al., 2006; Hamouda et al., 2007). Endogenous expression is found in human endothelial cerebral CMEC/D3 cells (Levoye et al., 2006) and in 1-10% of HEK293 cells, depending on the source/passage number of the HEK cells (our own unpublished observations). Overexpressed and endogenous GPR50 is detected at 66/67 kDa by Western blotting (Hamouda et al., 2007; Grünewald et al., 2009). It is common for GPCRs to oligomerise (Bouvier, 2001) and dimerisation is thought to be of functional importance (Milligan, 2004). Using various in-house produced and commercially available antibodies GPR50 was detected as a dimer by Western blotting, by us and others, endogenously and when overexpressed (Levoye et al., 2006; Hamouda et al., 2007; Grünewald et al., 2009).

2.1.3 RTN3 and RTN4 (Nogo) expression

Reticulons (RTNs) are primarily localized to the endoplasmic reticulum (ER) but are also found in the plasma membrane (Oertle et al., 2003b). They are involved in membrane shaping of tubular ER (Voeltz et al., 2006; Anderson and Hetzer, 2008). Within the reticulon homology domain (RHD) are two long (30-35 residues) hydrophobic segments, which determine the membrane topology with the ER and plasma membrane (Voeltz et al., 2006; Teng and Tang, 2008). Many different membrane topologies have been suggested (GrandPre et al., 2000; Thomson et al., 2005; Voeltz et al., 2006) reviewed in (Teng and Tang, 2008) (Fig 2.1). Most experimental evidence supports a topology where the Nogo-A and -B (and perhaps –C) N-terminus and Nogo-66 domain face the extracellular/ER luminal side and C-terminus faces the cytoplasm (Fig 2.1A-B) (Oertle et al., 2003b; Acevedo et al., 2004; Dodd et al., 2005; Miao et al., 2006). In this conformation Nogo-A and –B can

interact via their N-terminal and Nogo-66 domains with their receptors, in *trans* (when proteins are present on a different cell/membrane)(Schwab, 2010). The first hydrophobic segment of Nogo-C has been shown to form a hairpin structure within the ER membrane (Voeltz et al., 2006) (Fig 2.1 C). The second hydrophobic segment may also form a hairpin (Fig 2.1C) although this has not been confirmed (Voeltz et al., 2006). Therefore a topology where the Nogo-C C-terminus faces the ER lumen is also possible (Teng and Tang, 2008) (Fig 2.1D). For RTN3 on the other hand it has been shown that both hydrophobic domains can adopt this hairpin topology (He et al., 2007) (Fig 2.1E).

Nogo-A, -B and –C are a found on the plasma membrane of oligodendrocytes and in myelin (Huber et al., 2002), and also in neurons, myoblasts and 3T3 cells (Dodd et al., 2005). Neuronal Nogo-A is known to be expressed at the synapse (Lee et al., 2008). Endogenous and overexpressed Nogo proteins can complex together in various cell types (Dodd et al., 2005) and this may apply to all RTNs. On the cell surface a punctate staining of Nogo proteins was found, an indication of expression in distinct microdomains (Acevedo et al., 2004; Dodd et al., 2005), perhaps on lipid rafts (Acevedo et al., 2004). Nogo-A is expressed as 200 kDa, Nogo-B as 55 kDa and Nogo-C as 25 kDa protein by Western blotting using several different antibodies (Oertle and Schwab, 2003; Dodd et al., 2005).

The three main RTN3 isoforms detected in tissues are RTN3A1, RTN3A2 and RTN3A4b (Di Scala et al., 2005). RTN3A1 migrates at approximately 24 kDa. RTN3A2, the isoform interacting with BACE1 (He et al., 2004; Murayama et al., 2006) was detected at 27 kDa and corresponds to RTN3 transcript variant 1 (NCBI) or RTN3-204 (Ensmbl). RTN3A4b (corresponding to RTN3 variant 2 (NCBI) or RTN3-202 (Ensembl)) has a mass of approximately 100 kDa. Like the RTN4 isoforms RTN3A1, RTN3A2 and RTN3A4b are enriched in the ER/microsomal fraction of the cell (Di Scala et al., 2005).

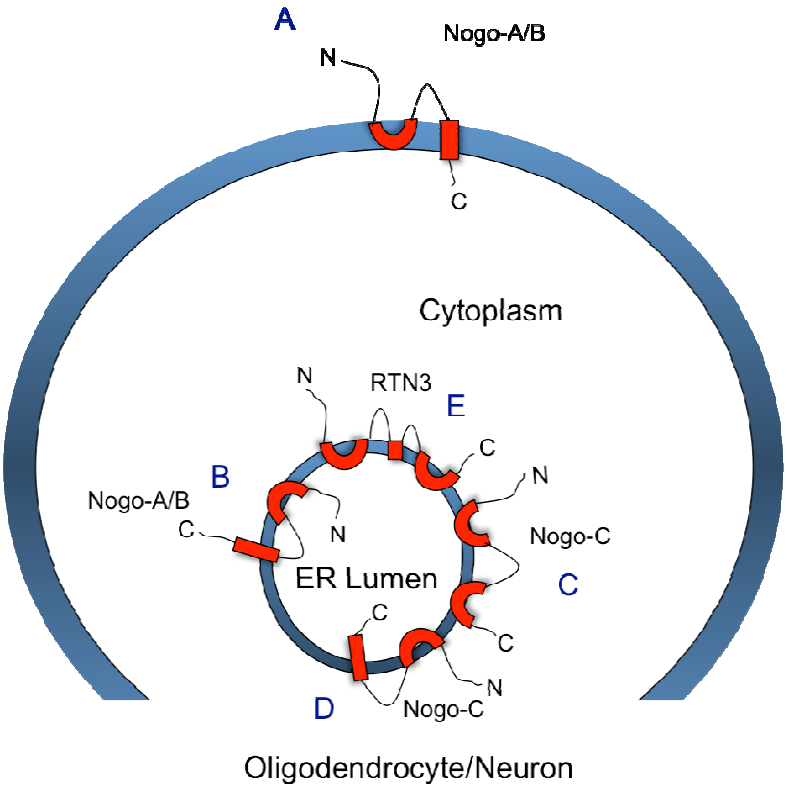

Figure 2.1 *Membrane topologies of reticulon proteins. Pictured is a schematic of some of the proposed membrane topologies as supported by experimental evidence. (A) The N-terminus and Nogo-66 domain of Nogo-A were shown to have neurite outgrowth inhibiting and growth cone collapsing characteristics via interaction with or modulation of the Nogo-receptor (Oertle et al., 2003b) and are therefore likely to face the extra cellular side. Similarly, the N-terminus of Nogo-B is shown to interact with the Nogo-B receptor (Miao et al., 2006). (B) RTNs are however predominanlty present in the ER membrane and the same topology as in (A) may be present there. (C, E) However most studies suggest a topology where the N- and C-termini of Nogo-C and RTN3 face the cytosol where the relatively long (30-35 residues) transmembrane domains are likely to form hairpin structures (Grandpre et al., 2000, He et al., 2007, Voeltz et al., 2006). Yet another topology is also possible (D) (Voeltz et al., 2006; Teng and Tang, 2008).*

2.1.4 CDH8 expression

Cadherins are calcium-dependent, single-pass transmembrane, cell-cell adhesion molecules. CDH8 is therefore expected to be expressed on the plasma membrane, at cell-cell contacts, as was shown after overexpression in L cells (Kido et al., 1998). Cdh8 is expressed in a punctate pattern in the dorsal horn of the mouse spinal cord and at the synapse (Suzuki et al., 2007).

In human and mouse the full-length isoform is predicted to be 88 kDa (Ensembl). Two forms of Cdh8 have been detected by western blotting in rat brain, a weakly expressed 130 kDa and a 95 kDa (truncated) form. The truncated form was present in the soluble fraction and the (more characteristic of classic cadherins) 130 kDa isoform in the insoluble fraction after untracentrifugation of whole brain homogenate (Kido et al., 1998). The authors suggest the 130 kDa isoform is full-length Cdh8 but is sensitive to trypsin digestion. In addition the 130 kDa isoform was shown to co-immunoprecipitate with cadherin binding partner beta-catenin.

2.1.5 ABCA2 expression

ABCA2 is a multipass transmembrane protein suggesting it is also expressed on the cell surface. When overexpressed it is however primarily localised to the lysosomes as shown by colocalisation with marker LAMP1, and to some extent to the ER and Golgi in HEK293 and HeLa cells (Vulevic et al., 2001). A more cytoplasmic staining pattern of endogenous Abca2 was previously reported in (Broccardo et al., 2006), indicating a likely difference in localisation between endogenous and overexpressed ABCA2. Human ABCA2 is expressed as a 270 kDa isoform by Western blotting of transfected HEK293 cells using a protein-specific antibody (Vulevic et al., 2001).

2.1.6 Introduction to experiments

The putative interactors as shown in Table 1.1 (Chapter 1) were identified in yeast. This system has limitations as proteins are expressed in the nucleus only whereas previous data suggests our proteins of interest are only expressed in the plasma membrane and in light membrane containing compartments such as the ER, Golgi and endolysosome in mammalian cells. Also, as mechanisms like protein folding could differ between yeast and mammalian cells, we sought to verify the yeast-two-hybrid results by performing co-immunoprecipitation (co-IP) and immunocytochemistry in mammalian cells.

Co-IP experiments were performed by overexpressing GFP-tagged and untagged constructs of GPR50, Nogo-A, Nogo-C, RTN3, CDH8 and ABCA2 in HEK293 (Human Embryonic Kidney) or HEK293T cells. HEK293T cells are HEK293 cells transformed by expression of the large T antigen from SV40 virus, and therefore have a higher transfection efficiency of plasmids with an SV40 origin of replication. For immunocytochemistry both overexpressed and endogenous proteins were investigated in HEK293 and SH-SY5Y neuroblastoma cell lines and primary cultured mouse neurons. In addition the effects of co-expressing the reticulons and GPR50 on GPR50 localisation was also investigated.

2.2 Methods

2.2.1 Expression constructs

All expression construct used in this thesis are listed in Table 2.1. Ultimate ORF entry clones containing full-length human GPR50 (IOH63602) and RTN4 transcript variant 1 (Nogo-A, IOH53642), RTN4 transcript variant 3 (Nogo-C, IOH4069), RTN3 (transcript variant 1, IOH10268) and CDH8 (IOH42822) in pENTR221, were obtained from Invitrogen (Paisley, UK). Additionally, a True Clone™ full-length clone termed GPR50-TTC was obtained from Origene (Rockville, USA). Full length ABCA2 in a pcDNA3.1/Hygro© vector (Invitrogen) was a kind gift from Kenneth Tew (Medical University of South Carolina, MUSC). The eGFP construct (pEGFP-N1, Clontech) was a kind gift from Laura Hyndman (University of Edinburgh). The Tif1α in pDEST53 (Invitrogen) was used as a control and was made by Christoph Grünewald (MMC, UoE, unpublished). The GPR50 C-terminal domain (GPR50 CTD) and GPR50$^{\Delta 502\text{-}505/T532A}$ CTD constructs were made by Hazel Kinnell and Alison Condie (University of Edinburgh). GPR50$^{\Delta 502\text{-}505/T532A}$ was made from GPR50 (IOH63602) using site-directed mutagenesis (see 2.2.4 below).

Entry clones were cloned by recombination into pDEST40, pDEST47 and pDEST53 vectors to create untagged and N-terminal GFP tagged constructs (LR clonase II, Gateway®, Invitrogen, Table 2.1). Untagged proteins were expressed by not removing the stop codons present in Invitrogen ORF entry clones, otherwise resulting in C-terminally V5/GFP-tagged proteins. Subcloning of these constructs was performed during my MSc in Neuroscience by Research project.

To select for expression constructs, the vectors were used to transform competent E. coli (One Shot Omnimax 2-Ti, Invitrogen) or DH5α (Invitrogen), and plasmid DNA was extracted using Qiagen Miniprep or Maxiprep kits (Crawley, UK) as per manufacturer's instructions. All clones were sequenced (see 2.2.5 below) and

checked for expression of proteins of the expected molecular weight by Western Blot (see 2.2.14 below) in HEK293 cells.

Name	Tag	Vector/Promoter	Residues	Accession
GPR50-TTC	-	pCMV,	1-617	GI:150170721
GFP-GPR50	GFP (N-terminal)	pDEST53, CMV	1-617	GI:73909216
GPR50	-	pDEST40, CMV	1-617	GI:73909216
GPR50$^{\Delta 502\text{-}505/T532A}$	-	pDEST40, CMV	1-613	GI:166714277
GFP-CTD	GFP (N-term)	pDEST53, CMV	283-617	GI:73909216
GFP-CTD$^{\Delta 502\text{-}505/T532A}$	GFP (N-term)	pDEST53, CMV	283-613	GI:166714277
GFP-Nogo-A	GFP (N-term)	pDEST53, CMV	1-1192	GI:47519561
Nogo-A	-	pDEST47, CMV	1-1192	GI:47519561
RTN3	GFP (N-term)	pDEST53, CMV	1-236	GI:41393611
Nogo-C	GFP (N-term)	pDEST53, CMV	1-199	GI:47519538
GFP-CDH8	GFP (N-term)	pDEST53, CMV	1-799	GI:16306538
CDH8	-	pDEST40, CMV	1-799	GI:16306538
ABCA2	-	pcDNA3.1/Hygro, CMV	1-2436	GI:150417982
TIF1α	GFP (N-term)	pDEST53, CMV	1-1050	GI:47419910
eGFP		pEGFP-N1, CMV		

Table 2.1 *Expression constructs used in this study. Subcloning of the constructs was performed during my MSc Neurosience Neuroscience by Research project.*

2.2.2 Primer design

Primers were designed using The Primer 3 http://frodo.wi.mit.edu/primer3/ (Rozen and Skaletsky, 2000). Genomic sequence information was obtained from the University College Santa Cruz (UCSC) genome browser and Ensembl (www.ensembl.org). The following parameters were used to select primers: Primer

Tm Min: 55, Opt: 60, Max: 63; Max Tm difference: 1, Primer GC%: Min: 20, Opt: 50, Max: 80; GC clamp: 1. Specificity of the primer sequence was checked using UCSC In-silico PCR (Kent et al., 2002), which searches a sequence database with a pair of PCR primers. The primers were synthesised by Sigma Aldrich. All primers were diluted to 100µM with TE buffer upon receipt and stored at -20°C. Primers and conditions used in this thesis are described in Table 2.2. These primer sequences were designed by Pippa Thomson (a) or Invitrogen (b-c) and were kindly provided by Pippa Thomson, Ben Pickard and Christoph Grünewald, which is noted in the legend of Table 2.2. Primers were either used for touch-down PCR (TD) and/or for sequencing (BD 3.1) (Table 2.2).

Name	Forward sequence	Reverse Sequence	PCR programme	Product size
GPR50 indel[a]	ttcatttcaagcctgcttcc	cttagggtggctggtagtgg	TD55, Seq 3.1	200/188
RTN4 ex4-6[a]	agcattgtgagcgtaacagc	accattaaacaaggcaccaac	TD53, Seq 3.1	309
CDH8 ex8-11[a]	ctgacctggagaggcagttc	gctgctcagtggaggatttc	TD55	467
RTN3 ex3-5[a]	ctgtcaccatcagcttcagg	atcagccacatgaagacagc	TD55	238
M13[b]	gtaaaacgacggccag	caggaaacagctatgac	Seq 3.1 TD55	-
T7[b]	taatacgactcactataggg	-	Seq3.1	
AttB1/2[c]	ggggacaagtttgtacaaaaaagcaggct	ggggaccactttgtacaagaaagctgggt	Seq 3.1 TD55	-
pDEST40[c]	gcttatcgaaattaatacga	accgaggagagggttaggga	Seq 3.1	-
pDEST53[c]	tgagtttgtaactgctgctggg	acagatggctggcaactagaag	Seq 3.1	-
pDONR[c]	gtaaaacctacggccag	caaataatgattttatttattttga	Seq3.1 TD55	-

Table 2.2 *Primers used for PCR and Sequencing. [a]Provided by Dr Pippa Thomson; [b]provided by Dr Christoph Grünewald, [c]provided by Dr Ben Pickard.*

2.2.3 Polymerase chain reaction (PCR)

The PCR reactions were performed in a Thermo non-skirted 96-well plate. Invitrogen reagents were used in 10 µl reactions: 1 µl 10x PCR buffer, 0.3 µl 50 mM $MgCl_2$, 0.2 µl 20 nM dNTPs, 0.2 µl of each 100 µM primer, 0.1 µl Taq polymerase; (Invitrogen), 1 µl 50-100 ng dsDNA). All amplification were performed in a PCR thermal cycler, PTC-225 (MJ Research) using touch-down (TD) 53 and 55 programmes at an initial denaturation of 93 ºC for 1 min, followed by 10 cycles of 93 ºC for 20 s, touch-down annealing from 63ºC to 53ºC (or 65ºC to 55ºC) for 30 s, and 72ºC for 1 min, followed by 10 cycles at an annealing temperature of 53ºC (or 55ºC), and a final extension of 72ºC for 10 min. The PCR products were mixed with Orange G loading buffer and were resolved on 1-2% agarose gel against a 1kb ladder (Invitrogen). Electrophoresis was performed in 0.5% TBE buffer at 100 V for 30-45 min.

2.2.4 Site-directed mutagenesis

$GPR50^{\Delta 502\text{-}505/T532A}$ was generated using the Stratagene QuikChange II Site Directed Mutagenesis kit (Agilent Technologies) in two consecutive steps: first removing residues 502-505 (TTGH), and subsequently generating the Thr532Ala point mutation that is in linkage disequilibrium (LD) with the deletion, from the GPR50 pENTR221 (Invitrogen) construct. Primers incorporating the mutations were designed using Stratagene's QuikChange online primer design programme: *http://www.stratagene.com/qcprimerdesign*
The first set of primers used to remove 12 base pairs at residues 1552-1563 were:
sense: 5'-cagccaccctaaacccatcaagccagctaccagcca-3' and
antisense: 5'-tggctggtagctggcttgatgggtttagggtggctg-3'. The second set used create a single base pair change from A to G at position 1594 were:
sense: 5'-gccaccctaagcccgctgctgctgacaac-3' and
antisense 5'-gttgtcagcagcagcgggcttagggtggc-3'.

Site-directed mutagenesis reaction mixes were prepared as follows:
5 µl of 10× reaction buffer (Agilent Technologies)
5 or 50 ng of dsDNA template
125 ng of sense primer
125 ng of antisense primer
1 µl of dNTP mix (Agilent)
ddH_2O to a final volume of 50 µl
1 µl of *PfuUltra high fidelity* DNA polymerase (Agilent)
Negative control reaction mixes contained 50 ng of DNA and only the sense primer.

The mutated DNA was amplified by PCR reaction. Cycling conditions were as follows: Hot start at 95ºC for 30s, then 18 cycles of 95ºC for 30 s, 55ºC for 1 min, and 68ºC for 4 min.

Dpn1 restriction enzyme was then added to the reaction and incubated at 37ºC for 1 hour to digest the non-mutated parental DNA. The Dpn1-treated DNA was then transformed in to super competent XL1 Blue E coli cells (Agilent Technologies). Colonies were screened by PCR using GPR50 'indel' exon 2 primers (Table 2.2) and PCR programme TD55 and were further confirmed by sequencing using Big Dye 3.1 reagents (see below).

2.2.5 Sequencing

The PCR Sequencing reactions were performed in a thermo non-skirted 96-well plate, using BigDye® Terminator Ready Reaction Mix v3.1 (Applied Biosystems) in a total volume of 10 µl, with 1µl BDv3.1, 2µl 5x sequencing buffer (Applied Biosystems), 3pmol primer, 150-500 ng dsDNA, up to 10µl dH20. The primers used for sequencing are listed in Table 2. Sequencing reactions were performed on a PTC-225 Peltier thermal cycler (MJ Research). Cycling conditions were as follows: Hot start at 96ºC for 1min, then 25 cycles of 96ºC for 10s, 50ºC for 5s, and 60ºC for 4 min.

Sequencing products were purified by ethanol/EDTA precipitation. To each well 5 µl 125 mM EDTA was added, followed by 60 µl ethanol. After incubation for 10 min in the dark, reactions were centrifuged at 3000 g for 30 min at 8ºC in a Jouan CR422 centrifuge. This was followed by a wash with 70% ethanol and centrifugation at 3000 g for 15 min at 8ºC. Samples were air dried for 10min in the dark and stored at -20ºC. Nucleic acid sequences were read by Agnes Gallacher at the Medical Research Council Human Genetics Unit. Sequences were checked using Chromas Lite version 2.01 (Technelysium Pty Ltd).

2.2.6 Mammalian cell culture

All media and chemicals were purchased from Invitrogen, unless stated otherwise. HEK293, HEK293T and SH-SY5Y cells (ECACC) were cultured in DMEM with 10% fetal bovine serum (FBS). Cultures were kept at 37^{o}C with constant humidity, 95% air and 5% CO_2. For transient transfections Lipofectamine 2000 was used according to the manufacturer's instructions (see 2.2.8 below).

2.2.7 Primary neuronal culture

Hippocampal and cortical neuronal cultures were prepared from embryonic day 18 (E18) CD1 mice as described previously (Okabe et al., 2003; Bradshaw et al., 2008). Date of plug was considered E0. Neurons were seeded at 50-100 cells/mm^2 on poly-D-Lysine (Sigma-Aldrich, St. Louis, USA) coated coverslips in 12 well cluster plates, and cultured in neurobasal medium supplemented with 2% B-27, 2mM Glutamax-1 and Penicillin/Streptomycin for 14-28 days-in-vitro (DIV). Cultures were kept at 37^{o}C with constant humidity, 95% air and 5% CO_2. For transient transfections Lipofectamine 2000 was used according to the manufacturer's instructions (see below).

2.2.8 Lipofectamine transfection protocol

The total amount of OptiMeM, DNA and Lipofectamine used per transfection are shown in Table 2.3. First, the plasmids and Lipofectamine 2000 were incubated in 2 separate vials with OptiMeM for 5 min. The two solutions were added together and incubated for a further 20 min. Before addition of the transfection mix the plated cells were briefly washed with OptiMeM. The transfection mix was added to the cells and left to incubate for 6 hours at 37^{o}C with 5% CO_2. After 6 hours the medium was replaced with prewarmed DMEM/FBS (HEK/SHSY5Y cells) or Neurobasal/B27/Glutamax (neurons), and left overnight, for a period of 14-16 hours.

	10 cm	6 wells	12 wells	24 wells
DNA	12 µg	4 µg	2 µg	1 µg
Lipofectamine	40 µl	8 µl	4 µl	2 µl
OptiMeM	4 ml	750 µl	500 µl	200 µl

Table 2.3 *Lipofectamine 2000 transfections*

2.2.9 Antibodies

The primary antibodies used in this thesis are listed in Table 2.4a-b.

Antibody Name	immunogen	Supplier, host
GPR50 (G-15)	Within residues 400-450 of GPR50 of human origin (accession number Q13585)	Santa Cruz Biotechnology, Santa Cruz, CA (sc-50590), goat polyclonal
GPR50 (Abcam)	C-terminal peptide residues of human GPR50	Abcam, Cambridge, UK (ab13190), rabbit polyclonal
GPR50 E62	C-terminal peptide residues 378-392 HPDRASGHPKPHSRS of human GPR50	In-house (produced by Eurogentec, Seraing, Belgium), rabbit polyclonal
GPR50 E63	C-terminal peptide residues 516-530 TTADYPKPATTSHPK of human GPR50	In-house (Eurogentec), rabbit polyclonal
Nogo-A (H-300)	Within residues 701-1000 of human Nogo-A	Santa Cruz (sc-25660), rabbit polyclonal
Nogo (N-18)	N-terminus of human Nogo	Santa Cruz (sc-11027), goat polyclonal
CDH8 E60	N-terminal peptide residues 44-55 LELNSLGEEQRILNR of human CDH8	In-house (Eurogentec), rabbit polyclonal
CDH8 E61	C-terminal peptide residues 785-799 (RLGELYSVGESDKET) of human CDH8	In-house (Eurogentec), rabbit polyclonal
CDH8 (C-18)	Peptide mapping at the C-terminus of human Cadherin-8	Santa Cruz, (sc-6461). Goat polyclonal
ABCA2	Residues 1499–1522 of human ABCA2	Kenneth Tew, MUSC (Vulevic et al., 2001), rabbit polyclonal

Table 2.4a *Antibodies used in this thesis.*

Antibody Name	immunogen	supplier	Marker for	Reference
Pan-cadherin	Synthetic peptide DYDYLNDWGPRFKKLA DMYGGGDD conjugated to KLH, corresponding to amino acids 889-912 of Chicken N-Cadherin	Abcam (ab6528), mouse monoclonal	Plssma membrane	(Diekmann et al., 2010)
VLA2a (Integrin A2)	Residues 42-245 of human VLA-2α	BD Biosciences, San Jose, Ca (611016), mouse monoclonal	Plasma Membrane	(Kirkland and Ying, 2008)
Calreticulin	Calreticulin-maltose binding fusion protein	Abcam (ab22683). Mouse monoclonal	Endoplasmic reticulum	(Kenny et al., 2009)
β-actin	Synthetic peptide DDDIAALVIDNGSGL conjugated to KLH, corresponding to amino acids 1-15 of Xenopus laevis beta Actin	Abcam (ab6276). Mouse monoclonal	Cytoskeleton , filopodia, lamellipodia	(Leung et al., 2006)
TUJ1 (β-tubulin III)	Microtubules derived from rat brain. Specific for neuronal β-tubulin III	Covance Richmond, CA, USA (MMS-435P 250), mouse monoclonal	Microtulules in immature neurons	(Markakis et al., 2004)
PSD-95	Purified recombinant rat PSD-95	ABR, Golden, CO (MA1-046), mouse monoclonal	Postsynaptic density	Clapcote et al., 2007
Synaptophysin	rat retina synaptosome	Sigma (S 5768), mouse monoclonal	Presynaptic membranes, vesices	Clapcote et al., 2007
alpha-Tubulin	Synthetic peptide conjugated to KLH derived from residues 1-100 of Human alpha-Tubulin.	Abcam (ab4074), rabbit polyclonal	Microtubules	(Feng et al., 2010)
GFP	Antibody is a mixture of two antibodies, clones 7.1 and 13.1, raised against recombinant Aequorea victoria GFP	Roche Applied Science, Burgess Hill, UK (11 814 460 001). Mouse monoclonal	Green fluorescent protein	(Keller et al., 2009)

NeuN	Tissue / cell preparation (purified cell nuclei from mouse brain).	Abcam (ab77315), mouse monoclonal	Mature neurons	(Rump et al.).
GFAP	GFAP from pig spinal cord	Sigma, St Louis, MO (G3893), mouse monoclonal	Astrocytes	(Tran et al., 2006)
O4	White matter of corpus callosum from bovine brain	R&D systems, Abingdon, UK (MAB1326), mouse monoclonal	Oligodendrocytes	(Aguirre and Gallo, 2004)
Vimentin	Cytoskeletal vimentin extract of calf lens	Abcam (ab8978), mouse monoclonal	Tanycytes	(Schnitzer et al., 1981)
5-HT	Serotonin coupled to BSA with paraformaldehyde	Immunostar, Hudson, WI (20080) rabbit polyclonal	Serotonin	Lee et al., 2003)
Dopamine Beta Hydroxylase	Full length native protein purified from adrenal medulla	Abcam (ab43868), rabbit polyclonal	Noradrenaline	(Coradazzi et al., 2010; Zhang et al., 2010)
Tyrosine Hydroxylase	Purified rat pheochromocytoma tyrosine hydroxylase	Abcam (Ab111), mouse monoclonal	Dopamine	(Brenz Verca et al., 2003).

***Table 2.4b**. Marker antibodies used in this thesis.*

2.2.10 Immunocytochemistry

Cells were fixed 24 hours after transfection by incubation with ice cold methanol for 10 min. Cells were washed with PBS containing 0.02% bovine serum albumin (BSA, Sigma-Aldrich) and blocked for 30 minutes in PBS/BSA with 10% serum from secondary antibody host. The following primary antibodies in PBS/BSA were incubated for 1 hour at room temperature: anti-GPR50 (C-ter, Abcam, 1:1000), anti-GPR50 (G-15, Santa Cruz, 1:1000); anti-GPR50 E62 (1:1000), anti-GPR50 E63 (1:1000), anti Nogo-A (H-300, 1:1000), anti-TUJ1 (1:2000), anti-CDH8 E61

(1:1000), anti-GFP (1:1000), anti-β-actin (1:100,000). Secondary antibodies Alexafluor 488 goat anti-mouse or -rabbit (1:500, Molecular probes, Invitrogen), Alexafluor 594-conjugated goat anti-mouse or -rabbit IgG (1:800), Alexafluor 488/594 donkey anti-goat, -rabbit or –mouse IgG (1:500/1:800) in PBS/BSA with 10% serum, were applied for one hour at room temperature. Glass coverslips were mounted onto slides using a drop of mowiol (Sigma-Aldrich) with DAPI (Vectashield, Vector Laboratories, Peterborough, UK, 2 µg/ml).

2.2.11 Microscopy

Confocal images of neurons and SH-SY5Y cells (Figs 2.8, 2.14, 2.17) were captured sequentially (line) on an Olympus Fluoview 1000 confocal laser scanning microscope (UPlanSApo 60x/1.35 oil objective) at image size 1024x1024 using Kalman filter mode 3. The remaining images were taken on a Zeiss Axioskop 2 fluorescent microscope (Zeiss Plan-Neofluar 40x/1.3 and 100x/1.3 oil objectives).

2.2.12 Colocalisation Image analysis

The Intensity Correlation Analysis (ICA) plugin for image J is described in detail in Li et al., (2004), the Pearson's and Manders' correlation coefficients in Manders' et al., (1993). Briefly, the ICA generates the Intensity Correlation Coefficient (ICQ), which describes if the intensities of two images vary in synchrony i.e. are dependent. The ICQ values are distributed between -0.5 and +0.5. Random staining: ICQ~0; segregated staining: 0>ICQ>-0.5; dependent staining 0<ICQ≤+5.0. Manders' Overlap coefficient is based on the Pearson's correlation coefficient with average intensity values being taken out of the mathematical expression, meaning that it will indicate positive overlap when one signal is stronger then the other at the same location. The values are distributed from 0 to 1, the former corresponding to non-overlapping images and the latter reflecting 100% co-localisation between both images.

There instructions on how to use the ICA plugin were followed: http://www.uhnresearch.ca/facilities/wcif/software/Plugins/ICA.html. Briefly,

representative confocal images showing staining of GPR50 and Nogo-A were selected and Olympus .oib files were imported into image J using the bioformats importer plugin (http://www.loci.wisc.edu/ome/formats-imagej.html). Images were background subtracted and thresholds were set. Image Correlation Analysis was selected for axonal/dendritic regions of interest (ROI). Frequency, scatter plots and ICA plots were selected. The results spreadsheet displayed Pearson's R (Rr), Manders' Overlap Coefficient (Manders, 1993)(R), red:green pixel ratio (Ch1:Ch2, was ~1 for selected images) and the Intensity Correlation Coefficient (ICQ) (Li et al., 2004). To determine if ICQ values are higher then 0, statistical analysis of N number of images/cells was performed using single sample t-Tests. Values are presented as mean (± SE).

2.2.13 Quantitative analysis of GPR50 distribution

SH-SY5Y cells were seeded at $1x10^5$ cells on glass coverslips in 12 well dishes. Cells were transfected with untagged GPR50 or $GPR50^{\Delta 502\text{-}505/T532A}$ and GFP-RTN3, GFP-Nogo-C, untagged Nogo-A or eGFP as a control using Lipofectamine 2000. Immunocytochemistry was performed using GPR50 G-15 (1:1000), ER marker Calreticulin (1:1000) and GFP (1:1000) or Nogo-A (H-300, 1:1000). Over three independent experiments 120 images were randomly collected, blind to the condition. The number of cells that showed GPR50 staining in the plasma membrane, ER or both was counted. A two-way ANOVA with Bonferroni's post-test was performed using Prism. A graph showing the percentage of GPR50 transfected cells (±SE) where GPR50 is in the plasma membrane, ER or both was also produced in Prism.

2.2.14 Immunoprecipitation and Western blotting

HEK293T cells were grown on 10 cm dishes until 95% confluent and then transfected as above. Twenty-four hours after initiation of transfection, cells were lysed using RIPA buffer (50 mM Tris pH 7.4, 150 mM NaCl, 1% NP-40, 0.1% SDS, 0.5% sodium deoxycholate, plus protease inhibitors (Complete, Roche)). Lysates

were incubated on a rotary wheel for 30 min at 4°C, and subsequently cleared from insoluble material at 13,000 rpm at 4°C. The supernatant was incubated for 2 hours with 3 µg of anti-GPR50 (SC). Protein G-sepharose beads (Sigma) were added to the lysate, and incubated for 90 min. Beads were collected by centrifugation for 3 min at 10,000 rpm and washed three times with RIPA (all at 4°C). The beads were resuspended in 40 µl Laemmli sample buffer with 100 mM DTT and boiled for 5 minutes or heated at 40°C for 10min in non-denaturing conditions and to allow better GPR50 detection. Supernatants were analysed by Western blotting. Immunoprecipitation and 10-15 µg lysate samples were separated on 4-12% NuPage Bis-Tris or 3-8% NuPage Tris-Acetate gels (Invitrogen) against Precision Plus all blue protein standards (Biorad) and transferred onto PVDF membrane (Invitrogen). Membranes were stained briefly using Ponceau S (Sigma) to verify transfer of proteins from the gel and to determine equal loading. After blocking for 1 hour at room temperature in PBS with 0.2% Tween-20 (PBS-T) plus 5% skimmed milk powder, the membranes were incubated overnight at 4°C with the following primary antibodies in PBS-T with 5% milk: anti-GPR50 (G-15, 1:5000), anti-GPR50 C-ter (1:1000), anti-GPR50 E62 (1:5000), anti-GPR50 E63 (1:5000), anti-Nogo-A (H-300, 1:2000), anti-Nogo (N-18, 1:1000), anti-ABCA2 (1:1000), anti-CDH8 E61 (1:3000), anti-GFP (1:1000). Membranes were incubated with horseradish peroxidase conjugated secondary antibodies: swine anti-rabbit (1:3000; DAKO A/S, Glostrup, Denmark), rabbit anti-goat (1:5000, DAKO), rabbit anti-mouse (1:2000, DAKO) in PBS-T for 30 min at room temperature. After incubations membranes were washed 3 x 15 min with PBS-T. The signals were detected using chemiluminescence (ECL-Plus, Amersham Biosciences, GE healthcare, Chalfont St.Giles, UK) and exposure to X-ray film.

2.3 Results

2.3.1 Antibody characterisation

Throughout this thesis several in-house produced and commercially available antibodies were used. To test these antibodies I overexpressed GFP-tagged and untagged proteins (see Table 2.1) for detection in HEK293(T) cells by Western Blotting and immunocytochemistry. Detection of endogenous protein expression was tested in primary cultured mouse neurons and HEK293(T) cells. The antibodies are briefly described here and details are provided in Table 2.4a. Marker antibodies used are described in Table 2.4b.

2.3.1.1 GPR50 antibodies

Overexpressed GPR50 was previously detected in the plasma membrane of HEK293 cells using C-terminal antibodies produced by Hamouda et al. (2007). Using these antibodies GPR50 was detected by Western blotting at 66 kDa (monomer) and 130 kDa (dimer) (Hamouda et al., 2007). In this thesis, two commercially available GPR50 antibodies were used, a rabbit polyclonal from Abcam and goat polyclonal from Santa Cruz (G-15, SC). As shown in Fig 2.2 both antibodies detect both overexpressed untagged GPR50 (Fig 2.2A) and endogenous (Fig 2.2D-E) GPR50 on the cell surface of HEK293T cells. However N-terminally GFP-tagged GPR50 does not localise correctly to the plasma membrane (Fig 2.2B), likely because of the absence of a signal sequence mediating receptor integration into the plasma membrane upstream of the GFP sequence. Approximately 1% of HEK239T cells express GPR50 endogenously. Both antibodies colocalise with plasma membrane marker pan-Cadherin (Fig 2.2A). Endogenous Gpr50 was detected by the G-15 antibody in a punctate pattern in cortical mouse neurons seeded at E18 and cultured for 28 days (Fig 2.2F). Both antibodies detect overexpressed untagged GPR50 at approximately 67 kDa, and GFP-GPR50 at 92 kDa by Western Blotting (Fig 2.2C). Possible dimers are detected in untransfected HEK293T cells but in GPR50

overexpressing cells these are masked by a smear (Fig 2.2C, see paragraph on GPR50 oligomeriation below).

Additionally, rabbit polyclonal antisera GPR50 E62 and E63 were raised against sequence derived C-terminal peptide residues 378-392 and 516-530 of human GPR50 (Fig 2.3A, Table 2.4a). Final bleeds from immunized rabbits were affinity-purified against their respective peptides by Eurogentec (Double XP program), and these purified antisera were used in all experiments.

GPR50 E62 and E63 detect overexpressed GFP-GPR50 in HEK293T cells (Fig 2.3B). GPR50 E63 also detected endogenous GPR50 on the cell surface of HEK293T cells (Fig 2.3C). E62 did however not detect any endogenous GPR50 in one experiment and it was therefore decided to use E63 only in future experiments. Both antibodies however detect overexpressed GPR50 in HEK293T cells by Western blotting at 67 kDa (Fig 2.3D). GPR50 E63 detects immunoprecipitated GPR50 from HEK293T cells transfected with various full-length and C-terminal only GPR50 constructs (Fig 2.3E). Again a high molecular weight smear is detected with these antibodies when overexpressing full length GPR50, which is absent from the C-terminal domain only sample (Fig 2.3E). This indicates the transmembrane domains and/or cell surface expression is important for this pattern to emerge.

2.3.1.2 GPR50 oligomerisation

GPR50 is known to dimerise (Levoye et al., 2006) and dimers were also detected here (Fig 2.2-2.3) and by others (Hamouda et al., 2007) by Western blotting. The high molecular weight smear detected with all four GPR50 antibodies in this thesis may indicate further oligomerisation. It may also indicate glycosylation of GPR50 (Lanctot et al., 2005). There are however no consensus N-glycosylation sites present in the GPR50 sequence (Hamouda et al., 2007). The high molecular weight smear however disappeared when samples were heated at 40°C for 10 min prior to loading on SDS-PAGE instead of boiling (Fig 2.3F). This suggests that boiling increases GPR50 high molecular weight aggregates which are unable to migrate properly into the gel. This is known to be the case for multi-pass transmembrane proteins (Ren et al., 2009)

Figure 2.2 *Characterisation of GPR50 C-terminal antibodies: Abcam ab13190 (C-ter) and Santa Cruz SC50590 (G-15). (A) HEK293T cells were transfected with untagged GPR50-TTC. Both C-ter and G-15 antibodies colocalise to the plasma membrane as indicated by plasma membrane marker pan-cadherin. The background signal from the secondary antibodies (DAG, donkey anti-goat Alexafluor 488 and GAR, goat anti-rabbit Alexafluor 594) is minimal in the absence of the primary antibodies. (B) HEK293T cells were transfected with GPR50-GFP. Both C-ter and G-15 antibodies colocalise with the GPR50-GFP signal, which appears to be more internal than GPR50 TTC (untagged). Cells were counterstained with DAPI. Scale bars: 50 µm (C) HEKT cells were transfected with several GPR50 constructs: 1. Untransfected, 2.GPR50-TTC, 3. untagged GPR50 (pDEST40), 4. GFP-GPR50. Western Blotting of lysates shows that anti-C-ter and anti-G-15 both recognize overexpressed GPR50 at the correct sizes (GPR50TTC=67 kDa; untagged GPR50=67 kDa, GPR50-GFP=92 kDa). GPR50 dimers are also detected at 134 kDa in both overexpressed and untransfected samples. This Figure was partly published as supplementary material in Grünewald et al., 2009. Molecular and Cellular Neuroscience. Copyright Elsevier 2009.*

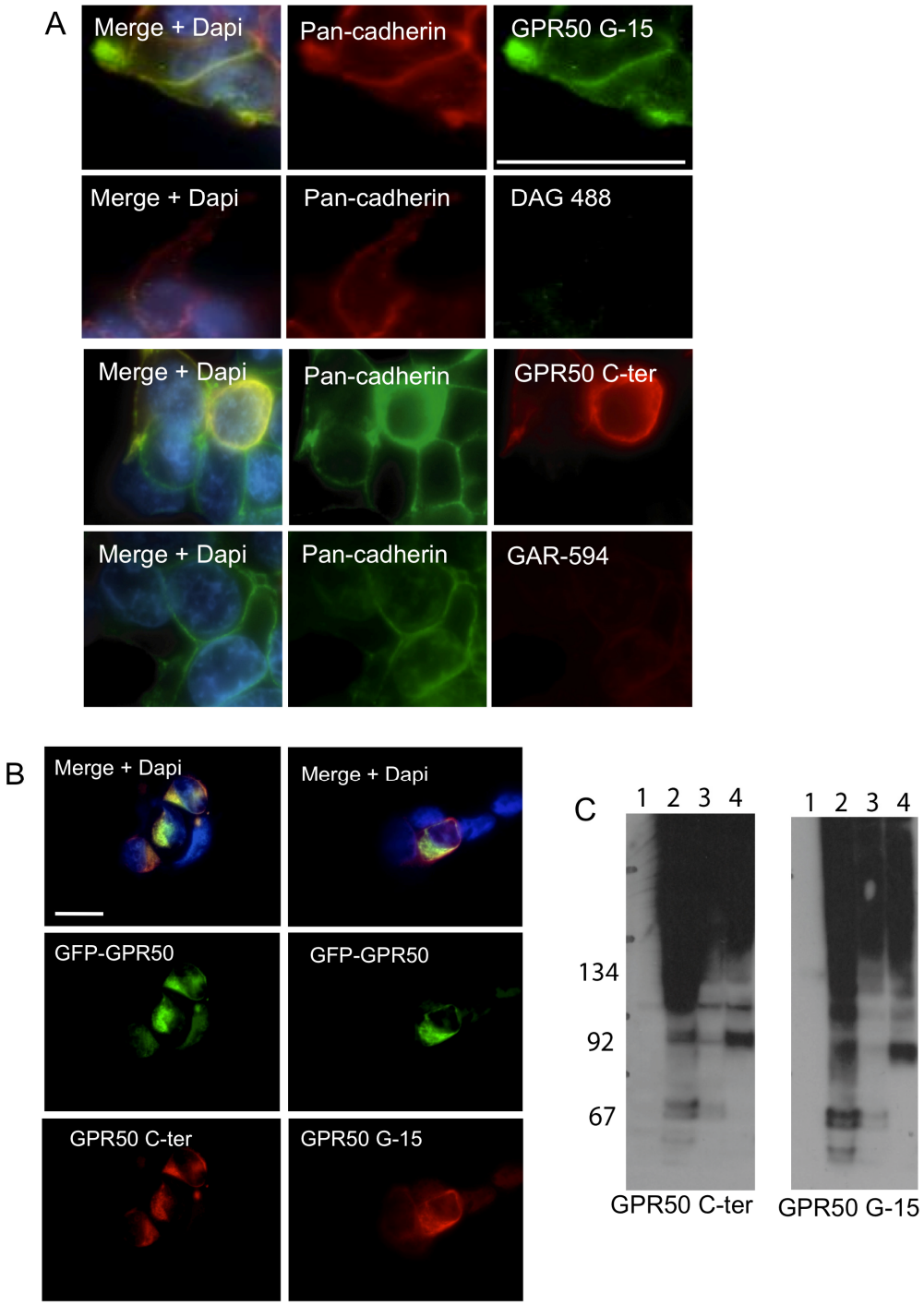

Figure 2.2. *Characterisation of GPR50 C-terminal antibodies: Abcam ab13190 (C-ter) and Santa Cruz SC50590 (G-15).*

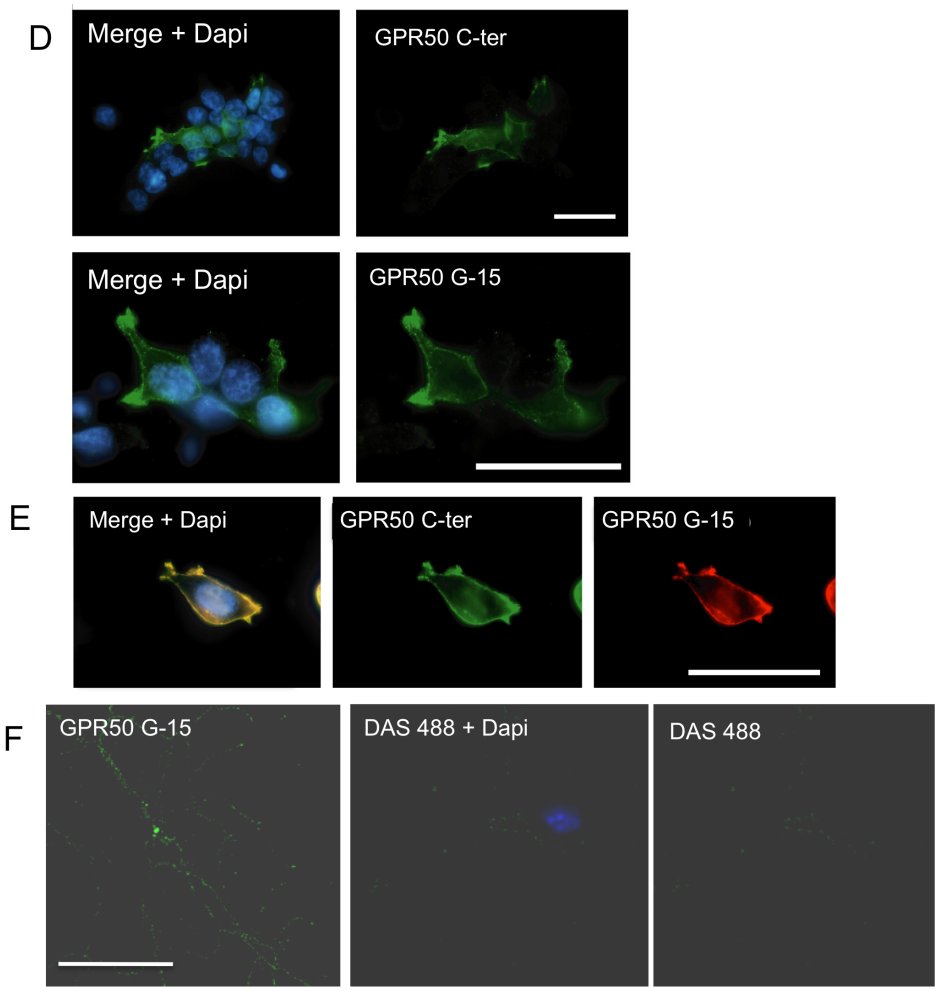

Figure 2.2. *Characterisation of GPR50 C-terminal antibodies: Abcam ab13190 (C-ter) and Santa Cruz SC50590 (G-15). Endogenous GPR50 in HEK293 cells and primary neurons. (D) HEK293T cells were stained with C-ter and G-15, which recognize endogenous GPR50 in the plasma membrane. (E) The signal of both GPR50 antibodies overlaps in the plasma membrane of HEK293T cells. (F) Primary cortical mouse neurons were stained with G-15, which recognises endogenous Gpr50 in a punctate pattern. Application of the secondary antibody (Alexafluor donkey anti-sheep, DAS, 488) only gives minimal background staining. Cells were counterstained with DAPI. Scale bars: 50 µm. Parts of this Figure published as supplementary material in Grünewald et al., 2009. Molecular and Cellular Neuroscience. Copyright Elsevier 2009.*

Figure 2.3 *Characterisation GPR50 C-terminal antibodies: E62 and E63. (A) Antibodies E62 an E63 were raised against C-terminal amino acid residues 378-392 and 516-530 of human GPR50 respectively. (B) HEK293T cells were transfected with GFP-GPR50 and stained with E62 and E63. (C) HEK293T cells were stained with E63 for detection of endogenous GPR50 E63 for detection of endogenous GPR50. HEK293T cells were also stained with a goat anti-rabbit secondary antibody (GAR, Alexafluor 594) only and minimal background staining was detected. Cells were counterstained with DAPI for nuclear staining. Scale bars: 50µm. (D) HEKT cells were transfected with GPR50 TTC. Lysates were run on SDS-PAGE and membranes were probed with serial dilutions of the E62 and E63 antibodies. Both antibodies recognise overexpressed GPR50 at 67kDa and also possible oligomers, similar to the GPR50 C-term antibody (Abcam) but stronger. (E) HEK293T cells were transfected with various GPR50 constructs: 1. untagged, 2. GPR50 TTC (67 kDa), 3. untagged GPR50 (pDEST40) (67 kDa), 4. GFP-GPR50 (92kDa), 5. GFP-CTD (75 kDa). Cells were lysed and immunoprecipitated using the G-15 antibody. GPR50 was detected by Western blotting using E63. (F) The high molecular weight smear that is detected by Western blotting of overexpressed GPR50 using G-15, C-ter, E62 and E63 antibodies disappears when heating the samples to 40℃ instead of boiling prior to loading on SDS-PAGE. HEK293 cells were left untransfected (1) or were transfected with untagged GPR50 (2). Shown is a representative Western blot when using G-15.*

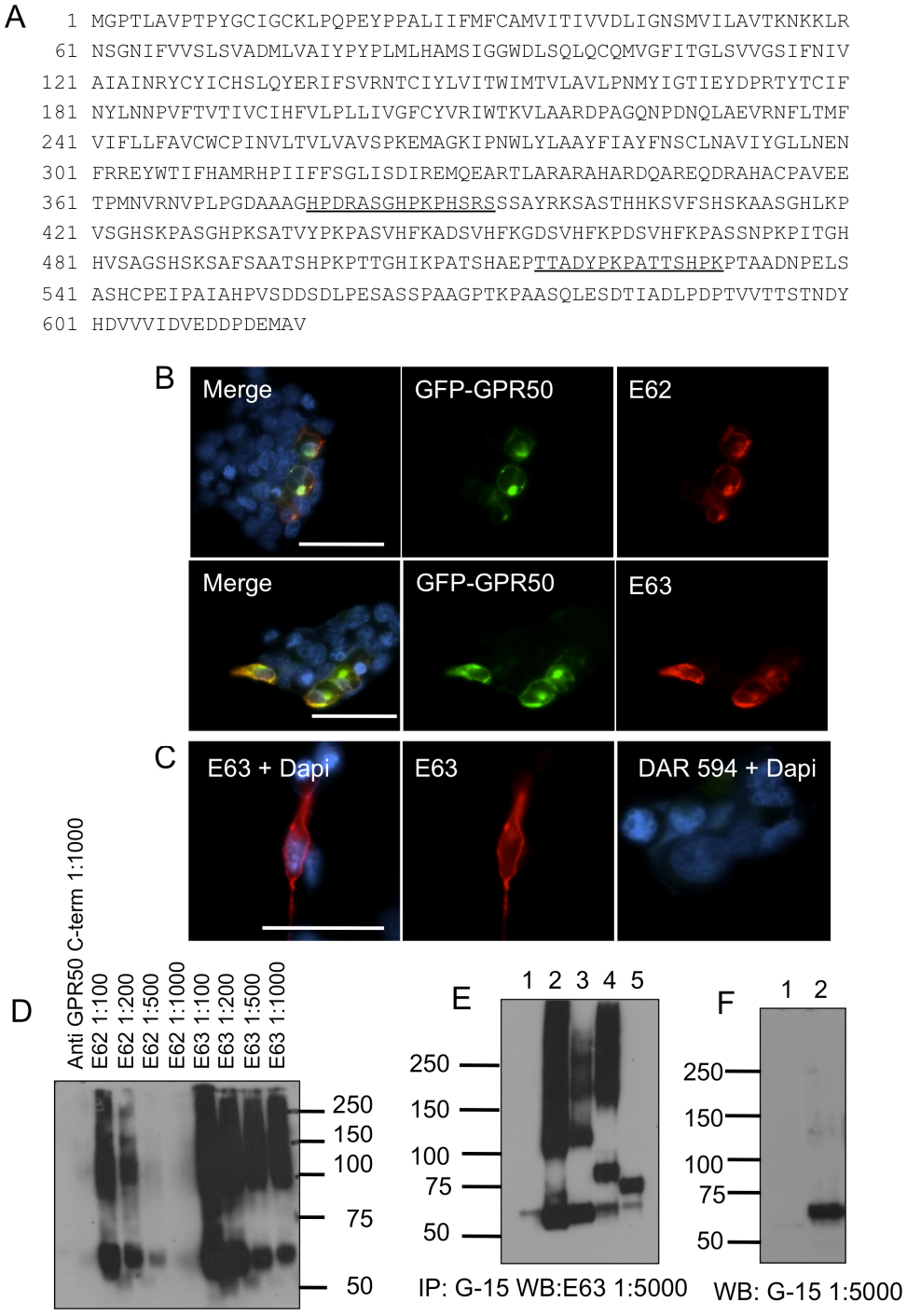

Figure 2.3 *Characterisation GPR50 C-terminal antibodies: E62 and E63.*

2.3.1.3 Nogo-A antibodies

I this thesis a rabbit polyclonal anti-Nogo-A (H-300, Santa Cruz) antibody is used that has previously been reported to detect Nogo-A at 180 kDa in human medulloblastoma cells (Satoh et al., 2005; Wojcik et al., 2007) and in in the cell soma, axons and dentrites of neurons in the rat somatosensory cortex (Shin et al., 2006). Polyclonal goat anti Nogo-A (N-18, Santa Cruz) has been previously shown to detect Nogo-A and Nogo-B at 180 and 46 kDa respectively by Western blotting of cultured human muscle fibers and COS7 cells (Acevedo et al., 2004; Wojcik et al., 2007), and Nogo-B by immunocytochemistry in cultured human muscle fibers (Wojcik et al., 2007) and a human endothelial cell line (Acevedo et al., 2004).

The H-300 antibody specifically detects endogenous and overexpressed Nogo-A in the ER and plasma membrane in HEK293 cells (Fig 2.4A-C) and in GFP-Nogo-A overexpressing and untransfected cultured mouse neurons (Fig 2.4D-F). H-300 detects overexpressed untagged Nogo-A and GFP-Nogo-A in HEK293 cell lysates at approximately 200 and 225 kDa respectively (Fig 2.4G). Overexpressing GFP-Nogo also results in an increase in untagged Nogo-A, perhaps in indication of the loss of the GFP tag (Fig 2.4G). The pan-Nogo N-18 antibody also detects overexpressed Nogo-A and GFP-Nogo-A at 200 and 225kDa by Western blotting (Fig 2.4G) and band at 50 kDa, which is possibly Nogo-B (Acevedo et al., 2004; Wojcik et al., 2007).

Figure 2.4 *Characterisation of commercially available Nogo-A antibodies. Nogo-A (H-300, Santa Cruz) detects overexpresssed and endogenous Nogo-A in mammalian cells. (A) HEK293T cells were stained with H-300 for endogenous Nogo-A detection and costained with ER marker calreticulin. (B) HEK293T cells were stained for calreticulin and a goat anti-rabbit secondary antibody (GAR, Alexafluor 594) only as control, and minimal background staining was detected. (C) HEK293 cells were stained with Nogo-A and plasma membrane marker pan-cadherin. Colocalisation signal is indicated by arrow. (D) Primary hippocampal mouse neurons at 14 DIV were transfected with GFP-tagged Nogo-A and overexpressed Nogo-A is detected by H-300. (E) This Nogo-A antibody also detects endogenous Nogo-A in primary hippocampal and cortical neurons cultured for 21 days. (F) Cortical neurons were stained with secondary antibody donkey anti-rabbit (DAR, Alexafluor 594) only, which gives minimal background staining. Cells were counterstained with DAPI for nuclear staining. Scale bars: 50 µm. (G) HEK293T cells were left untransfected (1) or transfected with GFP-Nogo-A (2). Lysates were processed for Western blotting with two Nogo-A antibodies: Nogo-A H-300 and N-18. Overexpressed Nogo-A was detected at 200 and 225 kDa.*

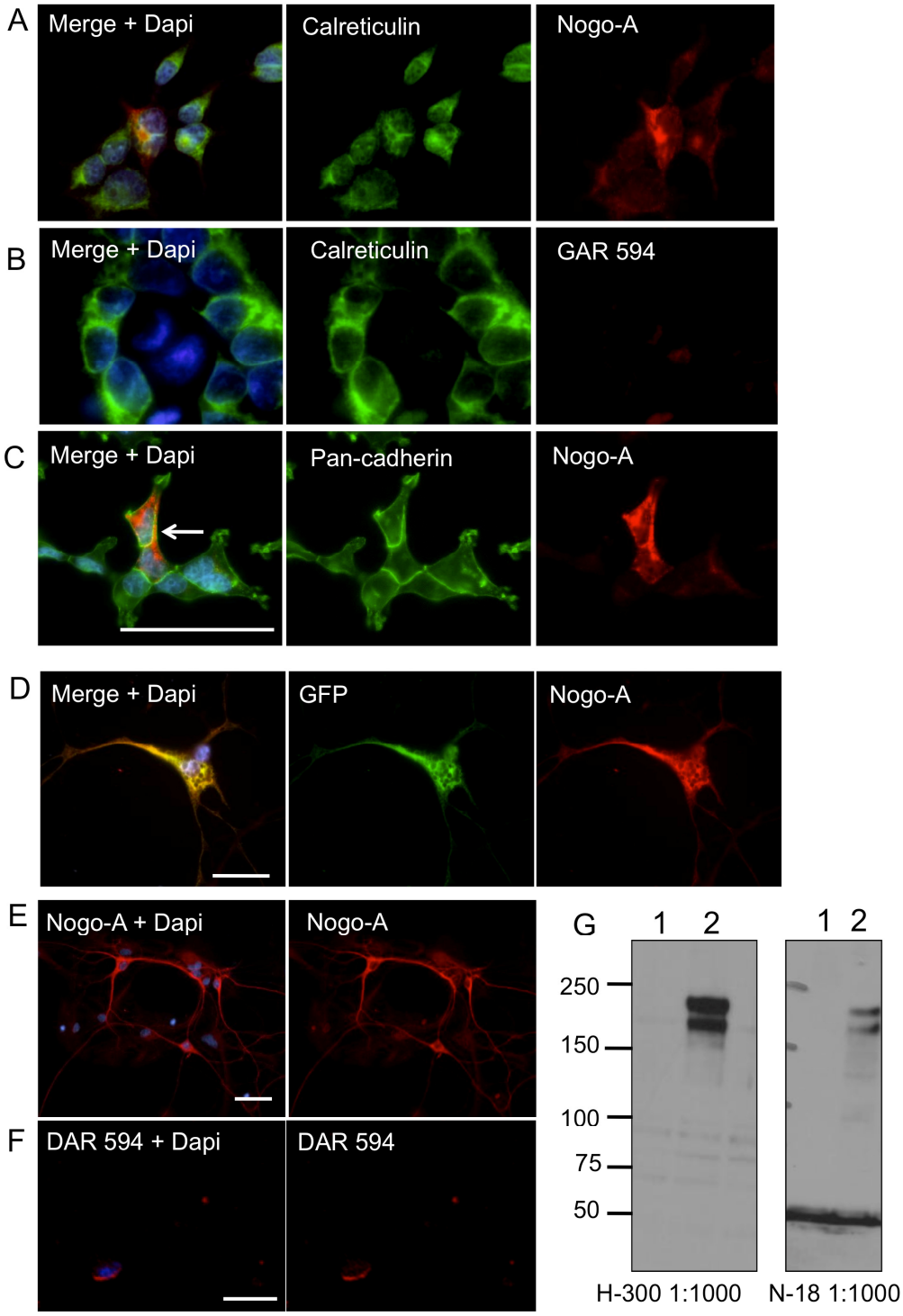

Figure 2.4 *Characterisation of commercially available Nogo-A antibodies.*

2.3.1.4 CDH8 antibodies

Exogenous CDH8 was previously detected in the plasma membrane at cell-cell contacts in L-cells (Kido et al., 1998). Punctate Cdh8 expression was earlier observed in the mouse spinal cord (Suzuki et al., 2007). CDH8 was detected as 130 and 95 kDa species by Western blotting of adult rat brain (Kido et al., 1998).

Rabbit polyclonal antisera CDH8 E60 and CDH8 E61 were developed, which were raised against sequence derived N-terminal peptide residues 44-55 and C-terminal peptide residues 785-799 of human CDH8 (Fig 2.5A, Table 5). Final bleeds from immunized rabbits were affinity-purified against both peptides by Eurogentec (Double XP program), and these purified antisera were used in all experiments. In addition a polyclonal goat antibody from Santa Cruz was used (C-18) for Western blotting only. All three antibodies detect overexpressed GFP-tagged human CDH8 at 125 kDa (Fig 2.5B), indicating a molecular weight of full-length CDH8 of 100kDa without the GFP tag. CDH8 E60 antibody detects a stronger additional band at approximately 60 kDa which not visible when using the other antibodies. CDH8 E61 detects overexpressed GFP-CDH8 on the cell surface of HEK293T cells (Fig 2.5C). Multiple sequence alignment of human and mouse peptide residues indicate high conservation in the C-terminal region but not at the N-terminus (Fig 2.6) suggesting E61 but not E60 is able to detect mouse CDH8 as well. CDH8 E61 detects endogenous Cdh8 in a punctate pattern in primary cortical mouse neurons seeded at E18 and cultured for 28 days (Fig 2.5D-E).

2.3.1.5 ABCA2 antibody

The ABCA2 antibody was first characterised in (Vulevic et al., 2001). Overexpressed ABCA2 in HEK293 and HeLa cells was shown to be expressed in endolysosomes and the trans-Golgi network (Vulevic et al., 2001; Broccardo et al., 2006). However, a more cytoplasmic staining pattern of endogenous Abca2 was reported in the soma and proximal processes of adult mouse oligodendrocytes and neurons (Broccardo et al., 2006), indicating a likely difference in localisation between endogenous and overexpressed ABCA2.

Here, the ABCA2 antibody was able to detect overexpressed ABCA2 in vesicle-like compartments of the cell soma by immunocytochemistry in HEK293T cells (Fig 2.7A), and primary cortical mouse neurons (Fig 2.7B). Note the neuron is colabelled with TUJ1, a marker for neurons (Fig 2.7B). In primary hippocampal mouse neurons and glia, cultured for 28 days, endogenous Abca2 shows a cytosolic expression pattern, more highly expressed in glia than neurons (Fig 2.7C-D). The ABCA2 antibody specifically detects overexpressed ABCA2 in HEK293T cells by Western blotting as a doublet at ~270 kDa (Fig 2.5E). In Vulevic et al. (2001) overexpressed ABCA2 from HEK293 cells was detected as a diffuse/smeary band above 250 kDa, possibly as a result of glycosylation (Vulevic et al., 2001). On the datasheet of a commercially availably antibody from Abcam (ab91571) the images show ABCA2 as a clear doublet at 270 kDa from HEK293T lysates, which much resembles the data in Fig 2.5E. The bottom band appears to correspond to ABCA2 as shown by IP on the abcam datasheet http://www.abcam.com/ABCA2-antibody-ab91571.html.

Figure 2.5 *Characterisation of CDH8 E60 and E61 antibodies. (A) Antibodies E60 an E60 were raised against amino acid residues 44-58 (N-term) and 785-799 (C-term) of human CDH8 respectively (Designed by Pippa Thomson) and produced by Eurogentec. HEK293 cells were transfected with GFP-tagged full length human CDH8. Lysates were run on SDS-PAGE and membranes were probed with a commercial CDH8 antibody and serial dilutions of the E60 and E61 antibodies. (C) HEK293T cells were transfected with GFP-tagged CDH8 and stained for GFP and CDH8 E61. (D) Primary cortical mouse neurons at E18 were cultured for 28 days and were stained using CDH8 E61 to detect endogenous Cdh8. The E61 antibody detects faint endogenous CDH8 in neurons in a punctate pattern. Primary cortical mouse neurons were stained with donkey anti-rabbit (DAR Alexafluor 584) only. Minimal background staining is observed. Cells were counterstained with DAPI for nuclear staining. Scale bars: 50 µm.*

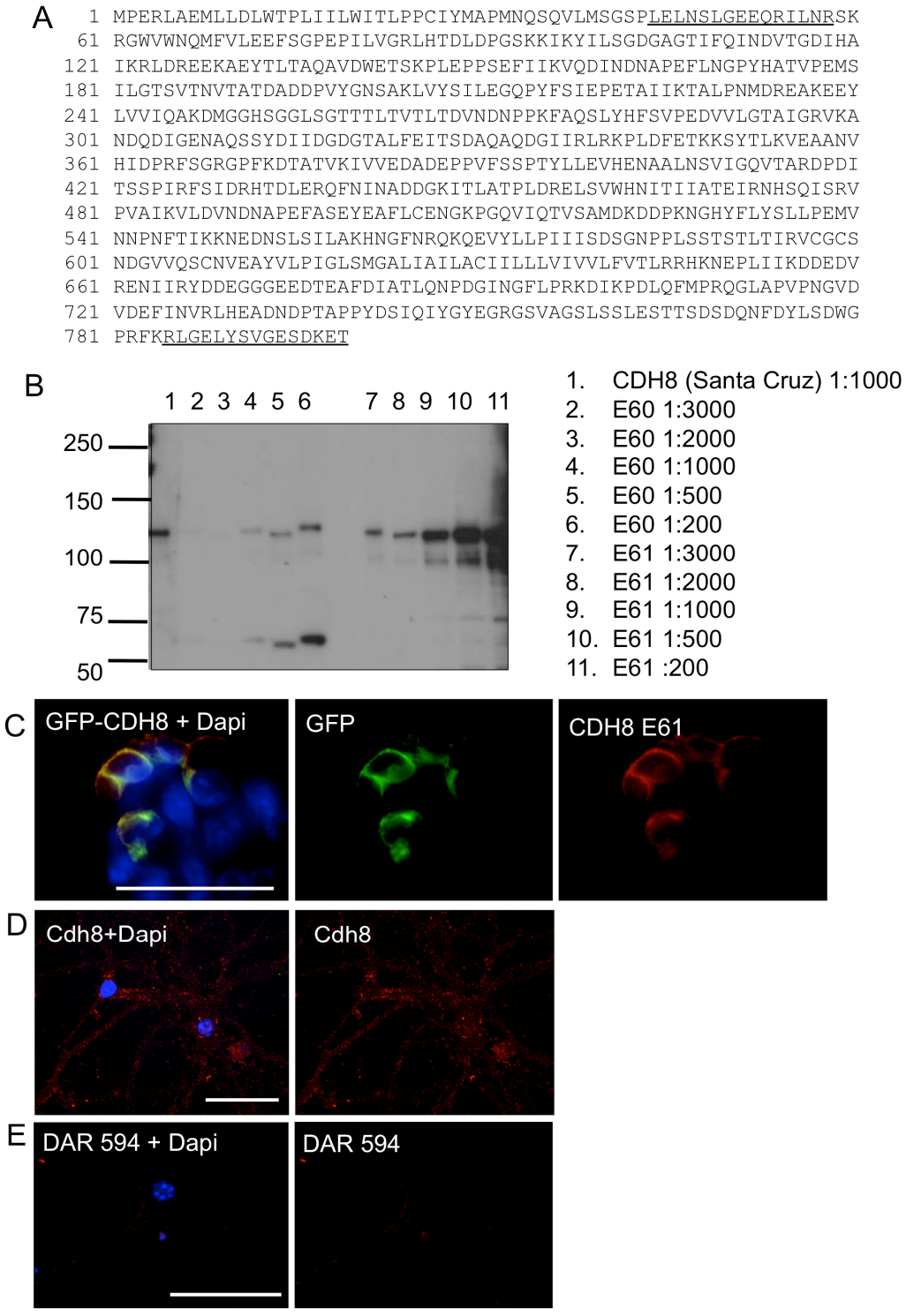

Figure 2.5 *Characterisation of CDH8 E60 and E61 antibodies.*

```
Mouse Cdh8      MPERLAETLMDLWTPLIILWITLPSCVYTAPMNQAHVLTTGSPLELSRQSEDMRILSRSK 60
human CDH8      MPERLAEMLLDLWTPLIILWITLPPCIYMAPMNQSQVLMSGSPLELNSLGEEQRILNRSK 60
                ******* *:***************.*:* *****::** :******.  .*: ***.***

mouse           RGWVWNQMFVLEEFSGPEPILVGRLHTDLDPGSKKIKYILSGDGAGTIFQINDITGDIHA 120
human           RGWVWNQMFVLEEFSGPEPILVGRLHTDLDPGSKKIKYILSGDGAGTIFQINDVTGDIHA 120
                ************************************************:******

mouse           IKRLDREEKAEYTLTAQAVDFETNKPLEPPSEFIIKVQDINDNAPEFLNGPYHATVPEMS 180
human           IKRLDREEKAEYTLTAQAVDWETSKPLEPPSEFIIKVQDINDNAPEFLNGPYHATVPEMS 180
                ********************:**.************************************

mouse           ILGTSVTNVTATDADDPVYGNSAKLVYSILEGQPYFSIEPETAIIKTALPNMDREAKEEY 240
human           ILGTSVTNVTATDADDPVYGNSAKLVYSILEGQPYFSIEPETAIIKTALPNMDREAKEEY 240
                ************************************************************

mouse           LVVIQAKDMGGHSGGLSGTTTLTVTLTDVNDNPPKFAQSLYHFSVPEDVVLGTAIGRVKA 300
human           LVVIQAKDMGGHSGGLSGTTTLTVTLTDVNDNPPKFAQSLYHFSVPEDVVLGTAIGRVKA 300
                ************************************************************

mouse           NDQDIGENAQSSYDIIDGDGTALFEITSDAQAQDGVIRLRKPLDFETKKSYTLKVEAANI 360
human           NDQDIGENAQSSYDIIDGDGTALFEITSDAQAQDGIIRLRKPLDFETKKSYTLKVEAANV 360
                ***********************************:************************:

mouse           HIDPRFSSRGPFKDTATVKIVVEDADEPPVFSSPTYLLEVHENAALNSVIGQVTARDPDI 420
human           HIDPRFSGRGPFKDTATVKIVVEDADEPPVFSSPTYLLEVHENAALNSVIGQVTARDPDI 420
                *******.****************************************************

mouse           TSSPIRFSIDRHTDLERQFNINADDGKITLATPLDRELSVWHNITIIATEIRNHSQISRV 480
human           TSSPIRFSIDRHTDLERQFNINADDGKITLATPLDRELSVWHNITIIATEIRNHSQISRV 480
                ************************************************************

mouse           PVAIKVLDVNDNAPEFASEYEAFLCENGKPGQVIQTVSAMDKDDPKNGHFFLYSLLPEMV 540
human           PVAIKVLDVNDNAPEFASEYEAFLCENGKPGQVIQTVSAMDKDDPKNGHYFLYSLLPEMV 540
                ************************************************:***********

mouse           NNPNFTIKKNEDNSLSILAKHNGFNRQKQEVYLLPIVISDSGNPPLSSTSTLTIRVCGCS 600
human           NNPNFTIKKNEDNSLSILAKHNGFNRQKQEVYLLPIIISDSGNPPLSSTSTLTIRVCGCS 600
                ***********************************:************************

mouse           NDGVVQSCNVEAYVLPIGLSMGALIAILACIILLLVIVVLFVTLRRHKNEPLIIKDDEDV 660
human           NDGVVQSCNVEAYVLPIGLSMGALIAILACIILLLVIVVLFVTLRRHKNEPLIIKDDEDV 660
                ************************************************************

mouse           RENIIRYDDEGGGEEDTEAFDIATLQNPDGINGFLPRKDIKPDLQFMPRQGLAPVPNGVD 720
human           RENIIRYDDEGGGEEDTEAFDIATLQNPDGINGFLPRKDIKPDLQFMPRQGLAPVPNGVD 720
                ************************************************************

mouse           VDEFINVRLHEADNDPTAPPYDSIQIYGYEGRGSVAGSLSSLESTTSDSDQNFDYLSDWG 780
human           VDEFINVRLHEADNDPTAPPYDSIQIYGYEGRGSVAGSLSSLESTTSDSDQNFDYLSDWG 780
                ************************************************************

mouse           PRFKRLGELYSVGESDKET 799
human           PRFKRLGELYSVGESDKET 799
                ********************
```

Figure 2.6 *Multiple sequence alignment of human and mouse CDH8 amino acid sequences. Underlined are the two epitopes of the N- and C-terminal antibodies E60 and E61. The sequence is well conserved except for the N-terminus, indicating that the E61 antibody is likely to also detect mouse Cdh8 contrary to the N-terminally raised E60 antibody.*

Figure 2.7 *Characterisation of the ABCA2 antibody (K.Tew). (A) HEK293T cells were transfected with ABCA2 and stained with ABCA2. Minimal background staining is observed in the absence of the primary antibody and application of goat anti-rabbit (GAR, Alexafluor 594). (B) Primary cortical mouse neurons of E18 were cultured for 14 days and transfected with ABCA2. Cells were stained with TUJ1 (B-tubulin III) and ABCA2. (C) Primary hippocampal mouse neurons of E18 were cultured for 28 days and were stained for ABCA2. The ABCA2 antibody detects endogenous ABCA2 in putative glia and neurons. (D) Primary hippocampal mouse neurons were stained with donkey anti-rabbit (DAG Alexafluor 584) only. Minimal background staining is observed. (E) HEK293T cells were transfected with ABCA2. Lysates were processed for Western blotting with the ABCA2 antibody, resulting in a band at 270 kDa in transfected sample (2) but not in untransfected lysate sample (1). Cells were counterstained with DAPI for nuclear staining. Scale bars: 50 µm*

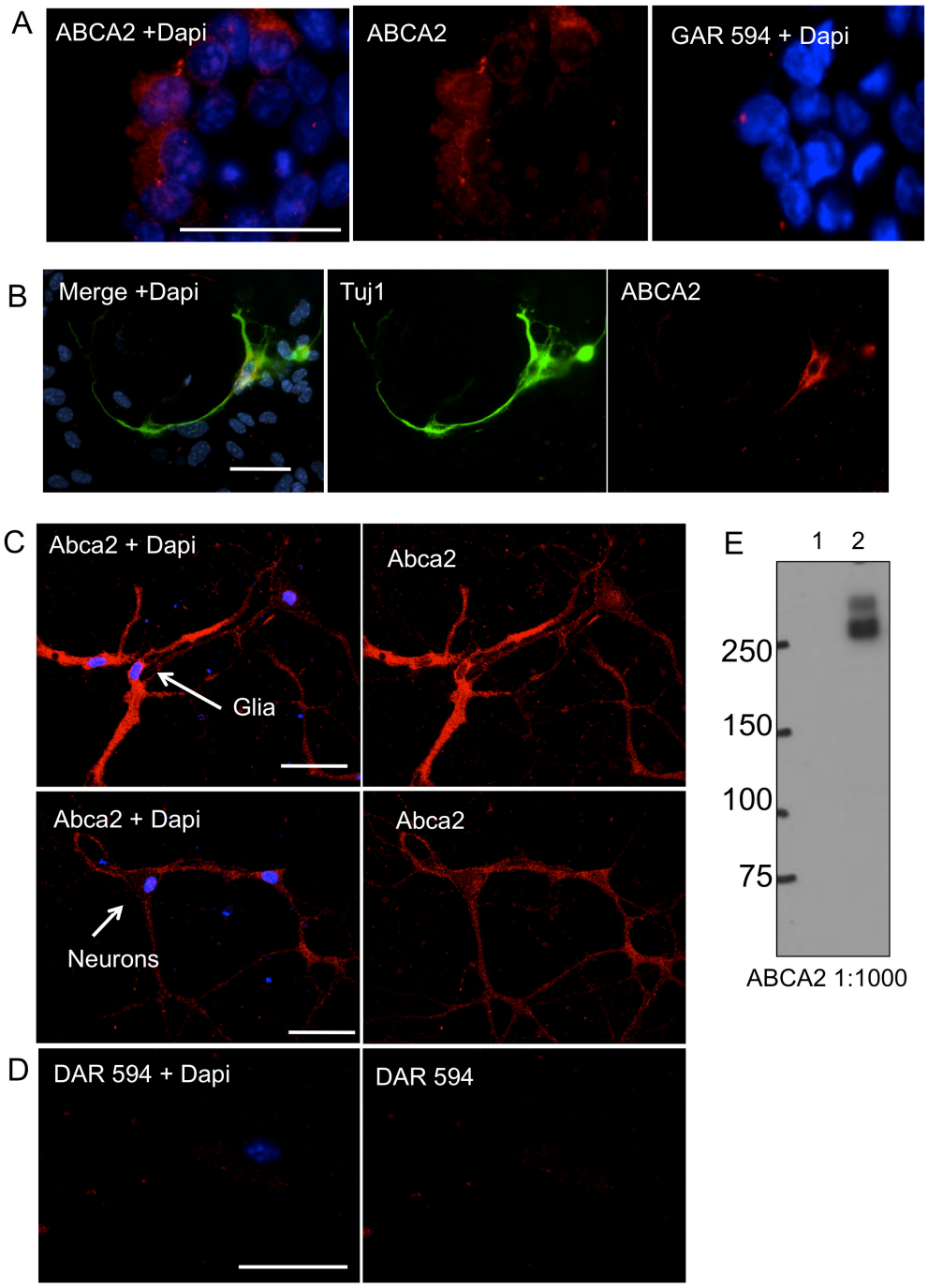

Figure 2.7 *Characterisation of the ABCA2 antibody*

2.3.2 GPR50 interacts with Nogo-A, Nogo-C, RTN3, CDH8 and ABCA2

2.3.2.1 Testing the interactions

In order to investigate the interactions in more detail various full-length and deletion constructs were made (see Table 2.1 for more details) and binding of RTN3, Nogo-A, Nogo-C, CDH8 and ABCA2 with these forms of GPR50 was tested. This was tested by performing immunocytochemistry and immunoprecipitation. Firstly, to directly replicate the Y2H study, GPR50 CTD only constructs were used. Secondly, experiments were performed using GFP-tagged full-length GPR50 (insertion only). Thirdly, after cloning of full length GPR50$^{\Delta 502\text{-}505/T532A}$, differential binding of untagged GPR50 and GPR50$^{\Delta 502\text{-}505/T532A}$ was investigated.

2.3.2.2 Interactions with GPR50 CTD only

In the Y2H screen, the C-terminal domain (CTD) of both the GPR50 ('insertion') and GPR50$^{\Delta 502\text{-}505/T532A}$ ('deletion') were used as bait (Grünewald et al., 2009). Nogo-A was captured by both forms, as was ABCA2 (see Table 1.1, Chapter 1). CDH8 was only isolated when using the deletion form, as was RTN3. Nogo-C on the other hand was only captured when the insertion form of GPR50 was used (Grünewald et al., 2009). However, because the number of clones that were isolated in each case was too low to reach significance levels, the interaction with both insertion and deletion forms needs to be tested.

Therefore HEK293T cells were cotransfected with GFP-tagged Nogo-A, CDH8 or untagged ABCA2, and either GFP-tagged C-terminal insertion (GFP-CTD) or – deletion (GFP-CTD$^{\Delta 502\text{-}505/T532A}$) constructs of GPR50 (Figure 2.8). These constructs spanned residues 283 to 617 (613 deletion), were made by Hazel Kinnell and Alison Condie (University of Edinburgh) and were already available in the lab. When pulling down GPR50 CTD using the GPR50 G-15 antibody, GFP-Nogo-A was predominantly co-precipitated by the H-300 antibody at 225 kDa but also some untagged Nogo-A, as indicated by a fainter band at 200 kDa. Similarly GFP-CDH8

was co-precipitated by Western blot at 125 kDa respectively using protein-specific antibodies. This was the case for both insertion and deletion forms of GPR50, indicating no difference in possibility to bind (Fig 2.8). These results were repeated twice. Although ABCA2 was co-precipitated as a doublet at 260-270 kDa with GPR50 CTD once (Fig 2.8), this could not be replicated. This result therefore needs to be treated with caution.

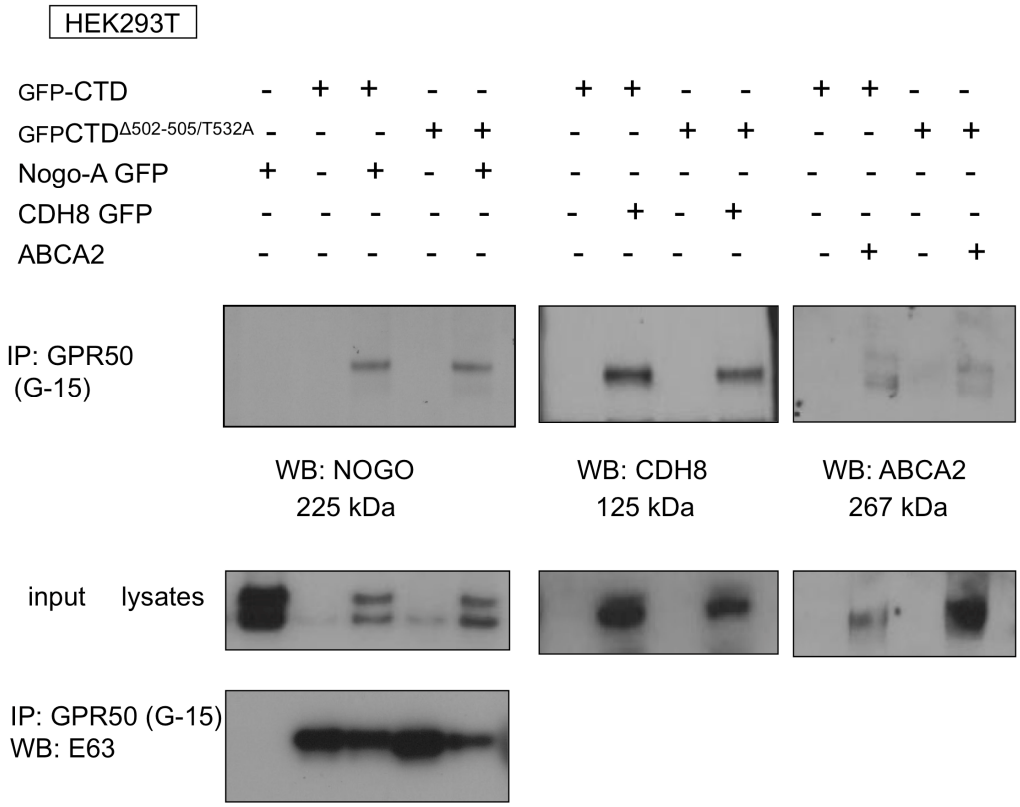

Figure 2.8 *The GPR50 CTD interacts with Nogo-A, CDH8 and ABCA2, irrespective of the deletion polymorphism. HEK293T cells were transfected with GFP-GPR50 CTD or GFP-GPR50 CTDΔTTGH or co-transfected with GFP-Nogo-A, GFP-CHD8 or untagged ABCA2. When lysates were precipitated with GPR50, Nogo-A, CHD8 and ABCA2 were all co-precipitated with both the CTD and CTD ΔTTGH, as shown by Western Blotting. Whereas the interaction of GPR50 CTD with Nogo-A and CDH8 could be replicated, this was not the case with ABCA2 and therefore this result needs to be treated with caution.*

2.3.2.3 Full length GPR50 interacts with Nogo-A

Because GPR50 CTD only does not localise correctly to the plasma membrane, the differential binding of full length GPR50 was investigated as well. In addition to co-IPs immunocytochemistry was performed in primary cultured neurons in order to test whether colocalisation could be detected and where this could be found.

For immunocytochemistry, primary cortical neurons were cultured for 15 days in vitro (DIV), and transfected with untagged GPR50 and GFP-Nogo-A. We detected some colocalisation between overexpressed untagged GPR50 and exogenous GFP-Nogo-A although GPR50 appears to be expressed more in dendrites and spines than Nogo-A (Fig. 2.9A, Grünewald et al., 2009). This indicates that GPR50 and Nogo-A may be available to interact in mammalian cells. As expected exogenous GPR50 is predominantly expressed in the plasma membrane and Nogo-A at a more intracellular location, most likely the ER or the cytoplasm. Interestingly overexpressed GPR50 also localises more strongly than Nogo-A to the tips of dendrites and spines (Fig 2.9B). In order to establish whether there is colocalisation between endogenous Nogo-A and Gpr50, immunocytochemistry was performed on primary cortical mouse neurons after 28 DIV. Endogenous colocalisation of a proportion of both proteins was found along dendrites, possibly in synaptic spines (Fig 2.9B).

In order to quantify colocalisation between exogenous and endogenous GPR50 and Nogo-A Pearson's correlation coefficient (exogenous: $Rr = 0.61 \pm 0.05$; endogenous: $Rr = 0.43 \pm 0.01$) and Manders' Overlap Coefficient (Manders, 1993) were calculated for axonal regions in several cells (N=6), indicating moderate to strong colocalisation (Grünewald et al., 2009). In addition the Intensity Correlation Analysis (Li et al., 2004) was used to test whether GPR50 and Nogo-A staining in axonal/dendritic sections (enlargement) was associated (Fig 2.9C for exogenous GPR50 and Nogo-A) see materials and methods Chapter 2.2.12). A dependent staining pattern was indicated by positively skewed ICA scatter plots (Fig 2.9C). In addition the ICQ values were consistently positive and highly significant (exogenous

+0.24 ± 0.03; $p < 0.001$; N=6; endogenous: +0.17 ± 0.01; $p < 0.001$; the values for the cells in Fig 2.9A and 2.9B only are given in the figure legend), arguing for a dependent association between exogenous and endogenous GPR50 and Nogo-A.

Next, imunoprecipitations were performed in HEK293T cells using GFP-tagged full-length GPR50 (insertion only) and GFP-Nogo-A. HEK293T cells were transiently transfected and a 225 kDa Nogo-A band was detected by western blot after immunoprecipitation with anti-GPR50 (G-15, Fig. 2.9C). The untagged Nogo-A appears however not to be co-precipitated with GFP-GPR50 this time. This may indicate dimerisation of the GFP tags and perhaps a false positive result. Therefore the experiment was repeated with untagged GPR50 and Nogo-A (see 2.3.2.4).

2.3.2.4 Full-length untagged GPR50 and GPR50$^{\Delta 502\text{-}505/T532A}$ also bind reticulons Nogo-A, Nogo-C and RTN3

Differential binding of untagged GPR50 and GPR50$^{\Delta 502\text{-}505/T532A}$ with Nogo-A and with reticulon family members Nogo-C and RTN3 was investigated next. To this end full-length GPR50 residues 502-505 were removed, and Thr was substituted by Ala at position 532 using site-directed mutagenesis (see *materials and methods* section 2.2.4 for more details).

First, immunocytochemistry was performed to test if GPR50 and GPR50$^{\Delta 502\text{-}505/T532A}$ both localise to the plasma membrane. This was performed in SH-SY5Y cells, as these are larger than HEK293 and have less of a tendency to form cell clumps and because neuroblastoma cells are more representative of neurons. Subcellular localisation in individual cells is therefore easier to detect. SH-SY5Y cells were transiently transfected with untagged GPR50 or untagged GPR50$^{\Delta 502\text{-}505/T532A}$. After colabelling cells with GPR50 (G-15) and plasma membrane marker pan-Cadherin, no apparent difference was found in localisation of GPR50 or GPR50$^{\Delta 502\text{-}505/T532A}$ (Figure 2.10).

Figure 2.9 *GPR50 interacts with Nogo-A in mammalian cells. (A) Primary cortical mouse neurons at E18 were cultured for 15 DIV. Neurons were co-transfected with untagged GPR50 and GFP-Nogo-A and stained the following day with GPR50 (SC) and GFP. The merged image (see enlargement) shows colocalisation in axons/dendrites (Grünewald et al., 2009). (B) Primary cortical mouse neurons were cultured for 28 days and stained for endogenous Nogo-A and Gpr50, indicating co-expression in dendrites and possibly synaptic spines. Intensity correlation analysis was performed on dentritic regions of interest (see enlargements in A and B) and the plots for exogenous GPR50 to Nogo-A together and individually shown below in (C). (C) Intensity correlation plots of Nogo-A versus GPR50. Red/green correlation plot with yellow pixels denoting colocalisation (left), respective plots of Nogo-A (middle) and GPR50 (right) against their (A-a) (B-b) values indicating the dependence of the stain of one protein versus the other (Li et al., 2004). Note the positive skew of the ICA plots indicating dependent staining. Values for these images only: A (exogenous): ICQ=+0.26. Rr = 0.66, R = 0.89; B (endogenous): ICQ = +0.17; Rr= 0.40; R = 0.83. Scale bar: 50µm. (D) HEK293T cells were transfected with full-length human GFP-Nogo-A and GFP-GPR50 constructs, individually or in combination. Lysates were immunoprecipitated with anti-GPR50 (SC) antibody and Nogo-A was co-precipitated in the GPR50 co-transfected sample only, as shown by Western blot analysis (Grünewald et al., 2009). Cells were counterstained with DAPI for nuclear staining. Scale bars: 50 µm. Figure adapted from Grünewald et al., 2009. Molecular and Cellular Neuroscience. Copyright Elsevier 2009.*

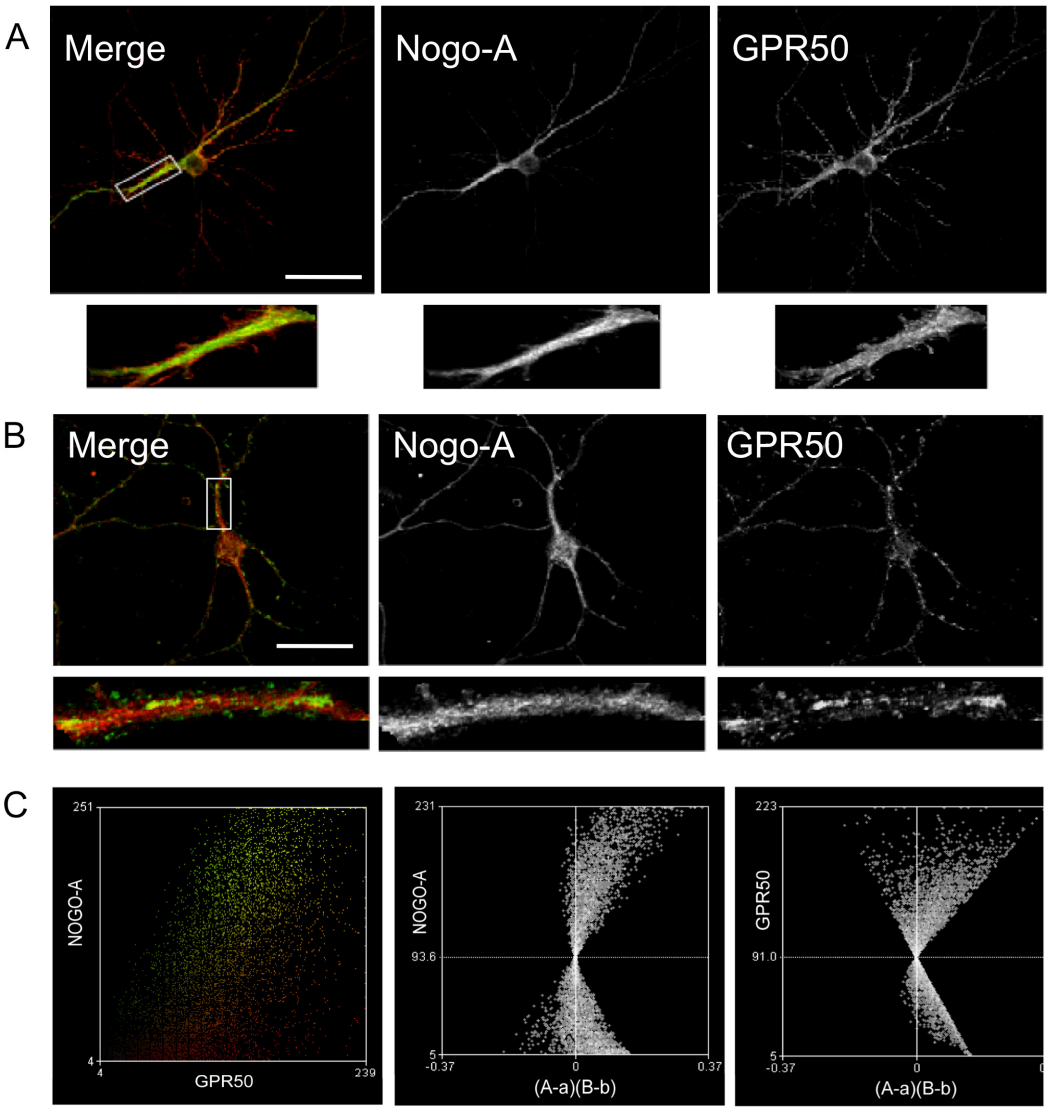
A
Merge
Nogo-A
GPR50
B
Merge
Nogo-A
GPR50
C
251
NOGO-A
4
4
GPR50
239
231
NOGO-A
93.6
5
-0.37
0
0.37
(A-a)(B-b)
223
GPR50
91.0
5
-0.37
0
(A-a)(B-b)
D
Nogo-A-GFP - + - +
GPR50-GFP - - + +
IP: GPR50
225 kDa
WB: Nogo-A
input

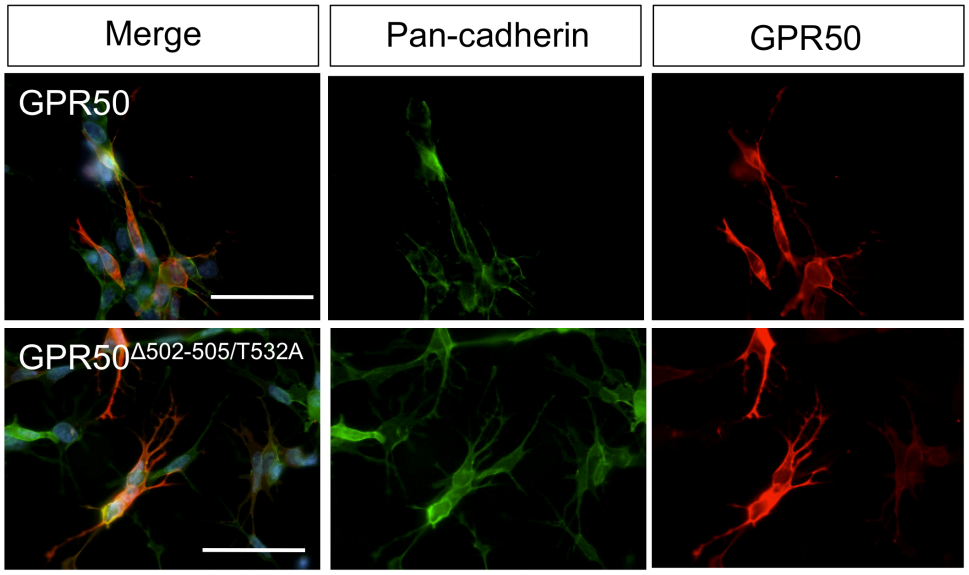

Figure 2.10 *Full-length GPR50$^{\Delta 502\text{-}505/T532A}$ localises to the plasma membrane, similar to GPR50. SHSY5Y cells were transfected with GPR50 or GPR50 $^{\Delta 502\text{-}505/T532A}$ and stained for GPR50 and plasma membrane marker pan-cadherin. Immunocytochemistry results show similar colocalisation of GPR50 and GPR50 $^{\Delta 502\text{-}505/T532A}$ with pan-cadherin at the plasma membrane. Cells were counterstained with DAPI. Scale bars: 50 µm.*

Next colabelling of GPR50 and GPR50$^{\Delta 502\text{-}505/T532A}$ with the reticulon proteins was performed. Colocalisation with Nogo-A as well as Nogo-C and reticulon family member RTN3 was investigated. Again SH-SY5Y cells were used for the reasons stated in the previous paragraph. Cotransfecting SH-SY5Y cells with GPR50 and Nogo-A resulted in costaining in the plasma membrane but mostly in ER-like structures (Fig 2.11). A similar pattern was seen with Nogo-C and RTN3 (Fig 2.12). Although the GPR50$^{\Delta 502\text{-}505/T532A}$ variant did not appear to visibly alter colocalisation compared to GPR50 (Fig 2.11-2.12), the GPR50 localisation seemed to be changed when cotransfected with reticulon proteins RTN3, Nogo-C and Nogo-A compared to GPR50 by itself (Fig 2.2). A larger fraction of GPR50 was present in what appeared to be the ER instead of the plasma membrane. This apparent difference was intriguing and was further investigated in 2.3.3.

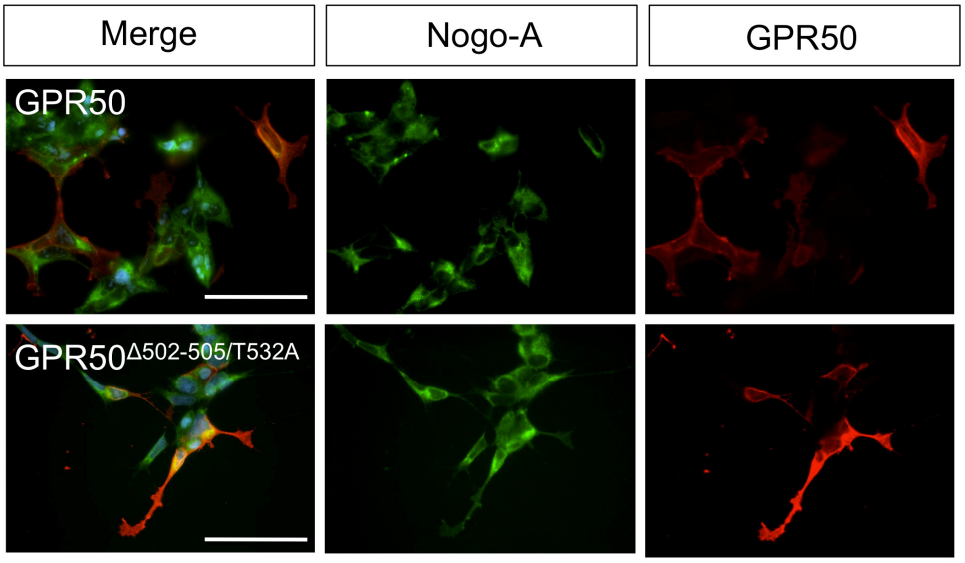

Figure 2.11 *Full-length GPR50 $^{\Delta 502\text{-}505/T532A}$ shows a similar colocalisation pattern as GPR50 with Nogo-A. SHSY5Y cells were cotransfected with GPR50 or GPR50 $^{\Delta 502\text{-}505/T532A}$ and Nogo-A. Immunocytochemistry results show similar colocalisation of GPR50 with Nogo-A at the plasma membrane and the ER. Cells were counterstained with DAPI. Scale bars: 50 µm.*

Next, to further test the binding of GPR50 to the reticulin proteins, immunoprecipitations were performed. HEK293 cells were transfected with untagged GPR50 or untagged GPR50$^{\Delta 502\text{-}505/T532A}$, and either untagged Nogo-A or GFP-tagged Nogo-C or GFP-tagged RTN3. After precipitating GPR50 using the G-15 (SC) antibody Nogo-A was repeatedly co-precipitated with both GPR50 and GPR50$^{\Delta 502\text{-}505/T532A}$ at 200 kDa (Figure 2.13) using a Nogo-A specific antibody (H-300). Similarly, Nogo-C (47 kDa) and RTN3 (50 kDa) (Fig 2.13) were repeatedly coprecipitated with GPR50 using a GFP antibody, indicating Nogo-A, Nogo-C and RTN3 bind GPR50 irrespective of the polymorphisms.

Interestingly, although equal amounts of GPR50 were precipitated (Fig 2.13) more Nogo-C and RTN3 seemed to be co-precipitated with GPR50$^{\Delta 502\text{-}505/T532A}$ compared to GPR50 (Fig 2.13). Although this needs to be replicated in future experiments, a preference in binding of RTN3 to GPR50$^{\Delta 502\text{-}505/T532A}$ is suggested by the Y2H results (Table 1.1).

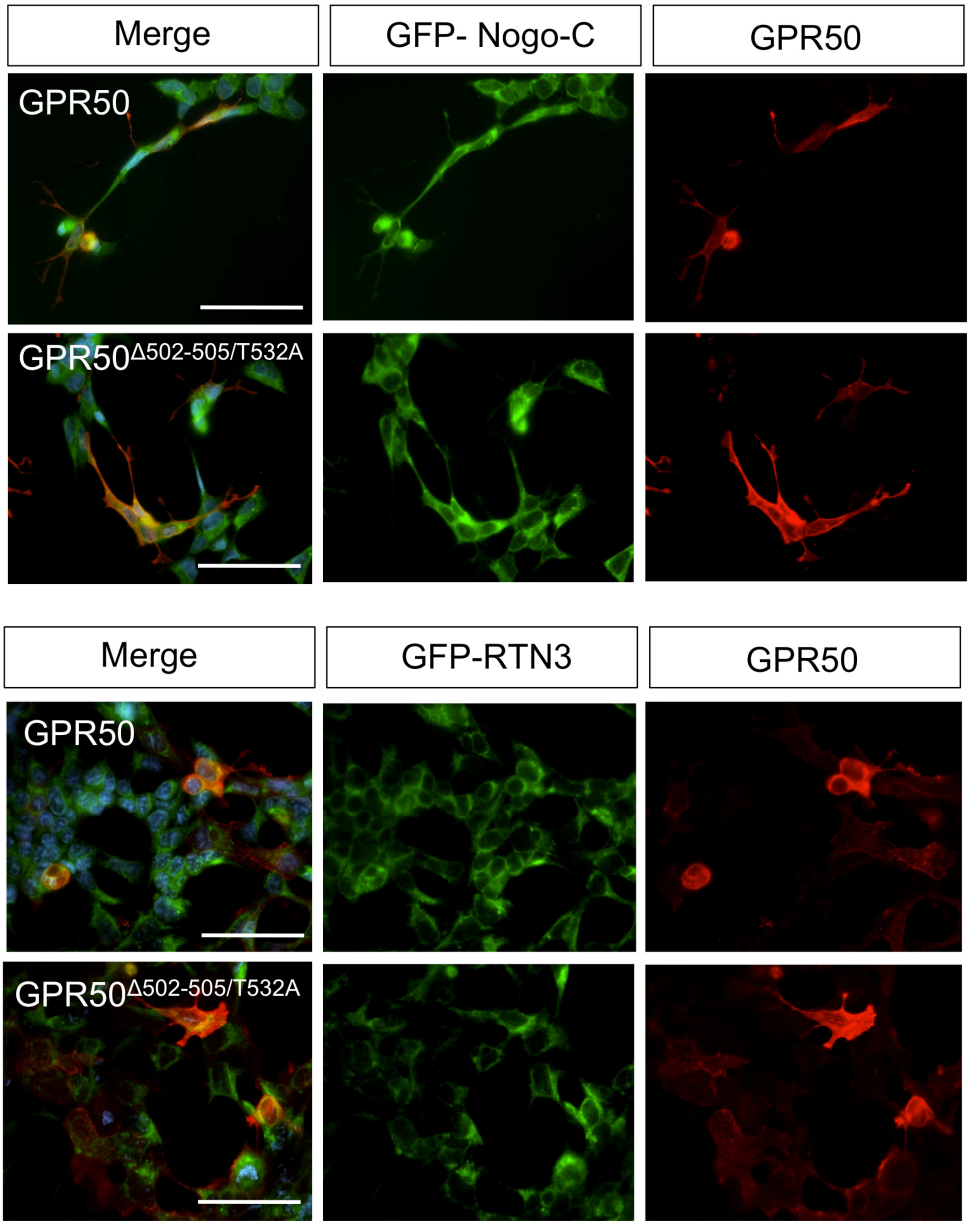

Figure 2.12 *Full-length GPR50$^{\Delta 502\text{-}505/T532A}$ shows a similar colocalisation pattern as GPR50 with Nogo-C and RTN3. SHSY5Y cells were cotransfected with GPR50 or GPR50 $^{\Delta 502\text{-}505/T532A}$ and Nogo-C (A) or RTN3 (B). Immunocytochemistry results (A,B) show similar colocalisation of GPR50 with Nogo-C and RTN3 at the plasma membrane and the ER. Cells were counterstained with DAPI. Scale bars: 50 µm.*

Full length GPR50 interacts with CDH8 and ABCA2

Similarly, in order to test interactions of full-length GPR50 with CDH8 and ABCA2, immunocytochemistry and co-immunoprecipitations were perfomed.

Immunocytochemistry experiments were performed in HEK293T cells and primary neurons (Fig 2.9A-B). In HEK293T cells overexpressed GPR50TTC colocalises with GFP-CDH8 in the plasma membrane (Fig 2.14A). In primary hippocampal neurons cultured for 28 DIV endogenous Gpr50 colocalises with CDH8 was found at synaptic contacts in primary cortical neurons cultured for 28 days (Fig 2.14B, enlargement).

In HEK293T cells overexpressed GFP-GPR50 colocalises with exogenous untagged ABCA2 in the cytoplasmic vesicles in a subset of cells, likely corresponding to the endolysosomal compartment (Fig 2.14C). However, the colocalisation may be affected by the N-terminal GFP tag of GPR50 (see also Fig 2.2). In primary hippocampal neurons cultured for 28DIV endogenous Gpr50 colocalises with Abca2 in axons and dendrites (Fig 2.14D, enlargement). The punctate staining pattern of Gpr50 and Abca2 may also indicate an (intracellular) pool of (peptide) molecules.

For co-immunoprecipiations HEK293T cells were transiently transfected with GPR50-GFP and CDH8-GFP or untagged ABCA2. CDH8 and ABCA2 were repeatedly detected by Western blotting as doublet bands after immunoprecipitation with anti-GPR50 (G-15, Fig 2.14E). The doublet band for ABCA2 had been detected previously in different experiments (Fig 2.7, 2.8) however the CDH8 doublet was not. This may indicate co-precipitation of the untagged form of CDH8 at 100 kDa as well as the tagged form at 125 kDa. However, because both GPR50 and CDH8 were GFP-tagged there is again the possibility that the positive co-IP result is caused by the dimerisation of GFP. Therefore the interaction needs to be investigated with untagged proteins.

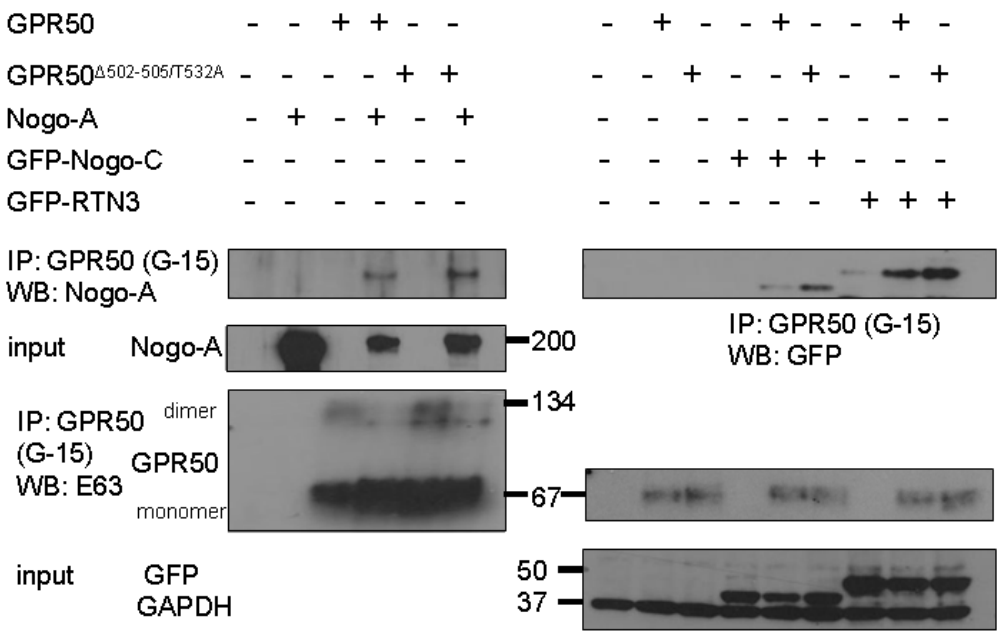

Figure 2.13 *Full-length GPR50$^{\Delta 502\text{-}505/T532A}$ also interacts with Reticulons Nogo-A, Nogo-C and RTN3. HEK293 cells were cotransfected with GPR50 or GPR50 Δ502-505/T532A and untagged Nogo-A, or GFP-tagged Nogo-C or RTN3. GPR50 was precipitated using the GPR50 G-15 SC antibody and co-precipitated Nogo-A was revealed by Western blotting with anti-Nogo-A (H-300, left hand figure). Co-precipitated Nogo-C and RTN3 were detected by immunoblotting with anti-GFP (right hand figure). More Nogo-C and RTN3 appears to be co-precipitated with GPR50Δ502-505/T532A compared to GPR50. (B) To further test this SHSY5Y cells were co-transfected with GPR50 or GPR50 Δ502-505/T532A and Nogo-A, Nogo-C or RTN3. After performing immunocytochemistry 120 images were randomly taken per condition and cells which showed colocalisation between GPR50 and the interactors were scored. Means of three experiments were compared and T-tests were performed using Graphpad Prism. These showed a non-significant increase in colocalisation of RTN3 with GPR50 Δ502-505/T532A compared to GPR50. A similar increase was not seen with Nogo-A or Nogo-C.*

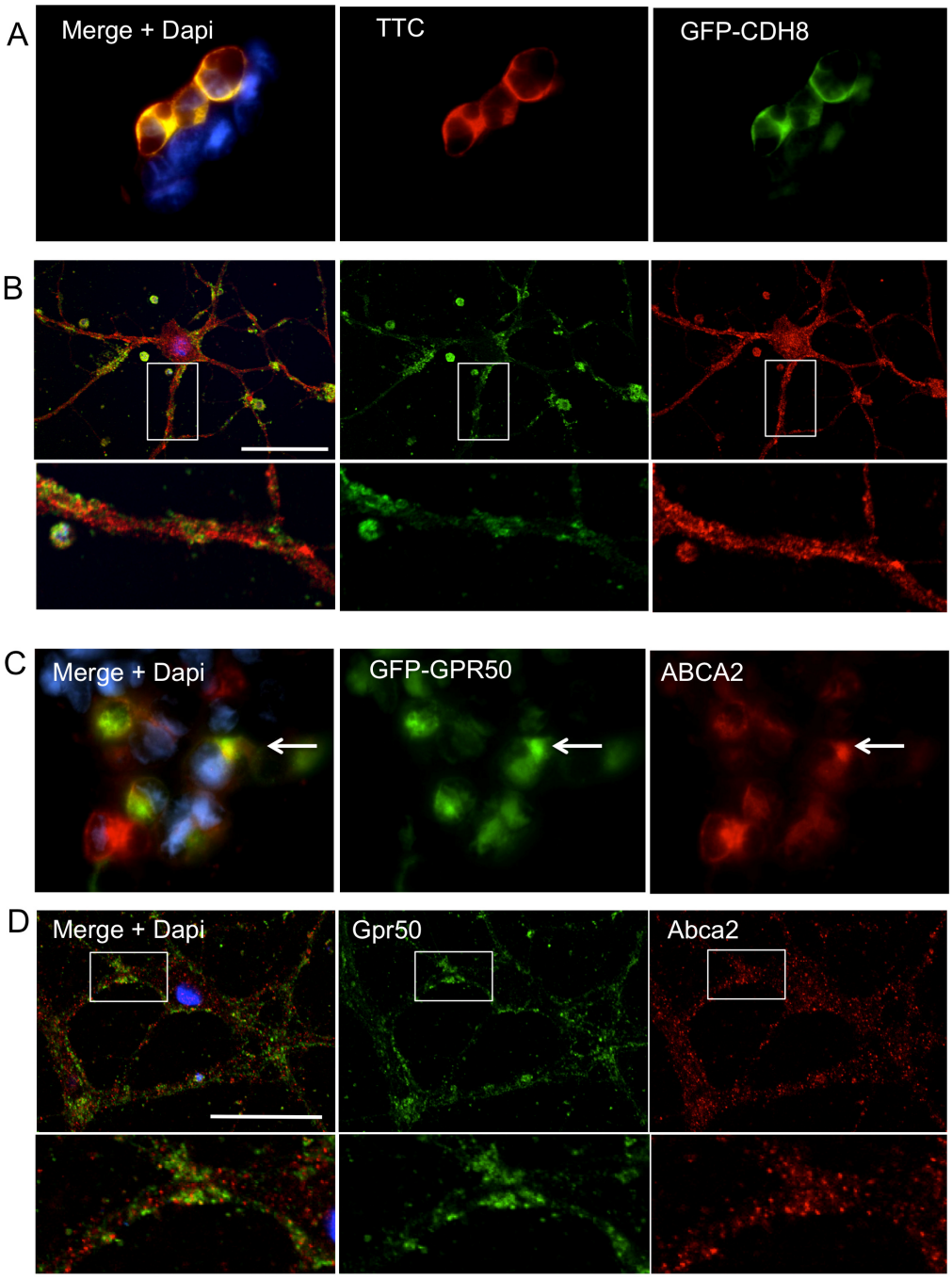
A
Merge + Dapi
TTC
GFP-CDH8
B
C
Merge + Dapi
GFP-GPR50
ABCA2
D
Merge + Dapi
Gpr50
Abca2

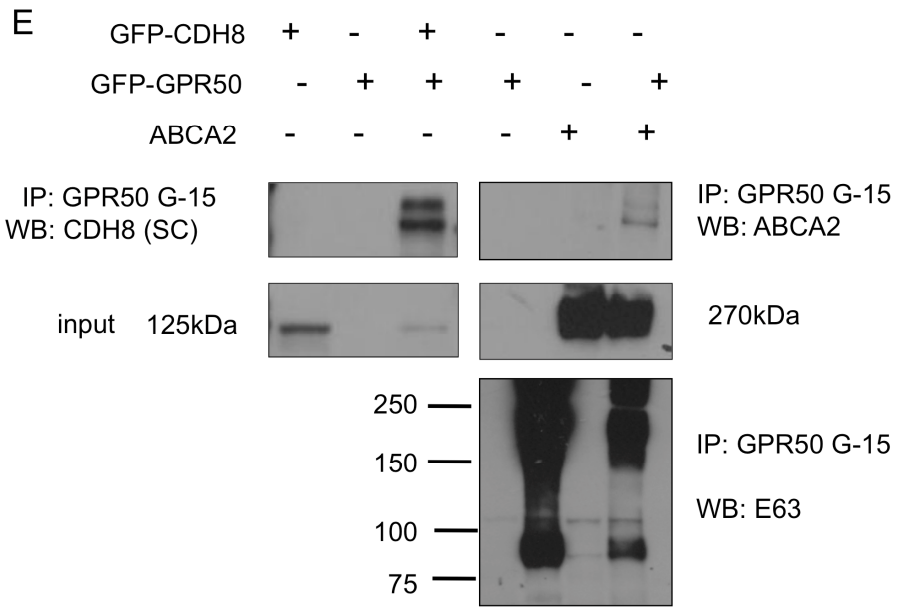

Figure 2.14 *GPR50 interacts with CDH8 and ABCA2 in mammalian cells. (A) HEK293T cells were co-transfected with GPR50-TTC and GFP-CDH8 and stained with GPR50 (C-term) and GFP. (B) Primary cortical mouse neurons were cultured for 28 days and stained with GPR50 G-15 or CHD8 E61 for detection of endogenous colocalisation. (C) HEK293T cells were co-transfected with GFP-GPR50 and ABCA2 and stained with GFP and ABCA2. (D) Primary cortical mouse neurons were cultured for 28 days and stained with GPR50 G-15 or ABCA2 for detection of endogenous colocalisation. Cells were counterstained with DAPI for nuclear staining. Scale bars: 50 µm. (E) HEK293T cells were transfected with full length human GFP-CDH8 or ABCA2 and GFP-GPR50, individually or in combination. Lysates were immunoprecipitated with anti-GPR50 (G-15, SC) antibody and CDH8 and ABCA2 were co-precipitated in the GPR50 co-transfected sample only, as shown by Western blot analysis.*

2.3.2.5 Interactions of untagged GPR50 and GPR50$^{\Delta 502\text{-}505/T532A}$ with CDH8 and ABCA2

Next, colocalisation and co-IP experiments were repeated using untagged GPR50 or GPR50$^{\Delta 502\text{-}505/T532A}$ with untagged CDH8 and ABCA2.

Performing immunohistochemistry using SH-SY5Y cells, GPR50 and GPR50$^{\Delta 502\text{-}505/T532A}$ both colocalised with CDH8 in the plasma membrane at cell-cell contacts. Colocalisation with ABCA2 was found in cytoplasmic vesicles in a small subset of cells. Again, no apparent difference in colocalisation was found between using GPR50 or GPR50$^{\Delta 502\text{-}505/T532A}$ in SH-SY5Y cells (Fig 2.15). This suggests CDH8 and ABCA2 have the ability to bind both forms of GPR50.

Co-immunoprecipitation studies of untagged GPR50 or GPR50$^{\Delta 502\text{-}505/T532A}$ with untagged CDH8 and ABCA2 were attempted in HEK293 cells. After immunoprecipitating GPR50 untagged CDH8 is expected to be detected by Western blotting at 100 kDa (Fig 2.16). However at this molecular weight non-specific bands are visible in the co-IP blot possibly blocking any real co-precipitated CDH8 (Fig 2.16). Reciprocal IP's using CDH8 E61 as IP antibody were performed but were so far unsuccessful and need further troubleshooting before conclusions can be drawn. In the case of ABCA2 there were issues with either the ABCA2 plasmid and/or the antibody resulting in apparent reduced (lysate) expression signal of ABCA2 by Western blotting (Fig 2.16). These technical issues meant no conclusions could be drawn and the experiments need to be repeated.

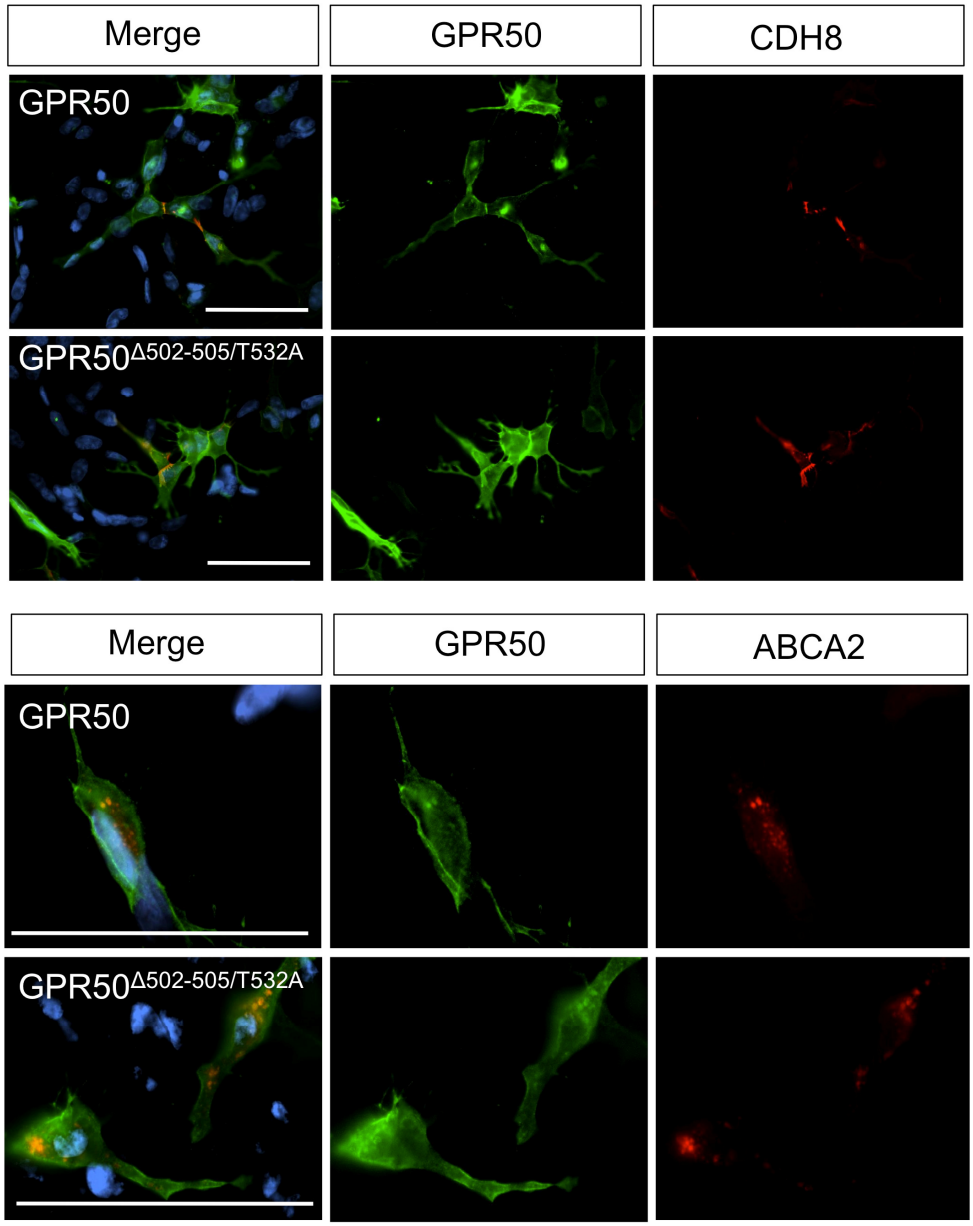

Figure 2.15 *Full-length GPR50$^{\Delta 502\text{-}505/T532A}$ shows a similar colocalisation pattern as GPR50 with CDH8 and ABCA2. SHSY5Y cells were cotransfected with GPR50 or GPR50$^{\Delta 502\text{-}505/T532A}$ and CDH8 (A) or ABCA2 (B). Immunocytochemistry results show similar colocalisation of GPR50 with CDH8 at the plasma membrane at cell-cell contacts (A) and at a lysosome-like location with ABCA2 (B). Cells were counterstained with DAPI. Scale bars: 50 µm.*

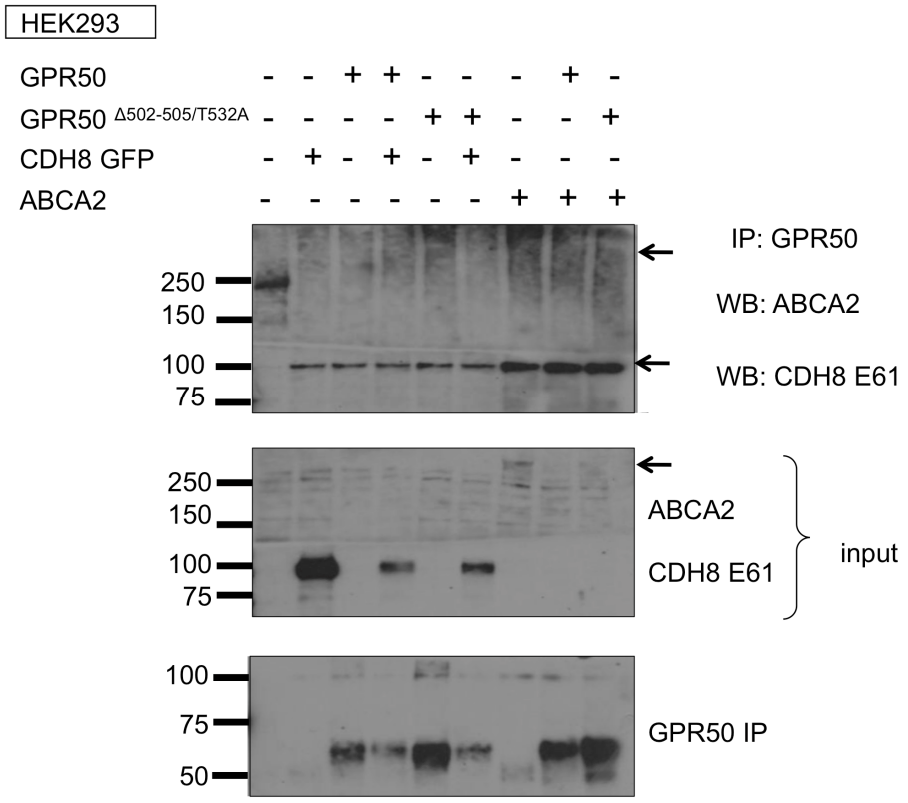

Figure 2.16 *Attempts to co-immunoprecipitate CDH8 and ABCA2 with GPR50 and GPR50$^{\Delta 502\text{-}505/T532A}$ were unsuccessful. HEK293 cells were cotransfected with GPR50 or GPR50$^{\Delta 502\text{-}505/T532A}$ and untagged CDH8 or ABCA2. GPR50 was precipitated using the GPR50 G-15 SC antibody but Western blotting with anti-ABCA2 didn't result in a positive signal (top arrow). The lysate signal of ABCA2 was very weak (bottom arrow) indicating problems with the plasmid and/or antibody. Similary, Western Blotting with anti-CDH8 61 resulted in a non-specific band at 100kDa (middle arrow), obscuring the results.*

2.3.2.6 Summary of interactions

The combined results of the colocalisation and co-immunoprecipitation findings are summarised in Table 2.5.

Constructs	GFP-CTD	GFP-CTD Δ502505/T532A	GFP-GPR50	GPR50	GPR50 Δ502505/T532A
GFP-Nogo-A	Co-IP	Co-IP	Co-IP	ICC	NT
Nogo-A	NT	NT	NT	Co-IP, ICC	Co-IP, ICC
GFP-Nogo-C	NT	NT	NT	Co-IP, ICC	Co-IP, ICC
GFP-RTN3	NT	NT	NT	Co-IP, ICC	Co-IP, ICC
GFP-CDH8	Co-IP	Co-IP	Co-IP, ICC	NT	NT
CDH8	NT	NT	NT	Co-IP inconclusive, ICC	Co-IP inconclusive, ICC
ABCA2	Co-IP inconclusive	Co-IP inconclusive	Co-IP, ICC	Co-IP inconclusive, ICC	Co-IP inconclusive, ICC

Table 2.5 *Results from interaction study. Indicated are replicable (3x) positive interaction/colocalisation results from co-immunoprecipitation (co-IP) and immunocytochemistry (ICC). When results were inconclusive this was indicated. NT, not tested.*

2.3.3 Reticulon proteins alter cellular localisation of GPR50

The colocalisation results in SH-SY5Y cells above (Fig 2.11-2.13) indicate colocalisation of GPR50 with RTN3, Nogo-C and Nogo-A in the ER, whereas GPR50 is normally predominantly found in the plasma membrane (Fig 2.2). This suggests an alteration of GPR50 localisation if favour of the ER. In order to test this, reticulon proteins or GFP as control were cotransfected with GPR50 or GPR50$^{\Delta 502-}$

$^{505/T532A}$ into SH-SY5Y cells (Fig 2.17A). After performing immunocytochemistry the number of cells showing GPR50 at the plasma membrane, ER or both were scored (Fig 2.17B). Initial pilot studies for this experiment were performed by S. Hempel, under my supervision, as part of her MSc project. The results indicate a significant decrease in plasma membrane localisation of GPR50$^{\Delta 502\text{-}505/T532A}$ in the presence of overexpressed RTN3 ($p<0.05$) or Nogo-C ($p<0.05$) and a significant increase in ER localisation of GPR50$^{\Delta 502\text{-}505/T532A}$ with RTN3 ($p<0.05$) compared to eGFP. There was also a non-significant but consistent decrease in plasma membrane and increase in ER localisation of GPR50 with RTN3, Nogo-A and Nogo-C, and of GPR50$^{\Delta 502\text{-}505/T532A}$ with Nogo-A, as compared to eGFP (Fig 2.17B). No difference was found between GPR50$^{\Delta 502\text{-}505/T532A}$ and GPR50 in any of the conditions. This experiment was not performed for CDH8 and ABCA2 because of time contraints. Although the localisation of GPR50 did not appear to be altered in the presence of CDH8 (Fig 2.15), there may be a difference with ABCA2 (compare Fig. 2.2 with 2.15), which needs to be further investigated.

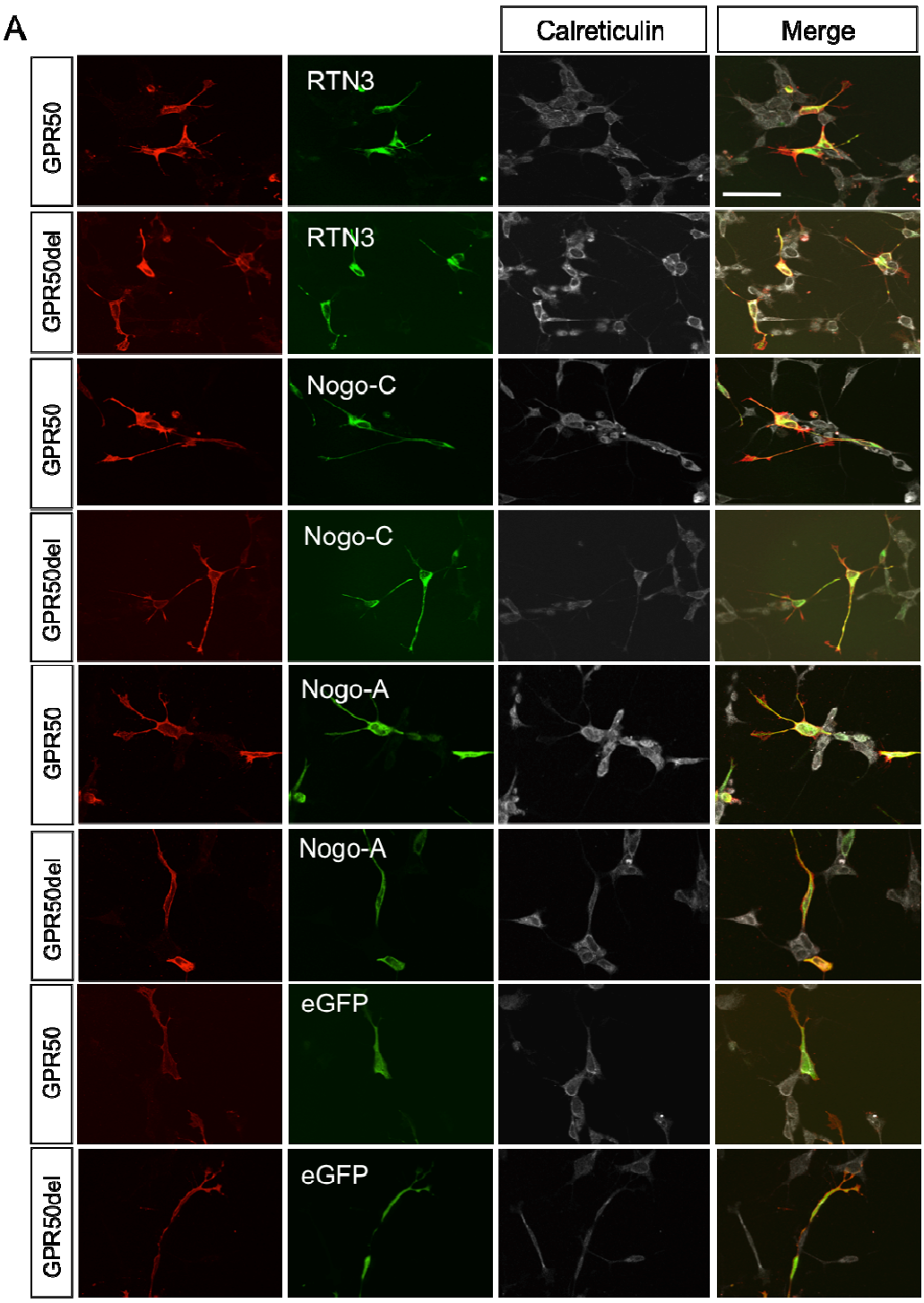

Figure 2.17A *Reticulon proteins alter the cellular localisation of GPR50. (A) SH-SY5Y cells were transfected with GPR50 or GPR50Δ502-505/T532A (GPR50del) and RTN3, Nogo-C, Nogo-A or eGFP as a control. Cells were triple labelled with GPR50 G-15 (red), Calreticulin (infrared) and GFP (green) or Nogo-A (H-300, green). Scale bar: 50 µm.*

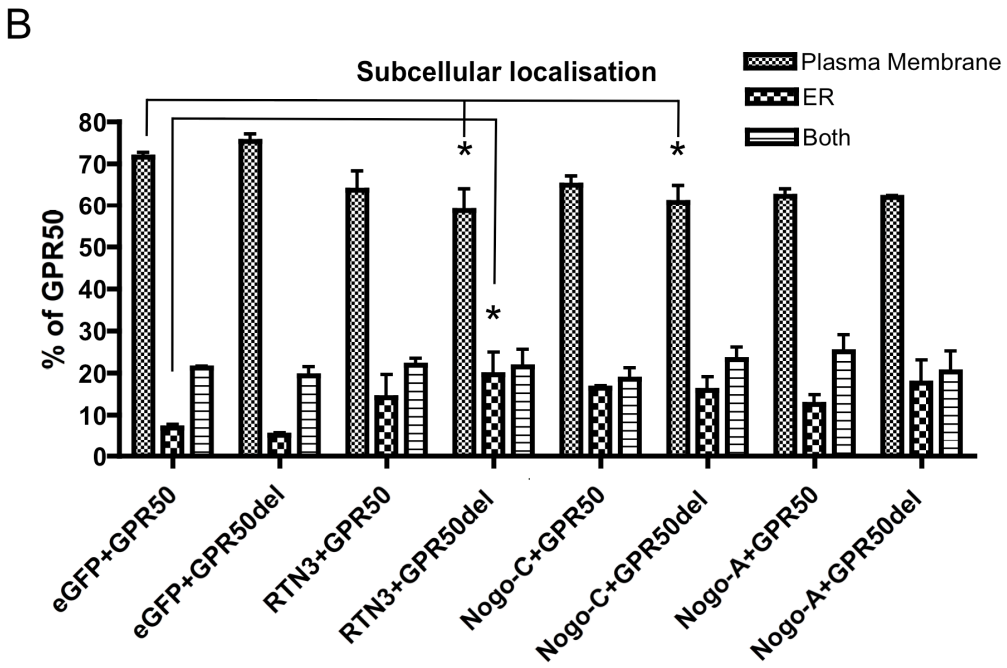

***Fig 2.17B**. Reticulon proteins alter the cellular localisation of GPR50. (B) Over three independent experiments 120 images were collected and the number of cells showing GPR50 at the plasma membrane, ER or both were counted.*p<0.05.*

2.4 Discussion

In this study we have shown that exogenous GPR50 colocalises and interacts with Nogo-A, Nogo-C, RTN3, CDH8 and ABCA2 in mammalian cells, although with some of the proteins the interaction was only shown when using GFP-tagged constructs (Table 2.5), introducing the possibility that the interaction is caused by GFP-dimerisation rather than a true interaction. The expression pattern of the proteins under overexpressed and endogenous conditions is in agreement with previous studies (Kido et al., 1998; Vulevic et al., 2001; Dodd et al., 2005; Broccardo et al., 2006; Hamouda et al., 2007). Endogenous expression and colocalisation of these proteins is found on axons and dendrites and at synaptic contacts, potentially indicating involvement in cell-cell signalling. A synaptic location of neuronal Nogo-A has been reported previously (Aloy et al., 2006; Lee et al., 2008). Cdh8 expression at the synapse would be in line with its previously detected localisation at synaptic junctions and suggested role in cell-cell adhesion at synaptic contacts (Suzuki et al., 2007).

2.4.1 GPR50 and RTN3/RTN4 (Nogo)

GPR50 interacts with RTN3, Nogo-C and Nogo-A as shown by colocalisation and co-immunoprecipitation (co-IP) of untagged and GFP-tagged constructs (Table 2.5), suggesting common pathways and functions for GPR50 and reticulon proteins. Reticulons play a role in neurite growth, BACE1 activity, ER structure/function and apoptosis (Schwab, 2010) and further research is needed to identify a role for GPR50 in these processes (also see Chapter 4).

Because reticulons have a mixed membrane topology (Fig 2.1) the exact location of the interaction is unclear. Looking at the results in this chapter the interaction could take place in the ER, cytoplasm and/or plasma membrane of the cell.

Within SH-SY5Y cells the interaction between overexpressed proteins appears to take place predominantly in the ER (Fig 2.11-2.12). This is possibly a result of ER

retention of GPR50 by reticulon proteins as is suggested by the results in Fig 2.17. RTN3 is known to affect the cellular location of interaction partner BACE1 (Shi et al., 2009). HEK293 cells stably expressing RTN3 showed an enrichment of BACE1 in the ER fraction and decrease on the cell surface. This ER retention results in decreased APP processing of BACE1 (Shi et al., 2009). Possible functions of GPR50 are also likely to be altered by mislocalisation of the receptor.

In neurons endogenous colocalisation was found in dendrites and possibly in synaptic spines (Fig 2.9, 2.14). It has been suggested that GPR50 interacts in *trans* with Nogo-A (proteins are present on the membrane of different cells, eg one presynaptic the other postsynaptic) and that GPR50 is a neuronal receptor for N-terminal Nogo-A (Schwab, 2010). This scenario is however unlikely as Nogo-A appears to interact with the C-terminal domain of GPR50, which is necessarily cytoplasmic. This was however shown with the GFP-tagged constructs only, and the experiment needs to be repeated with untagged GPR50 CTD and Nogo-A in order to confirm this. Furthermore colocalisation in immortalised cells and primary neurons suggest interaction in the same cell. It is however possible that there are more binding regions than only the CTD and further experiments are necessary to identify exact binding regions (see below). Nogo-A has previously been detected at presynaptic sites (Aloy et al., 2006; Lee et al., 2008). Subcellular fractionation studies may indicate a pre- and/or postsynaptic localisation for GPR50 and interactors, shedding light on whether GPR50-Nogo interactions are in *cis* (same membrane) or in *trans* (see next chapter).

Because the Y2H study identified several reticulon family members two GPR50 minimal interacting domains on Nogo/RTN proteins were identified (Grünewald et al., 2009) (Fig 2.18). The first binding site comprises 110 amino acids (residues 685-795), and lies within the Nogo-A-specific region (Fig 18, *GPR50 interacting domain 1,* GID1). The second binding site, identified through overlapping of the putative binding sites found on Nogo-C and RTN3, is 70 amino acids long and lies within the RHD. It therefore shows high homology to all known isoforms of RTN1, RTN3, and Nogo (Fig. 2.18, *GPR50 interacting domain 2,* GID2, residues 1008-1077). These

binding sites overlap with the *NiGΔ20* and *Nogo-66* regions that have previously shown to have growth cone collapsing and neurite outgrowth inducing properties (Oertle et al., 2003b). This may therefore indicate a role for GPR50 in these processes. However, these binding regions need to be confirmed by for instance deletion mapping and co-IPs with shorter forms of Nogo/RTN3.

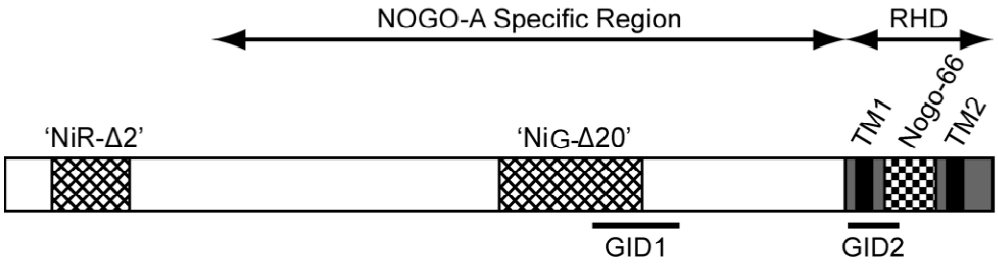

Figure 2.18 *The Y2H screen results predict two interaction sites of GPR50 on Nogo-RTNs. GPR50 interacting domain 1 (GID1) lies in the Nogo-A specific region. GID1 overlaps with the region homologous to the mapped rat regions NiG-Δ20 (human residues 87-185), which like the NiR-Δ2 (human residues 567-748) and Nogo-66 (human residues 1055-1120), appear to be responsible for the inhibitory effect on neurite outgrowth and the spreading of neurons (Oertle et al., 2003b). GPR50 interacting domain 2 (GID2) overlaps with Reticulon Homology Domain (RHD) present in all RTN4 isoforms and RTN1 and 3, and overlaps with the Nogo-66 region. Image from Grünewald et al., (2009) Molecular and Cellular Neuroscience. Copyright Elsevier 2009.*

Another important question is whether the interactions are direct. Reticulon proteins are known to interact with each other and complex together and it is therefore possible that GPR50 interacts with Nogo-A, Nogo-C or RTN3 only through other reticulon proteins. Co-immunoprecipitations with *in vitro* transcribed and translated (IVTT) proteins can be performed to confirm a direct interaction. Similarly, RNAi could be used to knock down the various reticulon isoforms to investigate the strength of the individual interactions. During this PhD several Nogo-C and RTN3 antibodies from commercial sources were tested however none of them resulted in a specific staining pattern. Therefore only GFP-tagged RTN3 and Nogo-C were used. For future studies it is important to acquire good specific antibodies and in the literature some RTN3 and Nogo-C antibodies produced 'in-house' have been

described (Oertle et al., 2003b; He et al., 2004; Shi et al., 2009). It might be worthwhile to obtain those in the absence of good commercially available antibodies.

2.4.2 GPR50 and CDH8

Exogenous untagged GPR50 colocalises with CDH8 in the plasma membrane at cell-cell contacts in SH-SY5Y and endogenous proteins colocalise at synaptic contacts in primary cortical neurons. CDH8 has previously been detected at these sites by others (Kido et al., 1998; Suzuki et al., 2007). Although positive interactions were detected with GPR50 and GPR50 CTD by co-IP, this was when using GFP-tagged constructs, and the experiment therefore needs to be repeated using untagged proteins. As was discussed above for reticulon proteins, more experiments are needed to investigate the interaction between GPR50 and CDH8 in more detail to determine whether there is a direct interaction and what the exact binding regions are.

Cadherins mediate adhesive interactions during development, both during axon growth and at the synapse (Ranscht, 2000). Each cadherin is predicted to be present at a subpopulation of synapses, perhaps acting as a molecular tag or postcode for neuronal connections (Ranscht, 2000). A positive GPR50-CDH8 interaction would indicate a role for GPR50 in (cortical) development or synapse formation and function. Cadherin has a role in promoting neurite extension, via the FGF receptor (Skaper et al., 2001), which is apparently opposite to Nogo's function in outgrowth inhibition. Cadherins form tight interactions with catenins and with the actin cytoskeleton. The membrane-actin interaction and cadherin activity can be modulated by Rho GTPases Cdc42, Rho and Rac1 (Kaibuchi et al., 1999; Kuroda et al., 1999). These Rho GTPases are effector molecules of Nogo signalling and are though to mediate the growth inhibiting characteristics of Nogo-A (Niederost et al., 2002). A possible connection between these signalling pathways is intriguing and calls for further investigation.

2.4.3 GPR50 and ABCA2

Colocalisation of GPR50 and ABCA2 is found in an endolysosomal-like location in the cell under overexpressed conditions but was endogenously detected at synaptic sites in primary neurons. This is in line with a perceived difference in ABCA2 expression under overexpessed or endogenous conditions (Vulevic et al., 2001; Broccardo et al., 2006). Similarly to CDH8 the interaction needs to be confirmed using untagged GPR50. Additionally, follow up experiments are needed to determine whether there is a direct interaction between GPR50 and ABCA2 and what respective binding regions are.

An interaction of GPR50 with ABCA2 may indicate a common role in lipid/sterol metabolism. ABCA2 is though to play a role in lipid metabolism, through homology with the HDL-cholesterol transporter Abca1(Kaminski et al., 2001) and is involved in the regulation of sphingolipids (Sakai et al., 2007). An intronic SNP in GPR50 is associated higher serum triglyceride and lower HDL (High Density Lipoprotein) levels (Bhattacharyya et al., 2006). GPR50 knockout mice have altered metabolism, as they display attenuated weight gain and reduced body fat on a high-energy diet as compared to wild-type animals. Moreover, on comparison, *Gpr50* knockout mice displayed hyperactive behaviour and a heightened metabolic rate. Abca2 knockout mice also display a stressed, 'skittish' behavour (Mack et al., 2007).

2.4.4 Effects of the polymorphisms on interactions

At first sight there is not a great difference between the co-localisation and co-immunoprecipitation results when using GPR50 or GPR50$^{\Delta 502\text{-}505/T532A}$. Both forms have the ability to bind Nogo-A, Nogo-C, RTN3, CDH8 and ABCA2. Only with RTN3 there is the suggestion of an increased interaction with GPR50$^{\Delta 502\text{-}505/T532A}$. As the interaction appears to be mainly found in the ER/cytoplasm under overexpressed conditions perhaps there is a difference in the 'basal' subcellular localisation between GPR50 and GPR50$^{\Delta 502\text{-}505/T532A}$. This was however not indicated by the results in figure 2.17 and there only seems to be a difference in the presence of RTN3. Co-immunoprecipitation is perhaps too coarse a method to detect subtle differences in binding affinities between variants. Several techniques are available that may be used to study this (see below).

2.4.5 Altered cellular localisation of GPR50 in the presence of reticulon proteins

Co-transfection of SH-SY5Y cells with GPR50$^{\Delta 502\text{-}505/T532A}$ and RTN3 and Nogo-C seemed to decrease the proportion of GPR50 in the plasma membrane and to increase the fraction present in the ER (only with RTN3). Although there may be a trend towards a similar effect with GPR50 and Nogo-A these differences were not significant (Fig 2.17). This suggests a possible ER-retention mechanism of GPR50 by RTNs, and in increased 'vulnerability' for the GPR50$^{\Delta 502\text{-}505/T532A}$ compared to GPR50. An ER retention mechanism by RTN3 was previously proposed for BACE1 and it is possible that this causes the negative modulation of BACE1 activity (Shi et al., 2009).

In this thesis the subcellular distribution was only investigated by immunocytochemistry. Additional subcellular fractionation studies are often performed to confirm this (Shi et al., 2009). With these fractionation studies it is however difficult to separate the ER membrane fraction from the plasma membrane fraction, as would be necessary here. One way of separating these is to perform surface biotinylation in living cells, and to test if the surface expression of GPR50 is decreased in the presence of RTNs as is predicted from this study. Another possibility for looking at surface expression is to use an N-terminal tag or an N-termial GPR50 antibody without membrane permeabilisation.

2.4.6 Future studies

In order to confirm interactions with CDH8 and ABCA2 co-IPs need to be performed using untagged proteins. Endogenous IPs should be attempted when it is clear where and when in the brain these proteins are highly co-expressed. In addition, to test whether interactions are direct IPs using *in vitro* transcribed and translated (IVTT) protein should be used. To map the interaction sites in more detail peptide array mapping should be undertaken, together with fine mapping using deletion constructs for co-IPs. With peptide array technology the protein sequence of protein 1 is spotted on nitrocellulose as short peptides, typically in 25-mers. The array is then

overlayed with recombinant protein 2 and probed with antibodies. Binding regions can be identified as spots on the array. With peptide arrays more exact data can be generated about binding regions, affinities and the effect of mutations of binding. An N-terminal GPR50 antibody may be useful to study GPR50 interactions on the plasma membrane only. The only GPR50 N-terminal antibodies that have been produced and reported of in the literature were however not able to detect GPR50 (Hamouda et al., 2007).

Although the data in this chapter indicated both GPR50 and GPR50$^{\Delta 502\text{-}505/T532A}$ are able to bind its interactors there are likely to be differences in binding affinities or stoichiometry between the two forms. Isothermal Titration Calorimetry is a very accurate if complicated biophysical technique for measuring the binding kinetics between two proteins. Another technique for determining binding constants is Surface Plasmon Resonance, although these techniques require protein purification. Common fluorescence microscopy techniques for assessing direct interactions of proteins in real time include FRET (Förster resonance energy transfer or fluorescence resonance energy transfer), BRET (Bioluminescence Resonance Energy Transfer) and FLIM (Fluorescence Lifetime Imaging Microscopy), where a donor (fluorescent) chromophore can transmit energy to an acceptor chormophore if it is in close proximity (Wallrabe and Periasamy, 2005).
These methods would help confirm or refute direct asociation under physiological conditions.

The results in this chapter suggest that GPR50 can interact with RTN3, Nogo-A, Nogo-C, CDH8 and ABCA2 under overexpressed conditions. The next question is where and when these proteins interact in the brain. This information can be used to attempt endogenous IPs of GPR50 and interactors. In the next chapter developmental expression of GPR50 and interactors in the developing and adult mouse brain is undertaken by performing rt-PCR and immunohistochemistry. Additionally subcellular fractionation of the adult mouse brain was performed to identify cellular compartment of high expression.

Chapter 3

Developmental expression of GPR50 and interactors in the CNS

3 Chapter Three: Developmental expression of GPR50 and interactors in the CNS

3.1 Introduction

The results in Chapter 2 indicate that GPR50 interacts with Nogo-A, Nogo-C, RTN3, CDH8 and ABCA2. The question is where and when are they able to interact. As we are interested in the function of the proteins in relation to mental disorders, I set out to investigate the expression in the central nervous system. This was studied using three methods: subcellular fractionation of adult mouse brain, rt-PCR of developing mouse brain, and immunohistochemistry in developing and adult mouse brain. The hypothesis is that GPR50 and its interactors are expressed at the same subcellular locations. In addition it is hypothesised that they show similar patterns of expression in the brain at similar stages of development, and may therefore be co-regulated.

The immunocytochemistry data in Chapter 2 suggest expression of GPR50, Nogo-A, CDH8 and ABCA2 along dendrites and in synaptic spines in neurons, suggesting a synaptic localisation. Immunocytochemistry in immortalised cell lines indicated co-localisation in plasma- and internal membrane fractions, such as the ER and the endolysosome. In order to test this further subcellular fractionation was performed from adult mouse brain including pre- and postsynaptic density fractions, similar to Clapcote et al. (2007).

The developmental expression in the mouse brain was also investigated, on the mRNA and protein level. Several techniques for mRNA and protein detection and quantification are currently available. For mRNA Northern blotting and RNase protection assay are considered the gold standards, since no amplification is involved, whereas rt-PCR (reverse transcription-polymerase chain reaction) is the most sensitive technique available. Compared to Northern blot analysis and RNase protection assay, rt-PCR can be used to quantify mRNA levels from much smaller

samples. In fact, under certain circumstances, this technique is sensitive enough to enable quantitation of RNA from a single cell (Rhoades et al., 2000).

Because we wanted to investigate several genes with varying levels of expression in many brain areas and at various timepoints we choose to perform rt-PCR for its sensitivity and ease. The rt-PCR experiments allowed us to address several questions:

1. Where and when is Gpr50 expressed?
2. Where are the interactors co-expressed?
3. Are the genes developmentally co-regulated?

In addition, the rt-PCR experiment allowed us to prioritise regions for future study by immunohistochemistry, which would otherwise have been too time consuming and costly. More details about the background and the setup of the rt-PCR experiment can be found under section 3.1.2.

Immunohistochemistry (and *in situ* hybridization for mRNA) is qualitative rather than quantitative but is best for visualizing exact locations of protein expression within regions and tissues. Its greatest disadvantage is that it is impossible to show that the staining corresponds to the protein of interest. For this reason primary antibodies must be well validated by Western blot or similar procedure. The antibodies that are used here were validated in Chapter 2 and all antibodies and markers used previously in the literature are detailed in Table 2.4a-b.

In this chapter mRNA levels of *Gpr50*, *Nogo-pan*, *Nogo-A*, *Nogo-C*, *Cdh8*, *Abca2* and *Srebf2* in the developing mouse brain were determined by rt-PCR. Because good antibodies were not available for all of these proteins immunohistochemistry was only performed for Gpr50, Nogo-A, Cdh8 and Abca2. For similar reasons subcellular distribution in adult mouse brain was investigated for Gpr50, Nogo-A, Cdh8 and Abca2.

In this introduction to Chapter 3 the expression of GPR50 and Nogo (-A, -B, -C), CDH8, ABCA2 and SREBF2 as previously reported in the literature is first summarised. Previous findings of expression in adult, embryonic and developing brain are described. After this summary concepts in real-time rt-PCR are introduced and the setup and optimisation of the rt-PCR experiment are explained in some detail.

3.1.1 Summary of expression of GPR50 and interactors as previously reported

3.1.1.1 GPR50

The first study of adult human *GPR50* reported expression in the pituitary and a weaker signal in the hypothalamus by Northern blot analysis and *in situ* hybridisation (Reppert et al., 1996). Rt-PCR and *in situ* results in sheep showed selective high expression in the dorsomedial hypothalamus (DMH), the pars tuberalis and –distalis of the anterior pituitary (adenohypophysis), the retina and the retinal pigmented epithelium (RPE) (Drew et al., 1998). Contrary to findings in human tissue (Reppert et al., 1996), expression of GPR50 was not found in the paraventricular nucleus (PVN) of the hypothalamus in sheep (Drew et al., 1998). Further studies in rodents (mice, rat, hamster) indicate the arcuate nucleus (Arc), subfornical organ (SFO), lateral hypothalamus (LH), anterior hypothalamus (AH), bed nucleus of the stria terminalis (BST), amygdala, preoptic nuclei and the olfactory bulb as regions of *Gpr50* expression (Drew et al., 2001) by rt-PCR and *in situ* hybridisation. In addition *Gpr50* was found to be expressed at high levels in ependymal cells (possibly tanycytes; Ivanova et al., 2008; Sidibe et al., 2010) lining the third ventricle in hamster (Barrett et al., 2006), mouse (Vassilatis et al., 2003) and rat (Drew et al., 2001) by *in situ* hybridisation. Using β-galactosidase inserted into the *GPR50* locus to show potential endogenous protein staining in *GPR50* knockout mice, *Gpr50* mRNA and putative protein was found to be expressed in the ependymal layer of the third ventricle and dorsomedial nucleus of the hypothalamus in mouse (Ivanova et al., 2008). Immunohistochemistry data support GPR50 protein expression in the

mouse hippocampus and rat pituitary (Hamouda et al., 2007) and mouse, human and rat 3rd ventricle and hypothalamus (Sidibe et al., 2010). The results from these studies are supported by *in situ* data in the Allen Brain Atlas database of gene expression http://www.brain-map.org/ (Jones et al., 2009), where enhanced *Gpr50* expression is found in the hypothalamus, olfactory bulb and third ventricular wall of the adult mouse brain. Although the BGEM website www.stjudebgem.org (Magdaleno et al., 2006) shows some *in situ* data in developing mouse brain, indicating high expression in the ventral hypothalamus and brainstem at E15, embryonic or developmental expression of GPR50 has not been reported elsewhere.

3.1.1.2 RTN4/Nogo

Expression of Nogo isoforms -A, -B and –C has been studied by rt-PCR, microarray, Northern blot, *in situ* hybridisation and immunohistochemistry, although the majority of studies have focused on rodent Nogo-A (Oertle and Schwab, 2003). *Nogo (Rtn4)* is ubiquitously expressed in the adult mouse brain, as can be seen from *in situ* data on the Allen Brain atlas (http://www.brain-map.org/). High expression of Nogo-C in the adult has been reported in the cerebral cortex, hippocampus, spinal cord, retina and optic nerve (Oertle and Schwab, 2003).

Using *in situ* hybridisation and immunohistochemistry, Mingorance-Le Meur et al. (2007) detected embryonic Nogo (-A) expression as early as E12.5 in the mouse hippocampus. At E14.5 Nogo-A staining was found throughout the entire rostrocaudal extent of the telencephalon, most notably in the olfactory bulb, tectum, cerebellum and spinal cord, with lower levels in the cortex, thalamus and hypothalamus. Nogo-A was also enriched in the CA1 and CA3 in the hippocampus at E14.5. At E18.5 Nogo-A is enriched in the white matter tracts of the corpus callosum, anterior commissure and fimbria-fornix (Mingorance-Le Meur et al., 2007).

In the developing brain Nogo-A is most predominantly present in spinal cord white matter, oligodendrocyte cell bodies, the cortex, hippocampus, habenula, cerebellum, optic nerve and retina (Huber et al., 2002; Oertle and Schwab, 2003). BGEM *in situ*

data indicate highest *RTN4* expression at P7 in the cortex, hippocampus and olfactory bulb.

3.1.1.3 CDH8

The type II Cadherin Cdh8 is predominantly expressed in the mammalian brain (Suzuki et al., 1991; Korematsu et al., 1998b). In the adult mouse brain *Cdh8* mRNA is highly expressed in the growth hormone (GH)- negative cells of the anterior pituitary (Chauvet et al., 2009). Attempts to identify the cell types that express Cdh8, using two previously well-characterised antibodies (Korematsu et al., 1998b; Suzuki et al., 2007), were unsuccessful (Chauvet et al., 2009).

Cdh8 is well studied in the embryonic and developing rodent brain. Korematsu and Redies (1997) have detected Cdh8 in the embryonic mouse brain by *in situ* hybridisation as early as E11.5/12.5 in the regions that will form the cortex (prosencephalon/telencephalon), ventral thalamus (prosencephalon/diencephalon), lateral ganglionic eminence and the pons (rhombencephalon). In the neonatal mouse brain (2-10 days) Cdh8 mRNA and protein is expressed in the (cingulate) cortex, striatum, globus pallidus, thalamus, subthalamic nucleus, entopeduncular nucleus, substantia nigra, amygdala, cerebellum and barrel cortex (Korematsu and Redies, 1997; Korematsu et al., 1998a; Korematsu et al., 1998b; Bekirov et al., 2002; Gil et al., 2002). Cdh8 is also highly expressed in the developing (first postnatal weeks) rat hippocampus (Bekirov et al., 2002; Bekirov et al., 2008). In the first postnatal weeks Cdh8 mRNA is expressed at high levels in the mouse entorhinal cortex (layer II), amygdala and in the hippocampal CA1, the distal part of CA3 and the dentate gyrus from birth (Bekirov et al., 2002). Korematsu and others (1998) however did not detect any expression in the hippocampus of neonatal mouse brain. *In situ* data show strong *Cdh8* expression in the cortex and weaker expression in parts of the olfactory bulb in P7 mouse brain (Akins et al., 2007). Cdh8 was also detected in the amygdala during development (Medina et al., 2004).

Characteristic of Cdh8 (and other cadherins) is a restricted, patterned, layered or regional expression within certain brain areas suggesting cadherins play a role in

subdivisional organisation of the developing brain (Korematsu and Redies, 1997; Suzuki et al., 1997; Korematsu et al., 1998a; Korematsu et al., 1998b; Bekirov et al., 2002; Gil et al., 2002; Neudert et al., 2008). In the first weeks postnatally Cdh8 is expressed in a decreasing dorsal to ventral gradient in the subiculum (Bekirov et al., 2002). Cdh8 expression may identify and contribute to functional neural circuits involving the development of the basal ganglia-thalamocortical (Alexander and Crutcher, 1990; Korematsu et al., 1998b) or the fasciculus retroflexus/habenulo-interpeduncular tract (Marchand et al., 1980). Cdh8 protein is also expressed in a patch-like distribution in the neonatal (P0 to P7) rat striatal matrix (Korematsu et al., 1998a), which has connections to cortical sensorimotor areas (Gerfen, 1984; Donoghue and Herkenham, 1986; Gerfen, 1992; Korematsu et al., 1998a). The BGEM database of *in situ* data indicates high expression at P7 in the cortex, basal ganglia, thalamus, hippocampus and amygdala.

Several cadherins have been found at the synapse during and after synaptogenesis (Fannon and Colman 1996; Uchida et al. 1996; Bozdagi et al. 2000; Togashi et al. 2002). A role for cadherins in dendritic sprouting and synaptic plasticity has been proposed (for a review, see Takeichi 2007).

3.1.1.4 ABCA2

ABCA2 is highly expressed in the mammalian brain (Luciani et al., 1994; Kikuno et al., 1999; Zhao et al., 2000; Vulevic et al., 2001; Warren et al., 2009), most notably by neural progenitors in the subventricular zone of the lateral ventricle and the dentate gyrus, regions important in adult neurogenesis (Broccardo et al., 2006). Abca2 expression was also found predominantly in white matter tracts and to a lesser extent in olfactory bulb and cerebellum in adult rat brain (Zhao et al., 2000). It is expressed by oligodendrocytes and by a subset of GABAergic and glutamatergic neurons (Broccardo et al., 2006). Nothing has been reported about its developmental expression pattern. The BGEM database suggest low of no expression around E15 but high(er) expression in the hippocampus, cerebellum and brainstem at P7.

3.1.1.5 Srebp2/SREBF2

Srebp2 was found to be highly expressed in the hippocampus and to a lesser extent in the cortex, striatum, thalamus, hypothalamus brainstem and cerebellum of the adult rat brain (Kim and Ong, 2009). In the adult mouse brain *Srebf2* mRNA expression is found in the cortex, olfactory bulb and hippocampal formation (Allen Brain Atlas, http://www.brain-map.org/). Neither embryonic nor developmental expression of SREBF2 has been reported in the literature.

3.1.2 Introduction to the real-time rt-PCR experiment

Below some concepts in real-time PCR and the materials used in this chapter are described.

3.1.2.1 Origene TissueScan rt-PCR mouse developmental panel

Although the developmental expression profile of Cdh8 has been extensively researched (see 4.1.2.3) not much is known about the developmental expression of Gpr50 or the other Y2H interactors. Therefore, mRNA expression of *Gpr50*, *Nogo-pan*, *Nogo-A*, *Nogo-C*, *Cdh8*, *Abca2* and *Srebf2* was investigated in the developing mouse brain. TissueScan Real-Time mouse developmental cDNA panels from different brain regions at E13, E15, E18, P7 and week 5 (total 48 samples, Origene) were obtained. Using this panel had several advantages: In this way it is possible to assess the gene profiles at many timepoints and regions, which would be technically difficult and time consuming when done in-house. Because the panel is made up of pooled RNAs it is possible to compare expression levels between genes on exactly the same sample. Additionally it is possible to assess correlations between genes, within regions and across timepoints. Similar use of the Origene TissueScan panels has been reported in the literature (De Luca et al., 2004; Gutierrez et al., 2008). More information on how the panels were produced can be found in under *Materials and Methods* (this chapter).

3.1.2.2 Introduction to real-time rt-PCR

Real-time quantitative PCR (qPCR) is characterised by the cycle number at which the amplified PCR product is first detected above a set threshold, rather than the amount of PCR product accumulated after a fixed number of cycles (with end-point quantitative PCR). In real time PCR the threshold is set at a point where DNA amplification is in the exponential phase. The greater the starting quantity of the target molecule, the earlier a significant increase in fluorescence is detected. This is measured by the threshold cycle parameter C_t (Fig 3.1). C_t is considered a more reliable measure of the starting copy number than end-point measurements, as a slight difference in a limiting component can have a large effect on the amount of product (Bieche et al., 1998). In addition the advantages of real-time PCR are the wide dynamic range, automated sample handling and short run time (Celi et al., 1994) in (Bieche et al., 1998). Disadvantages of the real-time method are the need for specific primer design and optimisation. Reactions need to be performed in a thermal cycler (96 wells) and reagents can be costly.

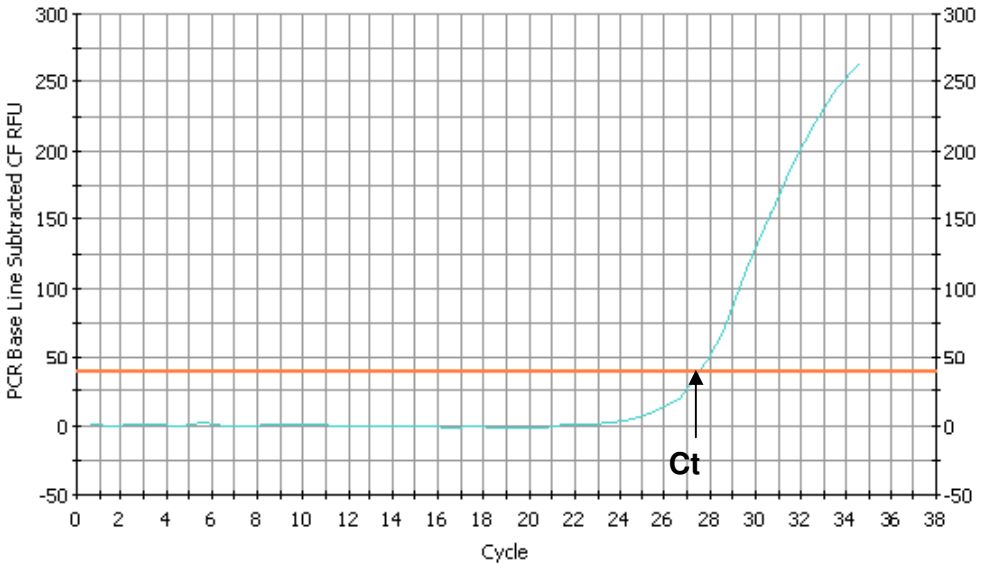

Figure 3.1 *Real time PCR trace graph for a single well on a 96-well plate. Cycle number is shown along the X-axis and arbitrary fluorescence units (these are fold increase over background fluorescence) are shown on the Y-axis. Quantitation of the amount of cDNA is done when the amplification is exponential, which is at the very beginning of the upturn of the curve. The orange horizontal line in the figure marks the threshold or Ct. More dilute samples will cross at later Ct values. In this example* $Ct=27.58$.

3.1.2.3 SYBR Green rt-PCR chemistry

SYBR Green reagent was chosen for quantifying mRNA using the Biorad thermal cycler (iCycler). SYBR Green provides the simplest and most economical format for detecting and quantifying PCR products in real-time reactions. SYBR Green binds double-stranded DNA, and upon excitation emits light. Thus, as a PCR product accumulates, fluorescence increases (see Fig 3.2A). The advantages of SYBR Green are that it is reasonably inexpensive, easy to use, and sensitive. The disadvantage is that SYBR Green will bind to any double-stranded DNA in the reaction, including primer-dimers and other non-specific reaction products, which results in an overestimation of the target concentration. Fluorescence may also vary with amplicon size. Despite this, for single PCR product reactions with well-designed primers, SYBR Green can work extremely well, with spurious non-specific background only showing up in very late cycles.

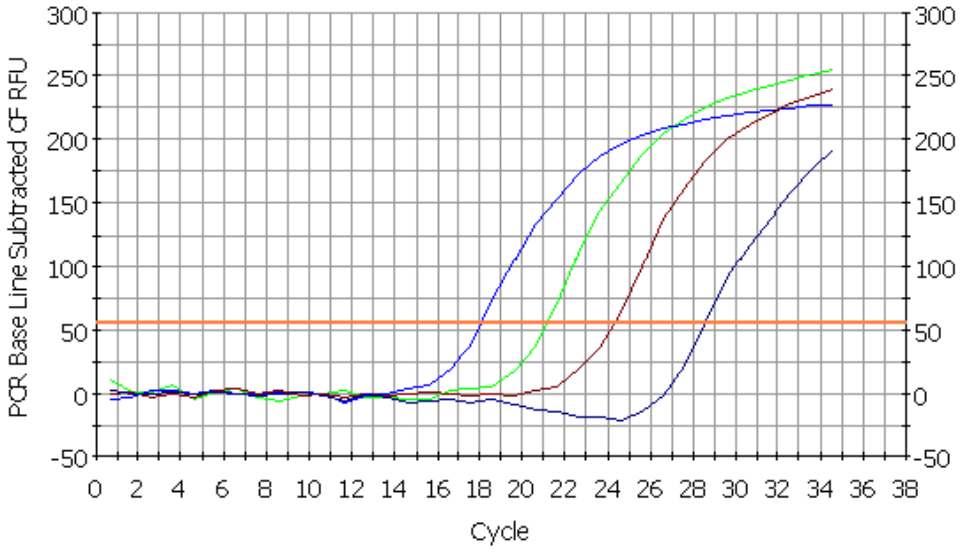

Figure 3.2 *Real-time PCR graphs (A) Example Real-Time PCR trace graph for a series of 10-Fold dilutions of a sample of DNA. The graphs should be equally apart at the threshold level (ideally 3.3 cycles).*

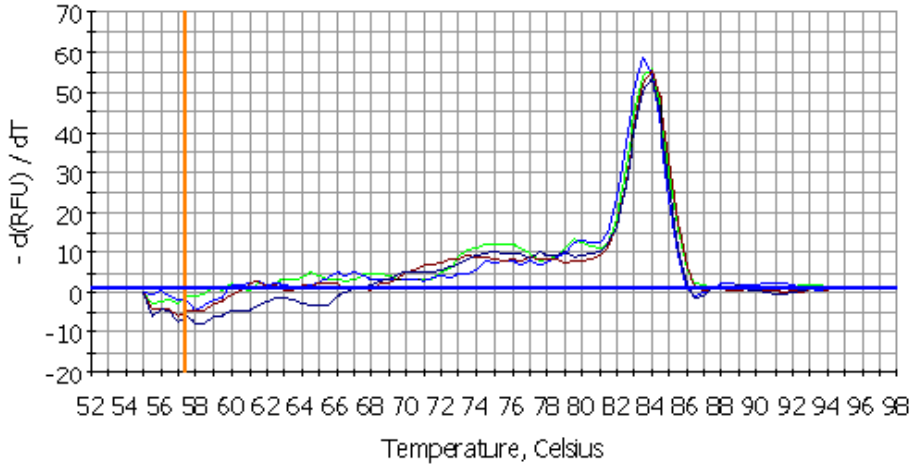

Figure 3.2 *Real-time PCR graphs (B) Example Melt Curve. Three replicates are shown. With the SYBR green method, primer dimer artifacts may be a problem since you are measuring total DNA synthesis and you need to be sure that you are measuring a Ct due to the real target for amplification. In this graph there is only one clear peak for each replicate, with no smaller ones at lower temperatures, indicating minimal primer-dimer artifacts and no non-specific binds.*

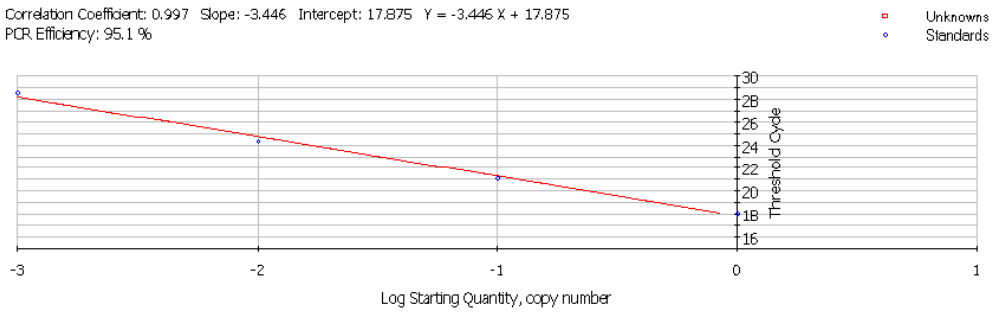

Figure 3.2 *Real-time PCR graphs (C) Example Standard Curve The Ct values for the dilutions are plotted against concentration, resulting in a linear graph. Ideally its correlation coefficient is 0.990 or more, with a slope of -3.3 and an efficiency of approximately 100%.*

3.2 Materials and methods

3.2.1 Antibodies

All antibodies and markers used in this chapter are described in Table 2.4a-b Rabbit polyclonal antiserum CDH8 E61 was raised against sequence derived C-terminal peptide residues 785-799 of human CDH8. Final bleeds from immunized rabbits were affinity-purified against both peptides by Eurogentec (Double XP program), and these purified anti sera were used in all experiments. Additionally we used GPR50 (G-15, goat polyclonal, Santa Cruz), Nogo-A (H-300, rabbit polyclonal, Santa Cruz), ABCA2 (Rabbit polyclonal, (Vulevic et al., 2001)), PSD-95 (mouse monoclonal, ABR), Synaptophysin (mouse monoclonal, Sigma), α-tubulin (rabbit polyclonal, Abcam), NeuN (mouse monoclonal, Abcam), 5-HT (rabbit polyclonal, ImmunoStar), GFAP (mouse monoclonal, Sigma), O4 (mouse monoclonal, R&D systems), Vimentin (Mouse monoclonal, Abcam), Tyrosine Hydroxylase (mouse monoclonal, Abcam) and Dopamine Beta-Hydroxylase (mouse monoclonal, Abcam).

3.2.2 Subcellular Fractionation

Ten 7-10 week old female C57BL/6 mice were purchased from Harlan (UK). Mice were sacrificed by cervical dislocation (schedule 1 procedure was performed by the animal facility staff) and brains were processed for subcellular fractionation and purification of synaptic fractions as described previously (Bradshaw et al., 2008; Clapcote et al., 2007; Grünewald et al., 2009). The fractions were analyzed by immunoblotting as described in Chapter 2 (section 2.2.14) with anti Nogo-A (H-300, 1:2000), anti-CDH8 E61 (1:3000), anti-ABCA2 (1:1000), anti-GPR50 (G-15, 1:1000), anti-PSD-95 (1:2000), anti-synaptophysin (1:10,000) and anti-α-tubulin (1:20,000). Rabbit anti-mouse (1:2000), rabbit anti-goat (1:5000) and swine anti-rabbit (1:3000) horseradish peroxidase conjugated secondary antibodies (DAKO) were used and membranes were treated described in Chapter 2 (2.2.14). This experiment was performed in triplicate, using three independent samples (30 mice total).

3.2.3 Real-time Reverse Transcription-Polymerase Chain Reaction (rt-PCR)

TissueScan Real-Time mouse developmental cDNA panels from different brain regions at E13, E15, E18, P7 and week 5 (total 48 samples) were purchased from Origene Technologies Inc. (Lot no.11/06, Rockville, MD). These first strand cDNAs were synthesized from poly-A^+ RNA using oligo(dT) primers, and were normalized to β-actin. The cDNAs were dried into the wells of the panel and were supplied frozen.

Real-time PCR using SYBR Green Supermix (100mM KCl; 40mM Tris-HCl, pH 8.4; 0.4M of each dNTP; iTaq, DNA polymerase, 50 units/ml; 6mM $MgCl_2$; SYBR Green I; 20nM fluoresein, and stabilizers; Bio-Rad Inc., Hercules, CA) was performed on the BioRad iCycler. Primers (Table 3.1) were selected using Primer3 software (http://primer3.sourceforge.net/), except for β-actin, which came supplied with the panel. The linear range of each primer pair was determined by producing standard curves in the Biorad iCycler, using mouse brain cDNA as template. Reactions were performed in duplicate. Amplification was achieved in 35 cycles of the following conditions: denaturation at 95°C for 30s; annealing at 60-65°C for 30s; and extension at 72°C for 30s. A melting curve was obtained starting at 55°C with 10s increments of 0.5°C for 80 cycles. Each PCR reaction generated a single amplicon as indicated by the melting temperature profiles. All PCR products were also checked by gel electrophoresis to confirm correct PCR product size against a 1kb ladder.

For analysis the fluorescence threshold value C*t* (the number of cycles required for the fluorescent signal to cross the threshold (ie exceeds background level) of each sample was calculated using the iCycler MyiQ system software.

The relative expression of the genes was determined using the deltaCt method, which generates raw (not normalized) data, relative to the sample with the highest expression. The data are further normalized using a method described by

Vandesompele et al. (2002), which is equivalent to using the delta-delta Ct method (see 4.2.4 below). It can be performed using the freely available geNorm software: (http://medgen.ugent.be/~jvdesomp/genorm/). Normalized expression data were obtained by dividing the raw gene-of-interest quantities for each sample by the normalization factors, which are the geometric means of the reference genes used in this study: ß-actin, Tbp, Hmbs and Cyclophilin B. Spearman correlations (r, (95% conficence interval), significance at $p \leq 0.05$) were performed using Graphpad Prism.

3.2.4 Normalisation of expression data

The relative expression of the 7 genes was determined using the delta Ct method, which generates raw (not normalized) data, relative to the sample (region) with the highest expression (lowest Ct value). The data are then further normalized using a method described by Vandesompele et al. (2002), which is equivalent to the more standard delta-delta Ct method but has the added advantage that it (1) takes the difference in amplification efficiency between target and reference gene(s) into account (for delta-delta Ct they should be equal), (2) allows easy inclusion of multiple reference genes, and (3) is easier to calculate in Excel (http://medgen.ugent.be/~jvdesomp/genorm/).

The normalisation of the expression data from the 7 genes of interest (GOI) was performed as follows (Vandesompele et al., 2002): First the Ct values from each gene of interest (GOI) were transformed into quantities, using the deltaCt formula, with the sample of the highest expression per gene set to 1:

$$Q = E^{\text{deltaCt}}$$

$$Q = E^{(\text{minCt} - \text{sampleCt})}$$

Q = sample quantity relative to sample with highest expression
E = amplification efficiency (2 = 100%; 1.90 = 90%, 2.10 = 110%)
minCt = lowest Ct value = Ct value of sample with highest expression

Next, the normalization factor (NF) was calculated by analyzing the geometric mean of the (selected) four reference genes (relative quantities).

$$NF_n = \sqrt[n]{REF_1 \,.\, REF_2 \,\ldots\, REF_n}$$

Geometric mean was calculated in Microsoft Excel, using the GEOMEAN(a, b, c, d) function, where a, b, c and d are the relative quantities of the reference genes. Finally, the normalized expression data were obtained by dividing the raw GOI quantities for each sample by the normalization factors (Vandesompele et al., 2002).

3.2.5 Immunohistochemistry

Female CD1 mice of approximately 10 weeks old were housed in groups of between 5-14 animals, depending on cage size. Females were taken to the male cage and left until a vaginal plug was found. The female was then housed with other females that were plugged on the same date. The date of the plug was E0. Mice were kept on a 12-hour light/dark cycle with lights on at 7.00h. Mice were fed on SDS RM1 expanded diet with water available *ad libitem*. Adult animals were killed by cervical dislocation. All the above procedures in 3.2.5 were performed by the animal facility staff.

Embryos were removed by hysterectomy and brains were directly transferred to ice cold PBS prior to fixation. Three adult female mice and three embryonic day 18 mice were used in this study. Brains were fixed in either 70% EtOH, 4% formaldehyde or methacarn (60%MeOH, 30% chloroform, 10% glacial acetic acid). E18 brains were fixed for 4 hours and adult brains for 16-18 hours. Brains were then transferred to 70% EtOH and stored at -20ºC until further processing.

Brains were embedded in paraffin wax and cut into 6µm sections on a Leica microtome onto gelatin coated superfrost plus slides (Thermo Fisher). Six coronal sections per animal from three individual 8-12 week old CD1 female and E18 mouse brains were processed for immunofluorescent detection of Gpr50 and interactors.

Intact coronal sections corresponding to approximately Bregma –0.655 mm, -1.455 mm, -2.88 mm, -3.58 mm, -4.655 mm and -5.555 mm were chosen from each animal to cover all brain regions evaluated (see Chapter 8 Supplementary information, supplementary images 1-6, from Allen Brain Atlas: http://www.brain-map.org/). Sections were dried at 37ºC overnight.

Sections were dewaxed in xylene and rehydrated in 100% and 70% EtOH. Before staining formalin-fixed sections were incubated in picric acid for 20 min and antigen retrieval was performed by microwave boiling slides in 50mM borate buffer pH8.0 for 15 min (Yamashita, 2007). For DAB staining sections were incubated in 3% H_2O_2 (Sigma) for 10 min to quench endogenous peroxidases, followed by three washes with PBS. With all fixation methods sections were loaded into Shandon Sequenza slide racks. Tissues were permeabilised in 0.1% triton X-100 (Sigma) in PBS for 30 min, washed twice in PBS/0.02%BSA and incubated in 6M guanidine hydrochloride to denature the proteins (Peranen et al., 1993). After washing the slides 3x with PBS/BSA sections were incubated in 10% serum from secondary antibody host in PBS/BSA for 30 min. Slides were incubated with the following primary antibodies in PBS for 16-18h: GPR50 (1:50), Nogo-A (1:100), CDH8 E61 (1:100), ABCA2 (1:500), 5-HT (1:250), Vimentin (1:250), NeuN (1:1000), GFAP (1:500), O4 (1:500), Dopamine Beta-Hydroxylase (DBH, 1:250), Tyrosine Hydroxylase (TH, 1:250). Slides were washed 3x with PBS/BSA before and after incubation with secondary antibodies.

For chromogenic detection of proteins biotinylated rabbit anti-goat (DAKO) was used at 1:500 for 30 min followed by ABC elite (Vector labs) for 30 min. Slides were removed from the sequenza and proteins were visualised by incubation with DAB (Vector labs). After counterstaining in Harris haematoxilin and lithium carbonate, slides were dehydrated in 70% and 100% EtOH and xylene. Coverslips were then mounted onto slides using pertex. For fluorescent detection slides were incubated for 1 hour with donkey anti-sheep (1:500, Alexafluor 488, Invitrogen) and donkey anti-rabbit (1:500, Alexafluor 594) of donkey anti-mouse (1:500, 594) in

PBS/BSA. Coverslips were mounted onto slides using Vectashield w/DAPI (Vector labs).

3.2.6 Imaging and semi-quantitative evaluation of regional expression

Confocal images of neurons were captured sequentially (line) on an Olympus Fluoview 1000 confocal laser-scanning microscope (UPlanSApo 10, 20 or 40x objective) at image size 1024x1024 using Kalman filter mode 3. Brightfield images were taken on an Olympus BX light microscope fitted with 4x, 10x, 20x and 40x objectives. Secondary antibody controls were performed by leaving out the primary antibody. Sections were compared to the adult coronal reference atlas of the Allen Brain Atlas: http://mouse.brain-map.org (Lein et al., 2007) (see supplementary images 1-6 from Allen Brain Atlas). For the visual evaluation of relative expression levels, each brain region was evaluated for DAB and fluorescence staining intensity based on the following scale: x, not investigated; –, no expression present; +, weak expression; ++, moderate expression; +++, strong expression.

3.3 Results

3.3.1 Subcellular fractionation of adult mouse brain

The colocalisation studies in primary cortical neurons (Chapter 2) suggest GPR50 and interaction partners are expressed at synaptic sites, while immunocytochemistry in HEK293 and SH-SY5Y cells indicated co-localisation in the plasma membrane, ER and endolysosome. To further investigate this and to identify the subcellular location of Gpr50 expression, subcellular fractionation of whole adult mouse brain including postsynaptic density (PSD) fractions 1-3 (Carlin et al., 1980; Cho et al., 1992; Niethammer et al., 2000; Clapcote et al., 2007) was performed (Figure 3.5A). The postsynaptic density is a cytoskeleton specialization at synapses. PSDs are usually composed of neurotransmitter receptors, molecular scaffolding molecules, cell adhesion molecules and a diverse set of other signalling proteins. The PSD is commonly studied in relation to molecular mechanisms of learning and memory, which are believed to take place at the synapse. In this experiment three different PSD fractions were extracted. The more detergent resistant/insoluble the fractions are (Two-Triton (PSD2)) and especially One-Triton plus Sarcosyl (PSD3)), the closer they are to the core of the PSD.

Western blotting of fractions (Fig 3.5B) shows that Gpr50, Nogo-A, Cdh8 and Abca2 are present in the homogenate, crude synaptosome (P2), light membrane (P3, includes ER, golgi, endolysosome) (Fig3.5B) fractions, and in the ER/Golgi-fraction of the crude synaptosome (ER/Golgi, Fig 3.5B), although Gpr50 is expressed at low levels in these fractions. GPR50 does not appear to be expressed in myelin, as is known for Nogo-A (Chen et al., 2000), suggesting it is not expressed by oligodendrocytes (Fig 3.5B).

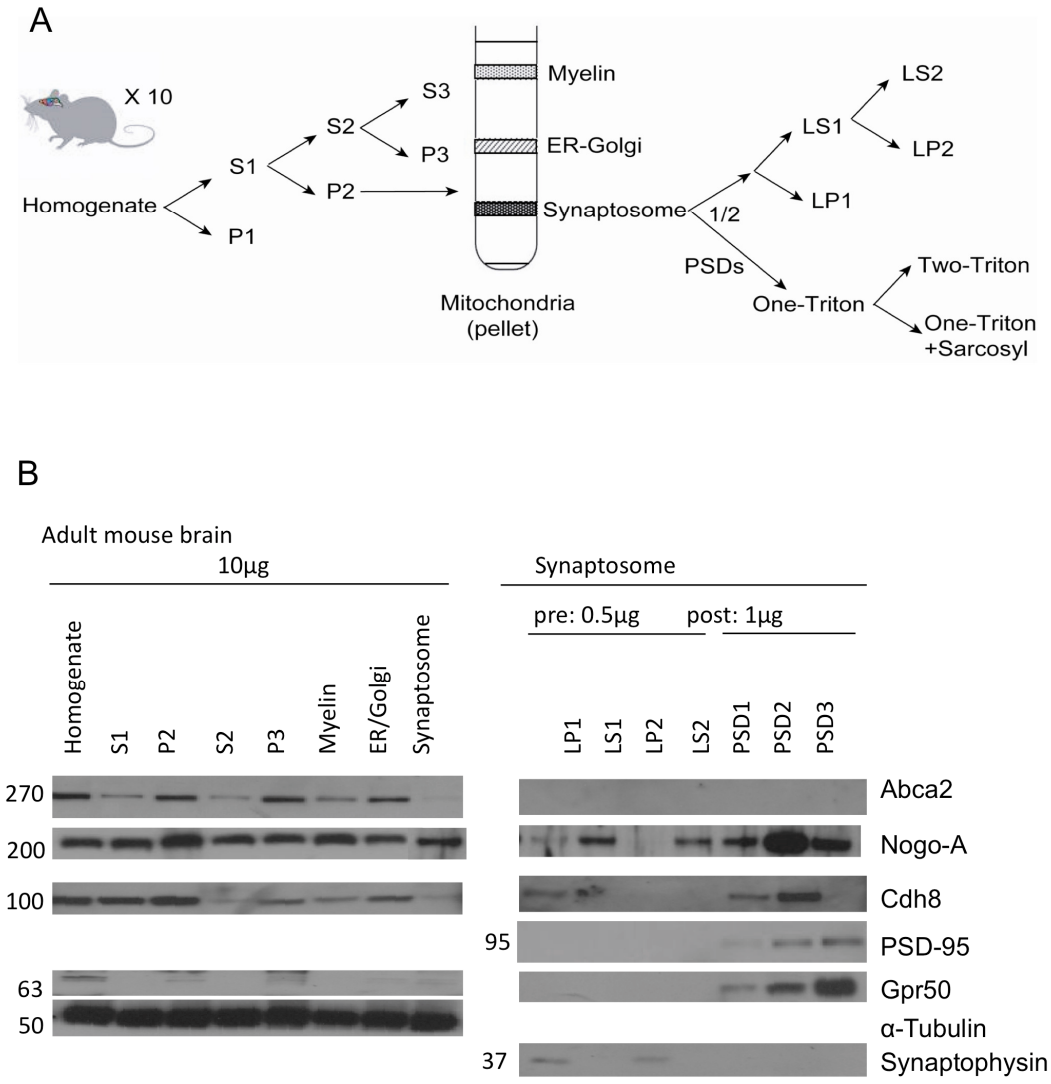

Figure 3.3 *GPR50 and interactors are enriched at the synapse after subcellular fractionation. (A) Subcellular fractionation protocol. Ten adult female mouse brains were homogenized and the homogenate (H) was subjected to multiple centrifugation steps, resulting in: the crude synaptosome (P2); light membranes (P3); myelin; ER-Golgi; synaptosome; synaptosomal membrane (LP1); (LS1) which consists of synaptosomal cytosol (LS2) and synaptic vesicle enriched fraction (LP2); and the three postsynaptic density fractions, PSD1 (One -Triton), PSD2 (Two-Triton), PSD3 (One-Triton + Sarcosyl). Western blotting of subcellular fractions shows enrichment of Gpr50, Nogo-A and Cdh8 in some or all of the post-synaptic density fractions, mainly the Two-triton fraction. Nogo-A and Cdh8 are also enriched pre-synaptically in the presynaptic membranes (LP1) and presynaptic vesicles (LP2). Controls were PSD-95, which is known to be enriched in the postsynaptic density, and Synaptophysin, which is enriched presynaptically. A-tubulin was used as a loading control. Figure published in part in Grünewald et al., 2009. Molecular and Cellular Neuroscience. Copyright Elsevier 2009.*

Interestingly Gpr50 is enriched in all of the PSD fractions, as indicated by the presence of postsynaptic density marker PSD-95 (Fig 3.5B) (Grünewald et al., 2009). Neuronal Nogo-A is ubiquitously expressed in almost all the fractions, including the PSD and the synaptosomal membrane (LP1) and the synaptic vesicles enriched (LP2) fractions (Fig 3.5) (Grünewald et al., 2009), as indicated by presynaptic marker synaptophysin. Neuronal Nogo-A has previously been reported to be present both pre- and postsynaptically in the developing or adult rat hippocampus (Lee et al., 2008; Grünewald et al., 2009). Cdh8 was also found to be enriched in the presynaptic membrane fraction and in the postsynaptic density fractions (Fig 3.5), in line with its previously detected localisation at synaptic junctions and suggested role in cell-cell adhesion at synaptic contacts (Suzuki et al., 2007), Although Abca2 was detected at low levels in the crude synaptosome, the Abca2 antibody appeared not sensitive enough to detect expression in the individual pre- and postsynaptic density fractions or it was not enriched in these fractions (Fig 3.5).

In addition to confirming a light membrane localisation for Gpr50, Nogo-A, Cdh8 and Abca2, this study identifies the synapse as a likely location for the interaction of these proteins.

3.3.2 Developmental expression of Gpr50 and interactors by rt-PCR

3.3.2.1 Primer design and optimisation

The primers used in this study (Table 3.1) were selected using Primer3 software version 0.4.0 (http://primer3.sourceforge.net/), except for reference gene *β-actin*, which came supplied with the cDNA panel (Origene). Among the selection criteria were: size between 100-200 bp, spanning an intron, balanced melting temperature (approx. 60ºC) and similar G-C content (between 20-80%). The primers used in this study and the parameters are shown in Table 3.1. To assess the quality of the primers several curves were generated in the Biorad iCycler, using mouse brain cDNA as template, after 35 cycles. 10-fold dilution ranges of template were used to determine the linear range of the primers. Samples that differ by a factor of 2 in the original

concentration of cDNA would be expected to be 1 cycle apart. Therefore each 10-fold dilution should result in a threshold cycle increase of 3.3 (see Fig 3.2A). After the real-time PCR amplification a melt curve is generated by raising the temperature a fraction of a degree and measuring the change in fluorescence (Fig 3.2B). At the melting point, the two strands of DNA will separate and the fluorescence rapidly decreases. Primer-dimer artifacts are a problem when measuring total DNA synthesis and one needs to be sure that a C*t* is measured due to the real target for amplification. To reduce primer-dimer artifacts Tm and primer concentrations were varied during optimisation. In addition, the linear range and PCR efficiency (90-110%) of each primer pair was determined by producing standard curves (Fig 3.2 C), of three replicates.

After optimization of the primers each PCR reaction generated a single amplicon (clear peak) as shown by the melting temperature profiles, and a good linear range, and correlation coefficient as shown by the standard curves generated by the iCycler (Table 3.1). As is expected from the literature there was quite some variability in abundance levels (Ct values) between genes (Table 3.2). The average delta-Ct value (35-Ct, ± SE) varied from 4.642 (± 0.270, Gpr50, lowest) to 12.403 (± 0.274, Nogo-pan, highest).

3.3.2.2 Selection of housekeeping genes

Although housekeeping gene *β-actin* was provided with the panel it is recommended to use more then one reference gene for normalisation (Vandesompele et al., 2002). Ideally a reference/housekeeping gene with a similar abundance level for accurate normalization is used. Therefore we choose several reference genes with varying abundance levels. Ideally these genes are also from different functional classes (Vandesompele et al., 2002). The number of reference genes necessary is dependent on how stable the reference genes are expressed in a specific sample, but there is a trade off between accuracy and practicality, as the number of target genes tested and the amount of cDNA available are also important. Vandesompele et al. (2002) recommend the minimal use of 3 reference genes and it was therefore decided to test a total of 4 reference genes, *Beta-actin* (provided with Origene panel), *TATA-binding*

protein (*Tbp*), *hydroxymethylbilane synthase* (*Hmbs*) and *Cyclophilin* (see Table 3.3), for stability. These genes were selected because their variation in abundance levels and function. *β-actin* is a high expressor with an average delta-Ct (35-Ct) value of 17.57 (±0.28), *Cyclophilin* has an average delta-Ct of 12.34 (±0.23), whereas *Hmbs* and *Tbp* expressed at lower levels, ΔCt = 8.49 (±0.29) and 8.12 (±0.41) respectively (Fig 3.3; Vandesompele et al., 2002).

We used geNorm, a freely available collection of VBA macros for Microsoft Excel to determine the most stable reference (housekeeping) genes (http://medgen.ugent.be/~jvdesomp/genorm/) from our set of 4. The most stable reference genes were determined by comparing the gene-stability measure (M) of these genes. The pairwise variation (V) between multiple reference genes determines how many genes should be included as a reference gene (for equations and calculations see Vandesompele et al. (2002)).

In our set Hmbs and Cyclophilin are the most stable and Tbp the least stable reference gene (Fig 3.4A). The authors suggest a cut-off value of V=0.15 between a selection of reference genes, if V>0.15 an extra reference gene should be included, provided it lowers the variation. After calculation of M and V using the geNorm applet, the pairwise variation of 2/3 strongest genes is 0.246 and when including Tbp $V^{3/4}$= 0.2, which suggests all 4 are required for accurate normalization (See Fig 3.4B). Ideally more reference genes should be added, however we decided that 4 reference genes was sufficient, as we are only testing 7 different genes and the cDNA panels were costly. This is in line with the recommendations of Vandesompele et al. (2002).

Gene name	Forward primer	Reverse primer	Size/Genomic	%GC	Tm	Correlation coefficient	ΔCt average	STDEV
Gpr50	TGGCTGTGACCAAGAACAAG	GTGACCAACCCGACCATC	172/2694 bp	50-61	63	0.982	3.625	1.20
Nogo-pan	TTGGCCCTGCTCTCTGTG	CCAATTCCTCTGATATGGCAAC	130/2649bp	45-61	63	0.992	12.403	0.68
Nogo-A	GGCTCGGGCTCAGTGG	CAGGACAGATGGGAAATCCTC	147/12806 bp	52-75	60	0.989	11.781	0.76
Nogo-C	GGCAAGAAATGGACGATCAG	AAGCTGGCACCAAACACC	103/14,853 bp	50-56	63	0.989	6.772	2.87
Cdh8	TGAGCCGCTCCAAAAGAG	TTGTGCCAGCTCCATCAC	156/121,178bp	56	63	0.989	9.153	0.97
Abca2	TTCATCCCGCTTGTCCTC	ATCAGGGCAAAGCGACTG	141/1148 bp	56	63	0.99	6.293	1.81
Srebf2	AGCCCGTCACCATCCAG	GGTCAACACAAGGGAATCTGTC	185/1654 bp	50-65	63	0.987	8.318	1.16
Control genes								
Actin-B	GATCTGGCACCACACCTTCTAC	TGGATGGCTACGTACATGGCTG	159/613bp		55	1.000	17.458	0.75
Tbp	GCCAGACCCCACAACTC	ACAGCCAAGATTCACGGTAG	182/2877 bp	50-64	60	0.991	8.115	1.01
Hmbs	CTGAAGGATGTGCCTACCATAC	AAGGTTTCCAGGGTCTTTCC	122/1084 bp	50	63	0.999	8.491	0.74
Cyclophilin	GGAGATGGCACAGGAGGAAA	CCCGTAGTGCTTCAGCTTGAA	75 bp/-	55-52	65	0.998	12.341	0.76

Table 3.1 *Primers and parameters used in this study. Shown are primer name, sequence of forward and reverse primer, cDNA/genomic DNA size (bp), GC%, Tmelt, calculated correlation coefficient from optimized primers, Average Ct value and STD error.*

Region	Gpr50	STD E	Nogo-pan	STD E	NogoA	STD E	NogoC	STD E	Cdh8	STD E	Abca2	STD E	Srebf2	STD E
E13														
Prosencephalon	3.933	0.252	11.185	0.245	10.58	0.015	3.395	0.795	7.585	0.355			5.055	0.745
Mesencephalon	4.770	0.124	11.755	0.005	11.49	0.135	5.105	0.995	8.69	0.01	6.08	0.015	8.55	0.02
Rhombencephalon	4.118	0.255	12.135	0.445	11.583	0.24	5.955	0.125	7.82	0.17	2.86	0.19	7.735	1.055
Spinal Cord	3.590	0.077	12.225	0.185	11.657	0.35	4.765	0.335	8.24	0.03	4.5	0.01	9.06	0.97
E15														
Telencephalon	2.553	0.316	11.695	0.375	11.217	0.28	4.22	0.37	8.91	0.56	3.125	0.245	7.66	0.59
Diencephalon	7.280	0.141	14.67	0.12	14.143	0.08	6.305	0.295	11.665	0.355	6.285	0.075	10.41	0.3
Midbrain	3.550	0.171	12.23	0.22	11.9867	0.11	4.52	0.46	10.455	0.515	5.33	0.23	7.75	0.74
Pons	5.680	0.190	12.575	0.505	12.737	0.03	4.49	0.31	9.995	0.355	5.245	1.245	7.695	0.185
Medulla	3.810	0.246	12.71	0.08	12.953	0.03	4.885	0.435	9.23	0.4	4.96	0.13	8.97	0.3
Spinal Cord	4.228	0.472	12.7	0.28	12.616	0.005	3.695	0.355	9.73	0.5	4.825	1.145	7.335	1.805
E18														
Frontal Cortex	4.937	0.786	12.82	0.2	12.38	0.13	2.89	0.28	9.075	0.495	4.61	1.32	7.755	0.875
Posterior Cortex	4.178	0.234	13.035	0.095	12.273	0.135			9.285	0.165	6.85	0.41	8.56	1.06
Entorhinal Cortex	2.440	0.296	12.36	0.12	11.87	0.075	2.14	0.5	8.815	0.065	4.275	0.175	6.445	0.255
Olfactory Bulb	3.435	0.370	12.135	0.055	11.326	0.15	3.365	0.475	8.97	0.85	3.64	0.4	7.3	0.15
Hippocampus	2.697	0.206	12.125	0.045	11.693	0.185	2.665	0.405	8.44	0.02	4.025	0.055	8.425	0.175
Striatum	4.143	0.131	13.08	0.39	11.43	0.04	2.655	0.565	9.645	0.075	4.855	0.535	7.895	0.335
Thalamus	6.615	0.362	12.935	0.105	12.613	0.02	4.245	0.105	10.36	0.04	6.22	0.45	7.68	0.49
Hypothalamus	7.893	0.275	13.175	0.105	12.36	0.185	4.535	0.965	9.87	0.25	7.06	0.22	8.56	1.03
Midbrain	5.780	0.212	12.155	0.035	11.966	0.03	3.355	0.635	10.365	0.405	5.935	0.145	8.035	0.075
Pons	4.563	0.408	11.76	0.31	11.167	0.04	3.3	1.6	9.815	0.145	5.215	0.935	6.685	1.095
Medulla	5.173	0.225	12.65	0.38	12.34	0.065	4.425	0.565	9.97	0.54	6.575	0.235	7.84	0.56
Spinal Cord	5.613	0.236	12.79	0.37	11.477	0.025	4.845	0.425	10.38	0.03	6.85		9.75	0.8
P7														
Frontal Cortex	4.048	0.341	12.795	0.215	12.607	0.04	8.01	0.07	10.62	0.05	6.92	0.49	9.22	0.37
Posterior Cortex	4.843	0.397	13.095	0.115	12.557	0.155	8.255	0.285	9.755	0.255	7.02	0.56	9.655	0.355
Entorhinal Cortex	1.740	0.301	11.055	0.385	10.777	0.66	6.15	0.23	8.69	0.27	4.365	0.195	7.82	0.22
Olfactory Bulb	4.760	0.309	12.145	0.015	11.857	0.17	7.73	0.25	8.445	0.135	6.255	0.025	8.035	0.105
Hippocampus	2.723	0.148	11.305	0.205	11.337	0.035	6.285	0.175	8.625	0.265	4.785	0.115	7.57	0.06
Striatum	4.268	0.149	12.32	0.05	11.723	0.04	9.42	0.14	9.935	0.035	5.72	0.19	7.545	0.175
Thalamus	4.708	0.498	12.29	0.25	11.787	0.31	7.275	0.065	9.435	0.205	6.735	0.185	7.855	0.335
Hypothalamus	6.665	0.227	12.84	0.03	12.31	0.045	8.53	0.34	9.44	0.43	5.275	0.425	8.765	0.365
Cerebellum	3.973	0.097	11.35	0.98	11.017	0.34	8.29	0.62	8.655	0.465	6.215	0.165	8.56	0.66
Midbrain	4.760	0.283	12.13	0.08	11.32	0.52	7.25	0.1	9.37	0.36	4.59	0.37	7.85	0.36
Pons	6.313	0.263	11.92	0.2	11.323	0.02	7.005	0.395	9.085	0.045	6.72	0.31	8.24	0.28
Medulla	4.175	0.241	11.965	0.455	11.756	0.33	7.545	0.385	8.655	0.005	6.63	0.28	11.435	3.865
Spinal Cord	5.500	0.159	12.54	0.23	11.853	0.31	5.27	0.27	8.255	0.145	6.055	0.355	8.695	0.095

Week 5														
Frontal Cortex	4.555	0.142	13.31	0.53	11.177	0.44	12.19	0.11	8.56	0.03	8.61	0.46	9.175	0.385
Posterior Cortex	1.885	0.215	11.01	0.42	10.433	0.54	10.435	0.185	6.59	0.59	4.655	0.405	7.14	0.04
Entorhinal Cortex	5.917	0.539	12.235	1.055	10.52	0.435	10.45	0.24	8.7	0.64	7.575	0.575	7.92	0.78
Olfactory Bulb	5.950	0.398	11.315	0.445	10.98	0.28	10.875	0.015	6.845	0.125	6.755	0.365	8.135	0.045
Hippocampus	5.623	0.198	13.185	0.595	11.74	0.38	10.72	0.08	9.64	0.51	10.28	0.89	8.775	0.235
Striatum	3.998	0.280	13.01	0.15	10.703	0.335	11.68	0.12	9.04	0.21	10.11	0.27	8.885	0.085
Thalamus	5.913	0.258	12.515	0.235	11.5	0.215	9.45	0.35	9.305	0.345	7.68	0.16	8.865	0.205
Hypothalamus	6.085	0.302	12.29	0.47	11.366	0.38	11.015	0.665	9.825	0.665	8.52	0.78	8.175	0.835
Cerebellum	3.450	0.294	13.125	0.385	11.193	1.11	10.45	0.96	10.165	0.365	9.185	0.445	7.92	0.8
Midbrain	4.795	0.253	12.715	0.085	11.243	0.17	10.125	0.195	8.715	0.015	9.105	0.475	8.28	0.23
Pons	5.660	0.148	12.67	0.31	13.057	0.27	9.705	0.325	8.78	0.02	8.8	0.44	12.23	2.61
Medulla	5.358	0.194	12.515	0.125	12.95	0.085	9.36	0.01	9.355	0.015	9.725	0.605	9.17	0.21
Spinal Cord	4.200	0.149	12.81	0.48	12.533	0.37	9.09	0.74	7.555	0.495	8.145	0.195	8.2	0.3
Average	**4.642**	0.270	**12.403**	0.274	**11.781**	0.215	**6.773**	0.390	**9.153**	0.271	**6.293**	0.389	**8.318**	0.575

Table 3.2 *Non-normalised delta Ct values (35-Ct, plus Standard Error) of Gpr50, Nogo-pan, Nogo-A, Nogo-C, Cdh8, Abca2 and Srebf2 after rt-PCR. There is a clear difference in abundance levels between the genes.*

Name	Accession Number	Function	Chromosomal location
B-Actin (Beta actin)	NM_007393	Cytoskeletal structural protein	Chromosome 5: 143,665,420-143,668,404
Tbp (TATA box binding protein)	NM_013684	General RNA polymerase II transcription factor	Chromosome 17: 15,636,852-15,654,391
Hmbs (Hydroxymethyl-bilane synthase)	NM_013551	Heme synthesis, porphyrin metabolism	Chromosome 9: 44,144,434-44,152,244
Cyclophilin (Peptidyl-prolyl cis-trans isomerase B (Ppib/CypB))	NM_011149	Cyclosporine-binding protein, associated with the secretory pathway	Chromosome 9: 65,908,062-65,914,428

Table 3.3 *Reference genes used in this study.*

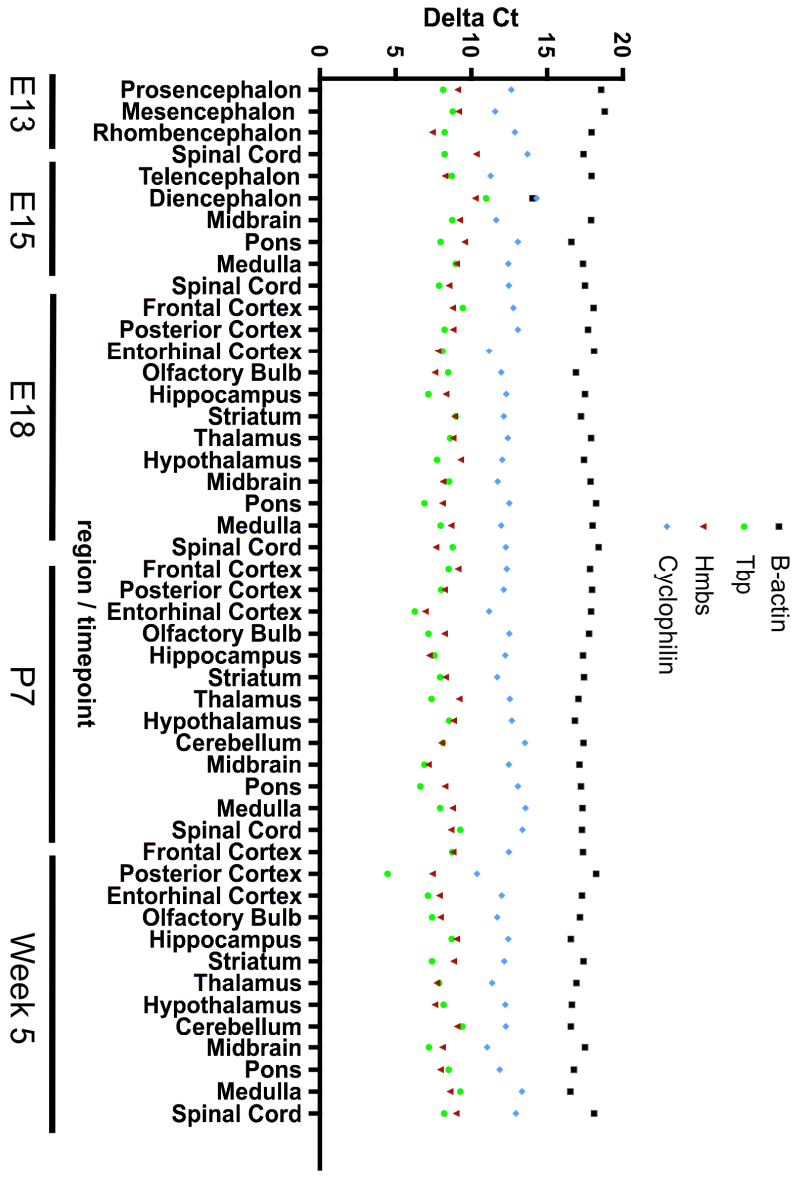

Figure 3.4 *Expression of the four control genes used in this study: Tbp, Cyclophilin, β-Actin and Hmbs. Graph 1 shows results from real time quantitative rt-PCR on Origene mouse developmental panel with 48 regional brain samples from 5 developmental stages: E13, E15, E18, P7, adult week 5. Quantification of non-normalised expression (in 35-CT values) indicates the variation in abundance levels between the genes. Variation within each gene is small.*

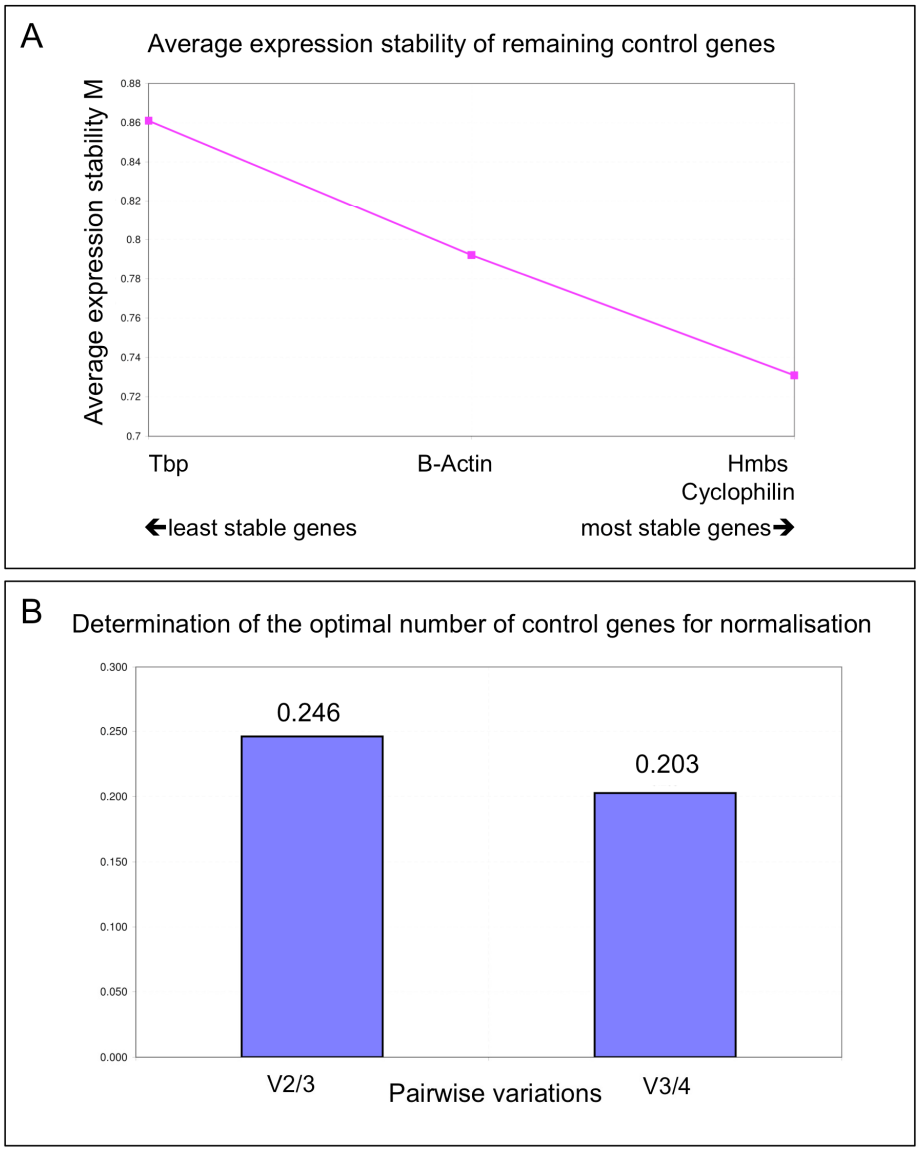

Figure 3.5 *Determination of optimum number of control genes using GeNORM. The optimum number of control genes was determined by calculating the expression stabitily (M, graph A) and pairwise variation (V, graph B) between the control genes using GeNORM (Vandesomepele et al., 2002).*

3.3.2.3 Normalised results

To determine where and when Gpr50 is expressed and available to interact with its interaction partners, rt-PCR was performed on a developmental mouse brain panel (Origene) covering 48 regional samples over 5 timepoints, E13, E15, E18, P7 and week 5. Data were normalised against four housekeeping genes with varying levels of expression (Ct value, Fig 3.3) to reflect the difference in expression levels between our genes-of-interest: *ß-actin, Tbp, Hmbs* and *Cyclophilin* (Table 3.3). Relative normalised expression of *Gpr50*, *Nogo-pan, Nogo-A, Cdh8* and *Abca2* are shown in Table 3.4 and visualised in Figure 3.6.

Gpr50 mRNA was detected in low levels from E13, peaked at E18 and increased again at week 5. At most developmental timepoints *Gpr50* appears to be localized to specific regions, with highest expression in thalamus, hypothalamus (diencephalon) and in the midbrain, pons and medulla (mesencephalon, rhombencephalon). *Gpr50* shows increased expression in frontal regions at 5 weeks only. *Nogo-A* mRNA expression is constant and was detected throughout all regions and timepoints. *Cdh8* expression is relatively constant but did show an increase in the posterior regions at E18 and frontal regions at P7. Both *Nogo-C* and *Abca2* expression is lower during development and increases at week 5. *Srebf2* expression was increased in spinal cord at E18, the medulla at P7 and the pons at week 5.

Region	Gpr50	Nogo-pan	Nogo-A	Nogo-C	Cdh8	Abca2	Srebf2
E13							
Prosencephalon	0.398	0.370	0.424	0.021	0.328		0.066
Mesencephalon	0.831	0.645	0.871	0.073	0.740	0.495	0.904
Rhombencephalon	0.545	0.918	0.984	0.137	0.454	0.062	0.511
Spinal Cord	0.141	0.377	0.395	0.024	0.226	0.071	0.548
E15							
Telencephalon	0.181	0.689	0.812	0.045	0.950	0.078	0.511
Diencephalon	0.812	0.933	0.771	0.025	0.740	0.087	0.527
Midbrain	0.286	0.787	1.024	0.042	1.907	0.255	0.426
Pons	0.942	0.702	1.150	0.028	0.975	0.165	0.276
Medulla	0.268	0.881	1.500	0.041	0.680	0.154	0.805
Spinal Cord	0.499	1.196	1.643	0.026	1.276	0.193	0.335
E18							
Frontal Cortex	0.637	0.992	1.062	0.011	0.639	0.127	0.347
Posterior Cortex	0.394	1.270	1.074		0.791	0.605	0.676
Entorhinal Cortex	0.202	1.398	1.522	0.014	1.088	0.204	0.268
Olfactory Bulb	0.285	0.794	0.718	0.021	0.811	0.090	0.342
Hippocampus	0.198	0.943	1.095	0.016	0.695	0.140	0.888
Striatum	0.360	1.232	0.576	0.010	0.930	0.151	0.394
Thalamus	2.570	1.267	1.449	0.033	1.679	0.430	0.390
Hypothalamus	7.015	1.620	1.302	0.042	1.310	0.797	0.777
Midbrain	1.768	0.885	1.204	0.023	2.146	0.454	0.640
Pons	0.906	0.823	0.893	0.028	1.912	0.355	0.302
Medulla	1.138	1.307	1.553	0.047	1.687	0.699	0.551
Spinal Cord	1.559	1.441	0.869	0.062	2.163	0.830	2.286
P7							
Frontal Cortex	0.368	1.085	1.375	0.384	1.886	0.651	1.143
Posterior Cortex	0.916	1.891	1.841	0.625	1.512	0.963	2.108
Entorhinal Cortex	0.187	0.795	1.146	0.311	1.562	0.336	1.101
Olfactory Bulb	0.931	0.983	1.252	0.476	0.715	0.627	0.687
Hippocampus	0.229	0.570	0.982	0.201	0.887	0.262	0.533

Striatum	0.604	1.050	1.070	1.372	1.708	0.411	0.453
Thalamus	0.651	0.799	0.869	0.256	0.971	0.627	0.433
Hypothalamus	2.220	0.980	0.987	0.474	0.782	0.191	0.684
Cerebellum	0.353	0.361	0.486	0.468	0.553	0.413	0.688
Midbrain	1.058	1.104	0.997	0.393	1.456	0.237	0.685
Pons	2.710	0.765	0.814	0.272	0.991	0.789	0.718
Medulla	0.360	0.509	0.697	0.251	0.486	0.478	4.830
Spinal Cord	0.799	0.662	0.620	0.046	0.315	0.273	0.564
Week 5							
Frontal Cortex	0.510	1.536	0.508	5.938	0.490	1.900	1.009
Posterior Cortex	0.323	1.189	1.415	8.384	0.643	0.630	1.047
Entorhinal Cortex	2.306	1.111	0.545	3.080	0.885	1.584	0.683
Olfactory Bulb	2.352	0.544	0.735	4.068	0.273	0.916	0.767
Hippocampus	0.939	1.168	0.618	1.865	0.810	4.806	0.639
Striatum	0.445	1.608	0.490	5.573	0.874	6.766	1.092
Thalamus	2.134	1.279	0.967	1.467	1.204	1.577	1.272
Hypothalamus	1.906	0.846	0.696	3.276	1.314	2.162	0.610
Cerebellum	0.169	1.000	0.386	1.397	1.012	2.087	0.314
Midbrain	1.163	1.857	1.016	2.864	1.033	5.042	1.025
Pons	1.364	1.110	2.087	1.340	0.666	2.549	10.883
Medulla	0.635	0.573	1.132	0.619	0.557	2.736	0.705
Spinal Cord	0.433	1.155	1.379	0.830	0.287	1.544	0.555

Table 3.4 *Normalised relative expression levels of Gpr50, Nogo-pan, Nogo-A, Nogo-C, Cdh8, Abca2 and Srebf2 after rt-PCR.*

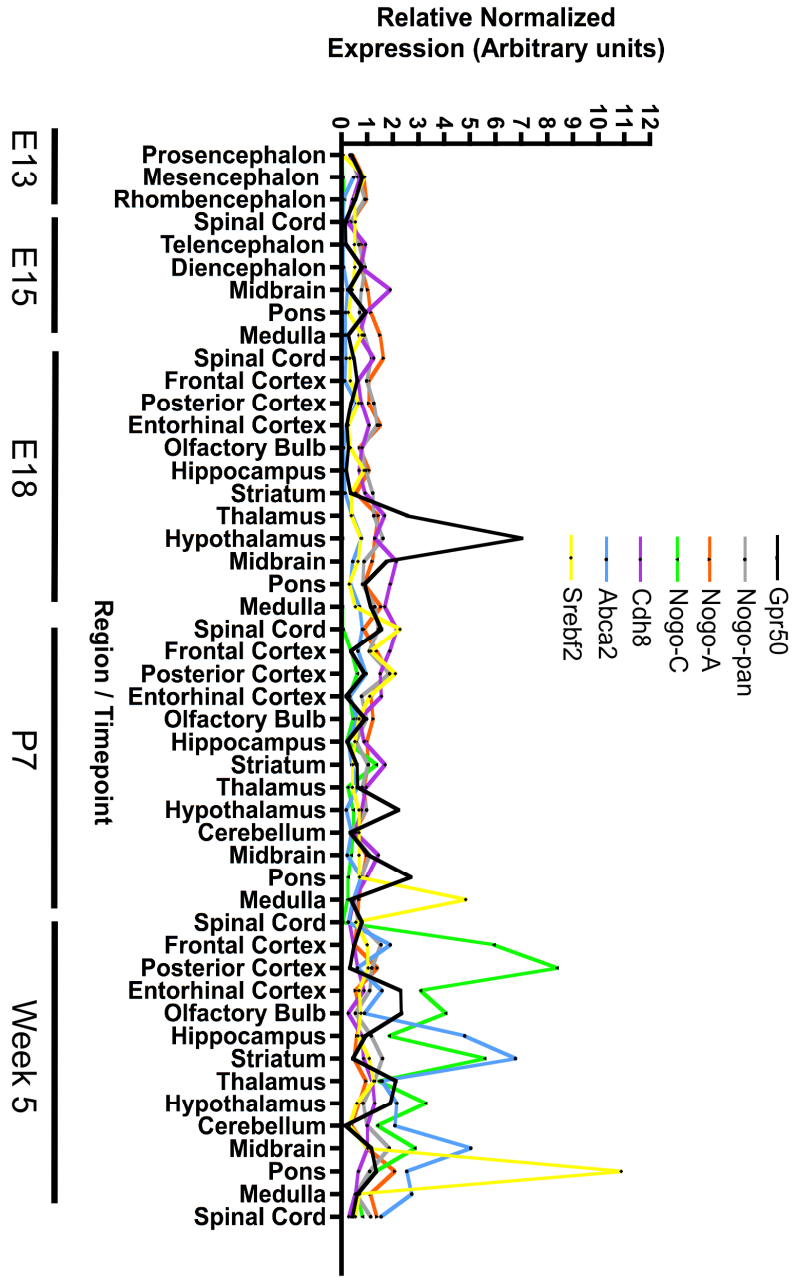

Figure 3.6 *Real-time quantitative rt-PCR on Origene mouse developmental panel with 48 regional brain samples from 5 developmental stages. Relative normalized expression values of Gpr50, Nogo-pan, Nogo-A, Nogo-C, Cdh8 and Abca2 normalised to b-Actin, Tbp, Hmbs and Cyclophilin B.*

The results suggest an increased expression of the genes around E18 and/or at 5 weeks, indicating possible co-regulation. Spearman correlations (r) were performed of the overall data (between the genes for all regions and ages, using the above genes plus *Nogo-pan* (detecting *Nogo-A, -B* and *–C*) (Fig 3.7). *Gpr50* correlates significantly with *Abca2* (Spearman's r (95% confidence interval); *p*-value): (r=0.43 (0.15-0.64); *p*=0.0028). Other significant correlations are *Nogo-pan* with *Cdh8* (r=0.39 (0.11-0.61); *p*=0.0068), *Nogo-pan* with *Abca2* (r=0.40 (0.12-0.62); *p*=0.0058), *Nogo-A* with *Cdh8* (r=0.32 (0.03-0.56); *p*=0.0268), *Nogo-C* with *Abca2* (r=0.77 (0.62-0.87); *p*<0.0001) and *Nogo-C* with *Srebf2* (r=0.55 (0.30-0.73); *p*<0.0001). As expected *Nogo-pan* correlates with *Nogo-A* (r=0.37 (0.09-0.60); *p*=0.0097). *Nogo-pan* does not correlate with *Nogo-C*, which is likely caused by the relative absence of *Nogo-C* at embryonic stages compared to *Nogo-A*.

Because Gpr50 shows increased expression around E18, Spearman correlations were calculated for age E18 only (Fig 3.8). At this timepoint *Gpr50* correlates significantly with *Nogo-C* (r=0.69 (0.14-0.92); *p*=0.0186), *Cdh8* (r=0.64(0.09-0.89); *p*=0.024) and again with *Abca2* (r=0.71(0.20-0.91); *p*=0.0102). Other significant correlations were found between Nogo-pan and *Abca2* (r=0.71 (0.20-0.91); *p*=0.0102), between *Nogo-C* and *Cdh8* (r=0.75 (0.24-0.93); *p*=0.0085), *Nogo-C* and *Abca2* (r=0.83 (0.43, 0.96); *p*=0.0015), and between *Cdh8* and *Abca2* (r=0.68 (0.15-0.90); *p*=0.0153). By contrast, no significant correlations were found at week 5. These results indicate possible co-regulation between Gpr50 and Abca2 overall and Nogo-C and Cdh8 at E18 only.

The rt-PCR results show an upregulation of Gpr50 and its interactors at E18 and week 5. Although the manufacturer of the cDNA panel describes week 5 as an adult stage this is generally considered adolescence in rodents, which is from weaning at postnatal day (P) 21 to P60 (Laviola et al., 2003; Hefner and Holmes, 2007). Adolescence in rodents can be further classified into *early* adolescence (prepubescent or juvenile, P21 to P34), *middle* adolescence (periadolescent, P34 to P46), and *late* adolescence (young adult, P 46 to 59) (Laviola et al., 2003). The rt-PCR results

suggest the late gestation (E18) and adolescent stages are important functional timepoints. These ages are relevant to mental illness, as E18 has been found to be an important developmental timepoint for processes of synapse formation and function, axon growth and guidance and survival and growth (Hinds and Hinds, 1976; Matsuki et al., 2005), processes that have been linked to the pathophysiology of psychiatric illness (Benes and Berretta, 2001; Coyle and Duman, 2003; Eastwood et al., 2003). Adolescence and early adulthood are generally when the first psychiatric symptoms (onset) occur (Joyce, 1984; Loranger, 1984).

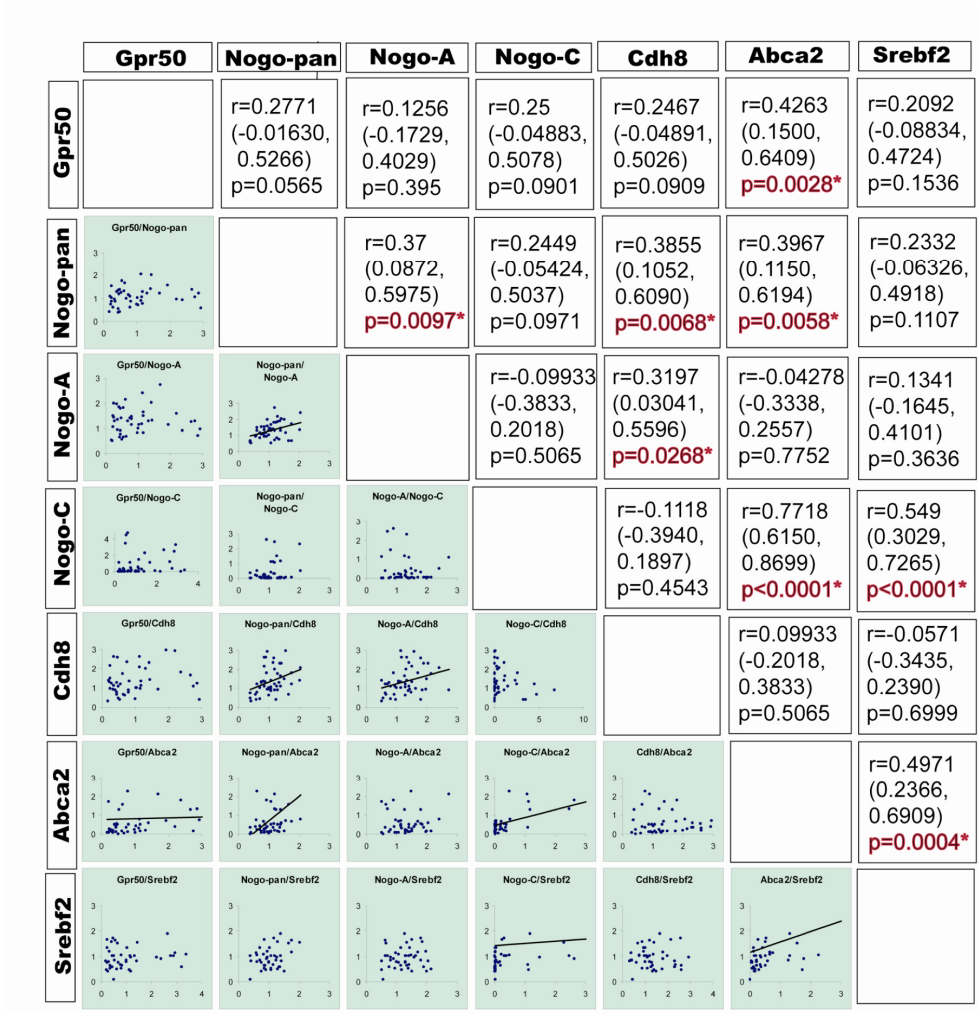

Figure 3.7 *Spearman correlations between rt-PCR data of all genes across all regions and timepoints. Data and correlation matrix were generated using Graphpad Prism and StatistiXL.*

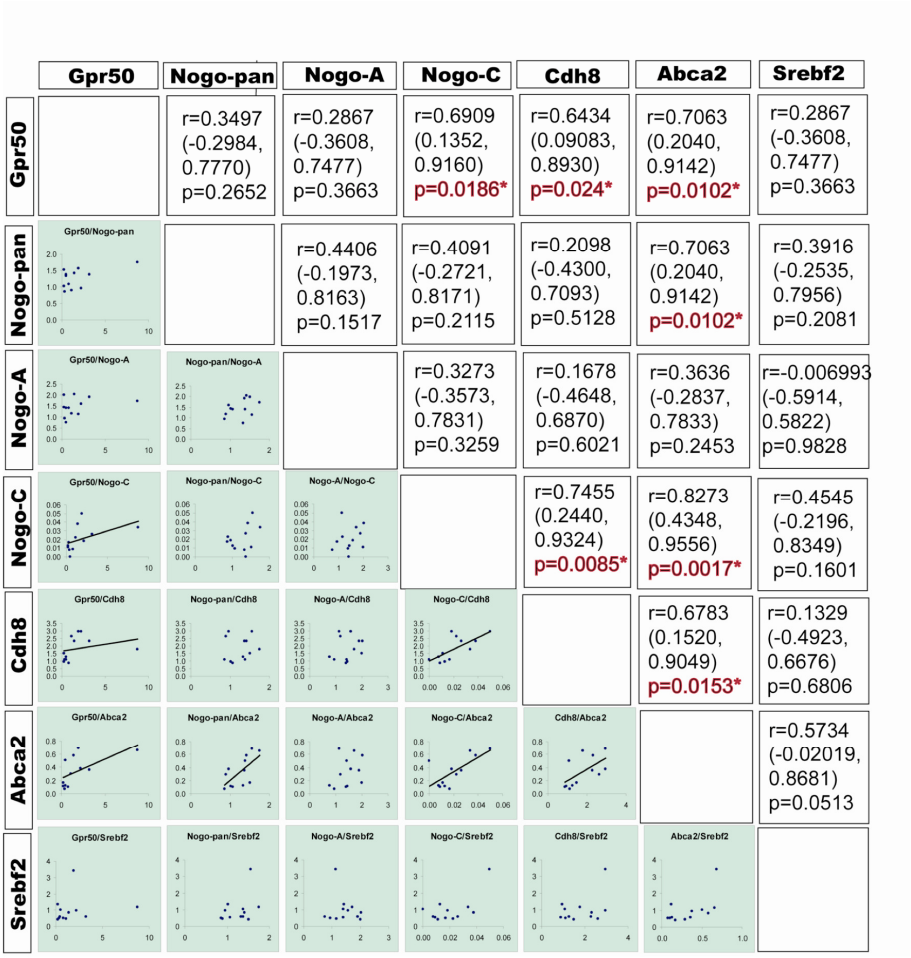

Figure 3.8 *Spearman correlations between rt-PCR data of all genes across all regions at E18 only. Data and correlation matrix were generated using Graphpad Prism and StatistiXL (Microsoft). Data and correlation matrix were generated using Graphpad Prism and StatistiXL.*

3.3.3 Expression of GPR50 and interactors by immunohistochemistry

Next we wanted to follow up the rt-PCR results at the protein level, by performing immunohistochemistry in the mouse brain. The rt-PCR results suggest E18 is an important developmental timepoint for Gpr50. We wanted to compare this to expression in the adult brain. Therefore the expression of Gpr50, Nogo-A, Cdh8 and Abca2 was investigated in 8-12 week old adult as well as E18 mouse brains.

3.3.3.1 Optimisation of tissue fixation

Several methods of tissue fixation are commonly used with 4% formaldehyde (or 10% formalin) the most common. Formaldehyde fixation however cross-links proteins with loss of antigenicity. Antigen retrieval methods are used afterwards to improve antibody sensitivity and reduce background staining, but these normally involve boiling tissues with possible loss of cell architecture. Fresh frozen tissue is also commonly used as it has improved antigenicity, but tissues are less rigid and stay less intact when compared to formaldehyde. Other commonly used fixatives are organic solvents, such as ethanol, methanol, acetone, acetic acid or a mixture of these. Heat-induced antigen retrieval is not necessary with these fixatives so antigenicity, tissue structure and cell architecture may be better preserved.

In initial trials on 4% formaldehyde fixed tissues the GPR50 G-15 antibody did not appear to give a reliable signal, even at 1:50 dilution, with standardised protocols in the lab. Trials with fresh frozen tissues fixed in acetone did produce a better signal but the tissues were damaged almost beyond recognition and were not suitable for the investigation of expression in specific nuclei. The standardised lab protocols all used 4% formaldehyde or 10% formalin fixed tissue with antigen retrieval in citrate buffer pH6.0, without further tissue permeabilisation. Kim et al (2004) tested several antibodies with different antigen retrieval buffers and noted that buffers at a higher pH of 8-9.5 often yield better results (Kim et al., 2004). Therefore a 50mM borate

buffer at pH8.0 was tested. In addition, pretreatment of the tissues with denaturant guanidine HCl/50mM tris buffer pH 7.5 for 10 min after permeabilisation with 0.1% triton X-100 for 30 min was tried (Peranen et al., 1993). These treatments improved GPR50 staining considerably, but were still not entirely satisfactory (Fig 3.9A).

Therefore fixation with 70% EtOH and Methacarn were also tested (see Materials and Methods). With these fixatives Gpr50 staining was found in similar areas but antigenicity was much improved (hypothalamic region, Fig 3.9B-C). The cytoarchitecture appeared better preserved and nuclei were counterstained more clearly then after formalin fixation. It was therefore decided to continue the study with adult and E18 brains fixed in 70% EtOH and methacarn. Secondary antibody controls showed minimal reactivity in the absence of the primary antibody (Fig 3.10A-B).

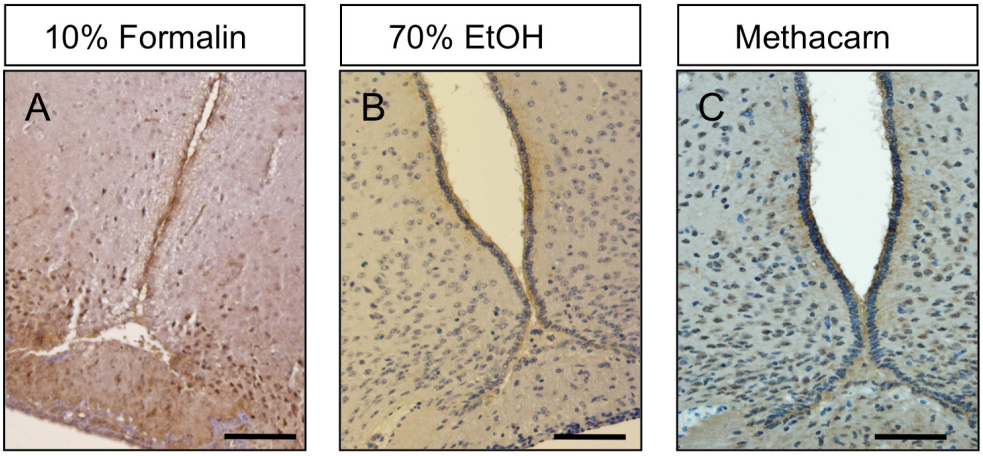

Figure 3.9 *Effects of fixation methods on Gpr50 immunostaining. Adult female CD brains were immerse fixed in either 10% formalin (A), 70% EtOH (B) or Methacarn (C), before being paraffin embedded. The section above includes the hypothalamus around the 3rd ventricle, where Gpr50 is known to be expressed. Formalin fixed tissues were subjected to picric acid treatment and antigen retrieval by boiling in borate buffer Ph 8.0 for 15 min. All sections were pretreated with 6M GndHCl/50mM Tris buffer pH7.5 before staining with GPR50 G-15 (1:50). Sections were counterstained with haematoxilin and lithium carbonate. Scale bars 100 µm.*

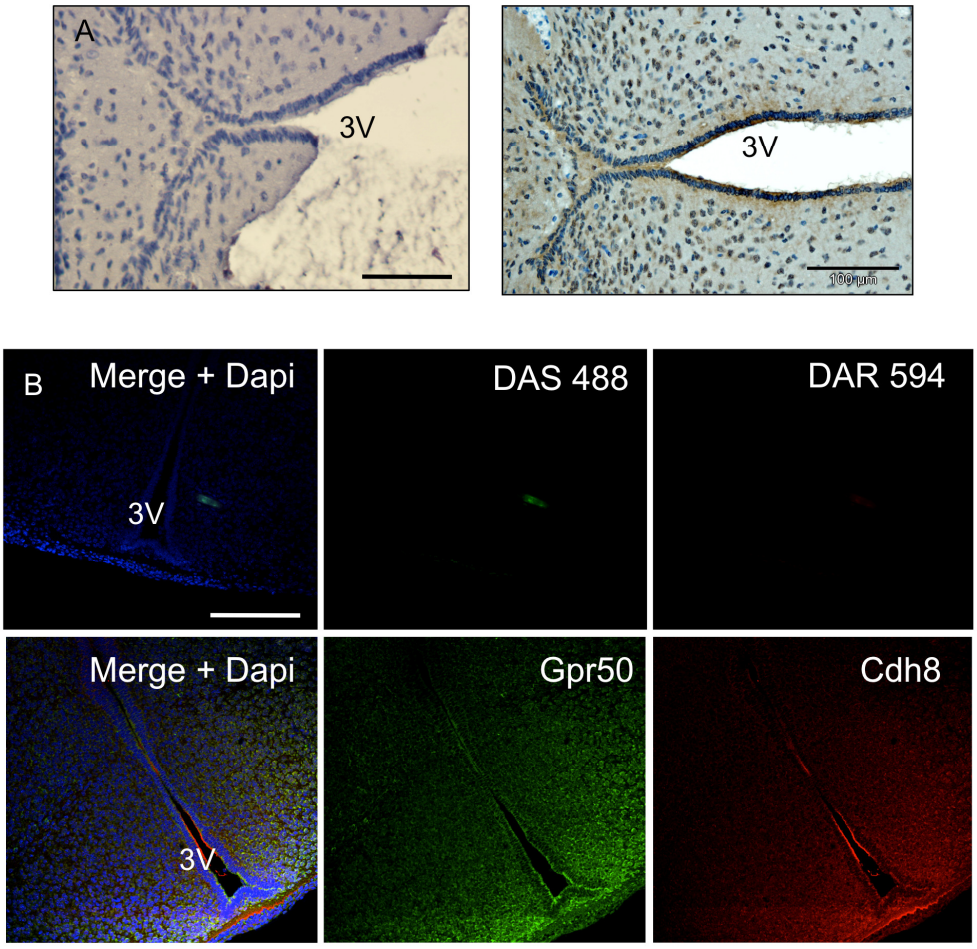

Figure 3.10 *Secondary antibody controls. (A) Chromogenic detection of biotinylated rabbit anti-goat (DAB). Methacarn fixed mouse adult brain tissue was probed with secondary antibodies only (left) of with Gpr50 (1:50, right). (B) Fluorescent detection with Alexafluor 488 (green) and 594 (red). Methacarn fixed mouse E18 brain tissue was stained with Donkey anti-sheep (DAS) and DAR=donkey anti-rabbit (DAR) secondary antibodies only (top) or with Gpr50 (1:50) and Cdh8 (1:100). Sections were counterstained with Harris haematoxilin (A) or Dapi (B). Scale bars: 100 µm.*

3.3.3.2 Gpr50 is expressed in several regions and levels in the brain

In order to find out more about subregional expression and to see if our proteins of interest are coexpressed at the cellular level, immunohistochemistry was performed in the adult and E18 mouse brain. In accordance with the rt-PCR results the coronal planes containing the hypothalamus and 3rd ventricle, the midbrain, pons, medulla and cerebellum were investigated (see materials and methods for details and supplementary figures for Allen Brain Atlas images of the regions studied). Both chromogenic and fluorescent detection methods were used. The relative normalised expression levels of *Gpr50* mRNA as measured by rt-PCR and levels of protein expression as detected by immunohistochemistry in E18 and adult mouse brain are summarised in Table 3.5. As was previously reported (Drew et al., 2001) and in agreement with the rt-PCR data, Gpr50 is highly expressed in the hypothalamus around the 3rd ventricle, the amygdala, amygdalar or piriform cortex, and the entorhinal and somatosensory cortices. Hippocampal expression of GPR50 was detected on the midbrain level in the adult brain only, in the polymorph layer of the dentate gyrus. At the midbrain level GPR50 is also expressed in the cortex and in agreement with the rt-PCR data the ventral pons. Gpr50 appeared to be moderately expressed in the ventral midbrain, in the substantia nigra pars compacta. If we look at more posterior regions in the brain Gpr50 expression is also found at low levels in the midbrain and pontine raphe nuclei, the cortex and the superior colliculus. In the pons and medulla Gpr50 is moderate to highly expressed in several brainstem nuclei, including the locus coeruleus. Gpr50 expression is also found in the inferior colliculus and in low levels in the Purkinje cell layer of the cerebellum (Table 3.5, for detailed images see 3.3.3.3 and further). There was much agreement in protein expression levels as measured by chromogenic and fluorescence detection except for the substantia nigra, which showed much clearer Gpr50 expression when using a HRP secondary antibody and DAB than when using fluorescent secondary antibodies (Fig 3.11). This perhaps reflects the relative sensitivity of these methods (Morris, 1991).

Region	Gpr50 mRNA	Gpr50 protein	Nogo-A	Cdh8	Abca2
E18					
Frontal Cortex	0.637	+++	Y	Y	N
Posterior Cortex	0.394	+++	Y	Y	N
Entorhinal Cortex	0.202	x	x	x	x
Olfactory Bulb	0.285	x	x	x	x
Hippocampus	0.198	-	N	N	N
Striatum	0.36	-	N	N	N
Thalamus	2.57	++	N	N	N
Hypothalamus	7.015	+++	N	Y	N
Midbrain	1.768	+	N	N	N
Pons	0.906	+	Y	Y	N
Medulla	1.138	++	Y	Y	N
Spinal Cord	1.559	x	x	x	x
Week 5/10					
Frontal cortex	0.51	x	x	x	x
Posterior cortex	0.323	x	x	x	x
Motor cortex		+	Y	N	Y
Somatosensory cortex		++	Y	N	Y
Visual cortex		++	Y	N	Y
Entorhinal cortex	2.306	++	Y	N	Y
Piriform cortex		++	Y	N	Y
Olfactory Bulb	2.352	x	x	x	x
Hippocampus	0.939				
dentate gyrus medial blade polymorph layer		+	N	N	N
hippocampus other		-	N	N	N
Amygdala		++	Y	Y	Y
Striatum	0.445	-	N	N	N
Thalamus	2.134	++	N	N	N
Hypothalamus	1.906				
suprachiasmatic nucleus		++	N	N	N
paraventricular nucleus		+	Y	N	N
ependyma of 3rd ventricle		+++	N	N	Y
dorsomedial hypothalamus		++	Y	N	N
ventromedial hypothalamus		++	N	Y	Y
lateral hypothalamus		+	Y	N	N
arcuate nucleus		++	Y	N	Y
median eminence		++	N	N	Y
Cerebellum	0.169				
Purkinje cell layer		+	N	N	N
Cerebellum other		-	N	N	N
Midbrain	1.163				
superior colliculus		++	Y	N	Y
periaqueductal grey		+	N	N	N
substantia nigra		+/++	N	N	N
Pons	1.364				

raphe nuclei		+	N	N	N
locus coeruleus		+++	N	N	Y
mesencephalic trigeminal nucleus		+	Y	Y	Y
pontine grey		++	N	N	N
Medulla	0.635				
inferior colliculus		++	Y	N	Y
gigantocellular reticular nucleus		++	N	N	Y
magnocellular reticular nucleus		++	N	N	Y
parvicellular reticular nucleus		++	N	N	Y
principal sensory nucleus of the trigeminal		++	N	N	Y
Spinal Cord	0.433	x	x	x	x

Table 3.5 *Expression levels of Gpr50 in the mouse brain.*
Column1: Relative normalized Gpr50 mRNA expression levels as measured by rt-PCR at E18 and week 5. Column 2: semi-quantitative evaluation of Gpr50 protein expression after immunohistochemistry at E18 and the Week 10. Scale: x, not investigated; –, no expression present; +, weak expression; ++, moderate expression; +++, strong expression. Columns 3-5: Co-localisation of Gpr50 and Nogo-A, Cdh8 or Abca2 as measured by by immunohistochemistry. Scale: x, not investigated; Y, colocalisation detected; N, no colocalisation detected.

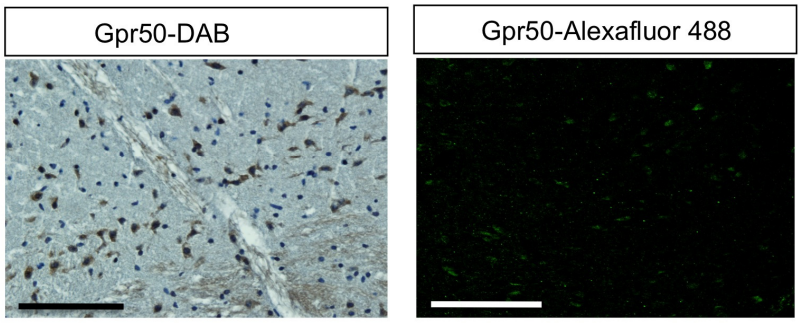

Figure 3.11 *GPR50 in the substantia nigra. Adult CD1 brains were fixed in 70% ethanol and stained with anti-GPR50. Both chromogenic (DAB, left) and fluorescent (Alexafluor 488, right) methods were used. These images show a midbrain section containing the substantia nigra. Section left was counterstained with haematoxilin. Scale bars: 100 µm.*

3.3.3.3 Gpr50 expression in different cell types

A few studies have investigated the specific cell type(s) that express GPR50. In the ependyma of the third ventricle Gpr50 is thought to be expressed by tanycytes as determined by location, morphology or co-labelling with tanycyte marker Vimentin (Garcia et al., 2003; Barrett et al., 2006; Sidibe et al., 2010) and by neurons in the dorsomedial hypothalamus (Sidibe et al.). However, in *Gpr50* knockout mice, β-gal expression driven by the *GPR50*-promotor stains the ependyma of the 3rd ventricle but did not co-localise with glucose transporter GLUT1, another marker for α- or β-tanycytes (Peruzzo et al., 2000; Berger and Hediger, 2001; Garcia et al., 2003), nor did the signal colocalise with astrocyte marker GFAP or neuronal progenitor and stem cell marker Nestin (Ivanova et al., 2008). There thus appears to be much uncertainly about the exact cell type expressing GPR50. As we identified novel regions of Gpr50 expression we carried out immunofluorescence colocalisation of Gpr50 with cell type markers NeuN (mature neurons), GFAP (astrocytes), O4 (oligodendrocytes) and Vimentin (tanycytes) in several regions in the adult and E18 mouse brain.

Gpr50 colocalises with NeuN in the ventral anterior hypothalamus (Fig 3.12A) and in the other areas of GPR50 expression, the cortex, midbrain, superior colliculus, pons, hippocampus and brain stem nuclei (Fig 3.13A-J). In the locus coeruleus colocalisation between Gpr50 and NeuN was not as clear (Figure 3.13J) but weak NeuN staining in locus coeruleus neurons has been reported before (Coelho et al., 2005). Gpr50 does not colocalize with GFAP, O4 or vimentin in any of these regions. Interestingly, no colocalisation was found with vimentin in the adult mouse brain (Fig 3.12B-C). In the anterior hypothalamus Gpr50 is present at the base of the ventricular ependyma but vimentin is expressed in the dorsal ependyma (Fig 3.12B). However more caudally in the hypothalamus, vimentin is expressed in the ventral ependyma, close to the median eminence, where Gpr50 was before but now Gpr50 has shifted dorsally (Fig 3.12C). When co-labelling with GFAP, some colocalisation is found on the lateral sides of the ependyma, although it is minor (Fig 3.13D). A similar pattern was detected at E18 (Fig 3.14A-C) where Gpr50 and vimentin expression appears to be mutually exclusive rather than colocalizing. In the 3rd ventricle at E18 no colocalisation was found with either of the other markers (GFAP (Fig 3.14D), O4 (not shown), NeuN (not shown)).

3.3.3.4 Gpr50 is expressed in monoaminergic neurons

The apparent expression of Gpr50 in several brain stem nuclei of behavioural importance is intriguing and was further investigated by co-labelling of Gpr50 with 5-HT (serotonergic marker), tyrosine hydroxylase (TH, dopaminergic and noradrenergic marker) and dopamine beta hydroxylase (DBH, noradrenergic neuronal marker) in the adult mouse brain (Fig 3.15A-E). The strongest Gpr50 expression is found in the locus coeruleus, where we found clear colocalisation with DBH (Fig 3.15A). Gpr50 is only expressed in low levels in the nucleus raphe magnus where it colocalises with 5-HT (Fig 3.15B). Other areas of 5-HT expression include the pontine gray and the substantia nigra, also show colocalisation with Gpr50 (Fig 3.15C-D). Gpr50 staining by immunofluorescence was much less clear in the substantia nigra than with DAB (Table 3.5), again probably due to the relative sensitivity of these methods (Morris, 1991). Colocalisation with 5-HT (Fig 3.15D) and TH (Fig 3.15E) was therefore found to be quite weak

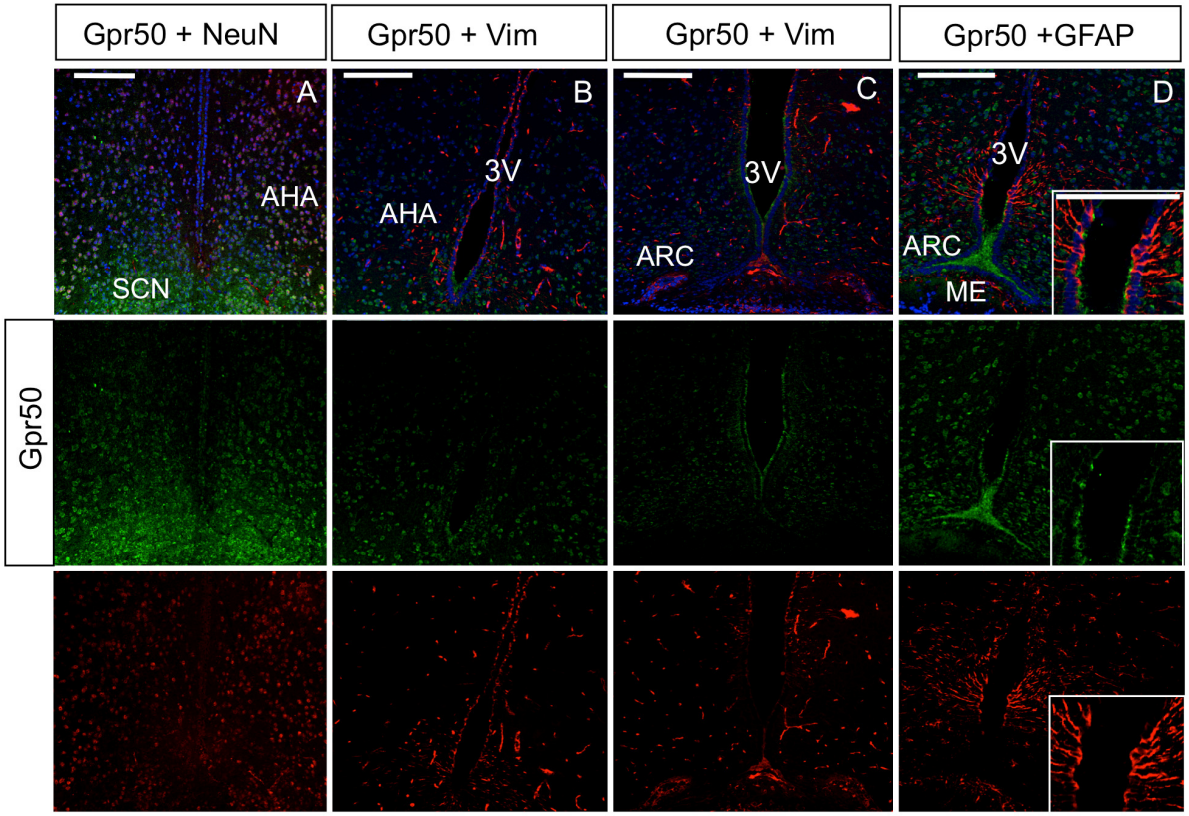

Figure 3.12 *Co-labelling of Gpr50 with NeuN, GFAP or Vimentin (Vim) throughout the rostrocaudal extent of the adult mouse hypothalamus. Adult CD1 brains were fixed in methacarn and stained for Gpr50 and NeuN (A), Vimentin (B, C) or GFAP (D, inset). SCN = suprachiasmatic nucleus, 3V=3rd ventricle, AHA=anterior hypothalamic area, ARC=arcuate nucleus, ME=median eminence. Nuclei were counterstained with DAPI. Scale bars: 100 µm*

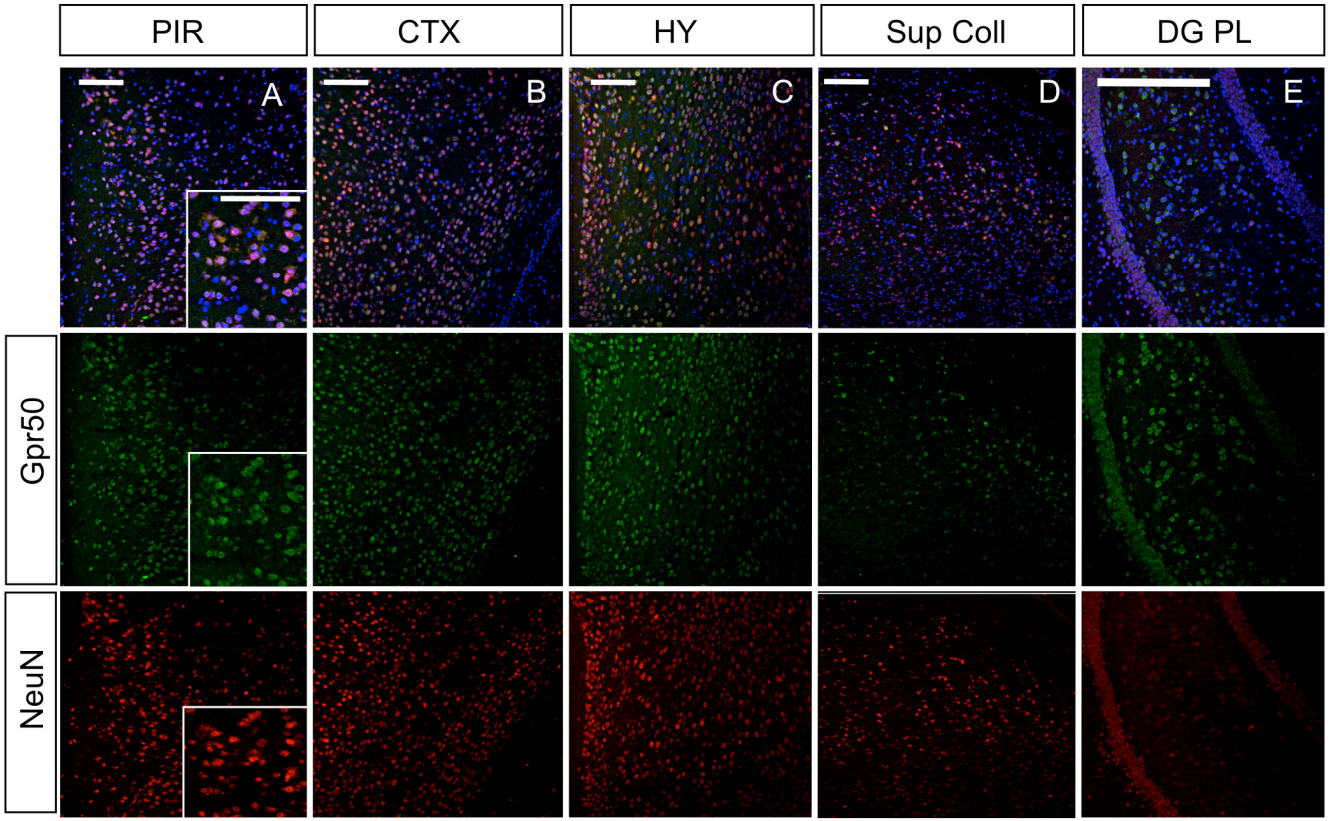

Figure 3.13 *Co-labelling of Gpr50 and NeuN in the adult mouse brain. CD1 brains were fixed in 70% EtOH and stained for Gpr50 and NeuN (A-J). PIR = piriform cortex, CTX = cortex, HY = hypothalamus, DG PL = Dentate gyrus polymorph layer, PG = pontine grey, MARN = magnocellular reticular nucleus, PARN = parvicellular reticular nucleus, PSV = principal sensory nucleus of the trigeminal, LC = locus coeruleus. Sections were counterstained with DAPI. Scale bar: 100 µm.*

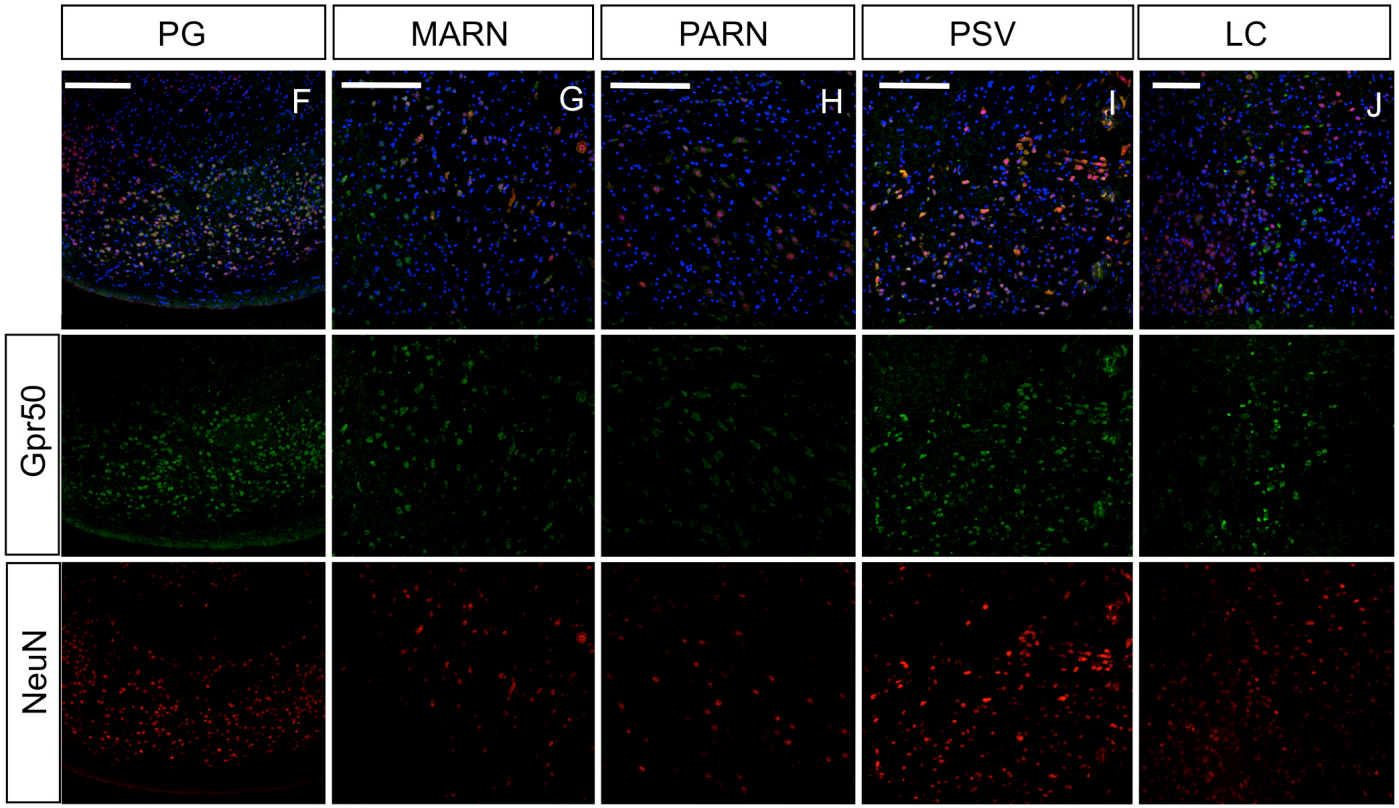

Figure 3.13. *Co-labelling of Gpr50 and NeuN in the adult mouse brain. CD1 brains were fixed in 70% EtOH and stained for Gpr50 and NeuN (A-J). PIR = piriform cortex, CTX = cortex, HY = hypothalamus, DG PL = Dentate gyrus polymorph layer, PG = pontine grey, MARN = magnocellular reticular nucleus, PARN = parvicellular reticular nucleus, PSV = principal sensory nucleus of the trigeminal, LC = locus coeruleus. Sections were counterstained with DAPI. Scale bar: 100 µm.*

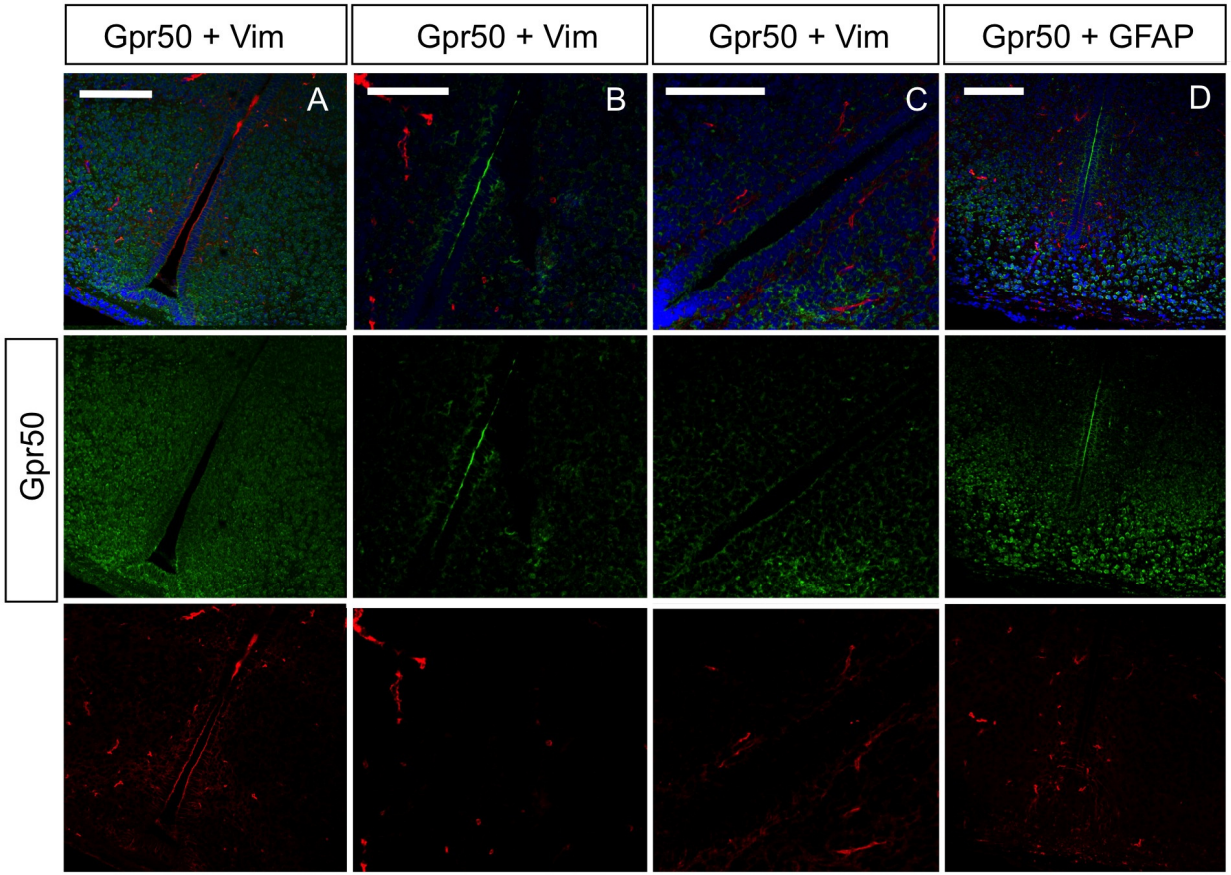

Figure 3.14 *Co-labelling of Gpr50 with Vimentin (Vim) or GFAP in the 3rd ventricular ependyma and the ventral hypothalamus in the E18 mouse brain. E18 CD1 brains were fixed in methacarn stained with Gpr50 and Vimentin (A-C) of GFAP (D). VM HY = ventromedial hypothalamus, 3V=3rd ventricle. Nuclei were counterstained with DAPI. Scale bars: 100 µm*

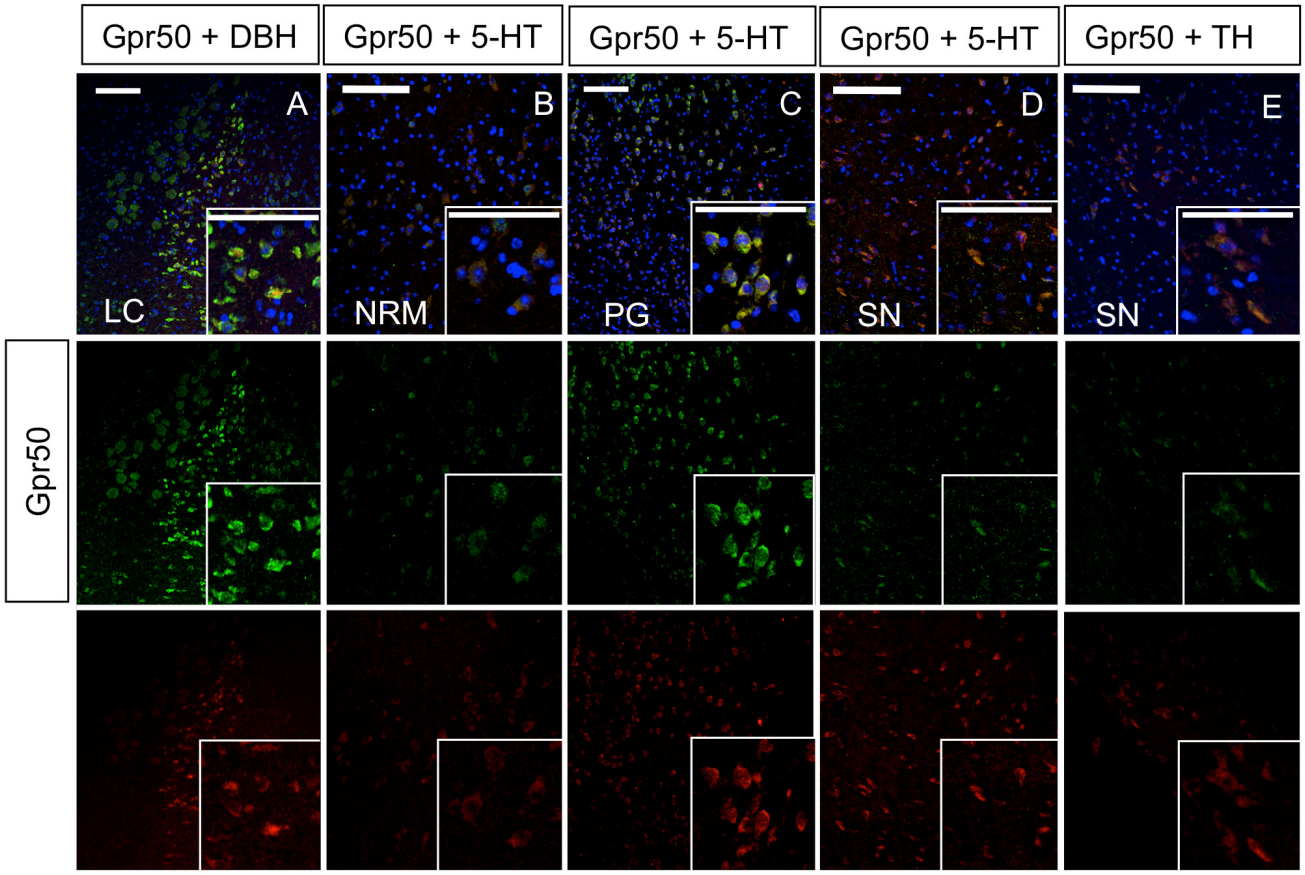

Figure 3.15 *Gpr50 colocalises with noradrenergic, serotonergic and dopaminergic markers. Adult mouse brains were fixed in 70% EtOH and stained for Gpr50 with dopamine beta hydroxylase (A), 5-HT (B-D) and Tyrosine Hydroxylase (E). LC = locus coeruleus, NRM = nucleus raphe magnus, PG = pontine grey, SN = substantia nigra. Sections were counterstained with DAPI. Scale bars: 100 µm.*

3.3.3.5 Gpr50 co-localisation with Nogo-A, Abca2 and Cdh8

Next we investigated whether Gpr50 colocalized with its interactors in the E18 and adult mouse brain: Nogo-A, Abca2 and Cdh8. In the adult mouse brain co-localisation of Gpr50 and Nogo-A was found in several areas in the hypothalamus: the paraventricular nucleus (Fig 3.16A and inset), arcuate nucleus/ventromedial hypothalamus (Fig 3.16B and inset), dorsomedial hypothalamus (Fig 3.16C and inset) and lateral hypothalamus (Fig 3.16D and inset). In each of these areas it appears to be a small subset of cells that express both. Colocalisation of Gpr50 and Nogo-A is more abundant in the amygdala (Fig 3.17A-B and insets), is also found in the superior colliculus (Fig 3.17C and inset) and the somatosensory cortex (Fig 3.17D and inset). In the brainstem nuclei co-localisation of Nogo-A and Gpr50 could be detected in the mesencephalic trigeminal nucleus only (Fig 3.17E). At E18 colocalisation of Gpr50 and Nogo-A was detected in the forebrain (Fig 3.18A-A'), the cortex at several levels (Fig 3.18B'B', C-C') and in the medullary hindbrain (Fig 3.18D-D').

Extensive colocalisation of Gpr50 and Abca2 in the adult mouse brain was detected in the ventral 3rd ventricular ependyma (Fig 3.19A-C, insets) and the lateral side of the epithelium (Figure 3.19B, inset). In the piriform and somatosensory cortices colocalisation of Gpr50 and Abca2 is widespread (Fig 3.19D-E), as is colocalisation in the brain stem nuclei of the medulla and pons: the parvicellular (PARN), magnocellular (MARN) and gigantocellular (GRN) reticular nucleus, the principal sensory nucleus of the trigeminal (PSV), and the nucleus raphe magnus (NRM) (Fig 3.19F, inset, G-I). Weak colocalisation between Gpr50 and Abca2 was found in the locus coeruleus and mesencephalic trigeminal nucleus (Fig 3.19I). As indicated by the rt-PCR results Abca2 expression is much lower in the embryonic than in the adult brain and no clear Abca2 staining could be detected at E18.

Our Cdh8 antibody detected weak expression in the adult mouse brain (Fig 3.20A-C). Here Gpr50 and Cdh8 appear to be expressed in a different subset of cells in the median eminence (Fig 3.20A) but are colocalising in the periventricular

hypothalamus (Fig 3.20B) and in the amygdala (Fig 3.20C). Cdh8 is also expressed in the mesencephalic trigeminal nucleus (Fig 3.20D).

In the embryonic brain Cdh8 expression is stronger then in the adult. At E18 Gpr50 and Cdh8 co-localise in the dorsal forebrain (Fig 3.21A-A'), the median eminence and 3rd ventricular epithelium (Figure 3.21B-B'). Colocalisation is also found in the cortex (Fig 3.21C-C') and roof plate of the pontine/medullary hindbrain (Fig 3.21D-D').

Colocalisation between Gpr50 and Nogo-A, Cdh8 and Abca2 in the E18 and adult female mouse brain by immunohistochemistry is summarised in Table 3.5 (Oertle et al., 2003b).

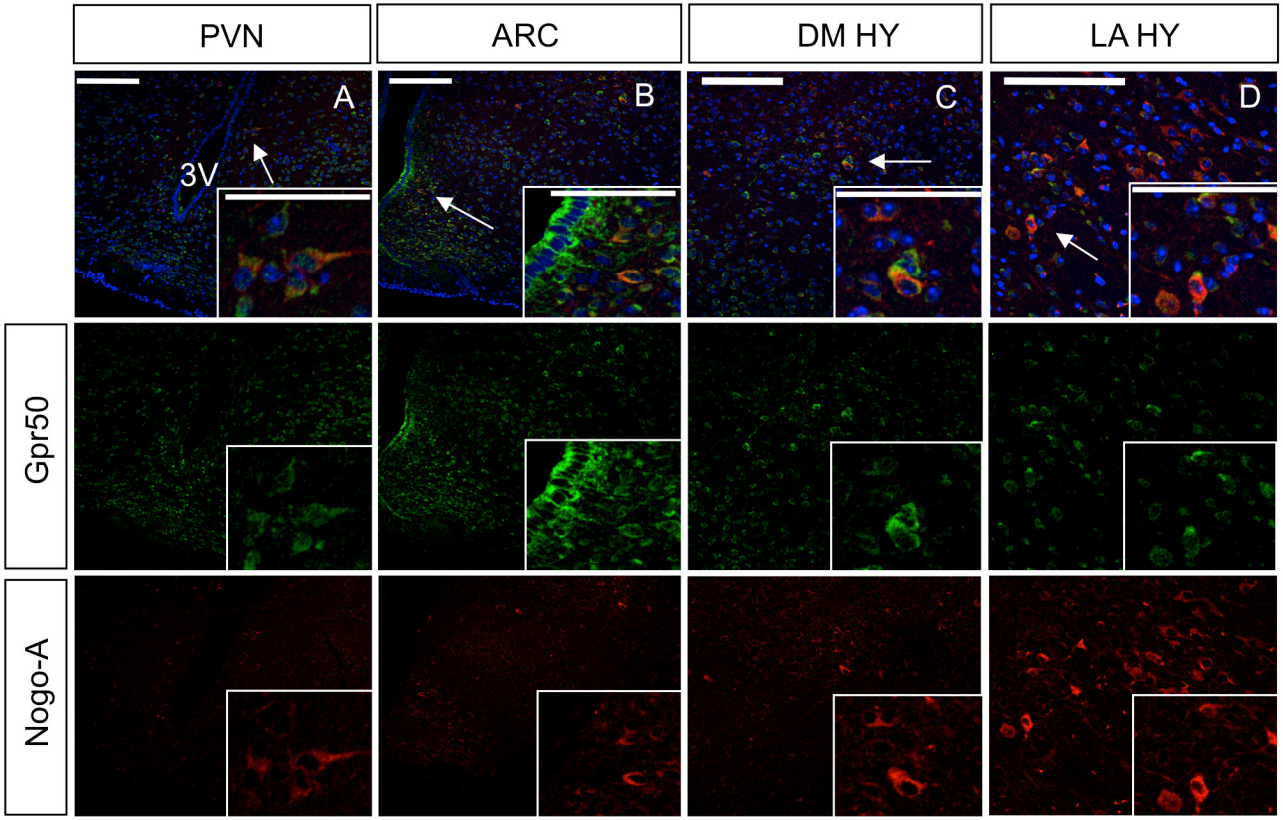

Figure 3.16 *Co-labelling of Gpr50 with Nogo-A in the adult mouse hypothalamus. Adult CD1 brains were fixed in methacarn or 70% EtOH stained with Gpr50 and Nogo-A (A-D). PVN=paraventricular nucleus, ARC=arcuate nucleus, DM HY= dorsomedial hypothalamus, LA HY = lateral hypothalamus, 3V=3rd ventricle. Scale bars: 100 µm*

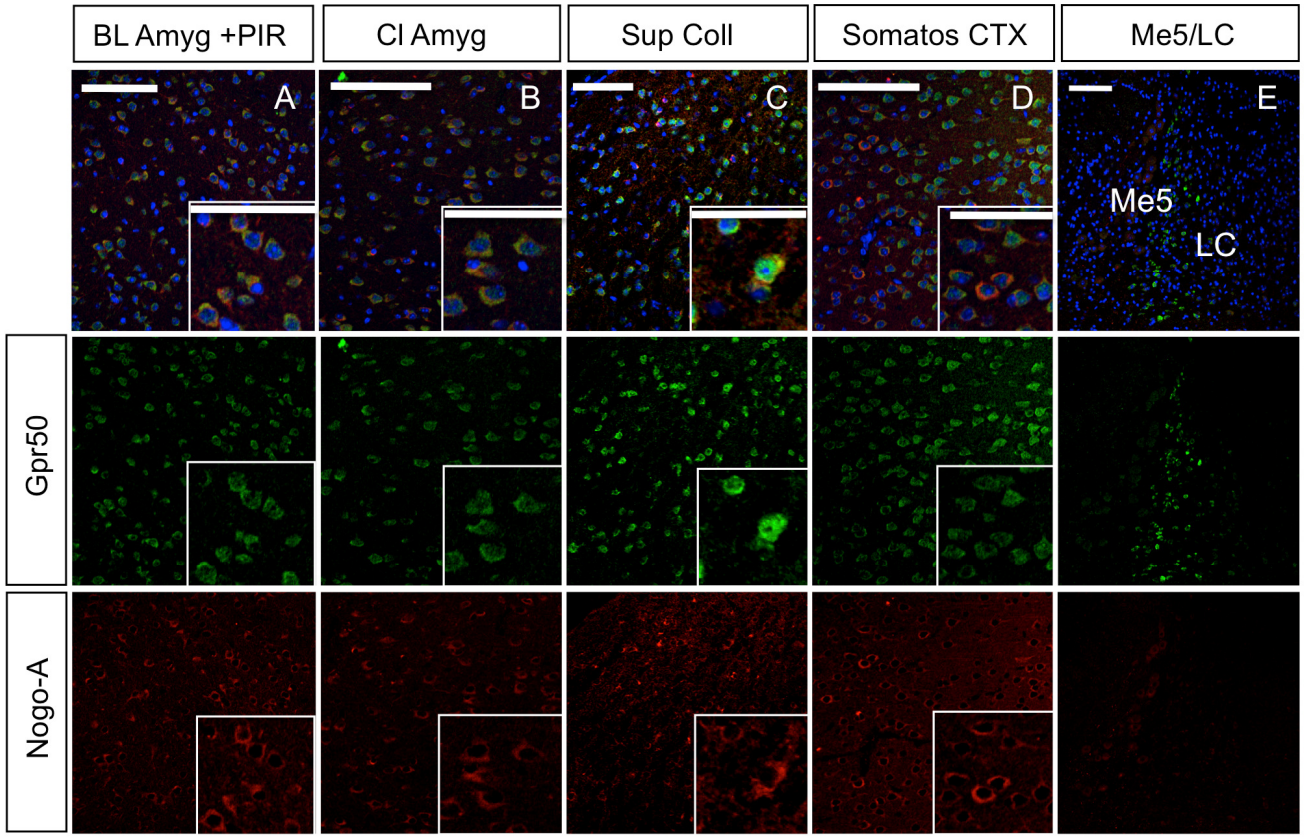

Figure 3.17 *Co-labelling of Gpr50 with Nogo-A in the adult mouse brain. Adult CD1 brains were fixed in methacarn or 70% EtOH and stained with Gpr50 and Nogo-A (A-D). BL Amyg = basolateral amygdala, PIR = Piriform Cortex, Cl Amyg = Central Amygdala, Sup Coll = Superior Culliculus, Somatos CTX = somatosensory cortex, LC= locus coeruleus, Me5= mesencephalic trigeminal nucleus. Scale bars: 100 µm.*

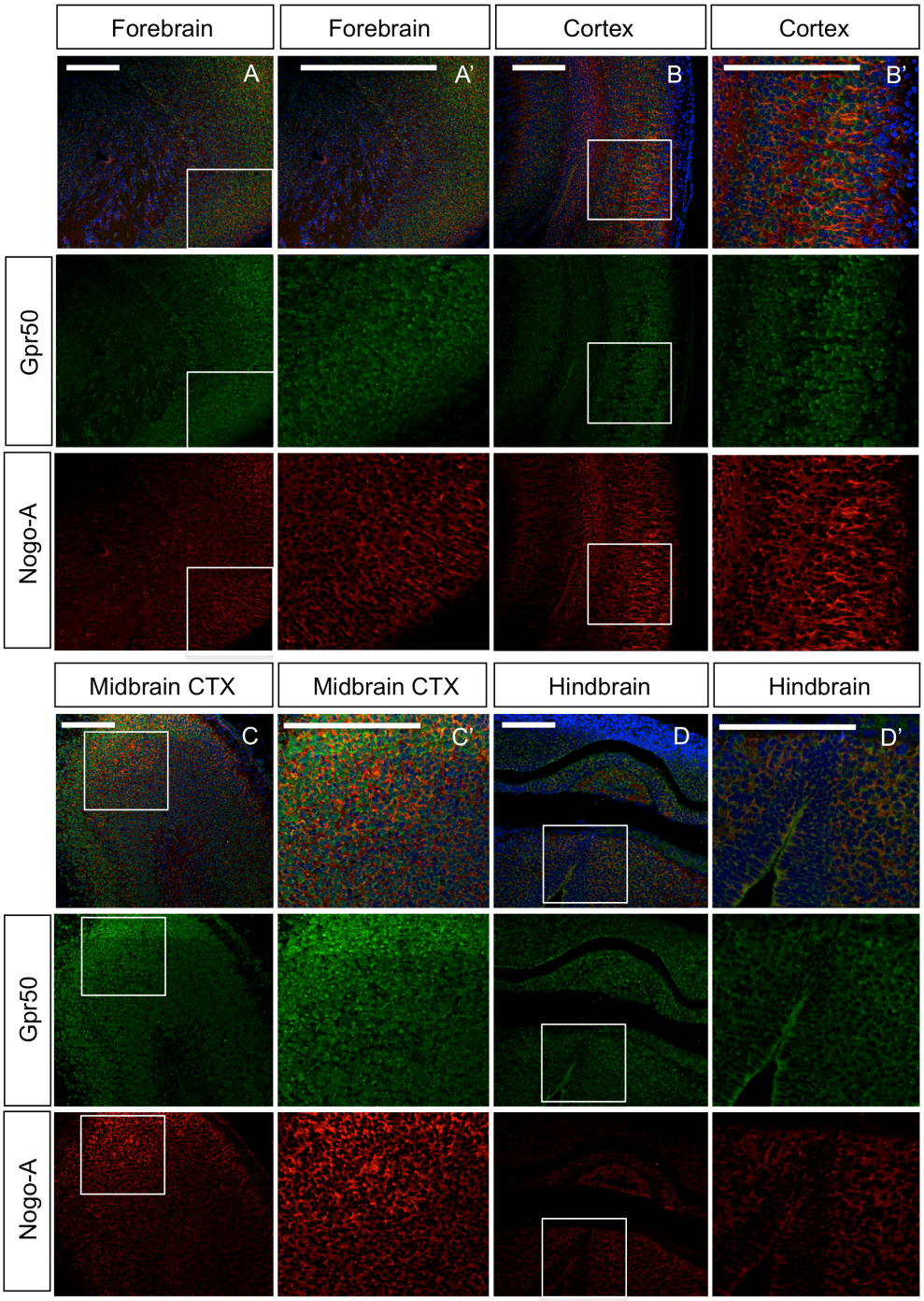

Figure 3.18 *Co-labelling of Gpr50 with Nogo-A in the E18 mouse brain. E18 CD1 brains were fixed in methacarn and stained with Gpr50 and Nogo-A (A-D with A'-D' enlargements). A-A': Dorsal forebrain, B-B': frontal Cortex, C-C: midbrain cortex, D-D': Medullary hindbrain. Sections are counterstained with DAPI. Scale bars: 100 µm.*

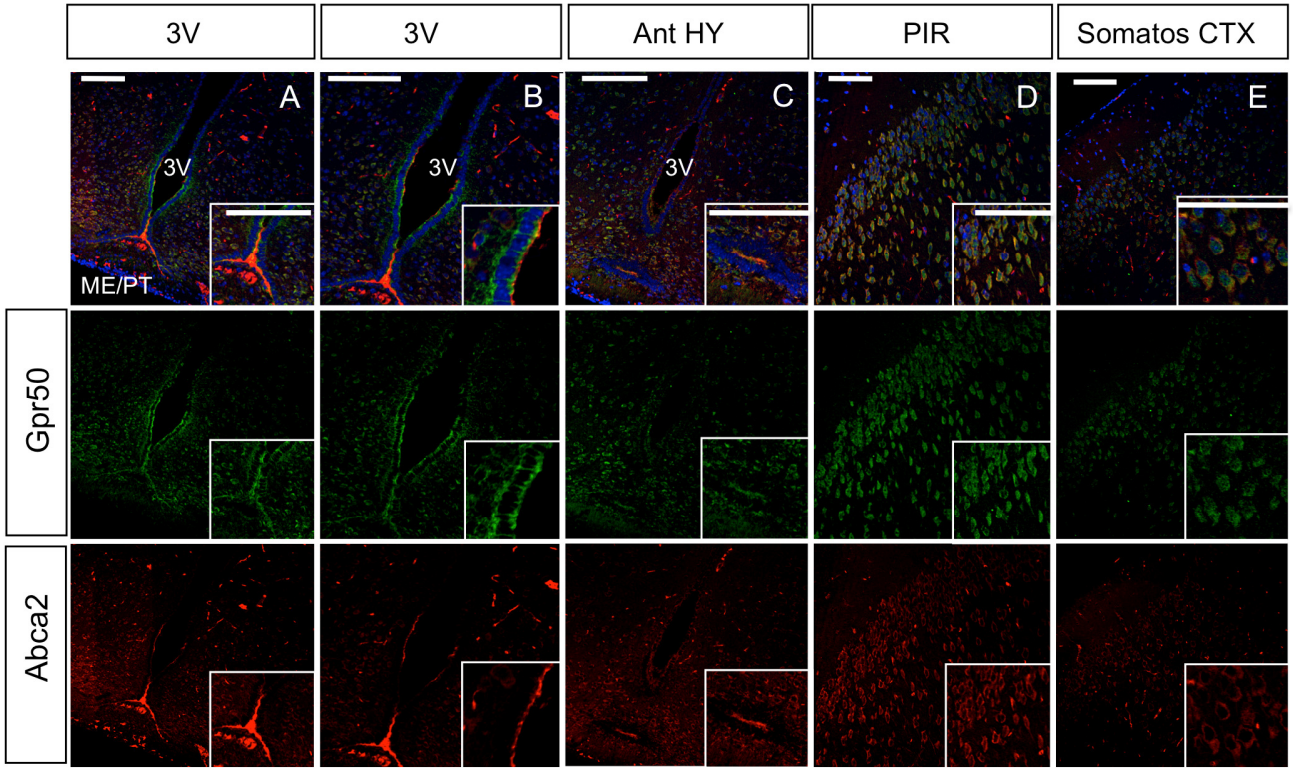

Figure 3.19 *Co-labelling of Gpr50 with Abca2 in the adult mouse brain. Adult CD1 brains were fixed in methacarn or 70% EtOH and sections were stained with Gpr50 and Abca2 (A-J). ME = median eminence, PT= pars tuberalis Ant HY = anterior hypothalamus, 3V = 3rd ventricle, PIR = piriform cortex, Somatos CTX = Somatosensory cortex., PSV = principal sensory nucleus of the trigeminal, GRN = gigantocellular reticular nucleus, PARN = parvicellular reticular nucleus, LC= locus coeruleus, Me5= mesencephalic trigeminal nucleus, NRM = nucleus raphe magnus. Nuclei were counterstained with DAPI. Scale bars: 100 µm.*

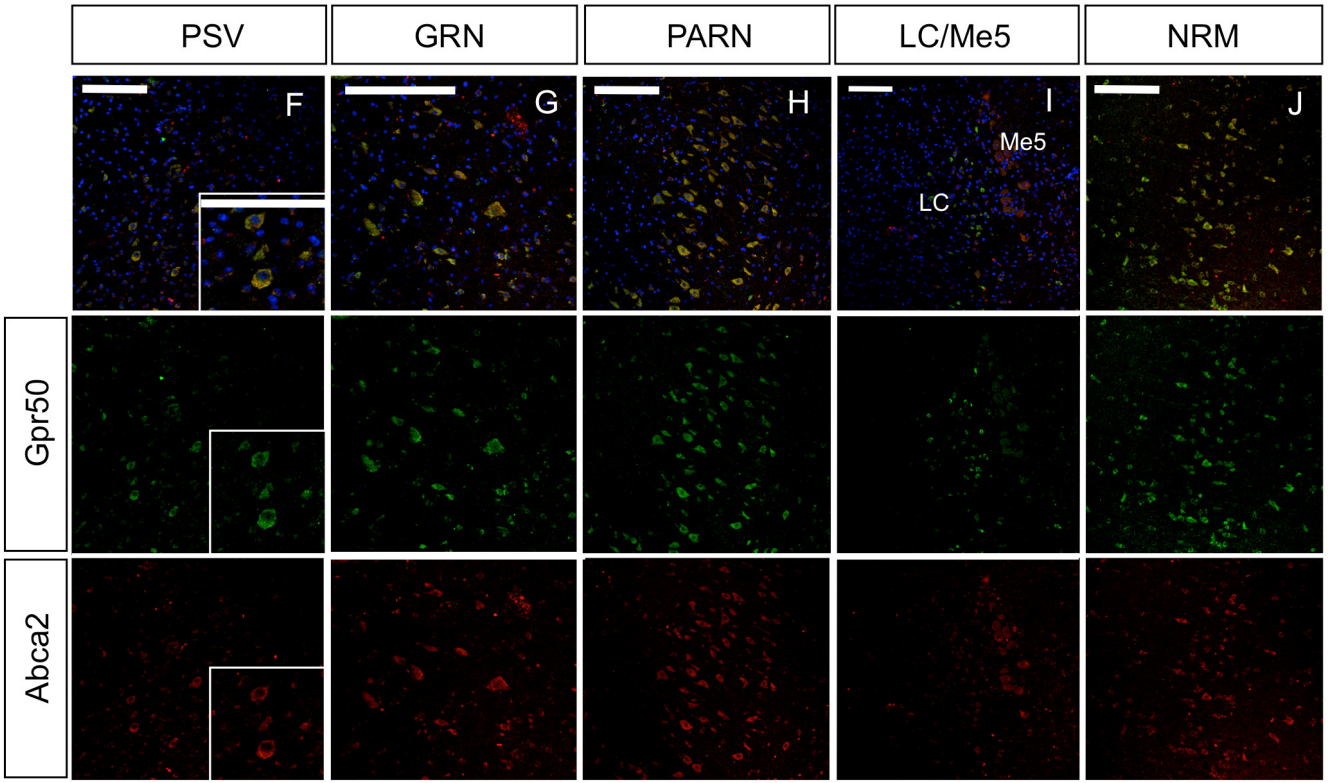

Figure 3.19 *Co-labelling of Gpr50 with Abca2 in the adult mouse brain. Adult CD1 brains were fixed in methacarn or 70% EtOH and sections were stained with Gpr50 and Abca2 (A-J). ME = median eminence, PT= pars tuberalis Ant HY = anterior hypothalamus, 3V = 3rd ventricle, PIR = piriform cortex, Somatos CTX = Somatosensory cortex., PSV = principal sensory nucleus of the trigeminal, GRN = gigantocellular reticular nucleus, PARN = parvicellular reticular nucleus, LC= locus coeruleus, Me5= mesencephalic trigeminal nucleus, NRM = nucleus raphe magnus. Nuclei were counterstained with DAPI. Scale bars: 100 µm.*

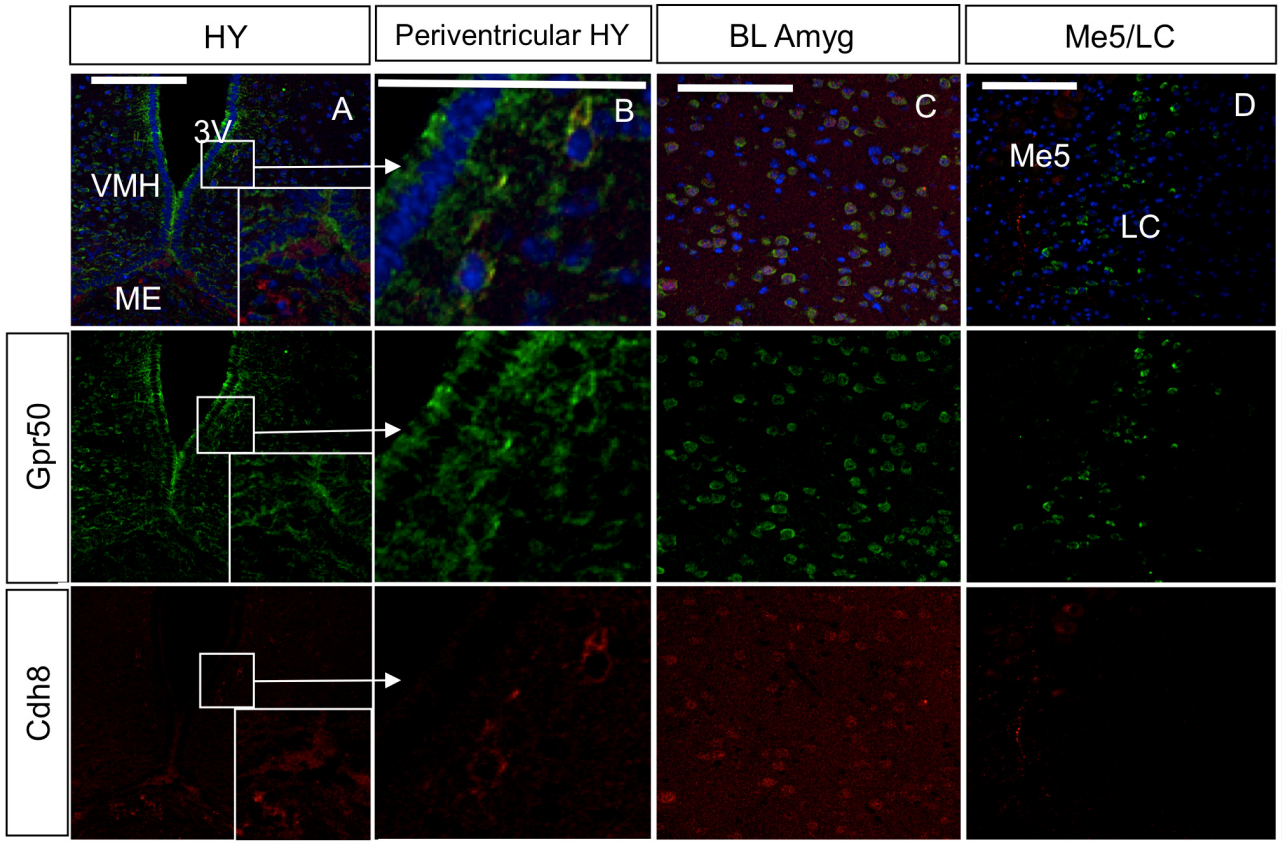

Figure 3.20 *Co-labelling of Gpr50 with Cdh8 in the adult mouse brain. Adult CD1 brains were fixed in methacarn or 70% EtOH and stained with Gpr50 and Cdh8 (A-D). HY=hypothalamus, VMH=ventromedial hypothalamus, ME = median eminence, 3V=3rd ventricle, BL Amyg = basolateral amygdala, Me5 =mesencephalic trigeminal nucleus, LC = locus coeruleus. Nuclei were counterstained with DAPI. Scale bars: 100 µm.*

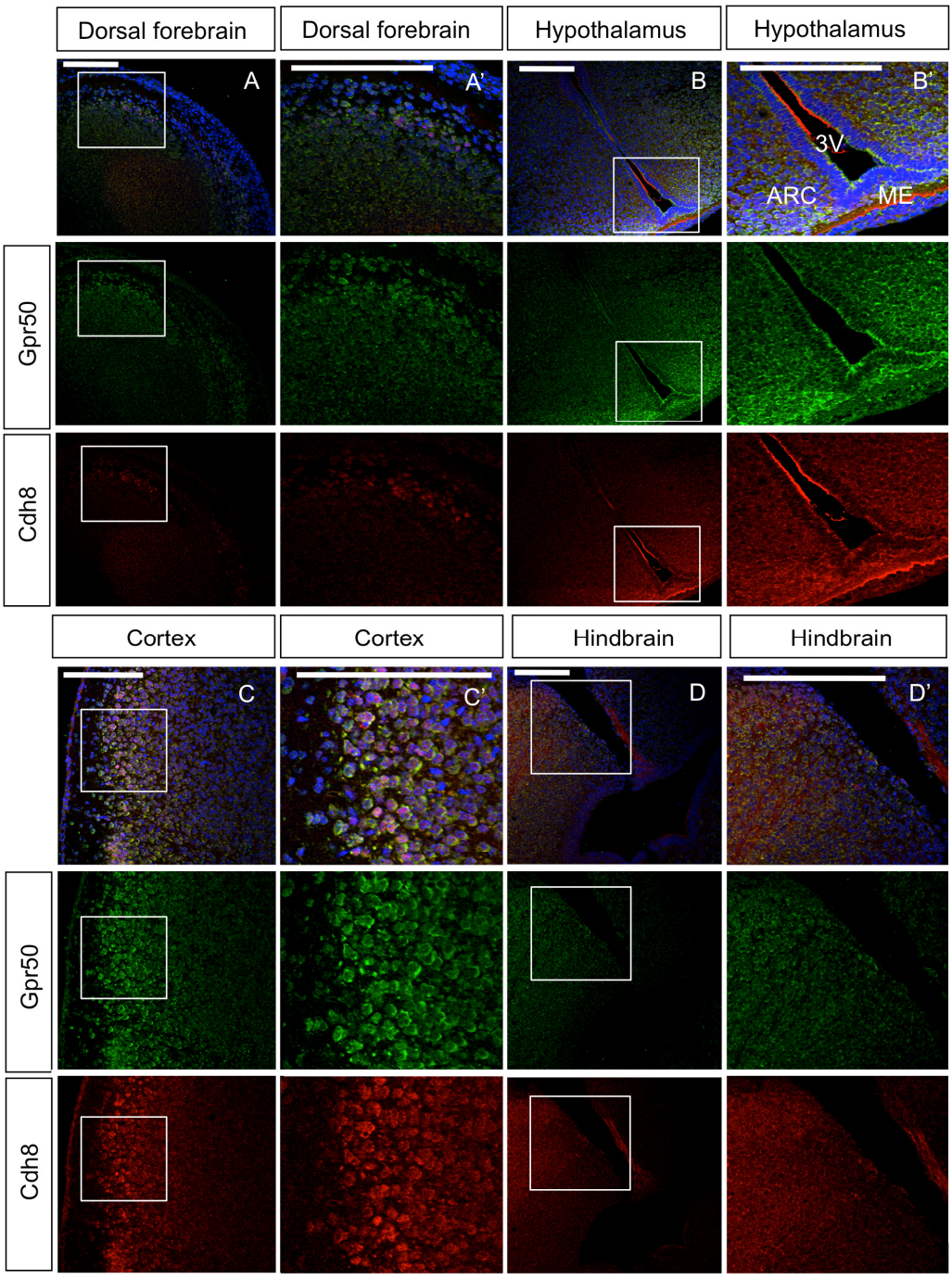

Figure 3.21 *Co-labelling of Gpr50 with Cdh8 in the E18 mouse brain. E18 CD1 brains were fixed in methacarn and stained with Gpr50 and Cdh8 (A-D with A'-D' enlargements). A-A': Dorsal forebrain, B-B': hypothalamus and 3rd ventricle, C-C' : cortex, D-D': Roofplate of the pontine/medullary hindbrain. 3V=3rd ventricle, ARC=arcuate nucleus, ME=median eminence. Sections are counterstained with DAPI. Scale bars: 100 µm.*

3.4 Discussion

3.4.1 GPR50 and interactors are enriched in the postsynaptic density

Subcellular fractionation of adult mouse brain indicates that Gpr50, Nogo-A, Cdh8 and Abca2 are all expressed in the light membrane fraction (P3), which includes structures such as the ER, Golgi, endolysosome and plasma membrane, and in the crude synaptosomal fraction (P2). This is in agreement with previous studies (Kido et al., 1998; Vulevic et al., 2001; Oertle et al., 2003b; Levoye et al., 2006), and the results of Chapter 2, and indicates the (internal) membrane fractions as an interaction site.

Increased expression of Gpr50 was found in the postsynaptic density fractions and this is highest in the 'core' PSD fraction (PSD3). Nogo-A and Cdh8 are present both post and presynaptically. This is in line with previous reports on synaptic expression of Nogo-A (Lee et al., 2008) and Cdh8 (Suzuki et al., 2007). This indicates that GPR50 and interactors are likely to be interaction partners at the synapse, and that GPR50 may interact in *cis* or in *trans* with its partners, either across the synapse or on the postsynaptic membrane. However, this needs to be confirmed by performing co-immunoprecipitations from synaptic fractions.

3.4.2 Developmental expression of GPR50 and interactors

This is the first study looking at the developmental expression of orphan GPR50. By rt-PCR, expression of *Gpr50* and several interactors is detected at E13 and peaks at E18, a developmental stage important for axon growth and guidance, synapse formation and function and survival and growth (Matsuki et al., 2005). The expression of *Gpr50* and *Nogo-C* and *Abca2* is also increased in adolescence, at 5 weeks. Early adulthood and adolescence are important timepoints in the development of psychiatric illness. The average age of onset of bipolar disorder and schizophrenia is in early adulthood (between 20 and 30 years) (Joyce, 1984). Early onset (in

adolescence) bipolar disorder is however common and is characterised by an increase in manic symptoms (Joyce, 1984; Geller and Luby, 1997).

The rt-PCR findings are in line with previous reports in the literature. *Gpr50* was previously found to be highly expressed in several nuclei of the hypothalamus (Reppert et al., 1996; Drew et al., 1998; Drew et al., 2001; Sidibe et al., 2010), which can be confirmed by our study. The 3rd ventricular wall is also likely to be part of the hypothalamic cDNA from the panel and a high hypothalamic expression could reflect this area. Gpr50 was also previously detected in the adult rodent amygdala, olfactory bulb (Drew et al., 2001), and in the hippocampus (Hamouda et al., 2007), although not specified which part.

As previously published Nogo and Nogo-A are ubiquitously expressed in most tissues (Funahashi et al., 2008)(Hasegawa et al., 2005), most highly espressed in white matter containing regions (pons, medulla, spinal cord), but also in the cortex during development (Oertle and Schwab, 2003). We found increased *Nogo-A* expression in the hippocampus at E18 but not at other stages. A higher expression in the cortical areas at P7 is in agreement with BGEM *in situ* hybridisation data (Magdaleno et al., 2006). A general increase in *Nogo-A* expression around birth was also reported by Huber et al. (2002).

Nogo-A protein expression has also previously been detected in the rat primary somatosensory cortex (Shin et al., 2006). *Nogo-A* mRNA was previously reported to be expressed in the paraventricular nucleus and ventromedial nucleus of the hypothalamus, the amygdala and cortex in the rat and human postmortem brain (Hasegawa et al., 2005; Satoh et al., 2005). We did not detect Nogo-A in the brain stem nuclei whereas high *Nogo-A* mRNA expression was previously found in the locus coeruleus and the substantia nigra pars compacta, the dorsal raphe and reticular nuclei (Hasegawa et al., 2005). We did however find Nogo-A in the adjacent mesencephalic trigeminal nucleus as predicted by mRNA expression (Hasegawa et al., 2005).

We could only detect significant expression of *Nogo-C* mRNA at 5 weeks, in line with previous findings (Huber et al., 2002). An increase in *Nogo-C* expression in adulthood was found previously in the hippocampus (Meier et al., 2003). This should be further investigated by performing immunohistochemistry with a Nogo-C-specific antibody.

Our observations of increased expression of *Cdh8* in cortical, striatal and midbrain areas at P7 corresponds to previous findings (Korematsu and Redies, 1997; Korematsu et al., 1998a; Korematsu et al., 1998b; Bekirov et al., 2002; Gil et al., 2002). We find an increase in *Cdh8* expression in the midbrain at all timepoints, which is in agreement with BGEM data at E15 and P7 (Magdaleno et al., 2006). Unlike Bekirov et al. (2002) we could not detect strong hippocampal Cdh8 expression at any developmental stage, which is in line with Korematsu and others (1998). Interesting is our observation of a shift in increased Cdh8 expression from anterior to posterior brain regions from E18 to P7. Similarly, Bekirov et al. (2002) detected in a decreasing Cdh8 dorsal to ventral gradient in the subiculum in the first few weeks postnatally, suggesting cadherins play a role in subdivisional organisation of the developing brain.

ABCA2 expression has only previously been reported in the adult brain, in the hippocampus and white matter areas (Zhao et al., 2000; Broccardo et al., 2006). An increase in *Abca2* expression after birth was previously found (Chen et al., 2004b; Tachikawa et al., 2005. We detected a general peak in mRNA expression at 5 weeks, especially in the hippocampus, striatum and midbrain (Table 3.4). In the adult brain high Acba2 protein expression was mostly detected in the hypothalamus around the 3rd ventricle, in the cortex and in several brain stem nuclei (Fig 3.18) and also in the corpus callosum. Strong Abca2 expression was detected in the median eminence and pars tuberalis and looked similar to the vimentin staining in these areas (this study). Vimentin has also been shown to be co-regulated with ABCA2 (Chen et al., 2004b; Mack et al., 2011). Although *Abca2* was detected in the developing brain by rt-PCR and previously by *in situ* hybridisation (Tachikawa et al., 2005) we could not detect

any protein expression with our antibody at E18. Other antibodies may detect Abca2 in the developing brain.

We detected high *Srebf2* expression in the spinal cord at E18, the medulla at P7 and the pons at week 5 (Tabel 3.4) suggesting a posterior to anterior expression gradient in the brainstem through development. *Srebf2* was previously detected in the brainstem (Kim and Ong, 2009). At P7 *Srebf2* is also more highly expressed in the cortex, and in the cortex, striatum and thalamus at 5 weeks, in agreement with previous studies in the adult rat and mouse brain (Jones et al., 2009; Kim and Ong, 2009). We did however not detect high mRNA expression in the hippocampus as was previously found (Kim and Ong, 2009). Protein expression should be investigated by performing immunohistochemistry using a specific SREBF2 antibody.

3.4.3 Novel sites of GPR50 expression

In addition to previously reported sites we found many novel sites of Gpr50 expression in the adult and E18 mouse brain by immunohistochemistry. Of particular interest is the expression in the brain stem nuclei as these include the substantia nigra, containing dopaminergic cells, the raphe nuclei (serotonergic cells) and perhaps most clearly the locus coeruleus (noradrenergic cells). GPR50 is also expressed in the polymorph layer of the dentate gyrus, which is the primary target for noradrenergic, serotonergic and cholinergic input to the hippocampus (Berger et al., 1981). Gpr50 also colocalises with monoaminergic markers TH, 5-HT and DBH suggesting a role in neurotransmitter signalling. These areas are highly interconnected with other areas in the brain and the neuromodulatory and behavioural properties of the monoaminergic neurotransmitters have been well researched. Dopamine plays a role in movement, reward and addiction, serotonin is implicated in appetite, mood and anxiety, and noradrenaline is involved in fight-or-flight reaction, stress and depression.

Gpr50 is also expressed in specific pontine/medullary nuclei: the parvicellular (PARN), magnocellular (MARN) and gigantocellular (GRN) reticular nucleus and the principal sensory nucleus of the trigeminal (PSV)

In the absence of a ligand for Gpr50 its expression in the brainstem and colocalisation with noradrenergic, dopaminergic, and serotonergic markers is intriguing and introduces the possibility that Gpr50 is a receptor for either neurotransmitter, or that Gpr50 is involved in the regulation of monoamine transmission. Given its localisation at sites controlling the HPA axis a neuropeptide ligand may also be possible.

3.4.4 GPR50 expression in neurons

Gpr50 appears to be expressed in grey matter only and is predominantly expressed by NeuN-positive postmitotic neurons. The expression pattern and morphology of Gpr50 expression neurons in the cortex and hippocampus resemble those of interneurons. GABA-expressing cortical interneurons arise from the ventral telencephalon/subpallium between E12.5 and E16.5 in mice (Wonders and Anderson, 2006). Specific subtypes of these neurons arise from different regions of the ganglionic eminence and express proteins and neuropeptides such as Parvalbumin, Somatostatin, Neuropeptide Y and Calretinin (Wonders and Anderson, 2006), which can be used as markers. Double labelling of Gpr50 with these interneuronal markers during neurogenesis and in adulthood is necessary to investigate which types of interneurons express Gpr50 and what their origins and molecular characteristics might be. Identifying the cell type could also give indications of a ligand for GPR50.

The other major site of Gpr50 expression is the ependyma of the third ventricle, where Gpr50 was previously detected, possibly in vimentin-positive tanycytes (Barrett et al., 2006; Sidibe et al.). Tanycytes are glial cells almost exclusively expressed in the ependyma at the base of the 3rd ventricle. They are derived from radial glia and are morphologically similar to astrocytes although they are GFAP

negative. There is some speculation as to the function of tanycytes and there are theories that tanycytes form the link between the CSF and portal vasculature and are involved in endocrine signalling (Lechan and Fekete, 2007). The fetal ependyma may play a role in neurogenesis, neuronal differentiation/axonal guidance, transport, and support, whereas the mature ependyma likely regulates the transport of ions, small molecules, and water between the CSF and neuropil and functions as a barrier that may protect the brain from harmful substances (Lechan and Fekete, 2007). Intermediate filament proteins vimentin (Sidibe et al., 2010) and GLUT1 (Garcia et al., 2003) are often used as markers for tanycytes although as with any marker there are limitations to their use (Peruzzo et al., 2000).

GLUT1 did not associate with Gpr50 in one study (Ivanova et al., 2008). GPR50 colocalisation with vimentin was only detected by Sidibe et al. (2010) and only in what appeared to be a small subset of GPR50-expressing cells in the mouse 3rd ventricular epithelium. No colocalisation was found with vimentin in Gpr50-expressing cells in the median eminence in the adult mouse brain at high magnification (Sidibe et al., 2010). This suggests GPR50 is also expressed by vimentin-negative ependymal and non-ependymal cells. Using different antibodies than Sidibe et al. (2010) we did not find any colocalisation of GPR50 with vimentin in the ependyma, median eminence or arcuate nucleus and the results here are therefore more similar to those of Ivanova et al. (2008). In our study, vimentin and Gpr50 even appeared to be mutually exclusive, both in the adult and E18 brain, which is intruiging. A typical elongated morphology of tanycytes in the dorsomedial hypothalamus is not visible in the vimentin-positive cells but does resemble the vimentin immunoreactivity in response to short day photoperiods (Kameda et al., 2003). The mice used in our study were kept on 12h day/night cycles so a decrease in tanycyte density is not expected. This suggests a different vimentin antibody should be tested as well. Although we can confirm the expression of Gpr50 in the ependyma of the 3rd ventricle we cannot confirm the type of cells showing expression.

3.4.5 GPR50 and interactors

In the E18 and adult female mouse brain Gpr50 colocalises with Nogo-A in neurons in the cortex and several nuclei hypothalamic and amygdalar nuclei. Expression in the paraventricular nucleus and arcuate nucleus suggests a combined role in neuroendocrine functions and control of the HPA axis (Swanson and Sawchenko, 1980; Herman and Cullinan, 1997). The ventromedial nucleus, dorsomedial nucleus and lateral hypothalamus are thought to play a role in metabolic regulation and control of food intake (Sakurai et al., 1998; Yang et al., 1999) and reward-seeking (Harris et al., 2005). The amygdala plays a role in fear conditioning and emotional memory (Adolphs et al., 1995) and reward learning (Baxter and Murray, 2002). Gpr50 and Nogo-A seem to colocalize in the same cells, as has been suggested previously (this thesis, Chapter 2). Thus Gpr50 does not appear to be a Nogo-A receptor on a different cell membrane (Schwab). As Gpr50 is expressed in these regions, it leaves open the possibility that Gpr50 influences Nogo-A expression as suggested earlier (Grünewald et al., 2009)

Gpr50 colocalisation with Abca2 in the adult female mouse brain is extensive, as was perhaps suggested by a significant correlation between Gpr50 and Abca2 mRNA expression at the final rt-PCR timepoint (5 weeks old, r=0.43; p=0.0028). Colocalisation is found in the ependyma of the 3rd ventricle, the median eminence and pars tuberalis but also in the cortex and in several brain stem nuclei in the pons and medulla involved in the autonomic regulation of feeding (PARN, MARN, PSV, raphe nuclei) (Ter Horst et al., 1991). This is intriguing as Abca2 has previously been implicated in lipid metabolism, through homology with the HDL-cholesterol transporter Abca1 (Kaminski et al., 2001) and involvement in the regulation of sphingolipids (Sakai et al., 2007). Expression in the 3rd ventricular ependyma, median eminence and pars tuberalis may indicate a role in transport of lipids from the CSF/hypothalamus to the portal blood.

In the adult mouse brain colocalisation between Gpr50 and Cdh8 was detected in the periventricular hypothalamus and amygdala but clearest colocalisation was found in

the E18 brain, in ependymal cells of the 3rd ventricle, the arcuate nucleus and the median eminence, suggesting a combined role in neuroendocine control. Colocalisation was also found in a small subset of cells in the dorsal forebrain, cortex and pontine/medullary hindbrain. *Gpr50* and *Cdh8* mRNA expression also correlate significantly at E18 (r=0.64; *p*=0.024). Correlation in prenatal development is interesting as cadherins are thought to play a role in subdivisional organisation of the developing brain (Korematsu and Redies, 1997; Suzuki et al., 1997; Korematsu et al., 1998a; Korematsu et al., 1998b; Bekirov et al., 2002; Gil et al., 2002; Neudert et al., 2008). Cdh8 expression is implicated in the formation of functional neural circuits involving basal ganglia- thalamocortical (Alexander and Crutcher, 1990; Korematsu et al., 1998b) or fasciculus retroflexus/habenulo-interpeduncular tract (Marchand et al., 1980) during development (Korematsu et al., 1998b). We found *Cdh8* to be expressed in a caudal to rostral peak in the E18 and P7 mouse brain and *Gpr50* was also high in caudal areas at E18. This may indicate a combined role of Cdh8 and Gpr50 in the development of these areas. Gene Ontology-analysis of the GPR50 yeast two-hybrid interactors also indicated neural development as a key process (Grünewald et al., 2009).

When looking at Table 3.5 there are only a few areas where all four proteins investigated are expressed: the amygdala and the mesencephalic trigeminal sensory nucleus (Me5). The amygdala is involved in emotional and social behavour, especially in fear conditioning (LeDoux, 1993; Adolphs et al., 2002). The Me5 receives sensory information regarding mastication (biting and swallowing), so is involved in the autonomic regulation of feeding. This suggests Gpr50 and interactors may have a shared role in emotional and metabolic control.

3.4.6 GPR50 in energy metabolism

Several of the regions where Gpr50 and interactors are expressed are involved in energy metabolism. The hypothalamic dorsomedial, paraventricular, and arcuate nuclei are involved in the regulation of feeding behaviour (Schwartz et al., 2000). The parvicellular (PARN), magnocellular (MARN) and gigantocellular (GRN)

reticular nucleus and the principal sensory nucleus of the trigeminal (PSV) play a role in autonomic regulation and orofacial motor control of food intake (Ter Horst et al., 1991). Whereas parts of the reticular formation control orofacial movements, the PSV receives primary efferents from pain, mechano and temperature receptors in the oral cavity. Efferents from the PSV transfer this signal to higher areas for instance the superior colliculus, cerebellum and the thalamus. The reticular formation receives input from the hypothalamus and sends projections to the raphe nuclei (Ter Horst et al., 1991).

Nogo-A, Cdh8 and Abca2 were detected in the Me5, which co-expressed Gpr50 in the same cells. The mesencephalic trigeminal nucleus is a sensory ganglion containing primary sensory neurons involved in the control of mastication, the automatic (unconscious) activities of food intake such as biting, chewing and swallowing. Me5 contains histaminergic neurons and depletion of neuronal histamine in Me5 resulted in a significant decrease in eating speed and longer duration of eating time, although the intake was not affected (Sakata, 1995). Me5 appears to be part of a histamine-controlled reflex, which also includes the ventromedial hypothalamus (VMH), and influences food intake through satiety (Sakata et al., 1997). These links to autonomic feeding mechanisms are interesting as *Gpr50* knockout mice appear to show increased energy metabolism, with attenuated weight gain and reduced body fat on a high-energy diet compared to wild-type animals (Ivanova et al., 2008). An intronic SNP in GPR50 was also associated and higher serum triglyceride and lower HDL cholesterol levels (Bhattacharyya et al., 2006).

3.4.7 Clues to GPR50 functioning: A role in stress and CRH signalling?

With GPR50 expression in areas involved in HPA-axis control and in monoaminergic cells we identify two systems involved in mediating both neuroendocrine responses to stress and the pathophysiology of bipolar disorder (Manji and Lenox, 2000). Both Gpr50 and Abca2 knockout mice show hyperactive

behaviour (Mack et al., 2007; Ivanova et al., 2008) perhaps an indication of stress-pathway activity. Although there was no significant difference, plasma corticosterone levels were consistently higher in the *Gpr50* null mice compared to wild type (Ivanova et al., 2008).

The mammalian neuroendocrine stress response in the HPA-axis is primarily regulated by corticotrophin releasing hormone (CRH) (Vale et al., 1981). CRH has been implicated in various diseases such as depression, bipolar disorder and Alzheimer's disease (Behan et al., 1996; Arborelius et al., 1999). Interestingly other effects of CRH, such as appetite control, energy metabolism and biological rhythms have also been linked to GPR50 expression (Richard et al., 2000; Swaab et al., 2005; Barrett et al., 2006; Bhattacharyya et al., 2006; Ivanova et al., 2008). All these systems are also disturbed in major mental illness. Investigating the relation between GPR50 and CRH or the CRH receptor would therefore be interesting.

3.4.8 GPR50 in neurotransmitter signalling

Investigating the interactions between the HPA axis and the monoaminergic neurotransmitter systems is key to understanding mental illness (Swaab et al., 2005). We found GPR50 to be highly expressed by noradrenergic neurons in the locus coeruleus (LC), and also in the serotonergic raphe nuclei and the dopaminergic substantia nigra. In addition Gpr50 was also expessed in the polymorph layer of the dentate gyrus, which is the primary target for noradrenergic, serotonergic and cholinergic input to the hippocampus (Berger et al., 1981). This suggests a role for GPR50 in the control of neurotransmitter signalling or regulation.

Although Gpr50 is expressed in these nuclei, the other proteins investigated appear not to be, with the exception of Abca2. Colocalisation of Gpr50 and Abca2 was observed in the LC only. The neurons in the LC have many afferent and efferent connections often modulated by stress (Cunningham and Sawchenko, 1988). Efferent projections to the hypothalamus include the cortex, hippocampus, cerebellum and brainstem (Loughlin et al., 1986). Noradrenergic neurons from the brainstem project

to paraventricular nucleus of the hypothalamus (PVN) and have a stimulatory role on hormonal activity. Blocking this pathway can reduce stress-induced changes in the HPA (reviewed by (Palkovits, 1999). LC's major inputs are from the nucleus paragigantocellularis and the nucleus prepositus hypoglossi, both in the rostral medulla, with minor afferents coming from the hypothalamic PVN and the spinal intermediate gray (Aston-Jones et al., 1986). Other inputs come from the medial/lateral preoptic nucleus, Arcuate nucleus and the dorsomedial nucleus of the hypothalamus, often in response to nociceptive stimuli (Cedarbaum and Aghajanian, 1978; Sim and Joseph, 1991).

Approximately 30% of neurons projecting to the LC are CRH-positive (Reyes et al., 2005). In the LC CRH acts as a neurotransmitter during stress (Valentino et al., 1993; Van Bockstaele et al., 1996). LC receives CRH input from a specific group of neurons in the PVN, the central nucleus of the amygdala and from areas in the pons and medulla, areas of Gpr50 expression. Axons containing several opioid receptors also innervate the LC (eg enkephalin, proopiomelanocortin, dynein) (Van Bockstaele et al., 1995; Reyes et al., 2006; Reyes et al., 2008).

Seasonal expression differences of *Gpr50* have been found in the ependyma of the 3rd ventricle in the Siberian hamster (Barrett et al., 2006) and recently an association was found between a GPR50 variant and seasonal affective disorder (Delavest et al., 2011), suggesting a possible role for GPR50 in biological rhythms.

3.4.9 The importance of sex in studying Gpr50

The GPR50 genetic associations with bipolar disorder and other major mental illness were found only in women (Thomson et al., 2005; Macintyre et al., 2010; Delavest et al., 2011), for reasons yet unclear. Animal studies so far have not been able to give a clear picture of GPR50 functioning and one reason may be that sex has not been accounted for. This is a general point as male animals are used more often in studies because they are easier to handle and cheaper than females (Wald and Wu, 2010). Previous studies on Gpr50 expression and behaviour have either used males only

(Barrett et al., 2006; Ivanova et al., 2008; Sidibe et al., 2010) or have not noted the sex of the animals (Drew et al., 2010). Some of the most male biased fields are endocrinology and physiology (Wald and Wu), where clear sex differences exist which cannot be ignored. Women are more vulnerable to stress-related psychiatric disorders, such as PTSD and major depressive disorder (Kuehner, 2003).

The locus coeruleus, one of the strongest sites of Gpr50 expression, may play a role in this, as it is a sexually dimorphic nucleus. It develops over a longer period and is generally larger in female rats (Luque et al., 1992; Pinos et al., 2001). Swim stress-induced activation of LC-neurons was greater in female then in male rats (Curtis et al., 2006) and was related to differential sensitivity of neurons to corticotrophin releasing hormone (CRH) postsynaptically. Sex-specific effects on other parts of the stress response are also significant. Women have higher cortisol levels and the endocrine responses are possibly more complex with oxytocin and female sex hormones influencing the HPA axis ACTH, CRH and cortisol levels during the oestrus cycle, breastfeeding and parturition (Chiodera et al., 1991; Swaab et al., 2005). Moreover CRH-BP is also expressed in sexually dimorphic pattern in the anterior pituitary, with greater expression in the female mouse, which is regulated by estrogen levels (Speert et al., 2002; Westphal and Seasholtz, 2006). Our finding of Gpr50 expression in the sexually dimorphic LC and the HPA axis might provide clues to its functioning and we stress the importance of taking sex differences into consideration in future studies.

3.4.10 Caveats to this study

There are a number of caveats we have to keep in mind when analyzing the expression of the genes as measured by rt-PCR. Firstly, the experiment was performed on a panel produced by Origene, which gives us little control on how the tissue was processed. We will therefore have to assume that this was performed correctly. Secondly, the cDNA in the panel was made from pooled RNA from different individuals and we used the same batch of panels for all experiments, which means no experimental replicates were performed, which will have effects on

statistical significance. Thirdly, Origene used *β-actin* to normalize the RNA to and also supplied *β-actin* primers to normalize the data against in rt-PCR. The company has in due time decided that *Gapdh* is a more stable control gene for developmental tissues, which it provides with panel now. This will have some effect on the expression levels. However, because we have used 4 reference genes to calculate a normalization factor (Vandesompele et al., 2002) we have controlled for the possible error that using one reference gene gives.

One might question the decision to perform Spearman correlations between genes with only a small number of samples per time point (from 4 regions at E13 to 13 at Week 5). The inferences that may be drawn should be viewed with some caution. But, in defense, the genes were not selected randomly but *a priori*, based on the interactions between the genes, as found by yeast-two-hybrid, co-immunoprecipitation and immunocytochemistry, from which a developmental co-regulation was hypothesized. Also, the correlations reported (Fig. 3.7-3.8) exist between genes that are expected to be correlated, like *Nogo-pan* and *Nogo-A*, and between sterol associated genes *Abca2* and *Srebf2*.

Another potential point of criticism is the age of the mice studied and the relevance to mental illness. The developmental panel did not include an adult but an adolescent stage (Laviola et al., 2003; Hefner and Holmes, 2007). Mice are able to mate at this age but are not fully grown yet. Ideally this needs to be followed up by extending the panel to 10 weeks, to be able to compare it with the immunohistochemistry data, and even older ages perhaps more relevant to neurodegenerative diseases. Because the cDNAs from these timepoints are not available on the same panel they would need to be made from fresh mRNA and any results are perhaps difficult to compare with those from the panel.

Similarly immunohistochemistry on different postnatal and adult stages may give a better picture of the true changes relevant to psychiatric or neurodegenerative diseases. Because of the importance of adolescence and early adulthood in the development of schizophrenia and bipolar disorder (Joyce, 1984), but also in fear-,

anxiety- and depression-related behaviors (Laviola et al., 2003; Hefner and Holmes, 2007) this calls for further investigation. Therefore it would be interesting to measure mRNA and/or protein expression and function of GPR50 and interactors over a broader range of ages through adolescence and early adulthood, from 4 to 10 weeks.

The subcellular fractionation was performed using adult (8-10 week old) mice brains. It would be interesting to follow this up with different ages in order to detect (subtle) changes in synaptic expression. Ages that can be suggested are E18, early postnatal and weeks 4-6. In addition co-IP analysis can be followed up by using subcellular fractions expressing Gpr50 and interactors (eg P2 and P3 and synaptosome) and also immunoprecipications from regions of co-expression in the brain such as the hypothalamus and amygdala.

Lastly, in the subcellular fractionation and immunohistochemistry studies we looked at female brains only. This was done because of the relevance of using a female sample to the results from association studies indicating a female only risk. A true comparison between males and females is however necessary in order to determine expression differences between sexes.

Another necessary follow-up study would be comparing the expression profiles of the interactors in wild-type, *GPR50* knockout and heterozygous mice as this would provide additional information regarding a direct regulatory role for GPR50 with respect to these GPR50 interactors.

3.4.11 Summary

We have found Gpr50 expression in both the embryonic and adult mouse brain and in the postsynaptic density. The regions of Gpr50 expression suggest an involvement in neurotransmitter signalling and in particular energy metabolism and/or stress response, which is consistent with previous studies of Gpr50 expression and function. We have identified potential interaction sites of GPR50 with Nogo-A, Cdh8 and Abca2, which can be verified by co-immunoprecipitation. The light

membrane fractions and the synapse are potential subcellular locations of interaction. Within the brain the amygdala, hypothalamus, cortex and brain stem nuclei are possible sites of interaction, both in the embryonic and adult brain. More detailed research is needed to investigate the role of Gpr50 and its interactors in stress, depression and metabolism.

Chapter 4

What is the function of GPR50's interactions?

4 Chapter Four: What is the function of GPR50's interactions?

4.1 Introduction

G protein-coupled receptors (GPCRs) form a link between the cell and their environment activating intercellular signalling pathways upon ligand binding. The C-terminal domain (CTD) is key as it binds ß-arrestin and other interacting proteins. As GPR50 is an orphan receptor its ligand and secondary messenger system are still unknown, although there is some genetic and functional evidence linking GPR50 to mood disorders (Thomson et al., 2005), (lipid) metabolism (Bhattacharyya et al., 2006; Ivanova et al., 2008) and alteration of melatonin receptor signalling (Levoye et al., 2006).

The GPCR CTD can also function as a scaffold for other proteins and its effects may therefore be further reaching than simply G-protein activation and signalling (Marinissen and Gutkind, 2001). Clues to the function of GPR50 may therefore lie in its interaction partners, as identified by yeast-two-hybrid screen (Grünewald et al., 2009). The screen identified several members of the reticulon family: Nogo-A, Nogo-C and RTN3, which have been confirmed as GPR50 interactors in Grünewald et al. (2009) and in this thesis. A wide range of functions has been suggested for reticulon proteins including neurite outgrowth inhibition, BACE1 activity inhibition, intracellular trafficking between the endoplasmic reticulum (ER) and Golgi, ER membrane morphogenesis, vesicle formation, and apoptosis (Schwab, 2010; Yang and Strittmatter 2007), although the exact mechanisms of action of remain to be elucidated.

4.1.1 Nogo in axonal outgrowth inhibition and regeneration

The function of the longest variant of RTN4, RTN4A or Nogo-A, in the mammalian brain has been characterized extensively to date. Nogo-A mediates neurite outgrowth inhibition and growth cone collapse in the nervous system via several regions (Oertle et al., 2003b): through its C-terminal Nogo-66 domain by binding to the Nogo receptor (NogoR) (Fournier et al., 2001), and through several N-terminal regions termed 'amino-Nogo', 'NiRΔ2' and 'NiGΔ20' (Oertle et al., 2003b; Schwab, 2010) for which no specific receptor or signaling mechanisms have been identified.

As shown schematically in Fig 2.18 (Chapter 2), the GPR50-interacting domains on RTN proteins, as predicted by the Y2H study (Grünewald et al., 2009), lie in the Nogo (-A) N- and C-terminal regions. GID1 overlaps partly with NiGΔ20 (Oertle et al., 2003b) and GID2 overlaps the first 20 amino acids of the Nogo-66 domain (GrandPre et al., 2000). It is therefore hypothesised that GPR50 expression may affect the inhibition of neurite outgrowth caused by these domains.

As a consequence of the growth inhibiting characteristics of Nogo-A its function is currently being investigated in models of spinal cord regeneration. However, although *in vitro* models of Nogo-A neurite outgrowth inhibition have been consistent, *in vivo* models of axon and spinal cord regeneration in *Nogo (-A)* knockout mice (Kim et al., 2003; Simonen et al., 2003; Zheng et al., 2003) or a triple knockout of *Nogo* with other myelin-derived neurite outgrowth inhibitors *OMgp* and *MAG* (Cafferty et al., 2010; Lee et al., 2010) have shown inconsistencies and fail to clarify the mechanisms of axon regeneration failure common to the mammalian CNS. Better results were obtained by blocking Nogo-A and the Nogo receptor function using inhibiting molecules and an antibody against Nogo-A is currently being tested in a clinical trial as a treatment for spinal cord injuries (reviewed in Schwab, 2010).

4.1.2 Reticulons and BACE1 activity

Additionally several recent studies have suggested the involvement of Nogo and other reticulon proteins in neurodegenerative and psychiatric disorders such as amylotrophic lateral sclerosis (ALS), multiple sclerosis, Alzheimer's disease (AD) and schizophrenia (Yang and Strittmatter 2007). Expression differences for Nogo-A and –C have been shown in post mortem forebrain samples from individuals diagnosed with schizophrenia, bipolar disorder and Alzheimer's disease (Novak et al., 2002; Gil et al., 2006). An insertion/deletion polymorphism in the 3' UTR of Nogo has shown association to schizophrenia in some, but not all studies (Novak et al., 2002; Tan et al., 2005). Mice lacking Nogo-A or the NgR showed behavioural changes that mimic some of symptoms of schizophrenia, such as impaired latent inhibition and sensorimotor gating, and increased perseverative behaviour and sensitivity to stimulants such as amphetamines (Budel et al., 2008; Willi et al., 2009; Willi et al., 2010).

AD is the most common form of neurodegenerative dementia, and involves progressive loss of neuronal cells and cognitive function (Citron, 2010). A major pathological feature in AD is the presence of amyloid plaques in neuronal cells (Alzheimer, 1907), which are formed by the aggregation of amyloid (Aβ) peptides. Aβ peptides are generated through the sequential proteolytic cleavage of the large transmembrane protein APP. APP is cleaved by aspartic protease β-amyloid converting enzyme 1 (BACE1) to produce an N-terminal fragment (sAPP), which is secreted, and a membrane-bound C-terminal fragment (CTF99). CTF99 is then processed by γ-secretase to produce the pathogenic Aβ peptides $A\beta_{40}$ and $A\beta_{42}$ (Vassar et al., 1999; Yan et al., 1999; Selkoe, 2002). He et al. (2004) and Murayama et al. (2006) demonstrated that all four human reticulon proteins interact with BACE1. The authors further showed that RTN3 and Nogo-C are negative modulators of BACE1 by preventing BACE1 access to its APP substrate, resulting in decreased production of Aβ peptide. Conversely, reducing the expression of RTN3 led to an increase in the production of Aβ peptide (He et al. 2004). Interestingly, expression of human RTN3 is decreased in the temporal lobes of AD patients (Yokota et al., 2006).

The NgR inhibits BACE1 cleavage and Aß formation by interacting with APP (Park et al., 2006). Nogo can also modulate axonal sprouting in AD models in an apparently separate mechanism from RTN3/NgR (Masliah et al., 2010). Although Nogo depletion on an APPswe background restores axonal sprouting it has no effects on APP neuropathology, eg amyloid deposition and microgliosis (Masliah et al., 2010).

BACE1 has other substrates in addition to APP, suggesting a variety of physiological functions for BACE1 (Vassar et al., 2009). All BACE1 substrates identified to date are (predominantly type-I (Hemming et al., 2009)) transmembrane proteins and include the axonal signal proteins neuregulin-1 (NRG1) and neuregulin-3 (NRG3) (Hu et al., 2006; Willem et al., 2006; Hu et al., 2008), cell-adhesion molecules NCAM1, L1CAM, Protocadherin 7 and 21, and P-selectin glycoprotein ligand-1, voltage-gated sodium channel (Na(v)1) beta2-subunit (beta2), Semaphorins, Ephrins and Sortilin (Lichtenthaler et al., 2003; Kim et al., 2007; Hemming et al., 2009) These proteins link BACE1 to a wide variety of functions including myelination, cell adhesion, contact-dependent intercellular communication and cognitive functions. While *BACE1* knockout mice fail to produce Aß and showed a reduction in age-dependent cognitive decline, they also showed deficits in spatial memory and lower anxiety levels at younger age compared to littermate controls (Laird et al., 2005). BACE1 null mice also show deficits in presynaptic release and synaptic plasticity in the hippocampal CA1 and CA3 regions, suggesting a role for BACE in the regulation of synaptic signaling (Laird et al., 2005; Wang et al., 2008).

BACE1 substrate NRG1 is a ligand for receptor-tyrosine kinases of the ErbB family and induces various signalling pathways, including in synapse formation, plasticity, neuronal migration, and myelination of central and peripheral axons (Falls, 2003; Michailov et al., 2004). In the absence of BACE1, accumulation of unprocessed NRG1 leads to reduced myelination of axons in both the peripheral and central nervous system (Hu et al. 2006; Willem et al. 2006). In addition, reduced cleavage of NRG1 by BACE1 also decreases remyelination of injured sciatic nerves (Hu et al. 2008). BACE1 knockout reduced the interaction of ErB4 with PSD-95 and induced

schizophrenia-like behaviour of impaired prepulse inhibition (PPI), novelty induced hyperactivity, sensitivity to a psychostimulant, reduced social recognition and impaired working memory in mice (Savonenko et al., 2008). Moreover a reduction of impaired PPI and hyperactivity was seen after the administration of atypical antipsychotic Clozapine (Savonenko et al., 2008). This is in agreement with genetic and functional data indicating that *NRG1* is an important susceptibility gene for schizophrenia (Stefansson et al., 2002; Hall et al., 2006).

Because GPR50 has been shown to interact with both Nogo-C and RTN3 (this thesis) it is hypothesised that GPR50 has an effect on BACE1 activity. An increase in GPR50-immunoreactive cells was detected in the postmortem Alzheimer brain (Hamouda et al., 2007) suggesting a link to the illness, perhaps via BACE1.

4.1.3 The GPR50$^{\Delta 502\text{-}505/T532A}$ variant

The Δ502-505/T532A variant of GPR50 is associated with an elevated risk in bipolar disorder and major depression in women (Thomson et al., 2005; Macintyre et al., 2010). To date no research has been published on the function of the deletion variant specifically, although Levoye et al (2006), seemingly unknowingly, used the deletion variant in their study that identified a functional interaction with melatonin receptors MT1 and MT2. The deletion has no apparent effect on the ability of GPR50 to bind its interactors Nogo-A, Nogo-C and RTN3 (this thesis) but there may be changes in the affinity. It would be interesting to find out if there are any functional effects of the GPR50$^{\Delta 502\text{-}505/T532A}$ variant that may explain its association with mental illness.

4.1.4 Introduction to experiments

In order to find out more about the function of GPR50 I performed neurite outgrowth assays in Neuroscreen-1 cells, a subclone of rat pheochromocytoma (PC12) cells (Cellomics, Thermo-Fisher). PC12 cells are tumor cells from the adrenal medulla and are commonly used for modelling neuronal differentiation and early neurite development (Greene and Tischler, 1976). They closely resemble primary

sympathetic neurons in response to NGF-treatment when plated on collagen-coated (or poly-D-Lysine or poly-L-Lysine-coated) substrates in serum-free RPMI medium (Greene and Tischler, 1976). PC12 cells have however the tendency to form clumps, which makes visualisation and quantification of individual cells and neurites difficult. In addition, PC12 cell need to be treated with NGF every second day for at least 7 days before they produce sufficiently long neurites. For these reasons we used Neuroscreen-1 cells which grow out quantifiable neurites after 2 days of NGF-treatment and which are less prone to clumping. I investigated the effect of overexpression of GPR50 and/or Nogo-A on neurite length and the number of neurites. In addition I assessed the effect of the GPR50 polymorphisms associated with mood disorders (Thomson et al., 2005) on neurite outgrowth.

I also performed *in vitro* BACE1/β-secretase activity assays in HEK293 cells (He et al., 2004), assessing the effect of RTN3/Nogo-C/Nogo-A, GPR50 and GPR50$^{\Delta 502\text{-}505/T532A}$ overexpression on BACE1 activity. The fluorescence-based assay of BACE1 activity makes use of a synthetic peptide BACE1 substrate (Abcam). Two reporter molecules, EDANS and DABCYL, are conjugated to amino acids on either side of the BACE1 cleavage site. In the absence of BACE1 enzyme activity, the fluorescence emissions of EDANS are suppressed due to the physical proximity of the dark quencher DABCYL. Cleavage of the substrate by BACE1 results in physical separation of the two reporter molecules, thus releasing fluorescence emissions by EDANS. The level of fluorescence activity observed is proportional to the activity of BACE1 in the respective sample lysates.

4.2 Methods

4.2.1 Expression constructs

All expression constructs used in this chapter are the same as those listed in Table 2.1. Entry clones containing full-length human GPR50 (IOH63602) and RTN4 transcript variant 1 (Nogo-A, IOH53642), RTN4 transcript variant 3 (Nogo-C, IOH4069), RTN3 (transcript variant 1, IOH10268) in pENTR221, were obtained from Invitrogen (Paisley, UK). The eGFP construct was a kind gift from Laura Hyndman (University of Edinburgh. The empty pDEST40 vector was a kind gift from Christoph Grünewald (University of Edinburgh). $GPR50^{\Delta 502\text{-}505/T532A}$ was generated using Site Directed Mutagenesis (Agilent Technologies, see 2.2.4 Chapter 2)

Entry clones were cloned by recombination into pDEST40 and pDEST53 vectors for untagged and N-terminal GFP tags (LR clonase II, Gateway®, Invitrogen). To select for expression constructs, the vectors were used to transform competent E. coli (One Shot Omnimax 2-Ti, Invitrogen), and plasmid DNA was extracted using Qiagen Miniprep or Maxiprep kits (Crawley, UK) as per manufacturer's instructions. All clones were sequenced (see 2.2.5 Chapter 2) and checked for expression of proteins of the expected molecular weight by Western Blot (see 2.2.14 Chapter 2) in HEK293 cells.

4.2.2 Mammalian cell culture

All media and chemicals were purchased from Invitrogen, unless stated otherwise. HEK293 cells (ECACC) were cultured in DMEM with 10% fetal bovine serum (FBS). Neuroscreen-1 (NS-1, Thermo Scientific/Cellomics, Pittsburgh, PA, USA) cells were cultured in RPMI with 10% horse serum (heat inactivated) and 5% FBS with Penicillin and Streptomycin (100 unit/ml and 100 µg/ml). Cultures were kept at 37°C with constant humidity, 95% air and 5% CO_2. For transient transfections Lipofectamine 2000 was used according to the manufacturer's instructions (see 2.2.7 Chapter 2).

4.2.3 Primary neuronal culture

Hippocampal neuronal cultures were prepared from embryonic day 18 (E18) CD1 mice as described previously (Okabe et al., 2003; Bradshaw et al., 2008). Neurons were seeded at 50-100 cells/mm^2 on poly-D-Lysine (Sigma-Aldrich, St. Louis, USA) coated coverslips in 12 well cluster plates and cultured in neurobasal medium supplemented with 2% B-27, 2 mM Glutamax-1 and Penicillin/Streptomycin for 14-28 days-in-vitro (DIV). Cultures were kept at 37^{o}C with constant humidity, 95% air and 5% CO_2. For transient transfections Lipofectamine 2000 was used according to the manufacturer's instructions (see 2.2.7 Chapter 2).

4.2.4 Antibodies

Antibodies used are described in 2.3.1 of Chapter 2 and details are provided in Table 2.4a-b.

4.2.5 Immunocytochemistry

Cells were fixed 24 hours after transfection, by incubation in ice cold methanol for 10 min. Cells were washed with PBS containing 0.02% bovine serum albumin (BSA, Sigma-Aldrich) and blocked for 30 minutes in PBS/BSA with 10% serum from secondary antibody host. The following primary antibodies in PBS/BSA were incubated for 1 hour at room temperature: anti-GPR50 (C-ter, 1:1000), anti-GPR50 (G-15, 1:1000); anti Nogo-A (H-300, 1:1000), anti-TUJ1 (1:2000), anti-GFP (1:1000), anti-β-actin (1:100,000). After 3x5min washes with PBS/BSA, secondary antibodies Alexafluor 488/594 donkey anti-goat, -rabbit or –mouse IgG (1:500/1:800) in PBS/BSA with 10% serum, were applied for one hour at room temperature. Glass coverslips were mounted onto slides using a drop of mowiol (Sigma-Aldrich) with DAPI (Vectashield, Vector Laboratories, Peterborough, UK, 2µg/ml). Images were taken on a Zeiss Axioskop 2 fluorescent microscope (Zeiss Plan-Neofluar 40x/1.3 and 100x/1.3 oil objectives).

4.2.6 Neurite outgrowth assay

Neuroscreen-1 cells were seeded at low density (50 cells/mm^2) on poly-L-Lysine (Sigma) coated coverslips and were transfected 24 hours later with 2 µg plasmid DNA and 4 µl Lipofectamine 2000 according to manufacturer's instructions. After 6 hours the transfection mix was replaced by serum-free RPMI with penicillin, streptomycin and 50 ng/ml NGF (from murine submaxillary gland, Sigma). After 48-72 hours, cells were fixed with ice cold methanol and immunocytochemistry was performed as above. 150-500 images of transfected cells were taken randomly per condition over three independent experiments on a Zeiss Axioskop 2 fluorescent microscope (Zeiss Plan-Neofluar 40x/1.3 objective). Protrusions longer than the soma diameter were classified as neurites. The number of neurites per cell was counted and the length of the longest neurite per cell was measured using ImageJ software (http://rsb.info.nih.gov/ij/), blind to the condition. The mean differences in length and number between conditions were calculated using a One Way ANOVA with Bonferroni's Multiple Comparisons Test in Graphpad Prism. A significance level of $p<0.05$ was used.

4.2.7 BACE1 activity assay

All reagents were supplied with the Beta-Secretase Activity Assay Kit (Abcam) unless stated otherwise. HEK293 cells were transfected according to the lipofectamine transfection protocol (2.2.8 Chapter 2). Equal amounts of each individual plasmid were used for single and double transfections. Cells were trypsinized with 500 µl TripleExpress solution (Invitrogen) on 10 cm plates 24 hours post-transfection, and resuspended in prewarmed DMEM/FBS. Cells were counted using a haemocytometer and an equal amount of cells (1 x 10^7 cells) was used for subsequent processing of each sample. Cells were washed in ice cold PBS with protease inhibitors (Roche) and lysed in 200 µl of ice cold BACE1 Extraction Buffer (Abcam). Cell lysates were incubated on ice for 10 minutes and sonicated (3 x 10 seconds with 1 min on ice in between each sonication). Cell lysates were centrifuged

at 10,000x g for 5 min to remove cell debris. Per condition 50 µl lysate, 50 µl BACE1 Reaction Buffer and 2 µl BACE1 substrate were added to a 96-well Costar black plate in duplicate. Controls for every experiment included: 'no substrate' controls for each condition; a 'background' control, by adding BACE1 Extraction Buffer instead of lysate, a 'positive control', containing active recombinant BACE1 enzyme; and a 'negative control', containing a BACE1 inhibitor. The 96-well plates were then incubated in the dark at 37ºC for 2 hours. Absorbance readings were obtained in an EnVision multilabel plate reader (PerkinElmer) with excitation wavelength 335-355 nm and emission wavelength 495-510 nm. The readings from no substrate and background controls were subtracted from the experimental samples. These absolute BACE1 activity levels were normalised to the readings from eGFP and/or pDEST40 transfected cells resulting in the relative normalised BACE1 activity levels. The mean differences in relative BACE1 activity were calculated using a One Way ANOVA with Dunnett's post hoc test in Graphpad Prism. A significance level of $p<0.05$ was used.

4.2.8 Western Blotting

In the BACE1 activity assay HEK 293 cells were lysed in BACE1 Extraction Buffer (Abcam, see above) and processed as in Chapter 2 (section 2.2.14). Western blotting was also performed from Neuroscreen-1 cells, lysed with RIPA buffer, and processed as in section 2.2.14. Membranes were incubated with the following primary antibodies in PBS-T with 5% Marvel: anti-GFP (1:1000), anti-GPR50 (G-15, 1:5000), anti Nogo-A (H-300, 1:2000), anti-GAPDH (Millipore, 1:100,000) overnight at 4ºC. Membranes were washed 3x10 min times in PBS-T, before being incubated with secondary horseradish peroxidise (HRP)-conjugated antibodies (swine anti-rabbit HRP, 1:3000; rabbit anti-goat HRP, 1:5000; rabbit anti-mouse HRP, 1:2000, DAKO), diluted in PBS-T for 30 minutes at room temperature. Following three washes with PBS-T, membranes were developed using chemiluminescence (ECL-Plus Western Blotting Detection System, Amersham Biosciences) and exposure to x-ray film.

Results

4.2.9 GPR50 affects neurite outgrowth

Although most studies have focused on outgrowth inhibition of Nogo-A by oligodendrocytes (Schwab, 2004), neuronal Nogo-A is also involved in neurite outgrowth (Mingorance-Le Meur et al., 2007; Montani et al., 2009). I therefore investigated whether GPR50 affects neurite outgrowth *in vitro* (Grünewald et al., 2009). For this we used Neuroscreen-1 (NS-1) cells, a PC12 cell clone, which will develop quantifiable neurites after 2 days of treatment with nerve growth factor (NGF, 50 ng/ml).

NS-1 cells were transiently transfected with untagged GPR50, GPR50-TTC, GFP-Nogo-A or eGFP as a control. Overexpressed GPR50, Nogo-A and eGFP all localised in the extensions and at the tips of neurites, as shown by co-labelling with early neuronal marker β-III tubulin (Fig 4.1B-I), making comparative analysis of outgrowth possible (Grünewald et al., 2009).

After transfection and treatment with NGF for 48 hours, immunocytochemistry was performed and images of transfected cells were randomly collected for each condition. The length of the longest neurite was measured and the total number of neurites per cell counted. Analysis of neurite length (Fig 4.1J) shows a significant increase in neurite length after transient expression of untagged GPR50 (100±4.11 µm) or untagged GPR50 'TTC' (110±3.33 µm) when compared to eGFP (79±3.51 µm) ($p<0.0001$) (Grünewald et al., 2009). In agreement with previous results (Montani et al., 2009), Nogo-A overexpression significantly shortens neurites (59±5.56 µm, $p<0.0001$) (Grünewald et al., 2009). However, in cells cotransfected with GPR50 and Nogo-A no significant difference in neurite length was observed as compared to eGFP (86±10.33 µm, $p>0.05$) (Grünewald et al., 2009). GPR50 thus not only extends neurites, but also appears to attenuate Nogo-A's outgrowth inhibition phenotype. The number of neurites per cell (Fig 4.1K) was significantly decreased upon transfection with Nogo-A (n=2.06±0.097) and Nogo-A plus GPR50

(1.99±0.125) as compared to eGFP (2.31±0.085, $p<0.001$) but no difference was found in the GPR50-transfected cells (2.40±0.049, $p>0.05$) (Grünewald et al., 2009). Interestingly, the Nogo-A results show marked similarity to a previous study (Montani et al., 2009). When looking at neurite outgrowth in neuronal DRG cultures from *Nogo-A* KO mice, an increase was found in neurite length but no effect was detected on the number of neurites.

In addition to longer neurites, the GPR50-overexpressed phenotype shows an increase in filopodia and lamellipodia-like structures in which GPR50 colocalises with β-actin (Fig 4.2A-C) (Grünewald et al., 2009). GPR50 is not able to induce neurite outgrowth in NS-1 cells in the absence of NGF (Fig 4.2D-E), although overexpressing GPR50 appears to induce filopodia formation (Fig 4.2E) as compared to eGFP (Fig 4.2D). In primary hippocampal neurons transfected with GPR50 an increase in synaptic spines is also observed as compared to eGFP (Fig 4.2F).

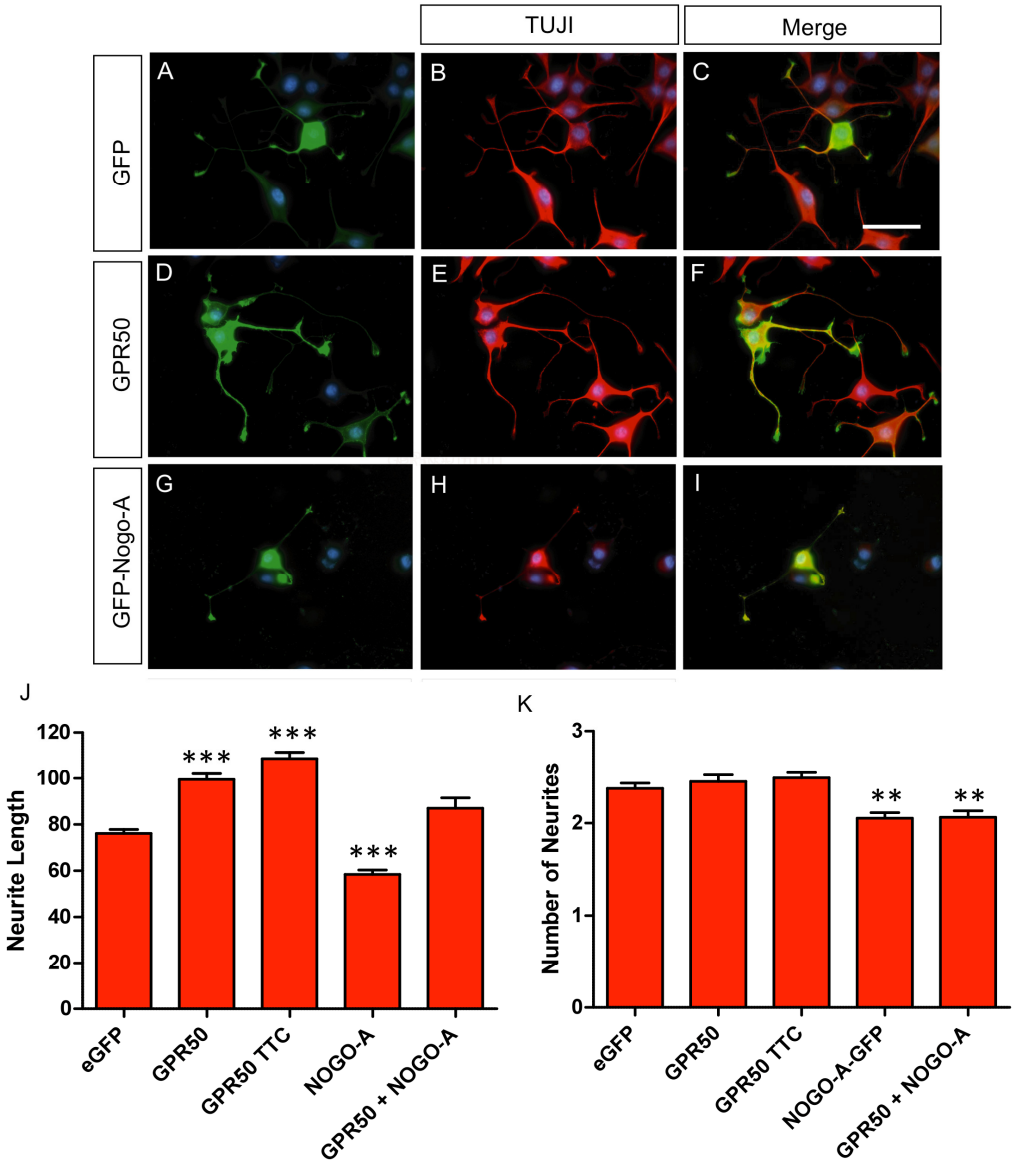

Figure 4.1 *GPR50 overexpression increases neurite outgrowth. Neuroscreen-1 cells were transiently transfected with eGFP, full length human untagged GPR50, full length untagged human GPR50'TTC', full length human Nogo-A or cotransfected with GPR50 and Nogo-A. After treatment with 50 ng/ml NGF for 48 h, transfected cells were labeled by expression of GFP (A, G) or GPR50 (Abcam, D). Co-staining with β-III tubulin (B-C, E-F, H-I) shows all overexpressed proteins are present throughout the cell body and into the neurites. Per condition 150-500 cells were randomly selected over five independent experiments. The length of the longest neurite (J) and number of neurites (K) per cell were determined for each condition. Bars show means (±SE). Cells were counterstained with DAPI. Scale bar: 50 µm. *** p<0.001, ** p<0.01. Image adapted from Grünewald et al., (2009) Molecular and Cellular Neuroscience. Copyright Elsevier 2009.*

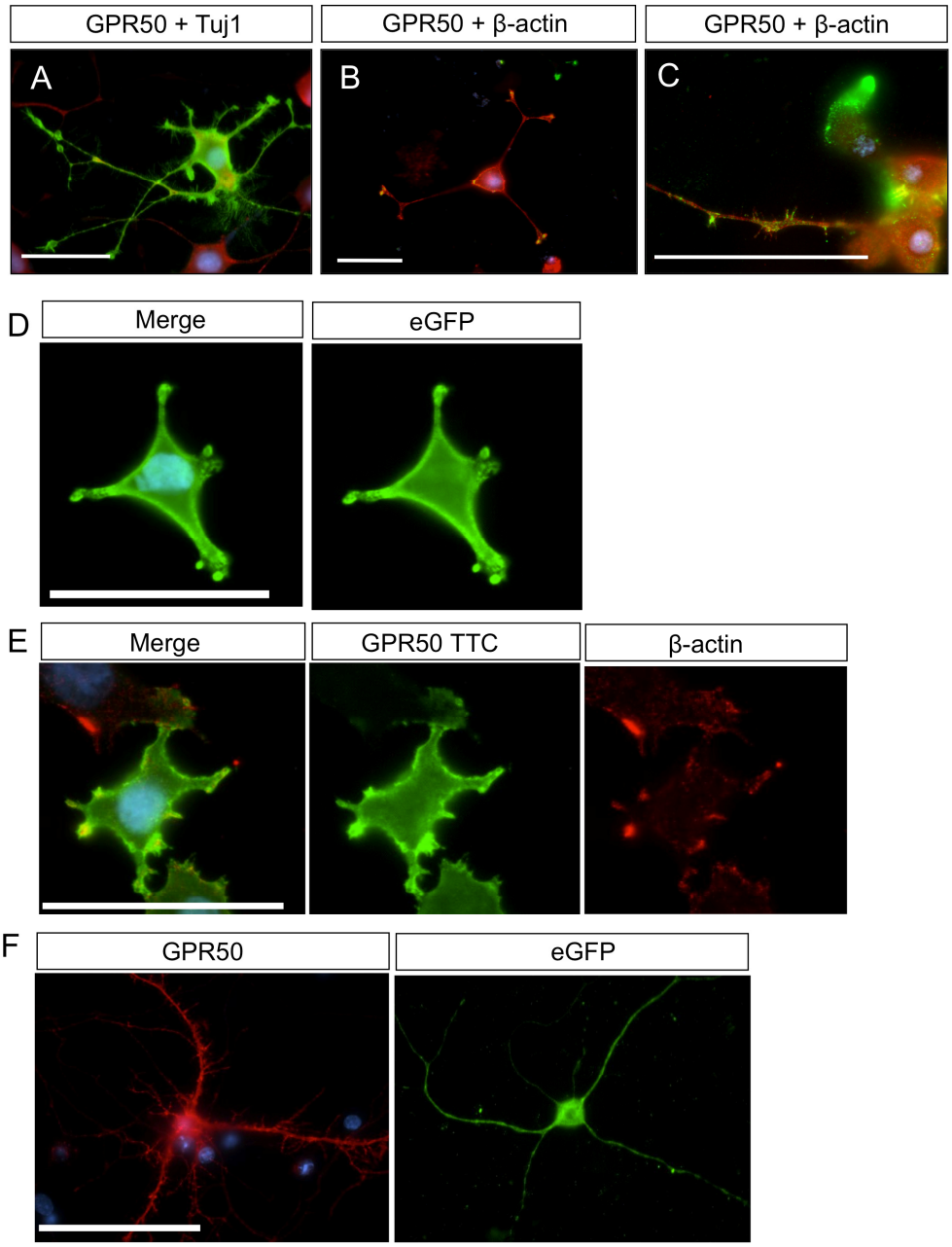

Figure 4.2 *GPR50 induces filopodia in Neuroscreen-1 and primary cultured neurons. NS-1 cells were transfected with GPR50-TTC (A-C), incubated for two days in serum-free medium with NGF and then labelled with GPR50 C-ter (A, green; B-C, red) and TUJ1 (A, red) and β-actin (B-C, green). NS-1 cells were transfected with (D) eGFP or (E) GPR50TTC, were cultured for two days in serum-free medium without NGF and stained with (D) GFP or (E) GPR50 G-15 and β-actin. (F) Primary hippocampal mouse neurons were transfected at 14 DIV with untagged GPR50 or eGFP and stained with GPR50 C-term antibody or GFP. Cells were counterstained with DAPI. Scale bar: 50 µm. Image partly adapted from Grünewald et al., (2009) Molecular and Cellular Neuroscience. Copyright Elsevier 2009*

4.2.10 GPR50$^{\Delta 502\text{-}505/T532A}$ further increases neurite outgrowth

The above neurite outgrowth experiment was repeated using GPR50$^{\Delta 502\text{-}505/T532A}$ to assess the effects of the deletion variant associated with mood disorders on neurite outgrowth. Overexpressed GPR50 and GPR50$^{\Delta 502\text{-}505/T532A}$ were both present at the tips of neurites, colocalising with β-actin (Fig 4.3A, arrows). A significant increase in neurite length was measured after overexpression of GPR50 (88.32±2.470) and GPR50$^{\Delta 502\text{-}505/T532A}$ (99.71± 2.507) compared to eGFP (72.32±2.207; $p<0.001$), moreover a further significant increase was found in GPR50$^{\Delta 502\text{-}505/T532A}$-overexpressing cells compared to GPR50 ($p<0.01$) (Fig 4.3B). Again no difference was found in the number of neurites between conditions ($p>0.05$, Fig 4.3C). To test whether this increase was the result of higher GPR50 expression of the GPR50$^{\Delta 502\text{-}505/T532A}$ construct NS-1 cells were transfected with GPR50, GPR50$^{\Delta 502\text{-}505/T532A}$ or GPR50 TTC or left untransfected. Western blotting was performed using the GPR50 G-15 antibody and GAPDH as a loading control. The results (Fig 4.3D) indicate that there is no difference in expression levels between GPR50 and GPR50$^{\Delta 502\text{-}505/T532A}$ but that GPR50 TTC is much higher GPR50 expressor as was previously shown (Chapter 2). This indicates that GPR50$^{\Delta 502\text{-}505/T532A}$ indeed increases neurite outgrowth further compared to GPR50.

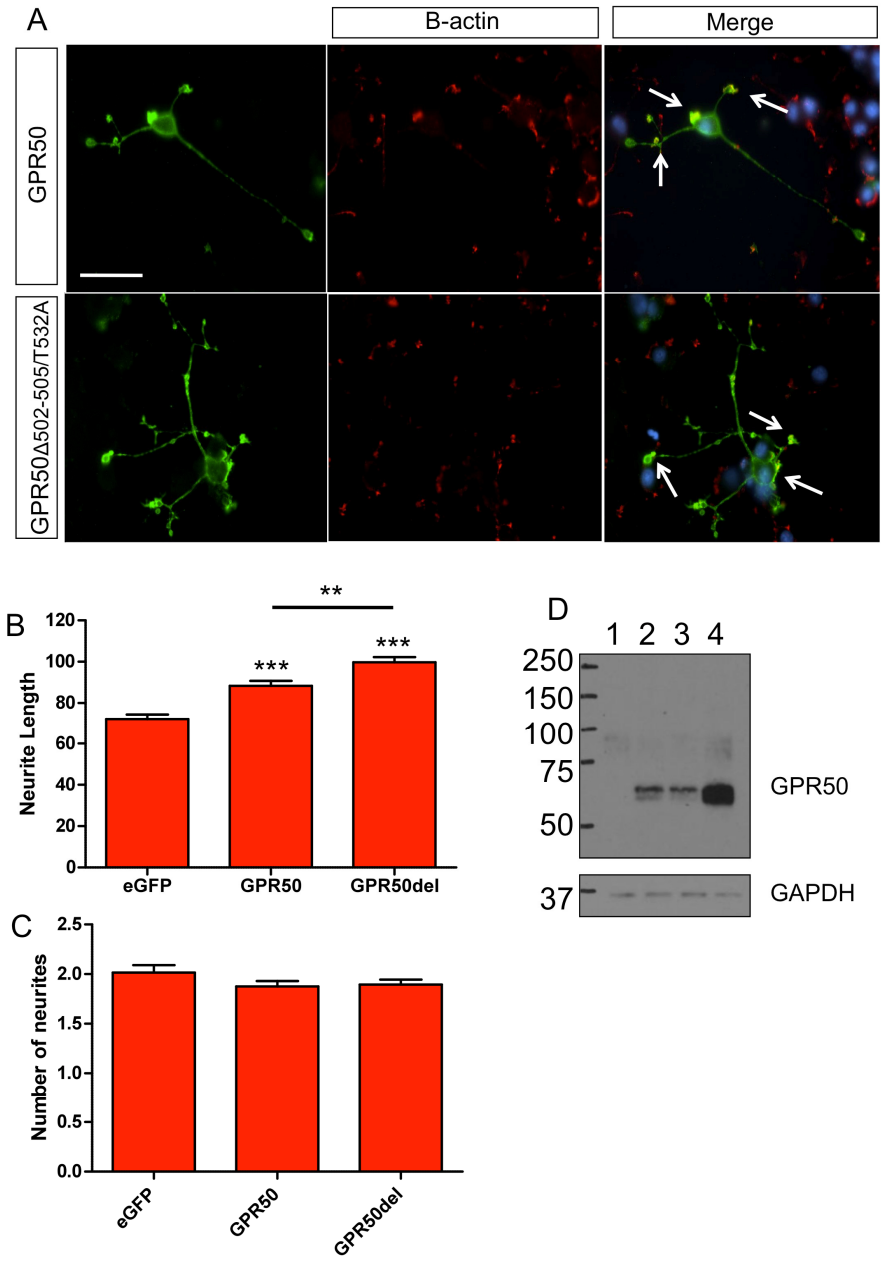

Figure 4.3 *GPR50Δ502-505 overexpression further increases neurite outgrowth. (A) NS-1 cells were transfected with GPR50 or GPR50Δ502-505/T532A and labelled with GPR50 (green) and β-actin (red). Cells were counterstained with DAPI. Scale bar: 50 µm. (B-C) After treatment with 50 ng/ml NGF for 48 h, transfected cells were labeled by expression of GFP or GPR50. Per condition 300 cells were randomly selected over three independent experiments. The length of the longest neurite (B) and number of neurites (C) per cell were determined for each condition. Bars show means (±SEM). *** p<0.0001, ** p<0.001. (D) NS-1 cells were left untransfected (1) or transfected with GPR50 (2), GPR50Δ502-505/T532A (3) or GPR50 TTC (4). Western blotting was performed using the GPR50 G-15 antibody and GAPDH as a loading control.*

4.2.11 Effect of reticulon proteins and GPR50 on in vitro BACE1 activity

As reticulon proteins are known to interact with BACE1 and inhibit its activity (He et al. 2004; Murayama et al. 2006), I wanted to establish whether GPR50 has any effect on BACE1 activity *in vitro*. HEK293 cells were used, which endogenously express BACE1 at relatively low levels, as they are able to produce small amounts of Aβ peptide (Hemming et al. 2009). A commercially available fluorescence-based BACE1 activity assay kit (Abcam) was used to assess the effect of overexpressing GPR50, the deletion variant GPR50$^{\Delta 502\text{-}505/T532A}$ (Thomson et al. 2005) and reticulon proteins Nogo-A, Nogo-C, and RTN3 on BACE1 activity, similar to the activity assay used by He et al., (2004).

The experiment was performed in two parts. The first part investigated the effects of untagged GPR50 (Δ502-505/T532A), untagged Nogo-A, GFP-Nogo-C and GFP-RTN3 on BACE1 activity. The second set of experiments looked at the combined effects of GPR50 (or Δ502-505/T532A) with Nogo-C or RTN3. EGFP and pDEST40 were used as controls and three independent experiments were performed. Two replicates from this first part were performed by MSc student Sophie Hempel (as part of her 4year IGMM PhD programme), the rest by myself. The sample lysates used in the fluorescence assay were checked by Western blot for correct expression of the respective proteins (Fig 4.4A).

The absolute non-normalised BACE1 activity data are shown in Fig 4.4B. These data were normalised to either GFP, for GFP-tagged constructs Nogo-C and RTN3, or the empty vector control (pDEST40) for all remaining untagged constructs. Cells cotransfected with untagged and GFP-tagged constructs were normalised to both eGFP and pDEST40. Because the experiment was performed in two parts it is necessary to establish whether the conditions between the two parts were similar. Only in this case the results from the two parts can justifiably be compared. Therefore T-tests were performed to test if absolute BACE1 activity of the control conditions was the same in both parts of the experiment. There was no significant

difference in absolute BACE1 activity between GFP or pDEST40 between part 1 and 2 of the experiment ($p>0.05$) and therefore the normalised data of single- and double-transfected cells can be compared.

The normalised results are shown in Fig 4.4C. As reported previously Nogo-C and RTN3 reduced BACE1 activity ($p<0.05$) (He et al., 2004; Murayama et al., 2006). No significant difference was seen however upon Nogo-A overexpression. Interestingly, over-expression of GPR50 significantly increased BACE1 activity ($p<0.05$, Fig 4.4C), whereas the GPR50 deletion variant, $GPR50^{\Delta 502\text{-}505/T532A}$ did not affect BACE1 activity. No difference in BACE1 activity was found when cells were cotransfected with GPR50 or $GPR50^{\Delta 502\text{-}505/T532A}$ and RTN3 or Nogo-C compared to control. GPR50 thus appears to partially counteract the BACE1 inhibiting characteristics of RTN3 and Nogo-C.

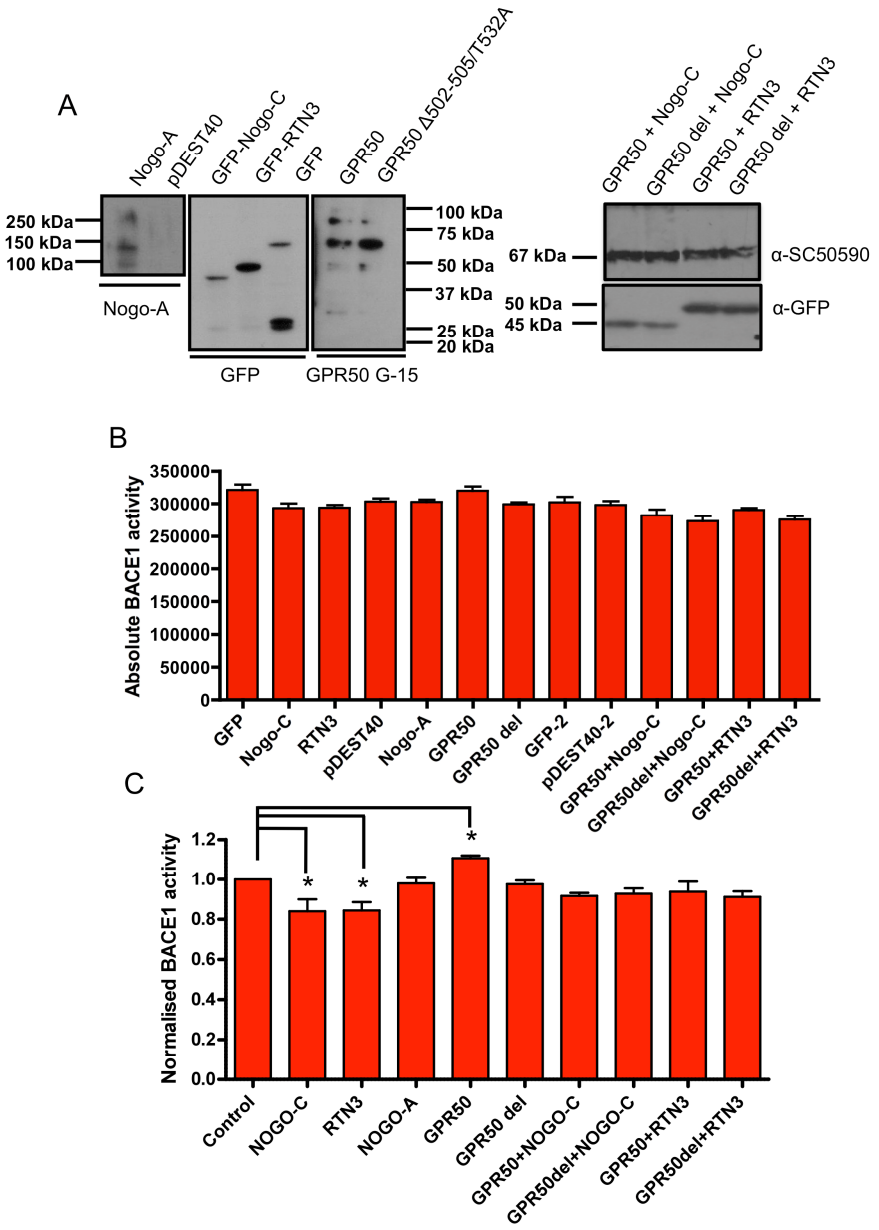

Figure 4.4 *Effect of reticulon proteins and GPR50 on BACE1 activity in vitro. (A) HEK293 cells were transfected with respective constructs (see legend and materials & methods). Cells were lysed using the BACE1 extraction buffer (Abcam), loaded on SDS-PAGE and checked for protein expression by Western blotting. 'GPR50del' = GPR50Δ502-505/T532A. (B) After incubation of lysates with reaction buffer (Abcam) and BACE1 substrate at 37°C, EDANS fluorescence emission caused by BACE1 cleavage was measured and absolute BACE1 activity readings taken from three independent replicates. (C) Relative BACE1 activity from three independent replicates. Absolute values were normalised to either the GFP (for GFP-tagged constructs) or to the empty vector control (pDEST40) reading (for untagged pDEST40 constructs, or both for cotransfected samples). Bars show means (±SE). * p<0.05.*

4.3 Discussion

In this chapter two functional assays were performed: neurite outgrowth and BACE1 activity. In both assays there is a significant effect of GPR50 overexpression. GPR50 appears to extend neurites and also increases BACE1 activity compared to controls.

4.3.1 GPR50 and neurite outgrowth

We have shown that GPR50 overexpression increases neurite ougrowth *in vitro* contrary to Nogo-A. The results also suggest that GPR50 attenuates the outgrowth inhibiting characteristics of Nogo-A. The $GPR50^{\Delta 502\text{-}505/T532A}$ variant further increases neurite outgrowth compared to GPR50.

Nogo-A is a potent neurite outgrowth inhibitor *in vitro* and *in vivo* (Schwab, 2004). One of the Nogo-A-signalling pathways is mediated by the neuronal Nogo-66 receptor (NgR) complex (Fournier et al., 2001) and second messengers RhoA and Rac1, which alter actin dynamics and organisation of the cytoskeleton (Fig 4.6) (Niederost et al., 2002; Fournier et al., 2003; Montani et al., 2009). GTPases Rho, Rac and Cdc42 are involved in actin dynamics by regulating cell adhesion and stress fibre formation (Rho), lamellipodia formation (Rac) and filopodia formation (Cdc42) (Nobes and Hall, 1995). It is likely that other Nogo-A signalling pathways exist as Nogo-A expression in the developing CNS precedes NgR expression (Mingorance et al., 2004) and other regions of Nogo-A can also inhibit outgrowth (Oertle et al., 2003b).

Although the neurite outgrowth inhibiting properties are mainly attributed to different regions of Nogo-A in oligodendrocytes (Oertle et al., 2003b), it is expressed in many different cell types, including developing and adult neurons (Mingorance et al., 2004; Dodd et al., 2005; Richard et al., 2005). In neurons, overexpressing Nogo-A causes destabilisation of inhibitory synapses in vivo (Aloy et al., 2006), inhibiting Nogo-A or the Nogo-receptor in adult mouse hippocampal slices results in an increase in long-term potentiation (LTP, Delekate et al., 2011), and ablation of

neuronal Nogo-A in knockout mice causes neurite extension (Montani et al., 2009) or branching of the major neurite (Mingorance-Le Meur et al., 2007). These studies indicate a role for neuronal Nogo-A as a negative regulator of plasticity and growth.

Our observations, that Nogo-A overexpression reduces neurite outgrowth in a neuronal-like cell line, support a role for neuronal Nogo in axonal formation and growth in development under non-pathological conditions (Mingorance et al., 2004; Richard et al., 2005). The opposite effect of increased outgrowth in GPR50-overexpressing neuronal cells is intriguing as it is remarkably similar to the effects seen in neuronal cultures from Nogo-A knockout mice (Fig 4.6) (Grünewald et al., 2009; Montani et al., 2009).

Whether GPR50 signals via Nogo-A and RhoA/Rac1 to alter neurite outgrowth or through Rac1 or another pathway calls for further investigation. Although there are indications that GPR50 increases filopodia in the absence of NGF (Fig 4.2), NGF is necessary for initiation of neurite outgrowth. This suggest Cdc42 activation by GPR50 rather then Rac1 (Nobes and Hall, 1995). Future studies performing Cdc42/Rac/Rho activity assays as well as targeting effector molecules of GTPase signalling pathways are necessary to confirm this.

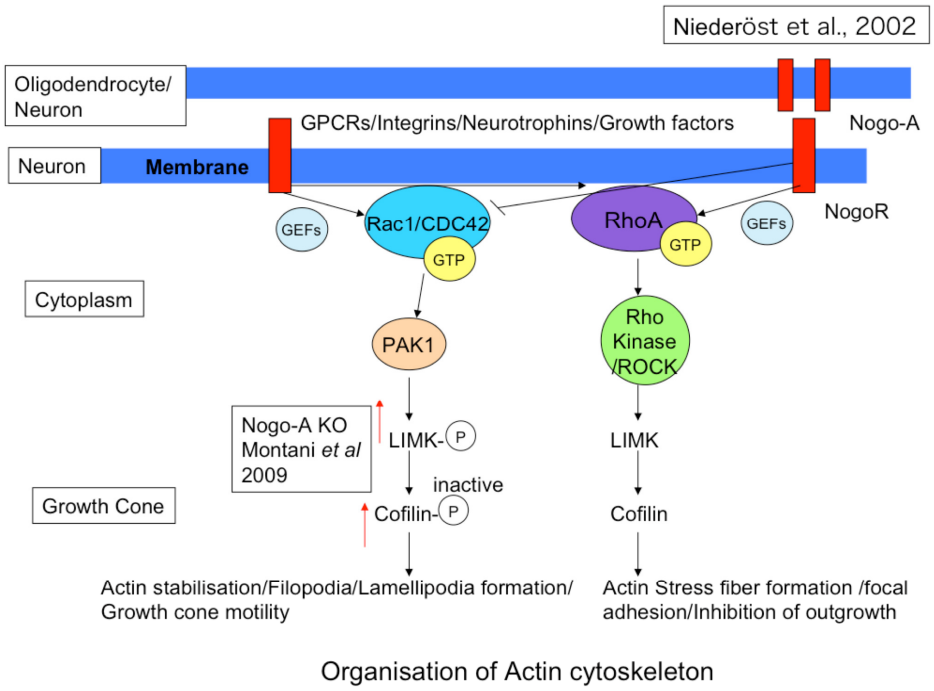

Figure 4.5 *Rho GPTases (RhoA, Rac1, Cdc42) and the organisation of the actin cytoskeleton. Nogo-A on the surface of oligodendrocytes or neurons can bind the Nogo receptor (NgR) via its Nogo-66 loop region (Fournier et al., 2001). NgR forms a complex with transmembrane proteins p75, LINGO1 and TROY (Nash at al., 2009). This leads to the activation of RhoA and ROCK pathway, via LIMK and Cofilin (Montani et al., 2009; Niederöst et al., 2002), and to neurite outgrowth inhibition. A parallel pathway, which is inhibited by Nogo-A (Niederöst et al., 2002) leads to Rac1 activation of PAK1 resulting in increased phosphorylation and inactivation of LIMK and Cofilin and to actin stabilisation and neurite outgrowth. These pathways can also be activated by other membrane receptors and signaling proteins (Siehler, 2009), perhaps GPR50 as well.*

Several of the other yeast two-hybrid interactors are also linked to neuronal development (CDH8, PCDH 9, SHOT1, PICK1), which increases the possible pathways in which GPR50 can affect neurite outgrowth. Cadherins can play a role in neurite extension (Skaper et al., 2001), through activating the fibroblast growth factor receptor (FGFR). By triggering second messenger cascades phospholipase C_γ (PLC_γ) is activated and voltage gated calcium channels are opened (Williams et al., 1994). This calcium influx is required for and sufficient to stimulate neurite outgrowth (Doherty et al., 1991). Whether this is also the case for CDH8 and PCDH9 needs to be further investigated.

Shootin-1 (SHOT1) is a brain-specific protein expressed during development, with a peak around postnatal day 4 (Toriyama et al., 2006). It localises to filopodia and lamellipodia and interacts with actin retrograde flow and with neuronal cell-adhesion molecule L1-CAM (also known as CDH2) (Shimada et al., 2008). The interaction is necessary for L1-dependent neurite outgrowth in hippocampal neurons. SHOT1 overexpression induces L1-dependent neurite outgrowth (Shimada et al., 2008). SHOT1 is involved in the development of neuronal polarisation. SHOT1 localises to a single neurite, which later develops into the axon and disrupting SHOT1 alters this asymmetric polarisation (Toriyama et al., 2006). Interestingly GPR50 overexpression only increase the length of the longest neurite and not the number of neurites suggesting it plays a role in axon formation as well.

PICK1 on the other hand has been shown to control and reduce synaptic spine size by inhibiting Arp2/3-mediated actin polymerisation (Rocca et al., 2008; Nakamura et al., 2011).

Interestingly other GPCRs are known to affect neurite outgrowth. GPR3, GPR6 and GPR12 are constituitively active and can induce neurite outgrowth in cerebellar granule neurons via activation of $G\alpha_s$ and cAMP and via inhibition of RhoA (Tanaka et al., 2007). In PC12 cells PACAP (Pituitary adenylate cyclase-activating

polypeptide) signaling through the GPCR PAC1 can induce neurite outgrowth via $G\alpha_s$ and $G\alpha_q$ (Vaudry et al., 2002), activating cAMP, PKA and EPAC, ERK and CREB. Interestingly there is some overlap with the pathway activated by NGF via the TrkA receptor in PC12 cells, although the processes are distinct (Vaudry et al., 2002). It is likely that many other recptors including GPR50 can influence these pathways via crosstalk or downstream signalling.

Without a ligand the GPR50 signalling pathway has remained unclear. This study however offers new insights into the pathways that could be investigated. GPCRs are able to activate Rho GEF and GTPases via $G_{\alpha 12/13}$ and several recently deorphanised GPCRs couple to $G_{\alpha 12/13}$ (Lee et al., 2006; Henstridge et al., 2009; Siehler, 2009). A preassociation of GPR50 with $G\alpha_i$, $G\alpha_q$ and G_β (but not $G\alpha_s$ or $G_{\alpha 12}$) has been found (Levoye et al., 2006). $G\alpha_i$ can activate Rac1 and RhoA (Singh et al., 2010) and $G\alpha_q$ was found to be necessary for morphological changes associated with cortical actin cytoskeleton redistribution in Drosophila photoreceptor cells (Kosloff et al., 2003). $G\alpha_i$ signalling inhibits cAMP and PKA production and activates protein kinases such as mitogen-activated protein kinases (MAPK) 1 and 2 and Akt. These kinases can stimulate neurite outgrowth in Neuro2A cells and the CNS (Ma'ayan et al., 2009). These pathways were shown to be activated by GPCR 5-HT1A/B, Cannabinoid 1 receptor and Dopamine D2 receptor stimulation (Ma'ayan et al., 2009). However, non-G-protein signalling is an important mechanism and ß-arrestins and G-protein-coupled receptor kinases, binding to the C-terminal domain, coordinate signal transduction by mediating silencing or desensitisation, trafficking, and G-protein independent signalling of 7-transmembrane receptors (Reiter and Lefkowitz, 2006). It is therefore possible that GPR50 excerts its function via ß-arrestin-dependent signalling.

Although neuronal Nogo-A accumulates in axonal growth cones, it remains in the central region and does not enter the filopodial processes (Mingorance-Le Meur et al., 2007). We have shown that GPR50 overexpression results in an increase in

filopodia and lamellipodia, in which GPR50 is present and colocalizes with actin. This difference in distribution is interesting and may be related to the opposite effects on outgrowth. Besides playing an important role in neurite outgrowth, filopodia are seen as precursors of dendritic spines (Mattila and Lappalainen, 2008), perhaps indicating a role for GPR50 and in synapse development.

Overexpression of the GPR50$^{\Delta 502\text{-}505/T532A}$ variant further increased neurite outgrowth, which is perhaps surprising since the polymorphism is associated with an increased risk in psychiatric illness. From this perhaps a decrease in neurite length would be predicted, in agreement with CNS volume reductions in mood disorders and findings that antidepressants and antipsychotics promote neurite outgrowth and brain grey matter volume (reviewed in Manji et al., 2000). This may however indicate neurite development is disturbed in GPR50$^{\Delta 502\text{-}505/T532A}$ variant. Since GPR50$^{\Delta 502\text{-}505/T532A}$ is a common variant (Thomson et al., 2005), the effects are not likely to be drastic, but it would be interesting to investigate possible differences in brain connectivity between people with GPR50 vs GPR50$^{\Delta 502\text{-}505/T532A}$ using functional imaging.

4.3.2 GPR50 and BACE1 activity

We have shown that GPR50 overexpression inceases BACE1 activity *in vitro*. Like He et al. (2004) and Murayama et al. (2006) we report that RTN3 and Nogo-C overexpression results in decreased BACE1 activity. Neither Nogo-A nor the GPR50$^{\Delta 502\text{-}505/T532A}$ variant alter BACE1 activity compared to control.

Interestingly, the effects of GPR50 on BACE1 activity may provide clues to its function in psychiatric illness, perhaps via NRG1. BACE1 has multiple substrates in addition to APP (see introduction to this chapter) and BACE1 is also responsible for the processing of NRG1, a signalling protein responsible for axon myelination (Willem et al., 2006). This is summarised in Fig 4.7. It is possible that GPR50, perhaps in response to an extracellular ligand, initiates a pathway that leads to the up-regulation of BACE1 and subsequent Aβ-generation and myelination.

Interestingly NRG1 is also a well-researched candidate gene for schizophrenia (Stefansson et al., 2002; Corfas et al., 2004; Hall et al., 2006). This implicates GPR50 in two pathological pathways, in Alzheimer's disease and psychiatric illness (Fig 4.7).

Aberrant sprouting of neurites is a common pathlogical feature in AD (Hashimoto and Masliah, 2003; Masliah et al., 2003). A similar mechanism has been proposed for schizophrenia although there is little evidence to support this (Stevens, 1992). GPR50 was detected in postmortem Alzeimer's brain (Hamouda et al., 2007) so it is possible that GPR50 plays a role in this mechanism. Interestingly it is proposed that Nogo may negatively regulate aberrant sprouting in AD (Masliah et al., 2010).

Yet another possibility is that GPR50 plays a role in the normal functioning of APP/BACE1. There is emerging evidence for a role of APP in neurite outgrowth (Leyssen et al., 2005; Hoe et al., 2009) neuronal proliferation and survival and cell adhesion (Hughes et al., 2010), synaptic development (Ashley et al., 2005) and interestingly G-protein-coupled receptor signaling (via G_0), (Nishimoto et al., 1993) under non-pathological conditions (Reinhard et al., 2005).

The results obtained in this study strengthen a role for GPR50 in brain disorders like AD and psychiatric illness, in agreement with previous studies (Thomson et al., 2005; Hamouda et al., 2007; Macintyre et al., 2010), and may even suggest a future role for GPR50 as a therapeutic target. More detailed research is however needed to substantiate these claims. The following questions may be relevant for future research.

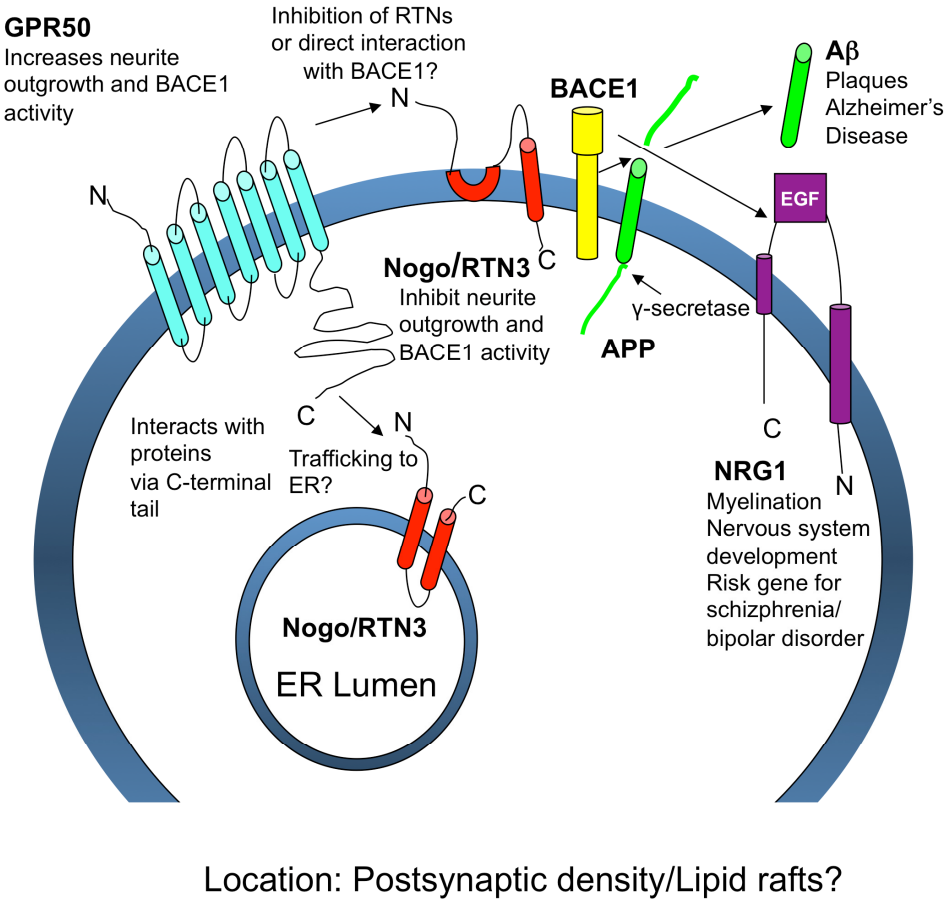

Figure 4.5 *Possible mechanisms of GPR50 functioning. GPR50 is shown to increase neurite outgrowth and BACE1 activity suggesting a link to Aβ deposition and Alzheimer's disease but also to NRG1 cleavage, myelination and psychiatric illness. Reticulon proteins on the other hand have been shown to inhibit neurite outgrowth and BACE1 acitivity suggesting GPR50 functions through inhibition of reticulon proteins. More research is needed to determine whether GPR50 interacts directly with BACE1 and what the downstream effects of BACE1 inhibition are. Nogo-A is known to signal via Rho kinase (ROCK) to destabilise the Actin cytoskeleton resulting in growth cone collapse. The effects of GPR50 overexpression on ROCK signaling and actin need to be investigated. GPR50, Nogo-A, BACE1 and APP all localise to the postsynaptic density suggesting they interact at the synapse. APP and BACE1 were previously shown to localise to lipid rafts indicating another possible interaction site within membranes or the PSD.*

4.3.3 Future studies

4.3.3.1 What are the effects of GPR50 knockdown/knockout?

So far we have only worked with overexpressed GPR50. This is due in part to the difficulty in obtaining a knockout mouse (mice have been produced by Organon/Schering Plough/Merck and Astra Zeneca, and KOMP (Knockout Mouse Project, UC Davis) have recently produced one). Knockdown of GPR50 using RNAi should however be easier to perform. The endogenous levels of GPR50 in common immortalised cell lines are however very low (1-10% of HEK293 cells) or not detectable (COS7, SHSY5Y, Neuroscreen-1) by rt-PCR, Western blotting or immunocytochemistry. As shown in Chapter 2 Gpr50 is detected in cultured neurons by immunocytochemistry. The effects of GPR50 knockdown on neurite outgrowth and BACE1 activity could therefore be tested in these cells.

4.3.3.2 Does GPR50 interact directly with BACE1?

While it has been found that reticulon proteins can directly bind and inhibit BACE1, it is not clear how GPR50 would achieve the up-regulation of BACE1 activity. Binding studies such as co-immunoprecipitation are needed to determine whether GPR50 has any direct or indirect interaction with BACE1, and whether this interaction involves reticulon proteins (for instance in a complex). APP has been shown to be expressed in presynaptic vesicles and in the PSD (Ashley et al., 2005) which suggests that GPR50/RTN3/4 may interact with APP/BACE1 at the synapse. Knockout models of reticulon proteins need to be included in order to test whether the functional effects are dependent on GPR50-RTN3/Nogo-C interactions.

A cell-based system in which GPR50 is endogenously expressed would be useful. Of all the cell lines that have been used in this thesis only HEK293(T) cells express GPR50 in 1-10% of cells. In the immunohistochemistry study several regions of the brain that express GPR50 were identified, most notably the hypothalamus and the locus coeruleus. Perhaps a cell line derived from these regions could be used. Recently a catecholaminergic cell-based system has been developed. CAD (Cath.a-differentiated) cells are a mouse neuronal cell line originating from the locus

coeruleus in which a neuronal phenotype can be induced following serum deprivation (Qi et al., 1997). Interestingly this system has so far been useful in studying APP and Aβ cell biology and Alzheimer's pathology (Muresan and Muresan, 2006; Muresan et al., 2009) and also DISC1 cell biology and psychiatric illness (Park et al., 2010).

4.3.3.3 Does GPR50 affect APP and NRG1 processing and Erb signalling?

Increased BACE1 activity suggests increased APP processing and extracellular Aβ, and an increase in NRG processing and myelination. Whether GPR50 overexpression can cause this needs to be tested. The $GPR50^{\Delta 502\text{-}505/T532A}$ variant does not increase *in vitro* BACE1 activity more then control and may thus result in reduced processing of NRG1 and myelination or prevent excessive Aβ production compared to GPR50. Myelin electrically insulates axons and is essential for the proper functioning of neuronal information processing (Sherman and Brophy, 2005). Loss of myelination can lead to cognitive defects and is known to be a contributing pathological feature in schizophrenia (Dwork et al., 2007) and possibly other psychiatric disorders. It is possible $GPR50^{\Delta 502\text{-}505/T532A}$ may lead to increased risk in psychiatric illness via abnormal myelination.

4.3.3.4 Do GPR50 and interactors affect surface/endomembrane expression (and therefore functionality) of BACE1?

Several of the GPR50 Y2H interactors have a role in cell sorting. SNX5 and SNX6 are members of the SNX family of proteins involved in membrane trafficking and protein sorting. It is believed that SNX5 and SNX6 are part of a retromer involved in endosome to *trans*-golgi network (TGN) transport (Hong et al., 2009). SNX6 was recently identified as a BACE1 interactor and a negative modulator of BACE1-mediated APP processing (Okada et al., 2010). It appears to do this by negatively modulating BACE1 retrograde transport from the endosome to the TGN. Y2H interactor Consortin (FLJ32001) is another TGN protein involved in the membrane targeting of interacting Connexin proteins (del Castillo et al., 2010). It is possible that these proteins is also involved in the sorting and targeting of BACE1.

RTN3 has been suggested to play a role in cellular trafficking between the Golgi and ER (Wakana et al., 2005). Recently it was shown that BACE1 localisation was altered upon RTN3 overexpression (Shi et al., 2009). HEK293 cells stably expressing RTN3 showed an enrichment of BACE1 in the ER fraction and decrease on the cell surface (Shi et al., 2009). BACE1 preferentially cleaves APP in an acidic milieu like the early endosome or Golgi and the ER is therefore not favourable. This increased retention of BACE1 and APP in the ER may explain the abnormal processing of APP and decreased Aß deposition, which is observed upon RTN3 overexpression. Results in Chapter 2 indicate that reticulon proteins have a similar effect of GPR50, decreasing its surface expression in favour of the ER. The strongest effects were seen on $GPR50^{\Delta 502\text{-}505/T532A}$ upon co-overexpression of RTN3 (Chapter 2). These results suggest that $GPR50^{\Delta 502\text{-}505/T532A}$ is more prone to ER retention and association with RTN3 and which perhaps causes a reduction in BACE1 activity compared to GPR50.

The transport and sorting of BACE1 to the different membrane compartments of the cells is tightly regulated and modulating the proportion of BACE1 in various compartments affects the cleavage of APP and other substrates (Small and Gandy, 2006). APP is cleaved by BACE1 at the cell surface and predominantly in early endosomes. BACE1 ad APP appear to be trafficked together from the cell surface to the endosomes and Aβ is generated in these areas (Kinoshita et al., 2003) but also in the Golgi and ER (Kuentzel et al., 1993; Chyung et al., 1997; Cook et al., 1997; Hartmann et al., 1997). Increased surface expression (reduced endocytosis) of APP has been shown to result in increased α-secretase and reduced β-secretase cleavage, leading to a decrease in secreted Aβ-40 and 42 (Hoe et al., 2009). It would be interesting to test if GPR50 overexpression can alter BACE1 localisation, and perhaps thereby its activity.

4.3.3.5 Is GPR50 associated with cholesterol-enriched lipid rafts as known for APP and BACE1?

Cholesterol is enriched in the brain, as it can hold 25% of total cholesterol in 2% of total body weight (Dietschy and Turley, 2001). Cholesterol has been implicated in

AD pathogenesis as total cholesterol and serum LDL correlated with Aß load in AD brains (Kuo et al., 1998) and individuals with higher cholesterol levels have a higher risk of developing AD (Kivipelto et al., 2001), which could be reversed by treatment with cholesterol lowering statins (Jick et al., 2000).

Several of GPR50's interactors are lipid associated or have a known role in lipid metabolism and have links to AD pathology. Oxysterol binding protein 2 is a member of a protein family involved in sterol synthesis and regulation (Im et al., 2005). SREBF2/SREBP2 is a ubiquitously expressed transcription factor that controls cholesterol homeostasis by stimulating transcription of sterol-regulated genes. Variations in SREBF2 are potential candidate CSF biomarkers in AD (Kim et al., 2011). Transgenic mice overexpressing SREBP2 showed accumulation of mitochondrial cholesterol and increased oxidative neuronal death in response to Aβ1-42 (Fernandez et al., 2009). ABCA2 shares the highest homology with the HDL cholesterol transporter ABCA1 and may also influence cholesterol transport (Kaminski et al., 2001) and sphingolipids (Sakai et al., 2007). Mace et al., (2005) identified a SNP in ABCA2 exon 14 associated with early onset AD. In further support of a role in AD, ABCA2 colocalizes with APP and Aβ, and overexpression of ABCA2 results in an increase in intracellular protein levels of APP and Aβ (Chen et al., 2004b). ABCA2 expression was also linked to the oxidative stress response and subsequent cell death, another pathological characteristic of AD (Chen et al., 2004).

Lipid rafts are small (10-200 μm), heterogeneous glycolipoprotein microdomains enriched in cholesterol and sphingolipids, predominantly present on the cell surface but also in endomembranes (Pike, 2006; Vetrivel and Thinakaran, 2010) They are rich in signalling proteins and are involved in signal transduction, sorting and membrane trafficking, regulation of the actin cytoskeleton (by altering cell polarity, motility of growth cones and lamellipodia) and cell adhesion (Simons and Toomre, 2000; Guirland et al., 2004). Lipid rafts have also been shown to be important for the functioning of spines and synapses (Hering et al., 2003). Interestingly, lipid raft protein Caveolin-1 has recently been shown to promote dentritic growth and

neurotransmitter signalling in primary neurons, even in the presence of myelin-associated inhibitors like Nogo (Head et al., 2011).

Both BACE1 and its substrates APP and NRG1 are present in lipid rafts (Frenzel and Falls, 2001; Riddell et al., 2001) as assessed by insolubility by Triton X-100. BACE1 processing of APP is thought to take place in lipid rafts and is dependent on the presence of cholesterol in rafts (Cordy et al., 2003; Ehehalt et al., 2003) however more recent data suggest otherwise (Vetrivel et al., 2009). Aβ is released from endosomes by specific vesicles and exit the cell membrane as exosomes, which are enriched in raft lipids (Rajendran et al., 2006).

APP, BACE1, GPR50, Nogo-A and CDH8 are present in the postsynaptic density, which is known to be rich in lipid rafts (Hering et al., 2003). Indeed, PSD-95 is a raft-enriched protein. One of the characteristics of the PSD is its insolubility in Triton X-100, which has long been used to identify lipid rafts (Hering et al., 2003), however other methods of identification and isolation are needed (Lichtenberg et al., 2005). There is therefore a good possibility that GPR50 (and its interactors) are raft proteins, both in the PSD and in other areas. The 2-transmembrane domain of RTN3 and Nogo-C are critical for modulation of BACE1 activity (Kume et al., 2009) suggesting a direct interaction within the membrane, perhaps in lipid raft domains. It would therefore be interesting to investigate the effects of GPR50 overexpression on BACE1 processing of its substrates specifically in lipid rafts.

4.3.4 Summary

To summarise, this study provides evidence that GPR50 plays a role in neurite outgrowth and in regulating BACE1 activity. Further studies are needed to establish whether GPR50 plays a role in these processes during development and/or pathological conditions and whether the effects are direct or via its (other) interactors. Building up from previous reports (Thomson et al. 2005; Macintyre et al. 2010; Hamouda et al. 2007), this study provides further clues for the functional

involvement of GPR50 in the pathogenesis of mood disorders and Alzheimer's disease, which makes GPR50 an exciting subject for future investigations.

4.3.5 Acknowledgements

The BACE1 assay was partly performed by IGMM PhD rotation student Sophie Hempel, under my supervision. She performed two replicates of part 1 of the BACE1 assay. Pilot studies giving a similar result with a different BACE1 activity assay kit (R&D systems) were performed by IGMM PhD rotation student Sarah McCulloch under my supervision.

Chapter 5

Structural analysis of the GPR50 C-terminal domain

5 Chapter Five: Structural analysis of the GPR50 C-terminal domain

5.1 Introduction

5.1.1 The GPR50 CTD sequence and structure

The GPR50 cytoplasmic domain (CTD) in humans spans 320 amino acid (aa) residues, roughly half of the total length of the GPR50 protein (617 aa). The GPR50 CTD is substantially larger than that of the related human Melatonin 1 (MT1) and 2 (MT2) receptors and its orthologue in non-mammalian species the Melatonin1c receptor (Mel1c) (Chapter 1 Fig 1.5). Compared to the relatively conserved transmembrane domains in GPCRs (Dufourny et al., 2008) (see also Introductory Chapter 1) not much is known about the structure of the CTD. We therefore set out to investigate some of the structural properties of the GPR50 CTD, and the significance of the polymorphisms within identified by Thomson et al. (2005). Interest in the structure of the CTD was raised by an unpublished report by Dinesh Soares (University of Edinburgh), as summarised below.

Using bioinformatics tools and through manual observation he detected several sequence and structural features. Firstly, an imperfect heptapeptide repeat was found, which is largely conserved among orthologues (Fig 5.1A), although the total number of repeats differs. Differences in heptapeptide numbers are also observed among the primates (e.g. human GPR50 contain 22, whereas chimpanzee and macaque GPR50 have 23 repeats, Fig 5.1A). This repeat region, albeit to a lesser extent - (only 10 repeats observed in humans) was also noticed by Dufourny et al (2008) and the authors note the resemblance of these repeats to the heptapeptide repeat in the RNA polymerase II CTD (Dufourny et al., 2008). From this, they hypothesised that this region may act as a functional scaffold for binding partners, as is the case for RNA polymerase II (Meinhart et al., 2005; Phatnani and Greenleaf, 2006). The CTD of RNA polymerase II can adopt a left-handed polyproline type II helix (PPII) under increasing hydrogen bond-promoting solvent trifluoroethanol concentrations

(Bienkiewicz et al., 2000), which could indicate a similar structure for the GPR50 CTD.

Another interesting feature in the GPR50 CTD sequence is the abundance of proline residues. Prolines make up 12% of the sequence, whereas the average number for SwissProt proteins is around 5% (Table 5.1). Proline-rich motifs and domains have been known to play important roles among signalling proteins (Kay et al., 2000) and in protein-protein interactions. The number of histidines in the CTD is also grossly overrepresented - 8.3% compared with unstructured proteins (1.51%) or to proteins in the SwissProt database (2.25%) (Table 5.1). Of course the GPR50 CTD is only part of the protein and the rest of GPR50 is highly structured (Fig 5.2 and Chapter 1 Figure 1.2, Dufourny et al., 2008).

Figure 5.1 *Heptapeptide repeats in the GPR50 CTD. (A) Orthologue multiple sequence alignment and sequence relationships. The C-terminal tail of GPR50 alignment was created using PROMALS (Pei and Grishin 2007) and is shown according to the colour scheme used in ClustalX version 1.83 (Thompson et al. 1997). Strictly conserved columns are shown with an '*', while conservatively substituted and semi-conserved columns are highlighted using ':' and '.', respectively. The sequence lengths in each case are indicated and the heptapeptide repeats boxed on the alignment. (D. Soares, Unpublished). (B) Twenty-two heptapeptide repeats in humans. The highly repetitive contiguous heptapeptide unit consists of an almost invariant histidine (H or aromatic) at position 'c' and lysine (K or charged amino acid) at position 'e'. The unit 'abcdefg' generally follows a semi-conserved pattern: a = S, T or small amino acid; b = G, V, X; c = H or aromatic; d = P, F; e = K or charged; f = P, S; g = A, X (where X = additional residues).*

A

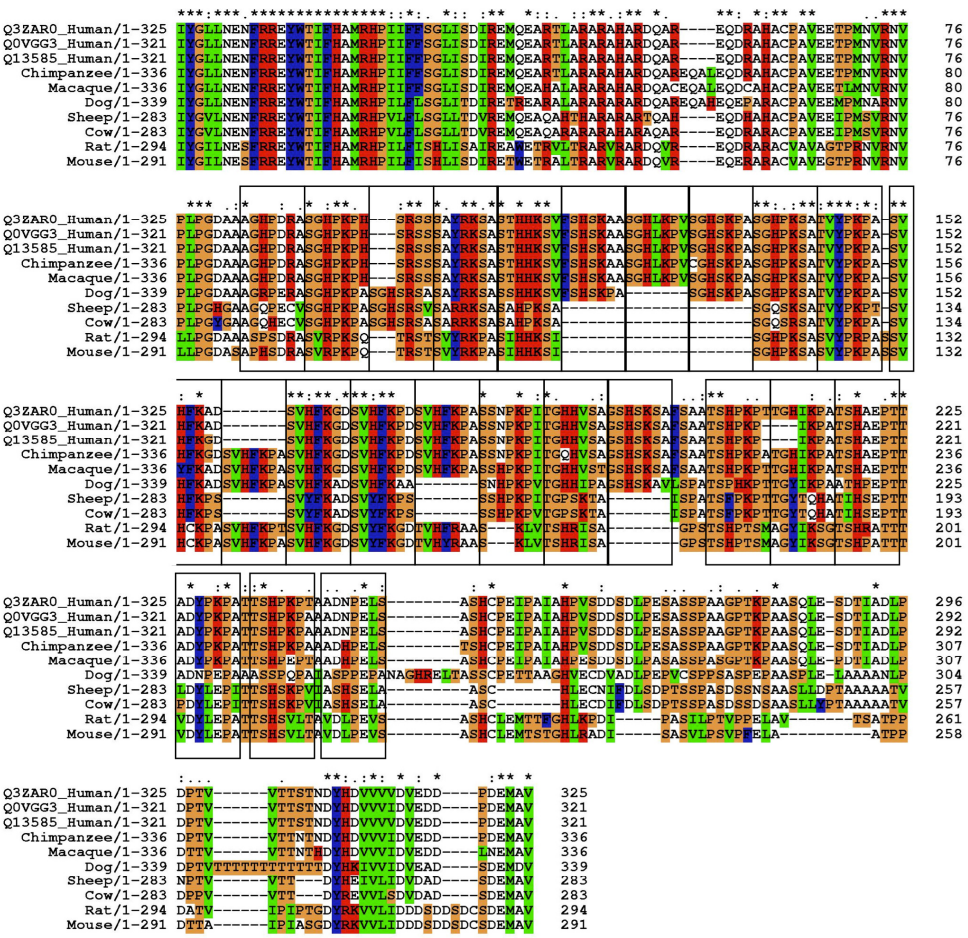
Q3ZAR0_Human/1-325
Q0VGG3_Human/1-321
Q13585_Human/1-321
Chimpanzee/1-336
Macaque/1-336
Dog/1-339
Sheep/1-283
Cow/1-283
Rat/1-294
Mouse/1-291

B

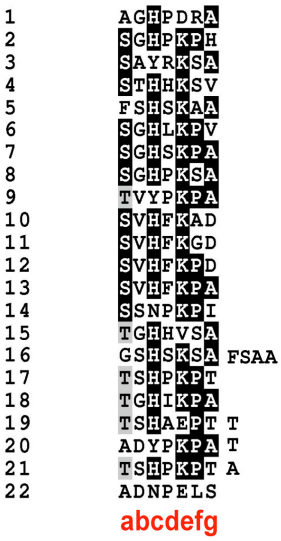
1 AGHPDRA
2 SGHPKPH
3 SAYRKSA
4 STHHKSV
5 FSHSKAA
6 SGHLKPV
7 SGHSKPA
8 SGHPKSA
9 TVYPKPA
10 SVHFKAD
11 SVHFKGD
12 SVHFKPD
13 SVHFKPA
14 SSNPKPI
15 TGHHVSA
16 GSHSKSA FSAA
17 TSHPKPT
18 TGHIKPA
19 TSHAEPT T
20 ADYPKPA T
21 TSHPKPT A
22 ADNPELS
abcdefg

Amino Acid	GPR50 313-617	GPR50 313-617 (Δ502-505, Thr532Ala)	Unstructured proteins	SwissProt proteins
Ala (A)	13.8	14.3	7.15	7.62
Arg (R)	3.9	4.0	4.21	5.19
Asn (N)	1.6	1.7	2.06	4.36
Asp (D)	7.2	7.3	5.05	5.25
Cys (C)	0.7	0.7	0.61	1.62
Gln (Q)	1.3	1.3	4.46	3.93
Glu (E)	3.9	4.0	14.25	6.47
Gly (G)	3.9	3.7	4.31	6.35
His (H)	8.5	8.3	1.51	2.25
Ile (I)	3.0	3.0	3.67	5.85
Leu (L)	2.6	2.7	5.44	3.54
Lys (K)	6.2	6.3	10.43	5.97
Met (M)	1.0	1.0	1.80	2.37
Phe (F)	2.6	2.7	1.66	4.10
Pro (P)	11.8	12.0	12.07	4.89
Ser (S)	13.4	13.6	6.91	7.08
Thr (T)	6.6	5.6	5.14	5.57
Trp (W)	0.0	0.0	0.32	1.21
Tyr (Y)	1.3	1.3	1.42	3.16
Val (V)	6.6	6.6	8.02	6.61

Table 5.1 *Amino acid compositions (in %) of GPR50 CTD insertion and deletion forms, along with amino acid frequencies of disordered and SwissProt proteins (taken from Tompa (2002)). Alanine, serine, proline and histidine are the most frequently occurring residues in the GPR50 CTD. Prolines and histidines occur with substantially higher frequency than would normally be expected in proteins. The amino acid frequencies in GPR50 CTD were taken from ProtParam (http://ca.expasy.org/tools/protparam.html). Data from SwissProt (http://www.expasy.org/sprot).*

5.1.2 Secondary structure prediction of GPR50 CTD

What could these features mean in terms of secondary structure? Repetitive sequences often correspond to repetitive structure (Andrade et al., 2001) and seven-

residue (heptad) repeats - labelled abcdefg (Fig 5.1B) - are frequently observed among coiled-coil proteins (Burkhard et al., 2001). However, the heptapeptide repeating unit in GPR50 lacks the two necessary conserved hydrophobic (apolar) residues at positions '*a*' and '*d*', or at any other register position within a seven-residue repeat unit, that are characteristic among coiled coil proteins (Fig 5.1B). Additionally, coiled-coil prediction using the COILS prediction server (Lupas et al., 1991) did not suggest any coiled-coil helices to be present (D. Soares, not shown).

Prolines are disorder promoting amino acids (Chakrabartty et al., 1994) and are therefore often overrepresented among unstructured proteins (Tompa, 2002) (Table 5.1). This is because the backbone nitrogen of proline is bonded to the Cδ of its side-chain, and is not available for hydrogen bond formation, a normally crucial ingredient for stable α-helix and β-strand creation. Indeed, secondary structure prediction using PsiPred (Jones, 1999; McGuffin et al., 2000) revealed an extended random 'coil' for the C-terminal region, with the exception of short segments 316-317 and 352-355, which are predicted to be β-strand and α-helix respectively, although with very low confidence (Fig 5.2, D. Soares, unpublished).

From the consensus disorder output (Fig 5.3, D. Soares, unpublished), ~75% of residues (243 out of 325 residues) are predicted to be disordered, made up from two major regions – residue positions 332-441 (110 residues), and 473-591 (119 residues). All seven servers/methods agreed on disorder for 123 out of 325 residue positions (~38%). This property could render this region intractable to experimental structure determination. The N-terminal region spanning residue positions 293-311 corresponding to a strongly predicted α-helix comprising part of the seventh transmembrane (Fig 5.2-5.3) or eighth membrane parallel helix (Palczewski et al., 2000; Choi et al., 2005; Conner et al., 2008) were predicted to be "ordered" by all servers/methods, with the exception of a single amino acid residue for one predictor.

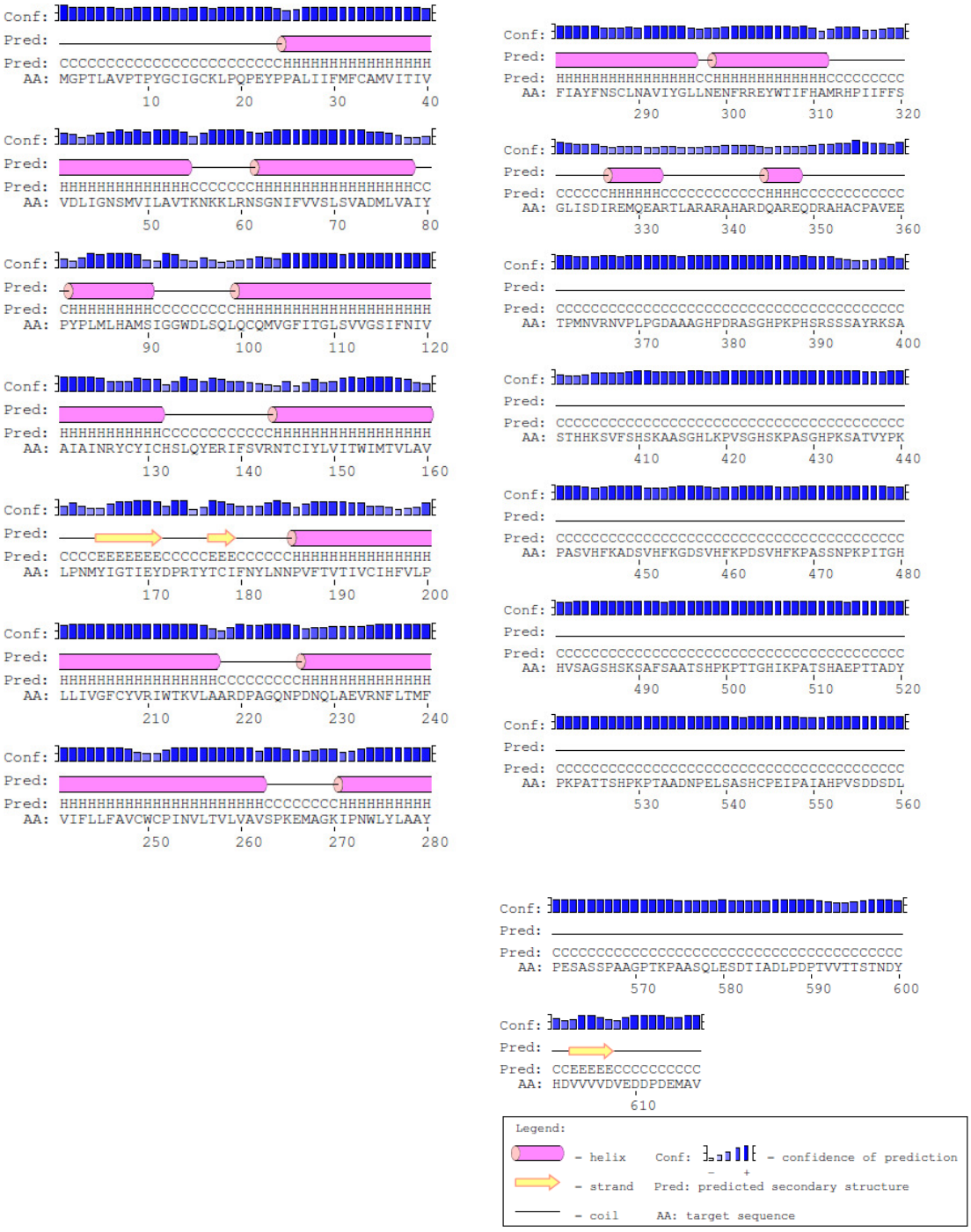

Figure 5.2 *PsiPred V2.5 (Jones, 1999; McGuffin et al., 2000) predicted secondary structure for full-length GPR50Δ502-505/T532A. The seven strongly predicted α-helices that correspond to the membrane-spanning regions are highlighted in pink. The C-terminal domain is predicted to contain predominantly random coil. Conf: Confidence.Pred: Predicted secondary structure (H = helix, E = strand, C = coil) AA: Target sequence (D. Soares, unpublished).*

Figure 5.3 *Predicted regions of disorder for the human GPR50 C-terminal tail sequence (blue) is shown using a range of servers/methods: DisEMBL™ version 1.5 (Linding et al., 2003); VSL2 at DisProt (Obradovic et al., 2005; Peng et al., 2006); FoldIndex© (Prilusky et al., 2005); PreLink (Coeytaux and Poupon, 2005); DRIP-PRED (http://www.sbc.su.se/~maccallr/disorder/) for details on method); PONDR® (Romero et al., 2001); and DISOPRED2 (Ward et al., 2004). In the case of DisEMBL™, the prediction output from REMARK-465 (missing coordinates in X-ray structure as defined by REMARK-465 entries in PDB) was considered, and in the case of VSL2 and PONDR®, the predictor models "VSL2B" and "VLXT" were used respectively. Each position was denoted by 'D' (and coloured red) for predicted disorder, or 'O' for predicted order. The consensus disorder (D), at the bottom of the sequence coloured magenta, was derived by applying a simple majority rule for each position (greater than or equal to 4) per server/method. Agreement for all servers on a position of disorder is shown by an asterisk '*', and for order indicated by an 'O' (shown in pink) alongside the consensus disorder prediction. The three polymorphisms are coloured light-green and underlined (D. Soares, unpublished).*

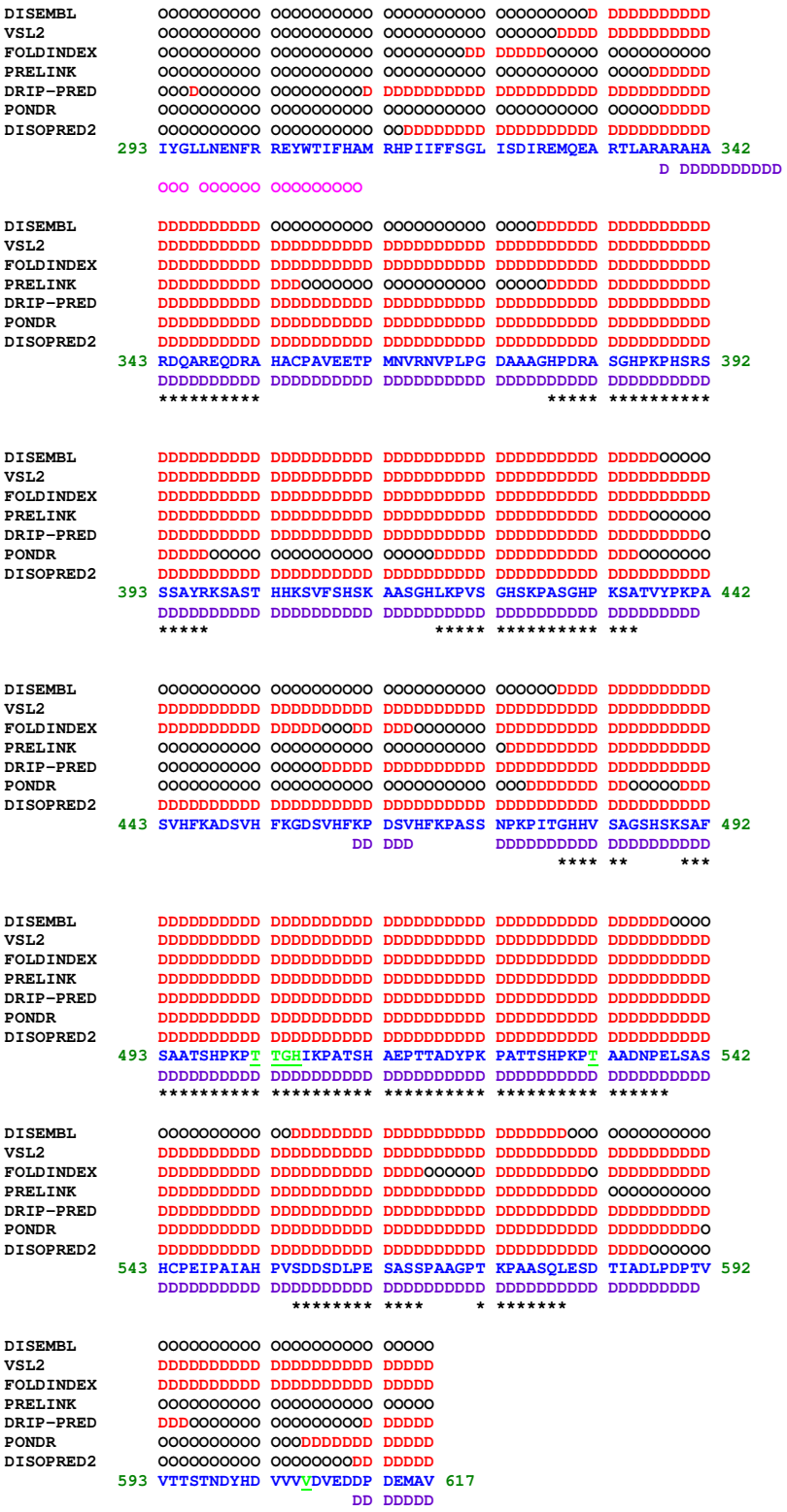
DISEMBL
VSL2
FOLDINDEX
PRELINK
DRIP-PRED
PONDR
DISOPRED2
293 IYGLLNENFR REYWTIFHAM RHPIIFFSGL ISDIREMQEA RTLARARAHA 342
343 RDQAREQDRA HACPAVEETP MNVRNVPLPG DAAAGHPDRA SGHPKPHSRS 392
393 SSAYRKSAST HHKSVFSHSK AASGHLKPVS GHSKPASGHP KSATVYPKPA 442
443 SVHFKADSVH FKGDSVHFKP DSVHFKPASS NPKPITGHHV SAGSHSKSAF 492
493 SAATSHPKPT TGHIKPATSH AEPTTADYPK PATTSHPKPT AADNPELSAS 542
543 HCPEIPAIAH PVSDDSDLPE SASSPAAGPT KPAASQLESD TIADLPDPTV 592
593 VTTSTNDYHD VVVVDVEDDP DEMAV 617

Repetitive proline motifs may also indicate a rare type II polyproline helix (Areschoug et al., 2002) as appears to be the case for RNA polymerase II (Bienkiewicz et al., 2000). To assess this likelihood for GPR50, a polyproline helix prediction was performed by D. Soares on the GPR50 sequence, using the method described by (Vlasov et al., 2005), and predicts 22% proline residues (Fig 5.4). However the results showed clear disagreement with many of the secondary structure predictions made by PsiPred (Fig 5.2) in the regions of the seven-transmembrane helices, and therefore it is difficult to conclude anything from this prediction.

```
 sequence ->    1 MGPTLAVPTPYGCIGCKLPQPEYPPALIIFMFCAMVITIVVDLIGNSMVI
structure ->    1 HPP-HHEPEHE-HE-HHPPPPHPPPEEEEEEEEEHEEPEEHHHH--HEEH

 sequence ->   51 LAVTKNKKLRNSGNIFVVSLSVADMLVAIYPYPLMLHAMSIGGWDLSQLQ
structure ->   51 HHHHHHHHHHH--PEEEEEHHHHHHHHHHHHPPPHHHHHEP--HHHHHHH

 sequence ->  101 CQMVGFITGLSVVGSIFNIVAIAINRYCYICHSLQYERIFSVRNTCIYLV
structure ->  101 -EHE-EPE-HPHE-EEE-PHHHHHHHHHE--HHPEEHHHPEEP-EPEEPP

 sequence ->  151 ITWIMTVLAVLPNMYIGTIEYDPRTYTCIFNYLNNPVFTVTIVCIHFVLP
structure ->  151 PPHEPHHHHEPP-PHE-EEHPPHHPEEPPHHHH-PPEEPEEPEPPEPPPP

 sequence ->  201 LLIVGFCYVRIWTKVLAARDPAGQNPDNQLAEVRNFLTMFVIFLLFAVCW
structure ->  201 PEPHEPPEPPHEHHHHHHHPHH-PPHHHHHHHHHHHHHHEEEPPHHHEHP

 sequence ->  251 CPINVLTVLVAVSPKEMAGKIPNWLYLAAYFIAYFNSCLNAVIYGLLNEN
structure ->  251 EPHHPPPEPEEEPHHHHPPPPPHHHHHHHHEPHEEPHHHEEEHHHHHHHH

 sequence ->  301 FRREYWTIFHAMRHPIIFFSGLISDIREMQEARTLARARAHARDQAREQD
structure ->  301 HHHPEEEPH-HEEEHHEPPH-PHHHHHHHHHHHHHHHHHHHHHHHHHHH

 sequence ->  351 RAHACPAVEETPMNVRNVPLPGDAAAGHPDRASGHPKPHSRSSSAYRKSA
structure ->  351 HHHHPPHHHHHPHHPHPPPPP-HHHH-HHHEPE-PHPPHHHH-HHHHHEE

 sequence ->  401 STHHKSVFSHSKAASGHLKPVSGHSKPASGHPKSATVYPKPASVHFKADS
structure ->  401 EEHHHHHHHE-HHHHH-HHHHHE-PPPPH--PPHEHEEEPPPEPEEPPHHH

 sequence ->  451 VHFKGDSVHFKPDSVHFKPASSNPKPITGHHVSAGSHSKSAFSAATSHPK
structure ->  451 --PP--PEPPEPHHEPPEHH--PPPPPP-EEP-H-PEHHHHHHHHEHPHE

 sequence ->  501 PTTGHIKPATSHAEPTTADYPKPATTSHPKPTAADNPELSASHCPEIPAI
structure ->  501 PHPHHPEPHEHHHEPEPHHEPEPH-PHPHPPPHHH-HHEEEEHEPHEPHH

 sequence ->  551 AHPVSDDSDLPESASSPAAGPTKPAASQLESDTIADLPDPTVVTTSTNDY
structure ->  551 HEPEPHHHPPPHPHHPHPH-PPEPPHHHHHEHEHHHPPPPHEPEEEEPHH

          sequence ->  601 HDVVVVDVEDDPDEMAV
         structure ->  601 HPEPPEPEE-PHHHHHH

H - α-helix
   E - β-structure
      P - PPII-(left)-helix
```

Figure 5.4 *Predicted secondary structure including polyproline prediction for full-length GPR50. The accuracy attained by this method, which is the first to predict polyproline helices is reported as ~60% (Vlasov et al. 2005) (D. Soares, unpublished).*

5.1.3 Predicted effects of deletion and missense polymorphisms

The ΔTTGH deletion and Thr532Ala polymorphism in the GPR50 CTD involve threonine residues, which were previously suggested to possibly harbour phosphorylation sites (Thomson et al., 2005). They are not however predicted by NetPhos version 2.0 (Blom et al., 1999) or PROSITE to correspond to potential phosphorylation sites (not shown), and hence a loss-of-phosphorylation effect is unlikely. However, a species-specific site cannot be ruled out entirely. The deletion of four residues would normally have serious consequences for protein folding, unless present in a solvent-exposed loop region that is not intimately associated via H-bonds or van der Waals interactions with the rest of the protein fold. Additionally, the ΔTTGH deletion directly affects the repetitive heptapeptide unit (between the 16^{th} and 17^{th} repeats). In addition, a putative 'P-X-X-P'-binding motif ('PIKP') is created upon the deletion of the 'TTGH' sequence in the variant human form, which could serve as a scaffold for proteins that recognise proline-motifs, such as Src homology 2 and 3 (SH2 and 3), postsynaptic density/disc-large/ZO1 (PDZ), WW domains and 14-3-3 proteins (Kay et al., 2000). Interestingly, two of the yeast 2-hybrid interactors (Grünewald et al., 2009) contain such domains: spectrin alpha, non-erythrocytic 1 (SPTAN1) that contains an SH3 domain, and protein interacting with PRKCA1 (PICK1) that contains a PDZ domain (D. Soares, unpublished). Although the number of clones of SPTAN1 and PICK1 identified in the screen was small (2 and 1 respectively), they were only identified as hits using the deletion variant of GPR50.

5.1.4 Introduction to experiments

In the absence of any known structural information it is difficult to determine what effects the polymorphisms might have on structure and function. Therefore a preliminary series of experiments was performed to gain insight into the structure of the GPR50 CTD and the effects of the polymorphisms on structure. A method often used to confirm secondary structure is circular dichroism (CD), a spectroscopy technique that measures the difference in absorption between left- and right handed

circularly polarised light (Beychok, 1966; Kelly et al., 2005). Measurements are performed in the far-UV spectrum and helical, sheet and disordered content can be derived with the use of deconvolution tools (e.g. Dichroweb (Whitmore and Wallace, 2004)). Far-UV CD spectra associated with various types of secondary structure are shown in Fig 5.5 (Kelly et al., 2005). CD is a valuable tool to assess differences in conformation as a result of structural, buffer or temperature changes. As with NMR and X-ray crystallography membrane proteins are difficult to study in their native state due to the sensitivity of the technique to pick up scattering from membrane structures. With this in mind the GPR50 CTD and GPR50 CTD $^{\Delta TTGH/T532A}$ excluding all transmembrane regions, spanning residues 313 to 617, were cloned, expressed and purified. After bacterial purification preliminary biophysical characterisation of the CTD, including circular dichroism, was undertaken.

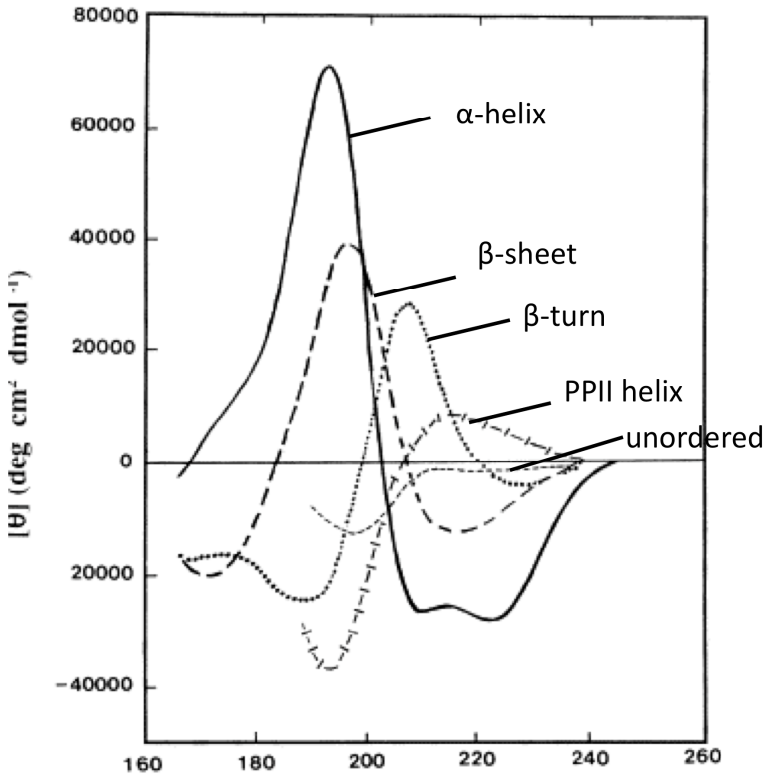

Figure 5.5 *Far UV CD spectra associated with various types of secondary structure. Solid line: α-helix; long dashed line: anti-parallel β-sheet; dotted line: type I β-turn; cross dashed line: extended 31-helix or polyproline II (PPII) helix; short dashed line: irregular structure. From Kelly et al., (2005). Biochimica et Biophysica Acta (BBA) - Proteins and Proteomics. Copyright 2005 Elsevier.*

5.2 Materials and methods

5.2.1 Cloning

Gateway compatible untagged, C-terminal non-cleavable His and N-terminal TEV cleavable His-tagged constructs of GPR50 amino acid residues 313-617 (insertion, ins) and 313-617 Δ502-505 Thr532Ala (deletion, del), were made via a two-step PCR reaction according to a proposed Edinburgh Protein Production Facility (EPPF) cloning strategy (Fig 5.6) using human cDNA. The primers used are detailed in Table 5.2.

PCR reactions were performed using Phusion high fidelity polymerase (Finnzymes, New England Biolabs) with 0.5 μM primers, on an PTC-225 PCR thermal cycler (MJ research) using a touch-down programme with an initial denaturation at 93ºC for 1 minute, followed by 10 cycles at 93ºC for 20 seconds, touch-down annealing from 65ºC to 55ºC for 30 seconds over 10 cycles, 72ºC for 1 minute, 55ºC for 30 seconds over 10 cycles, and a final extension of 72ºC for 10 minutes. PCR products were cloned by recombination into pDONR221 and subsequently pDEST14 vectors (Gateway, Invitrogen). Plasmids were transformed into competent DH5α cells. DNA was purified using the Qiagen Maxiprep kit. Plasmids were checked by sequencing using BigDye3.1 reagents (see 2.2.5 Chapter 2).

Construct	PCR step	Sense primer	Antisense primer
Untagged	Step 1	cggcaccctatcatattcttctc	cacagccatttcatcaggatc
	Step 2	ggggacaagtttgtacaaaaaagca ggcttcgaaggagatatacatatg	ggggaccactttgtacaagaaagct gggtccta
C-term His	Step 1	atatacatatgcggcaccctatcatatt cttctc	tgatggccatccacagccatttcatc aggatc
	Step 2	ggggacaagtttgtacaaaaaagca ggcttcgaaggagatatacatatg	ggggaccactttgtacaagaaagct gggtcctagtgatggtgatggtgac ggccatc
N-term His TEV	Step 1	attttcagggccggcaccctatcatatt cttctc	agctggggtcctacacagccatttc atcaggatc
	Step 2	ggggacaagtttgtacaaaaaagca ggcttcgaaggagatatacatatgtc gtactaccatcaccatcaccatcacg attacgatatcccaacgaccgaaaa cctgtattttcagggc	ggggaccactttgtacaagaaagct gggtccta

Table 5.2 *GPR50 CTD Primers used in this study. Step 1 primers were designed using Primer 3. Step 2 primers were a kind gift from Martin Wear (CTCB).*

Cloning Strategy and PCR Primers used in the EPPF.

All PCR products cloned into pDONR221 (BP reaction) and then into pDEST-14 (LR reaction)

A. Untagged

AttB1 *RBS* *ATG*
Fwd 5'-**GGG GAC AAG TTT GTA CAA AAA AGC AGG CTT CGA AGG AGA TAT ACA TAT G** – **gene specific 23 nt**-3' (72)

Rev 5'-**GGG GAC CAC TTT GTA CAA GAA AGC TGG GTC CTA** - **gene specific 23 nt**-3' (56)
AttB2 *Stop*

B. Cleavable (TEV) N-teminal His Tag

AttB1 *RBS* *ATG* *6 x His*
Fwd 5'-com-**GGG GAC AAG TTT GTA CAA AAA AGC AGG CTT CGA AGG AGA TAT ACA TAT GTC GTA CTA CCA TCA CCA TCA CCA TCA CGA TTA CGA TAT CCC AAC GAC CGA AAA CCT GTA TTT TCA GGG C**-3' (118)
TEV

Fwd 5'-cust-**CCG AAA ACC TGT ATT TTC AGG GC** – **gene specific 23 nt**-3' (46)
TEV

Rev 5'-cust-**GGG GAC CAC TTT GTA CAA GAA AGC TGG GTC CTA** - **gene specific 23 nt**-3' (53)
AttB2 *Stop*

C. Non-cleavable C-terminal His tag.

AttB1 *RBS* *ATG*
Fwd 5'-com-**GGG GAC AAG TTT GTA CAA AAA AGC AGG CTT CGA AGG AGA TAT ACA TAT G**-3' (49)

Fwd 5'-cust-**GCT TCG AAG GAG ATA TAC ATA TG** – **gene specific 23 nt**-3'(46)
RBS *ATG*

AttB2 *Stop* *6 x His*
Rev 5'-com-**GGG GAC CAC TTT GTA CAA GAA AGC TGG GTC CTA GTG ATG GTG ATG GTG ATG GCC ATC**-3' (57)
6 x His

Rev 5' cust-**TGA TGG TGA TGG TGA TGG CCA TC** – **gene specific 23 nt**-3'(46)

Figure 5.6 *The Edinburgh Protein Production Facility (EPPF) cloning strategy used for generating bacterial expression constructs. By Martin A Wear, University of Edinburgh.*

5.2.2 Protein purification

For testing of optimal growth conditions DNA was transformed into competent BL21(DE3) Star (Invitrogen), C41(DE3) or C43(DE3) *E. coli* cells. Cultures were streaked onto LB-carbenicillin (50 µg/ml) plates and incubated at 37°C overnight. Single colonies from each transformation were picked and grown in LB plus (50 µg/ml) carbenicillin for 4-5 hours at 37°C. Starter cultures were further grown in either auto induction medium (TB Overnight Express, Merck Biosciences) at 37°C overnight (o/n) or LB or 2XTY medium at 37°C until A_{600} = 0.60. IPTG (1 mM) was then added to induce protein expression and cultures were incubated at either 25, 30 or 37°C for 3 hours.

For bulk growth, DNA was transformed into competent BL21(DE3) and grown in 1l auto induction medium at 37°C overnight. Cells were centrifuged at 6000g for 15 minutes and pellets were resuspended in 30 ml IMAC 'buffer A' with added protease inhibitors (Complete, Roche). Cells were lysed using a Constant Systems cell disruptor at 22 kpsi and 8°C. Lysates were cleared at 50,000g for 45 minutes at 4°C and filtered through 0.22 um pore filters before being loaded onto Äkta automated liquid chromatography systems. Liquid chromatography was performed at 6°C. Lysates were first affinity-purified using a 1 ml HiTrap FF immobilised metal ion affinity chromatography (IMAC) column charged with Ni^{2+}-ions and eluted in two steps. First, a linear gradient of increasing concentrations (20-500 mM) of imidazole in 20 column volumes (CV), followed by 5 CV of 500 mM imidazole, all collected in 1 ml fractions. Selected fractions were further purified by size exclusion chromatography. Fractions were first concentrated to 4 ml using Vivaspin centrifuge columns (Sartorius Stedim Biotech) with a molecular weight cutoff of 10 kDa and loaded onto a 320 ml Superdex 200pg XK26/60 gel filtration column. Protein was eluted in 1.5 column volumes of PBS pH 7.4 (Gibco) and collected in 2 ml fractions.

5.2.3 SDS-PAGE and Western blotting

Samples were mixed with 2x laemmli sample buffer with added 300 mM ß-mercaptoethanol or 100 mM DTT and boiled for 3 minutes before being loaded onto Biorad 4-20% gels. Gels were run in MOPS-SDS-Tris buffer for 40 minutes at 150 V. Gels were stained using Simply Blue Safestain (Invitrogen) and destained using dH_2O. For Western blotting, proteins were transferred from gels onto PVDF membrane using semi-dry transfer buffer at 25 V for 45 minutes. Membranes were blocked in TBS (+ 0.2% v/v Tween 20, TBS-T) with 5% w/v bovine serum albumin for 1 hour. Membranes were incubated with anti GPR50 E63 (1:5000) (See Chapter 2 and Table 2.4 for characterisation of E62 antibody) or AP-His (1:2000) for 2 hours in blocking buffer. Following three 15 minute washes in TBS-T, membranes were incubated in swine anti-rabbit HRP (DAKO) or 5 ml alkaline phosphatase buffer with 33 µl NBT and 16.5 µl BCIP (Thermo Fisher, Pierce). GPR50 was visualised using ECL plus (Amersham) and exposure to X-ray film.

5.2.4 Desalting using PD-10 columns (GE healthcare)

PD-10 columns were equilibrated in 25 ml elution buffer (20 mM phosphate 100 mM NaF pH 7.0 or 10 mM ammonium acetate (pH 6.7). Samples were loaded onto the column and allowed to enter the resin. Up to 2.5 ml of elution buffer was added to the column and allowed to enter the resin. To elute 3 to 3.5 ml elution buffer was added to the column and collected as desalted fraction.

5.2.5 Dynamic Light Scattering (DLS)

Samples in 'IMAC buffer B' (pH 7.4), PBS (pH 7.4), or desalted using PD-10 columns (see 5.2.4 above) into 20 mM phosphate with 100 mM NaF (pH 7.0) or 10 mM ammonium acetate (pH 6.7) were measured on the Zetasizer Auto Plate Sampler (Malvern Instruments Ltd, UK). Dynamic light scattering measurements were performed on 50 µl aliquots in a 384 well plate, with laser set at 830 nm. Size

distribution of GPR50 was determined by performing 3 measurements of 18 x 10 seconds readings of each sample at 10ºC (± standard deviation). Thermal stability of proteins was determined by melting point analysis after heating the sample from 10 to 80ºC with 2ºC increments. Data was analysed on Zetasizer APS software (Malvern).

5.2.6 ESI (Electrospray Ionisation) Mass Spectrometry

(performed by Dr Elizabeth Blackburn of the CTCB)

Samples were desalted into 10 mM ammonium acetate pH 6.7 using Amersham PD10 columns. Protein concentrations were approximately 1 µM as measured on a SpectraMax M5 multimode platereader (Molecular Devices) at 280 nm. A 100 µl sample was mixed 1:1 with acetonitrile/0.2% v/v formic acid (5 mM ammonium acetate, 50% v/v ACN 0.1% v/v formic acid final concentration, pH 2.5) and incubated for 15 minutes to denature the protein. Positive ESI mass spectra were acquired using a single quadropole mass spectrometer (Micromass, Wyntheshawe, UK) equipped with a Z-spray electrospray ionisation source. Samples were injected directly into the source using a Harvard Model 22 syringe at a flow rate of 3 µl/min. Spectra were acquired over a range of 150 to 2000 m/z and for each sample 100 runs were performed.

5.2.7 MALDI (matrix assisted laser desorption/ionization) Mass Spectrometry

Protein samples were desalted into 20 mM phosphate 100 mM NaF pH 7.0 using PD10 columns (Amersham, see 5.2.4 above), and were used at a concentration of 10-50 µM. A 10 mg/ml solution of sinapinic acid (3,5-Dimethoxy-4-hydroxycinnamic acid) matrix was prepared and 1 µl of sample followed by 1 µl of matrix were spotted on a 100 well gold sample plate (Applied Biosystems) and left to dry. The plate was loaded into a Voyager DE STR MALDI-TOF (Applied Biosystems) instrument and Bovine Serum Albumine (BSA) was used as standard (for proteins of 20-100 kDa). For each measurement 200 laser shots were fired over different areas of the sample. The laser intensity was adjusted until the signal intensity reached

2000-8000. Data were processed in Data Explorer (Applied Biosystems) by applying baseline correction and noise filters to remove background.

5.2.8 Circular Dichroism

Samples were desalted in 20 mM phosphate 100 mM NaF pH 7.0 using PD10 columns (see 5.2.4 above). Protein concentrations ranged from 0.02-0.1 mg/ml as measured on a JASCO V-550 UV-VIS spectrometer at 280 nm. A 0.1 cm pathlength cuvette (Starna) was used for collecting spectra from 300-185 nm at 20ºC on a JASCO J-810 Spectropolarimeter. Four scans were acquired for each spectrum at a scanning speed of 10 nm/min, bandwidth of 1 nm and response of 2 seconds. Buffer spectra were recorded using identical parameters to the sample spectra and, after offsetting both spectra to zero at 260 nm, the buffer spectra were subtracted from the sample spectra using Spectra Manager software (Jasco).

No filtering or other smoothing techniques were used to reduce the noise levels. The subtracted image was saved as an ASCII file. ASCII files were uploaded into Dichroweb (Whitmore and Wallace, 2004, 2008) for data analysis. Analysis was performed using the CDSSTR method (Compton and Johnson, 1986; Manavalan and Johnson, 1987; Sreerama et al., 2000) and reference databases 2 and 5. CDSSTR is a modification of the Varslc algorithm, which uses the variable selection method to eliminate proteins from the reference set that do not contain characteristics present in the test protein. The NRMSD (normalised root-mean-square deviation) was used to assess the quality (precision) of the fitting between experimental data and predicted structural content as performed on Dichroweb. Values range from 0 for a perfect fit to 1 for no fit) and only values of 0.1 or less were considered. A low NRMSD value is necessary for establishing whether results are correct, but it is not sufficient in itself. It enables the user to evaluate the different algorithms and databases for the most appropriate conditions for their experiment (Whitmore and Wallace, 2004).

5.3 Results

In order to experimentally test the protein secondary structure predictions by Dinesh Soares, protein purification and circular dichroism (CD) was performed. Additionally, purified GPR50 CTD was characterised under different conditions using dynamic light scattering and mass spectrometry. Several constructs were generated for bacterial protein expression of GPR50 C-term insertion (aa. 313-617) and deletion (313-617 Δ502-505, Thr532Ala): N-terminal TEV cleavable His-tagged-, C-terminal non-cleavable His-tagged- and untagged GPR50 (See Table 5.2). Because of time and resource limitations only the TEV cleavable His-tagged constructs have been used here.

5.3.1 Optimisation of protein expression

To determine the best conditions for protein expression a small volume trial of 21 conditions per construct was performed. His-TEV GPR50 CTD (ins) and $CTD^{\Delta 502-505/T532A}$ (del) were subcloned by PCR from human cDNA using the EPPF cloning strategy with Gateway technology (See materials and methods and Fig 8). Plasmids were transformed into either BL21Star (DE3), C41(DE3) or C43(DE3) *E. coli* strains. Bacteria were grown under several conditions: in auto-induction medium at 37 ºC or in LB or 2xTY medium and IPTG induced at 25, 30 or 37ºC (see materials and methods). SDS-PAGE (Fig 5.7A: ins, B: del) shows that under several conditions a band is detected at approximately 50 kDa that is absent from the negative (non-induced) control. These samples were probed with the GPR50 E63 antibody and strong GPR50 expression at 45 kDa was detected in several conditions (Fig 5.7C-D). From these trials, BL21 with auto-induction medium was selected for bulk growth for both insertion and deletion variants.

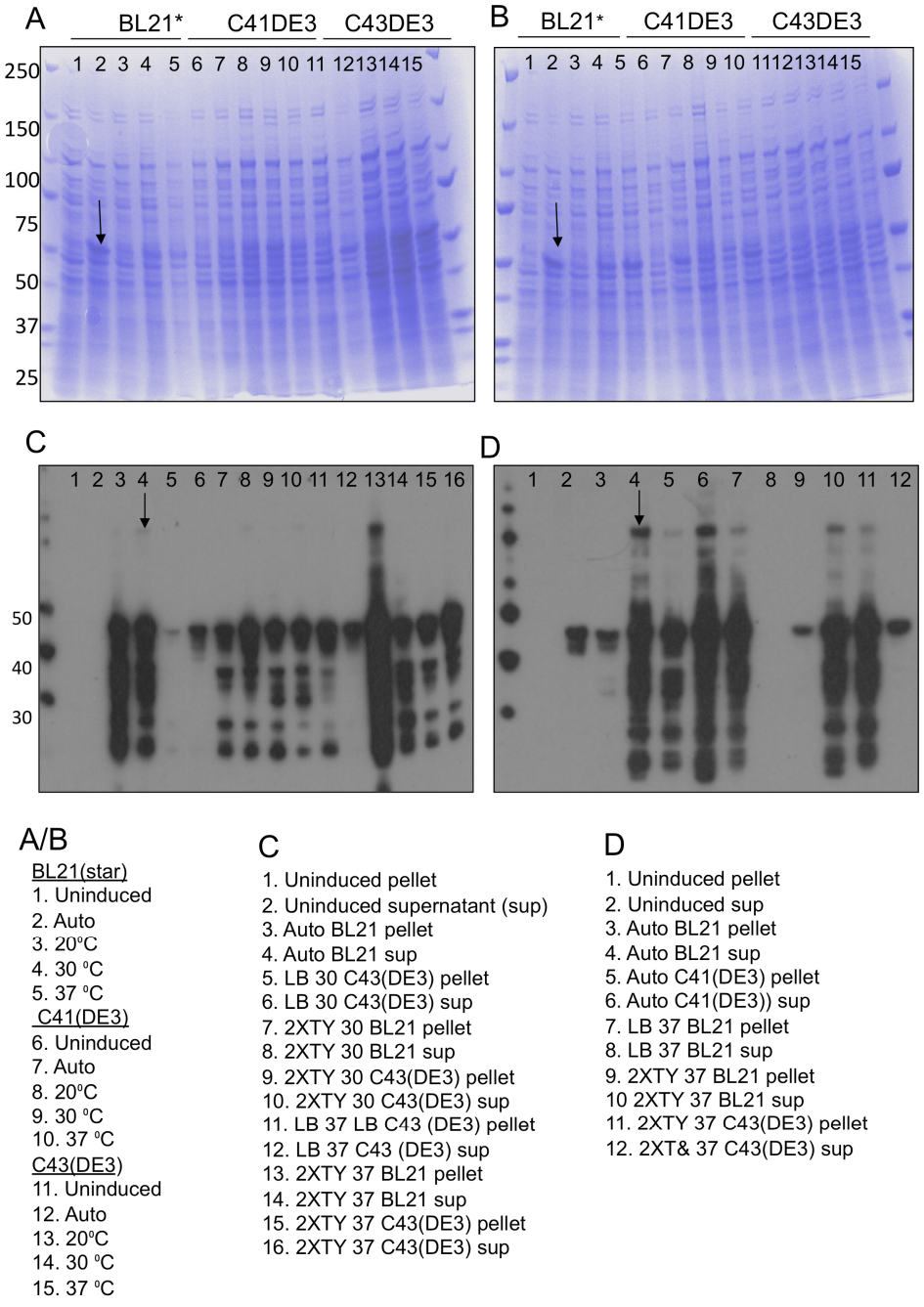

Figure 5.7 *Optimisation of growth conditions for protein expression. Three different E. coli strains (BL21 Star, C41(DE3), C43(DE3)) were used under different growth conditions and in three types of media: LB, 2xtY and auto induction (AI) medium. (A) GPR50 CTD insertion, (B) deletion (only LB and AI are shown here). Several conditions produced a band at ~50 kDa (arrows A, B). Lysates from these conditions were probed with a GPR50 E63 (C: insertion, D: deletion), which produced strong bands at 45 kDa. From these conditions BL21 Star in AI medium (arrows C, D) was selected.*

5.3.2 Protein purification

For purification, GPR50 CTD insertion and deletion were transformed into BL21 Star (DE3) and grown as 1 litre cultures o/n. Pelleted cells were lysed, and cleared lysates were affinity purified on an IMAC column using Äkta liquid chromatography systems. The elution profile for His-TEV GPR50 ins is shown in Fig 5.8A. There are two peaks in the profile, one from fractions C1-C7 (Sample A, 26%B, 130 mM imidazole) and a later one from D8-E1 (Sample B, 100%B, 500 mM imidazole). These fractions were loaded onto SDS-PAGE as shown in figure 5.8B. Bands migrated slower through the gel than predicted (observed: ~45 kDa, predicted: 35,106 Da ins and 34,767 Da del). This discrepancy may be attributed to the type of gel used; the SDS-PAGE was performed using precast gels from Invitrogen, while the Biorad gels produced bands closer to the predicted molecular weight (See Fig 5.7C-D and Fig 5.9). However it may also be an indication of lack of structure as unstructured proteins have the endency to run slower on SDS-PAGE because of their unusual amino acid composition and low capacity for SDS binding (Tompa, 2002; Li and Song, 2007). Fractions from Sample A were further purified using a size exclusion chromatography step. The elution profile shows many peaks corresponding to different sizes of proteins (Fig 5.8C), and SDS PAGE of selected fractions shows that the largest peak contains bands corresponding to the size of GPR50 CTD ("Sample A final", Fig 5.8D). These fractions were pooled and concentrated using <30 kDa size exclusion Vivaspin concentrators, retaining the >30 kDa fraction. This sample was further characterised as Sample A. Fractions from IMAC peak 2 appear very pure by SDS-PAGE (Fig 5.8B) and were characterised as a separate Sample B. His-tagged GPR50 is detected by Western blotting, using both GPR50 and His antibodies, in both Samples A and B (Fig 5.9A-B), albeit in different intensities and sizes.

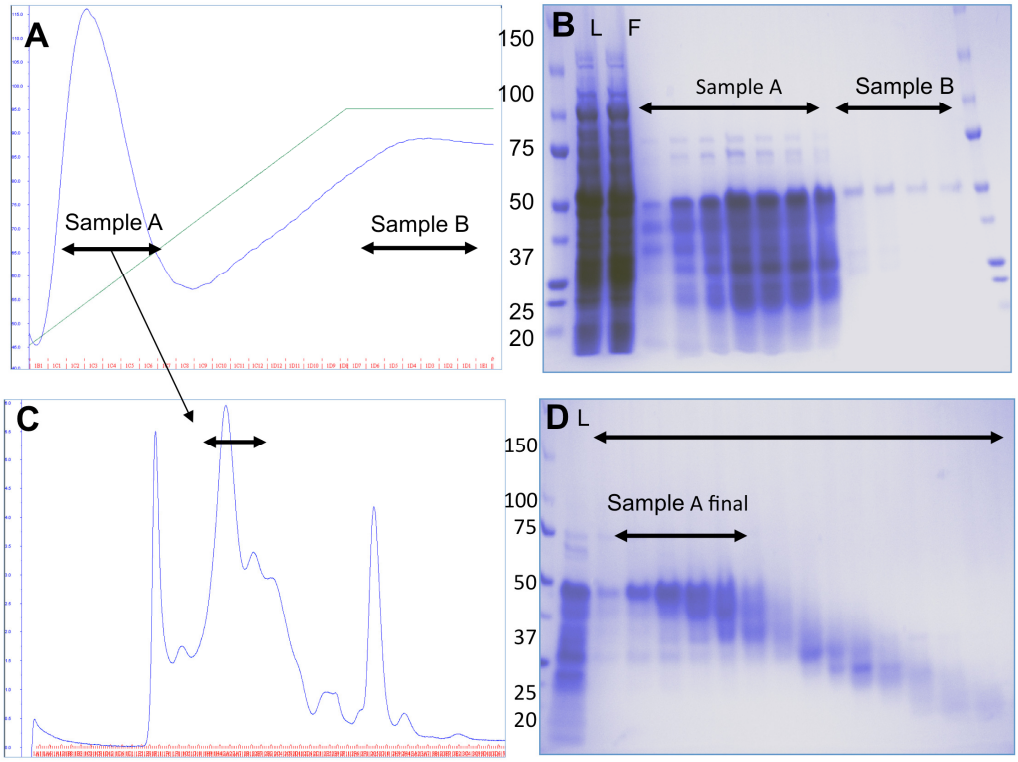

Figure 5.8 *Protein purification of TEV his GPR50 ins (GPR50del not shown but profile looked similar). Lysates from GPR50 ins expressing cells were loaded onto an IMAC column and the elution profile (A) showed two peaks (Samples A and B). Samples were loaded onto SDS-PAGE and stained with Simply Blue safestain (B). Samples A were further purified by gel filtration chromatography. The elution profile (C) shows many peaks of which the tallest one (C, arrows) was loaded onto SDS-PAGE (D) and stained with Simply Blue safestain. 'Sample A final' (D) was selected and further characterised, along with Sample B (A, B). L=whole protein extract (Load) F= unbound sample (Flow-through).*

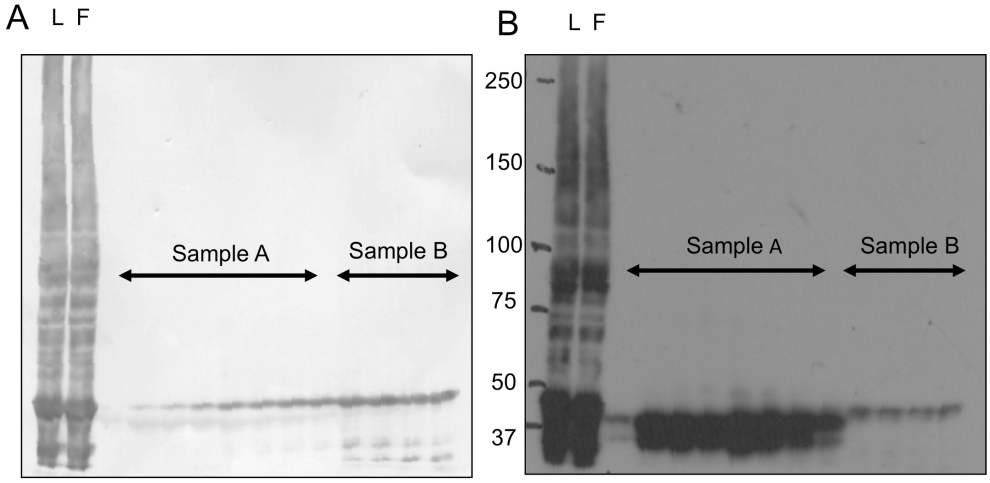

Figure 5.9*TEV his GPR50 ins IMAC purified fractions (Sample A: early peak; Sample B: late peak, see Fig 9) were loaded onto a tris-actetate gel (Invitrogen) and proteins were transferred onto PVDF membrane. The membrane was probed with anti-polyHis-AP (A) and anti-GPR50 E63 (B). L=whole protein extract (Load) F= unbound sample (Flow-through).*

5.3.3 Biophysical characterisation

5.3.3.1 Protein size distribution and stability

5.3.3.1.1 Dynamic Light Scattering

To determine particle size, distribution and stability of the GPR50 CTD in different samples and buffers Dynamic Light Scattering (DLS), otherwise known as photon correlation spectroscopy, was performed (http://www.malvern.com/common/downloads/campaign/MRK656-01.pdf) on *Sample A* and *Sample B,* separately (see Fig 5.8-5.9). See Materials and Methods for more details.

5.3.3.1.1.1 Sample A

Results from DLS analysis of GPR50ins and del 'Sample A' in PBS (pH 7.4) are shown in Figure 11. Concentrations of samples measured were 1 mg/ml (ins, 11A; del, 11C) and 0.125 mg/ml (ins, 11B; del, 11D). The protein samples appear to be single species (99.9%-98.4% pure, indicated by 'Mass', Fig 5.10A-D). Although the intensity of aggregates was high (indicated by bigger peaks with large diameter on

the left hand side of each subfigure), these only formed 0.1% of total mass (note, DLS is extremely sensitive at detecting even small traces of aggregation). Polydispersity (Pd, a measure of the homogeneity of macromolecules in solution) values of <20% would indicate a monodisperse (monomeric or non-aggregated) sample suggesting that GPR50ins A (Fig 5.10A-B) is more polydisperse (multimeric or aggregated) than GPR50del A (Fig 5.10C-D). GPR50 ins A has a hydrodynamic diameter (D_h) of 7.67 (± 1.86) nm (Fig 5.10A) with a predicted molecular weight of 78.1 kDa, which may indicate dimerisation of GPR50 CTD (2x 35,107 = 70,241 Da (including His-tag)) as is also known for full length GPR50 (Levoye et al., 2006; Hamouda et al., 2007; Grünewald et al., 2009), although the prediction should be treated with caution as mass estimates are based upon globular proteins, which GPR50 CTD is not likely to be. Also, there are no mathematical models to quantify the proportions of monomer/dimer/multimer in a given sample (Hubmacher et al., 2008). GPR50ins A seemed reasonably stable (similar characteristics to undiluted, Fig 5.10A) at an 8x dilution (Fig 5.10B, 0.125 mg/ml, 99.6% pure; D_h = 7.035 (± 1.67) nm; predicted molecular weight (Mw) = 63.9 kDa, Pd = 23.7).

The characteristics for GPR50 del Sample A in PBS (pH 7.4) were similar, although more monodisperse (Fig 5.10C, 1 mg/ml; 99.1% pure; D_h = 7.734 (± 1.16) nm; Mw = 79.7 kDa, Pd = 15.0), with reasonable stability at 8x dilution (Fig 5.10D, 0.125 mg/ml, 98.4% pure, D_h = 7.139 (±1.11) nm, predicted Mw of 66.1 kDa, Pd = 15.5). GPR50 ins A in PBS had a melting point of 21.9 ºC (12E), indicating it would lose its stability around room temperature. The melting point of GPR50 del Sample A in PBS was not measured due to time constraints, but is likely to be similar.

5.3.3.1.1.2 Sample B

DLS was also performed on GPR50 ins and del IMAC 'Sample B', which was desalted into 20 mM sodium phosphate with 100 mM NaF (pH 7.0) prior to DLS measurements. The DLS characteristics of GPR50 ins and del from Sample B at 1 mg/ml were very different (Fig 5.11). For these, intensity and size measurements indicated a single large species with a hydrodynamic radius of 29.44 (± 6.52) nm (Fig 5.11A, ins) or 24.67 (±6.62) nm (Fig 5.11C, del), corresponding to a predicted

size of 1820 kDa (ins) or 1200 (del). Both GPR50 ins and del B were stable at 4x dilution although some aggregation was measured at 8x dilution: (ins B: 0.125 mg/ml; 99.4% pure; D_h = 28.99 (± 3.98) nm; mass = 1760 (Fig 5.11B); del B: 0.125 mg/ml; 98.2% pure; D_h = 27.92 (±3.74) nm; mass = 1610 kDa (Fig 13D)). GPR50 ins Sample B had a Tmelt of 22ºC (Fig 5.11E), indicating loss of stability at or near room temperature.

Previous DLS measurements on GPR50 ins Sample B in high salt IMAC 'buffer B' showed similar characteristics (hydrodynamic radius of 27.55 (±7.94) nm and a predicted size of 1560 kDa (Fig 5.12). Thus the formation of the large species is not likely a consequence of desalting (reduction in ionic strength of solution) the sample. It likely reflects a structural difference between the loosely bound monomeric/dimeric GPR50 Sample A and a multimeric Sample B that is tightly bound to the IMAC column due to multiple hexahistidine residues.

An increase in anti-His signal is also detected by Western blotting of Sample B as compared to Sample A (Fig 5.9A) with a decreased signal of anti-GPR50 in fractions B compared to A (Fig 5.9B). The GPR50 signal in Sample A is strong but corresponds to different (smaller) size bands, indicating that some of GPR50 may have lost its tag (Fig 5.9B). His-immunoreactive bands at lower molecular weight, that are not detected by the GPR50 E63 antibody, are also visible in Fig 5.9A. This may indicate the presence of His-oligomers or His-tagged C-terminally degraded GPR50, of which the E63 epitope is missing.

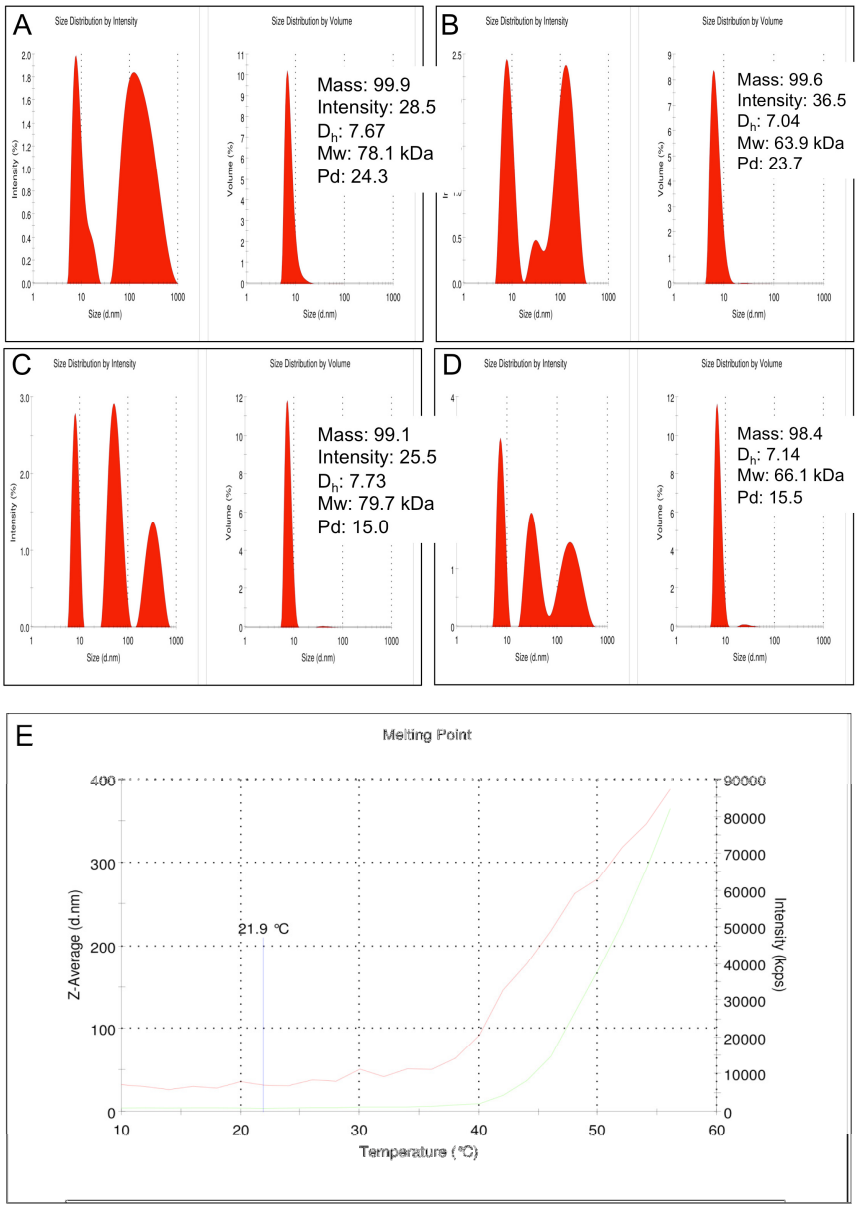

Figure 5.10 *Distributions of GPR50 C-term ins and del A particles in PBS by dynamic light scattering. Measurements were performed at 10 ℃. Eighteen acquisitions of 10s readings were recorded for each measurement and graphs represent the mean of the values for three measurements. DLS shows particle size by intensity (left of each subfigure) and volume (right of each subfigure). Mass indicates volume percentage (fraction) of a particular particle present in total solution. Intensity indicates the percentage (fraction) of light intensity scattered by that particular particle from the total amount of particles in solution. The intensity is proportional to particle size. Hydrodynamic radius (Dh) is the radius or size of a particle. Mw is the molecular weight (in kDa) predicted by the Dh. Pd is the polydispersity index, which indicates whether a sample is monomeric or free of aggregation (monodisperse, <20) or multimeric or aggregated (polydisperse, >20). (A) GPR50 ins Sample A (1mg/ml), (B) GPR50ins Sample A 1:8 dilution((0.125 mg/ml), (C) GPR50del Sample A (1 mg/ml), (D) GPR50del Sample A 1:8 dilution (0.125 mg/ml). (E) A melt curve for GPR50 ins A was generated by heating the sample from 10 to 80 ℃ in 2 ℃ increments. The recorded denaturing temperature (Tmelt) of GPR50 ins A is 21.9 ℃.*

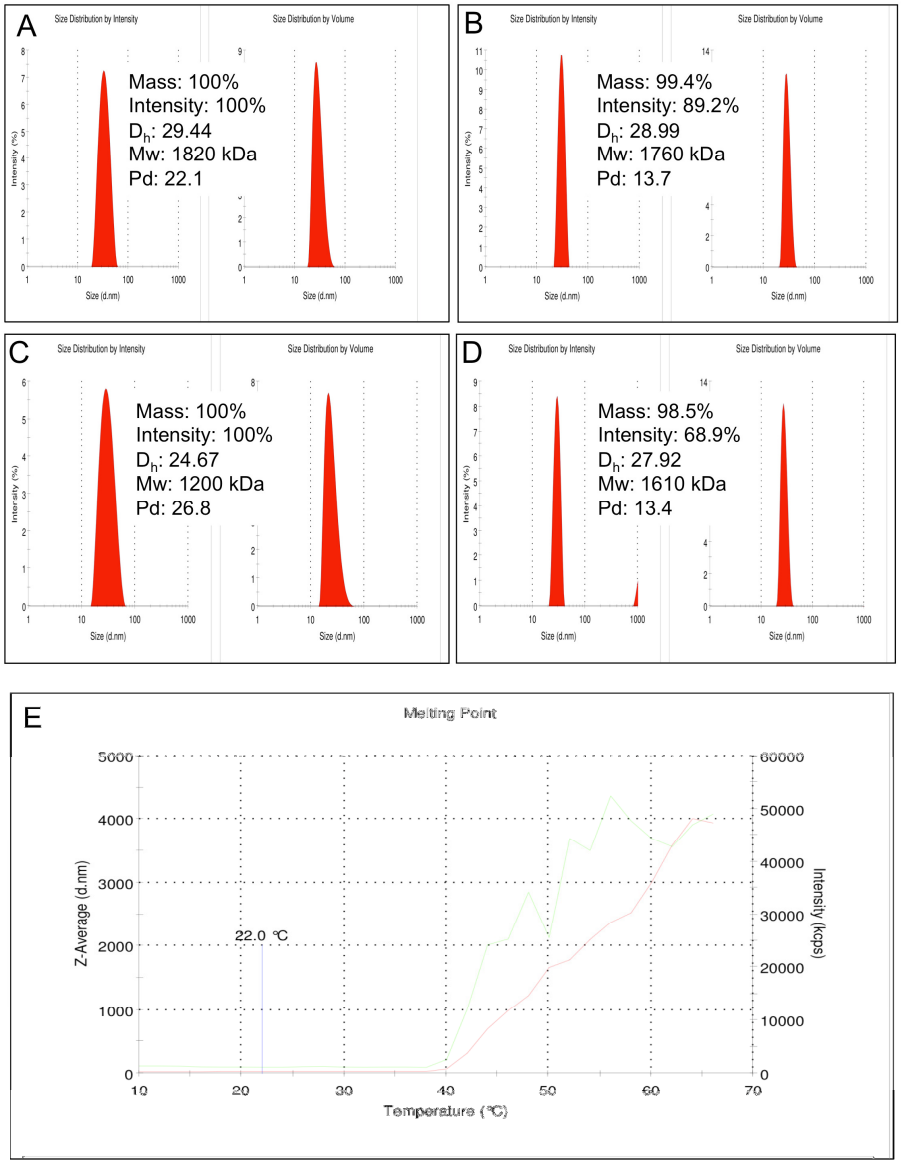

Figure 5.11 *Distributions of GPR50 CTD ins and del B particles in 20mM sodium phosphate 100mM NaF pH 7.0 by dynamic light scattering. Measurements were performed at 10℃. Eighteen acquisitions of 10s readings were recorded for each measurement and graphs represent the mean of the values for three measurements. DLS shows particle size by intensity (left of each subfigure) and volume (right of each subfigure). Mass indicates volume percentage (fraction) of a particular particle present in total solution. Intensity indicates the percentage (fraction) of light intensity scattered by that particular particle from the total amount of particles in solution. The intensity is proportional to particle size. Hydrodynamic radius (Dh) is the radius or size of a particle. Mw is the molecular weight (in kDa) predicted by the Dh. Pd is the polydispersity index, which indicates whether a sample is monomeric or free of aggregation (monodisperse, <20) or multimeric or aggregated (polydisperse, >20). (A) GPR50ins B (1 mg/ml), (B) GPR50ins B 1:8 (0.125 mg/ml), (C) GPR50del B (1 mg/ml), (D) GPR5 del B 1:8 (0.125 mg/ml). (E) A melt curve for GPR50 ins B was generated by heating the sample from 10 to 80℃ in 2℃ increments. The recorded Tmelt of GPR50 ins B is 22℃.*

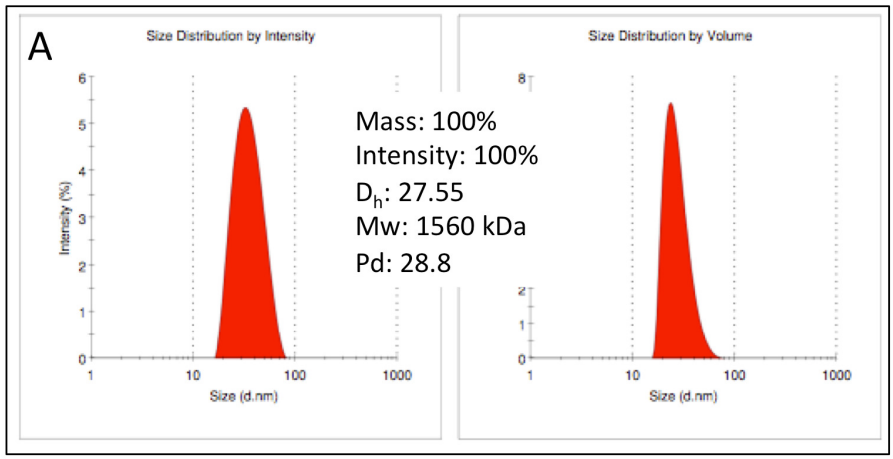

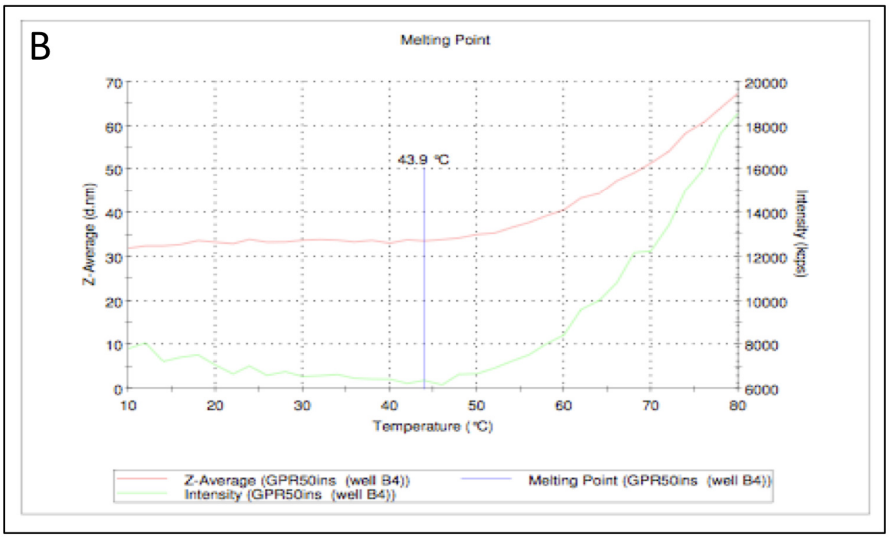

Figure 5.12 *Distributions of GPR50 CTD ins B (1mg/ml) particles in IMAC buffer B (25 mM Na_2HPO_4, 500 mM NaCl, 500 mM imidazole) by dynamic light scattering. (A) Measurements were performed at 10 ℃. Eighteen acquisitions of 10s readings were recorded for each measurement and graphs represent the mean of the values for three measurements. DLS shows particle size by intensity (left of each subfigure) and volume (right of each subfigure). Mass indicates volume percentage (fraction) of a particular particle present in total solution. Intensity indicates the percentage (fraction) of light intensity scattered by that particular particle from the total amount of particles in solution. The intensity is proportional to particle size. Hydrodynamic radius (Dh) is the radius or size of a particle. Mw is the molecular weight (in kDa) predicted by the Dh. Pd is the polydispersity index, which indicates whether a sample is monomeric or free of aggregation (monodisperse, <20) or multimeric or aggregated (polydisperse, >20) (A) DLS characteristics of GPR50 CTD ins B in IMAC buffer B. (B) A melt curve for GPR50 ins B was generated by heating the sample from 10 to 80 ℃ in 2 ℃ increments. The recorded Tmelt of GPR50 ins B is 43 ℃.*

5.3.3.1.2 Mass Spectrometry

5.3.3.1.2.1 ESI mass spectrometry

In an attempt to obtain accurate measurements of the mass of GPR50 CTD mass spectrometry was performed. Electrospray Ionisation (ESI) mass spectrometry resulted in a very noisy spectrum and a clear mass/charge pattern could not be distinguished (Fig 5.13A). Potentially interesting was the series of peaks with 44 u intervals left in the spectrum (400-600 m/z). These peaks were observed in GPR50ins/del A and GPR50ins/del B, with apparent increasing abundance of the 44 u interval peaks in the deletion variant compared to the bulk of the peaks. This is likely to be a sign of contamination by the non-ionic surfactant 4-(α,α-dimethylbenzyl)-phenol ethoxylate (Yokoyama et al., 2002) from glassware or instrumentation. As this contamination was not picked up before in the lab it is possible that it has high affinity for GPR50 CTD. The intensity of the peaks is no measure of how much contamination there is, it could be only a trace amount that is very volatile.

5.3.3.1.2.2 MALDI-TOF mass spectrometry

In order to find out if full length or multimeric intact GPR50 could be detected MALDI-TOF mass spectrometry was performed (Fig 5.13B). GPR50 ins/del A and B were analysed and peaks close to monomeric and dimeric GPR50 ins/del were detected (monomeric ins: 35528 Da, del: 34102/34265 Da; dimeric del: 72382.74 Da; Fig 5.13C), but also peaks at ~31 kDa again reflecting that some of the GPR50 CTD may have that lost its His-tag.

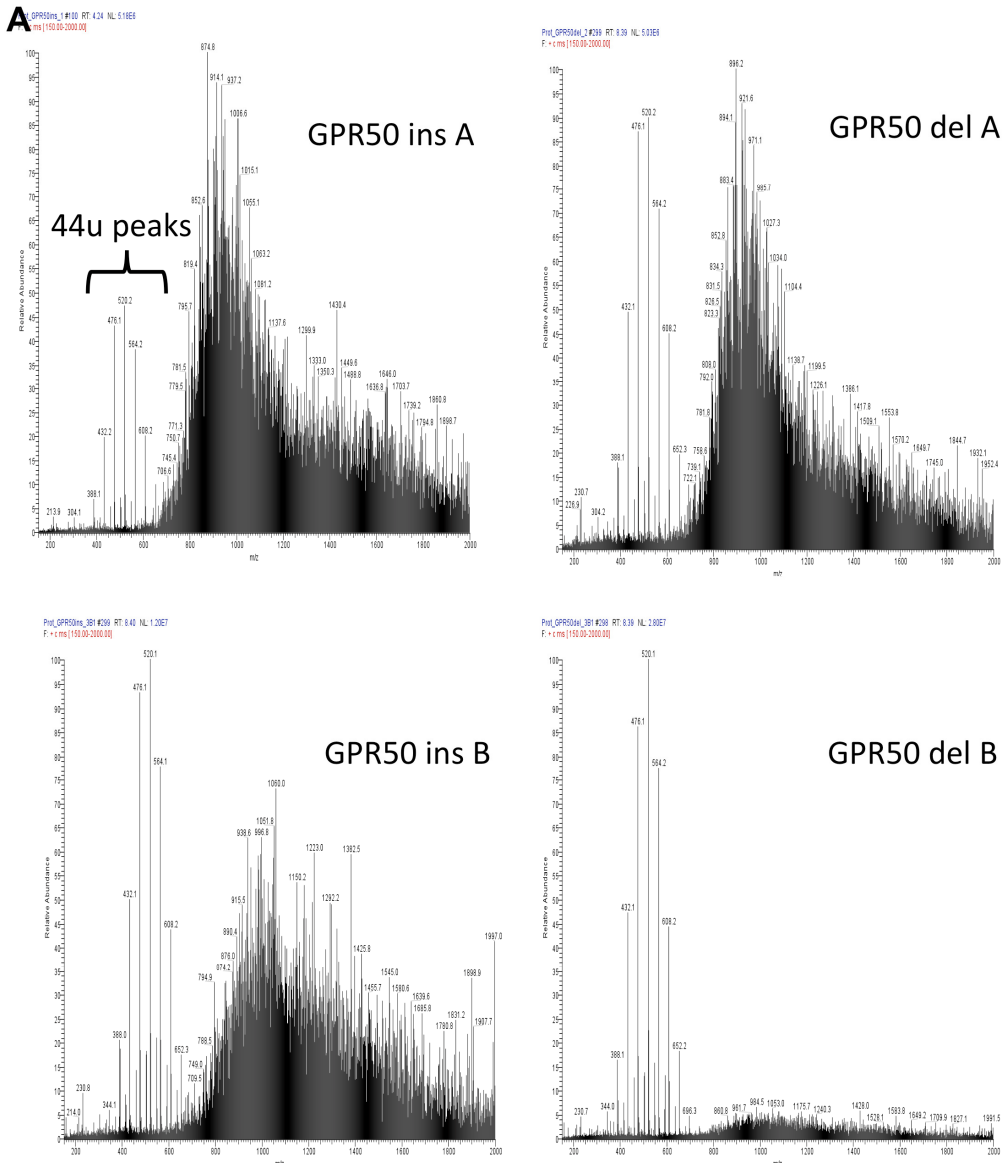

Figure 5.13 *Determination of GPR50 CTD molecular mass by Mass Spectrometry (A) ESI MS spectrum of GPR50 CTD ins/del Sample A and GPR50 ins/del Sample B. GPR50 CTD samples in 5mM ammonium acetate, 50% acetonitrile and 0.1% formic acid at pH 2.5 were injected into the electrospray ionisation source. Spectra were acquired over a range of 150 to 2000 m/z and for each sample 100 runs were performed.*

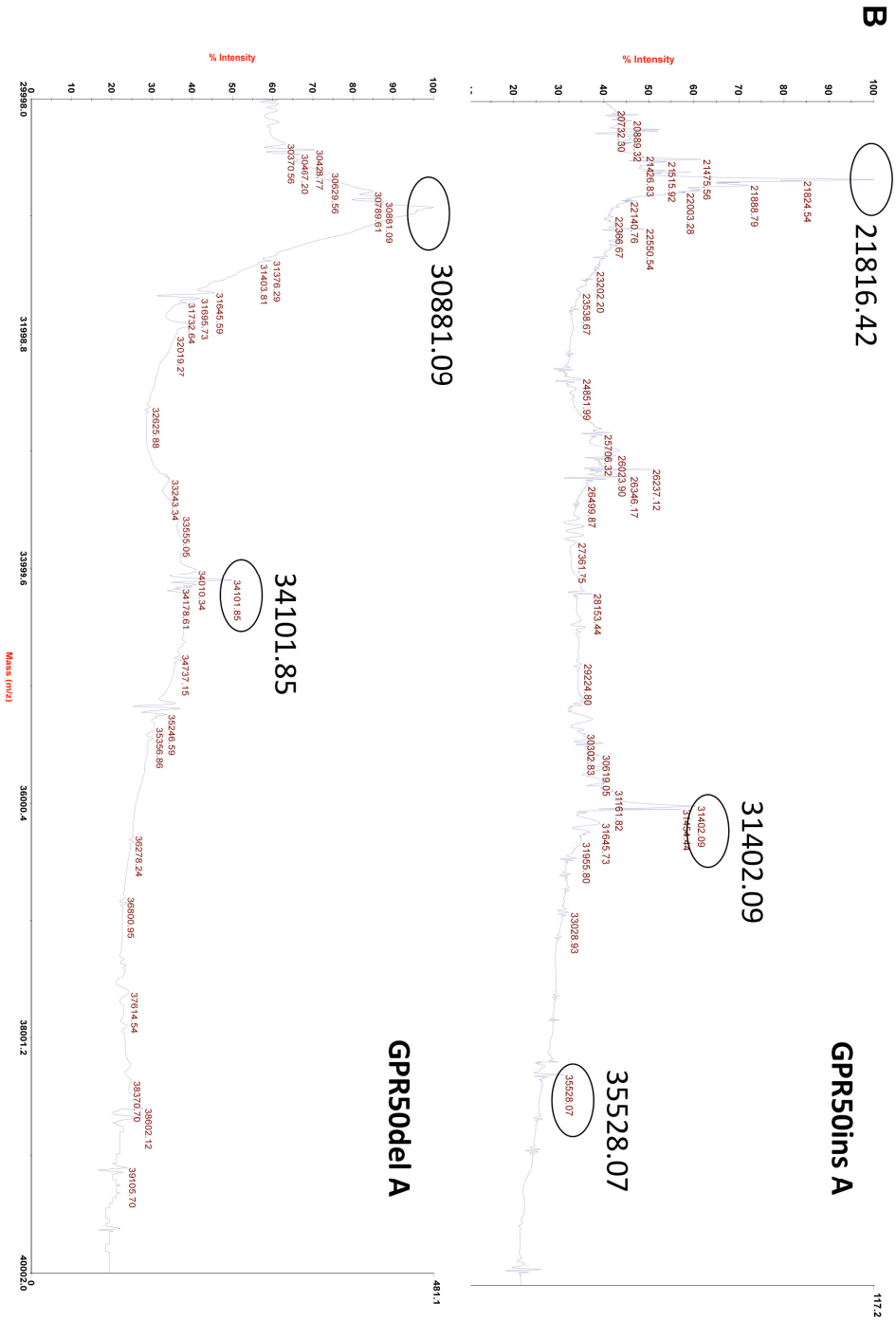

Figure 5.13 *Determination of GPR50 CTD molecular mass by Mass Spectrometry (B) MALDI-TOF analysis of purified GPR50 ins A (top) and del A (bottom) in 10 mM phosphate and 50 mM NaF/50% sinapinic acid matrix . The molecular mass estimations in daltons (Da) for the single mass ionization peaks are shown. Predicted molecular weight of TEV GPR50 del using ProtParam: 34767 Da; untagged: 31843 Da.*

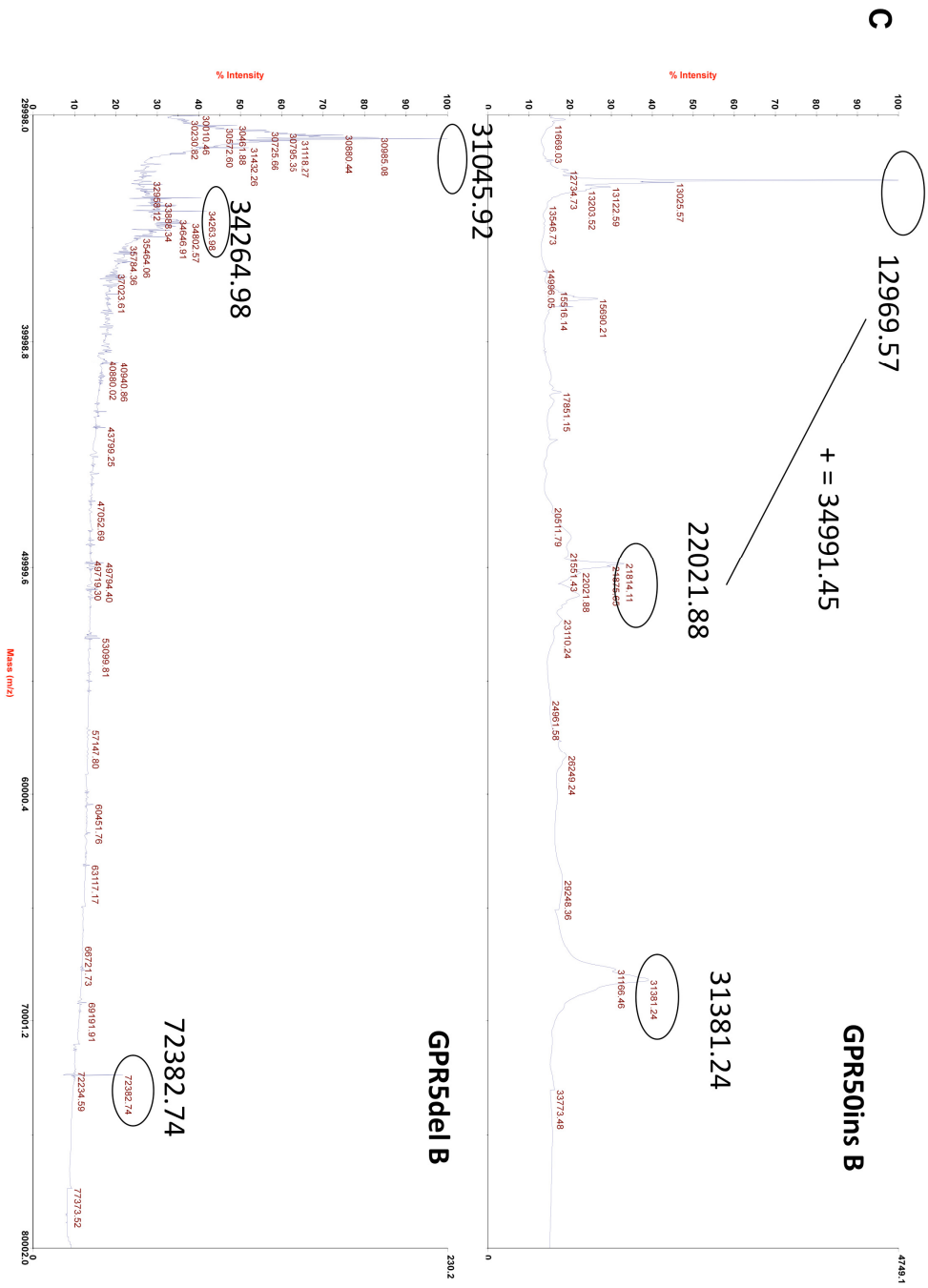

Figure 5.13 *Determination of GPR50 CTD molecular mass by Mass Spectrometry (C) MALDI-TOF analysis of purified GPR50 ins B (top) and del B (bottom) in 10 mM phosphate and 50 mM NaF/50% sinapinic acid matrix . The molecular mass estimations in daltons (Da) for the single mass ionization peaks are shown. Predicted molecular weight of TEV GPR50 del using ProtParam: 34767 Da; untagged: 31843 Da; dimer: 69543.*

5.3.3.2 Protein Secondary Structure

GPR50 CTD was predicted to be either largely unstructured, or some regions may form a polyproline type II helix, because of the number of proline residues within the repetitive motifs (Antonyraj et al., 1998; Bienkiewicz et al., 2000; Ma et al., 2001; Areschoug et al., 2002). In order to test this, circular dichroism (CD) was performed. When comparing CD spectra of GPR50ins A with del A (Fig 5.14) they both contain a minimum at ~200 nm, and a general profile characteristic of unstructured elements (Kelly et al., 2005). The minimum of GPR50del A seems to have however shifted slightly to a higher wavelength compared to ins A. This, combined with a slight decrease in signal at approximately 225 nm, may indicate that the proportion of α-helix in GPR50del is slightly higher than GPR50ins. A minimum at 195 nm and maximum at 220-230 nm as commonly observed in polyproline II structures was however absent. Instead a second minimum was observed around 220 nm characteristic of both α-helix and β-sheet (Kelly et al., 2005) (Fig 5.5), which is increased in the deletion variant. GPR50ins B and del B show similar spectra but an even greater increase of the 220 nm minimum, indicating increased helicity or structure (Fig 5.14).

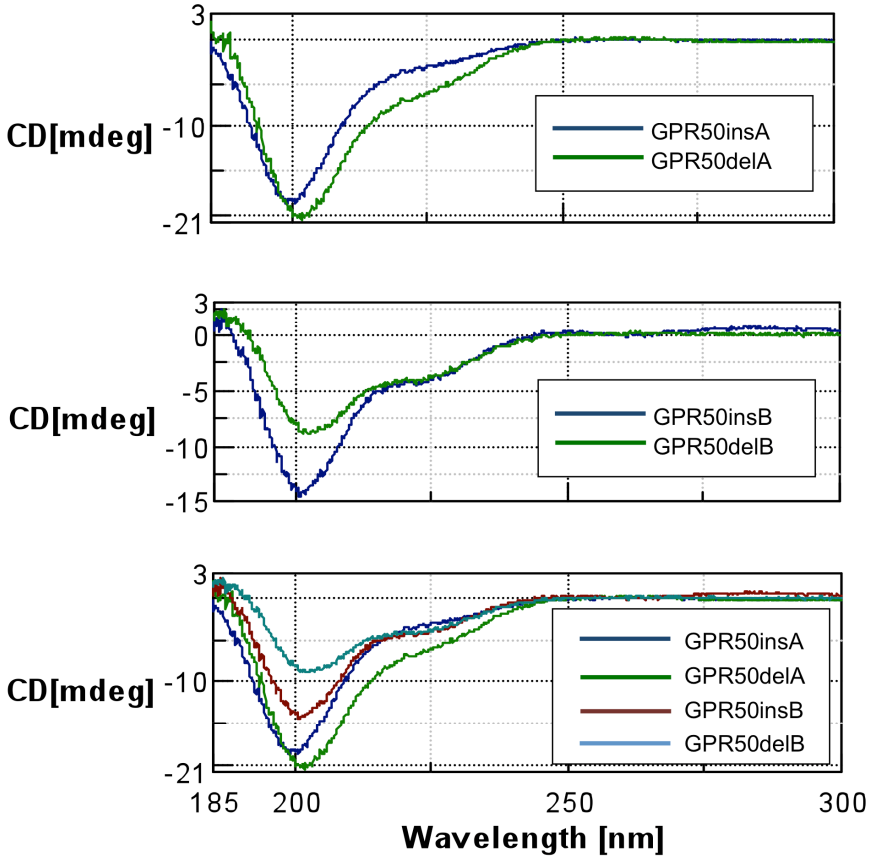

Figure 5.14 *CD spectra of GPR50 CTD. Comparing GPR50 ins/del samples A and B in a 20 mM phosphate and 100 mM NaF buffer, measured at 20℃ in a a 0.1 cm pathlength cuvette in a Jasco J-810 spectropolarimeter. Background was subtracted using Spectra Manager software. (Jasco). Graphs are presented in CD units (θ, mDeg).*

Using Dichroweb (Whitmore and Wallace, 2004, 2008) the traces were compared to databases with proteins whose structures have been determined experimentally by X-ray crystallography. The choice of database can greatly alter the results (Whitmore and Wallace, 2008) and it is therefore important to choose a database that reflects the protein of interest. Although there is no information available on the structure of GPR50, databases 2 and 5 were selected as they were the only two databases that were able to discriminate polyproline II helices. This is because the CD spectra in these two databases were collected from 300 to 178 nm increasing the resolution and

possibility to detect structures such as PPII helices and 3^{10}-Helices (Johnson, 1999). Tables 5.3 and 5.4 show the structural information of proteins in databases 2 and 5. Thirteen proteins are present in both databases, with 9 proteins unique to database 2 and 4 unique to database 5.

The CDSSTR deconvolution algorithm (Compton and Johnson, 1986; Manavalan and Johnson, 1987) was used as this produced the best fit when compared to ContinLL and Selcon3 (not shown). This algorithm produced small normalised root-mean-square deviation (NRMSD) values, reflecting small differences between the calculated and experimental CD spectra. CDSSTR has also been shown to perform better than other methods when using a small (29 protein) database (Sreerama et al., 2000).

Although the fit between experimental data and reconstructed data with databases 2 and 5 were both excellent (Fig 5.15A-B), the resultant calculations of structural content were very different (Fig 5.15C). Analysis of GPR50ins Sample A with database 2 predicted predominantly 'unordered' (46%), whereas database 5 indicated 25% helical and 17% sheet structure, with only 19% disorder. The numbers were similar using CDSSTR and ContinLL methods, indicating the difference is caused by the databases (Fig 5.14C). Although the trend of unstructured→GPR50 insA>GPR50delA>GPR50insB>GPR50delB→structured was detected when using both databases, the fraction results of database 2 seemed to reflect what was seen in the UV spectra better.

These differences are likely caused by difference in dataset content (Tables 5.3 and 5.4). Although the X-ray data for the 13 proteins in common are the same, the method of parsing the structure into secondary structural elements was different, as reflected in Tables 5.3-5.4 (Woody & Sreerama, pers comm). The authors of reference dataset 5 (Sreerama and Woody, 1994) utilised the Kabsch & Sander method (Kabsch and Sander, 1983) for assigning helix, sheet and turn residues, supplemented by a method for identifying PPII residues, whereas Johnson (dataset 2) used a different method as described in (Johnson, 1999). The two methods are meant

to agree well on helix and on PPII content, but database 5 is prone to giving higher β-sheet and β-turn and lower unordered content than Johnson's. This is because the Kabsch & Sander criteria for the ordered structures are 'looser' than Johnson's. The two methods give more similar results for proteins with high helix content, e.g. MGLB (Myoglobin), HBN (Haemoglobin), LDH (Lactate dehydrogenase), THML (Thermolysin), but differ with more β-sheet or unordered content, as seems to be the case for GPR50 (Woody & Sreerama, pers comm).

From structure predictions (Fig 5.2-5.3, D. Soares), we expect that a high disordered content reflects the structure of GPR50 better and the method and database used by Johnson (1999) may therefore be better for analysing the data. When using database 2 only the results indicated a difference between the insertion and deletion variants of the GPR50 CTD, with an increase in α-helical content from 14% (sample B: 25%) to 25% (B: 51%) in the deletion variant (Fig 5.15D). The polyproline type II content was similar in both insertion (8%, B: 9%) and deletion (9%, B: 5%) variants (Fig 5.15D).

A

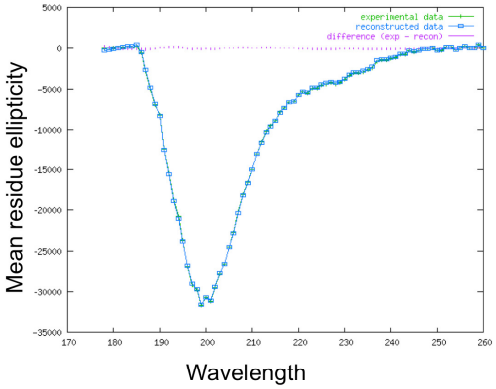

B

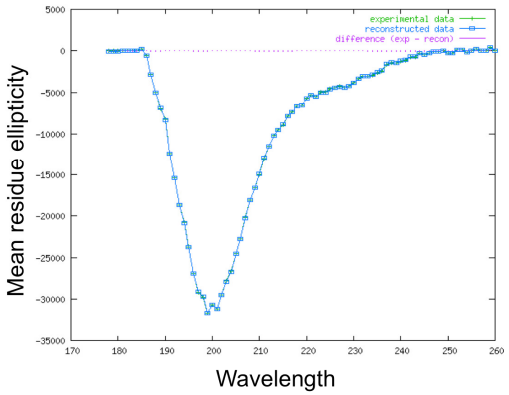

C

Method	Database	Helix	Sheet	Turn	PPII	Unordered	NRMSD
CDSSTR	5	0.25	0.17	0.25	0.14	0.19	0.013
Contin	5	0.22	0.17	0.33	0.17	0.12	0.178
CDSSTR	2	0.14	0.07	0.25	0.08	0.46	0.010
Contin	2	0.14	0.00	0.25	0.17	0.44	0.224

D

	Helix	Sheet	Turn	PPII	Unordered	NRMSD
GPR50 ins A	0.14	0.07	0.25	0.08	0.46	0.010
GPR50 del A	0.25	0.08	0.20	0.09	0.38	0.011
GPR50 ins B	0.25	0.12	0.19	0.09	0.35	0.005
GPR50 del B	0.51	0.08	0.16	0.05	0.21	0.002

Figure 5.15 *Structure content of GPR50 CTD using Dichroweb. Mean residue ellipticity of GPR50 ins A fitted using the CDSSTR method and database 2 (A) and 5 (B). (C) Databases 2 and 5 differed in their structure content prediction using two different methods, CDSSTR and Contin. (D) Structure content of all GPR50 CTD samples using the CDSSTR method and database 2.*

Database 5 Protein Symbol	α-helix	β-sheet	turn	PPII	Unordered
BNJN	0.028	0.491	0.206	0.159	0.117
CHYT	0.114	0.314	0.222	0.163	0.186
CYTC	0.418	0.000	0.164	0.199	0.218
ELAS	0.108	0.342	0.225	0.145	0.171
FLVD	0.320	0.218	0.279	0.061	0.112
HBN	0.760	0.000	0.125	0.035	0.080
LDH	0.390	0.087	0.228	0.024	0.270
LYSM	0.397	0.078	0.310	0.085	0.132
MGLB	0.804	0.000	0.078	0.033	0.085
PAPN	0.259	0.170	0.271	0.123	0.231
PRAL	0.063	0.499	0.193	0.055	0.240
THML	0.415	0.165	0.222	0.095	0.104
TPI	0.460	0.168	0.144	0.055	0.174
PGLU[1]	x	x	x	x	x
RUBR	0.171	0.154	0.269	0.231	0.173
SUBB	0.302	0.178	0.244	0.078	0.189
GPD	0.274	0.208	0.246	0.060	0.213
Average	0.33	0.192	0.214	0.100	0.168

Table 5.3 *Proteins in Dichroweb's reference database 5. X-ray data in Sreerama & Woody 1994. Biochemistry.* [1.] *data not available in paper.*

Database 2 Protein symbol	α-helix	3^{10}-helix	β-sheet	turn	PPII	Unordered
BNJN	0.00	0.00	0.34	0.10	0.12	0.44
CHYT	0.08	0.03	0.16	0.15	0.14	0.44
CYTC	0.39	0.03	0.08	0.09	0.08	0.34
ELAS	0.06	0.04	0.21	0.14	0.11	0.44
FLVD	0.25	0.06	0.17	0.20	0.02	0.30
HBN	0.67	0.08	0.00	0.10	0.00	0.15
LDH	0.35	0.07	0.14	0.12	0.03	0.29
LYSM	0.30	0.11	0.04	0.19	0.02	0.33
MGLB	0.70	0.11	0.00	0.05	0.02	0.17
PAPN	0.24	0.05	0.15	0.11	0.08	0.37
PRAL	0.05	0.04	0.35	0.07	0.04	0.46
THML	0.34	0.06	0.14	0.12	0.04	0.30
TPI	0.33	0.07	0.15	0.10	0.04	0.31
AZU	0.09	0.08	0.34	0.13	0.06	0.29
BLAC	0.09	0.04	0.34	0.13	0.04	0.37
CONA	0.01	0.01	0.36	0.12	0.07	0.42
HMRT	0.59	0.12	0.04	0.06	0.03	0.17
PPSN	0.11	0.10	0.39	0.11	0.09	0.19
RNAS	0.17	0.05	0.19	0.11	0.08	0.40
SUDS	0.00	0.04	0.24	0.16	0.09	0.47
T4LS	0.59	0.08	0.06	0.04	0.01	0.22
TRPN	0.09	0.03	0.19	0.14	0.14	0.41
Average	0.25	0.06	0.19	0.12	0.06	0.33

Table 5.4 *Proteins in Dichroweb's reference database 2. Ref: X-ray data, Johnson PROTEINS: Structure, Function, and Genetics 35:307–312 (1999).*

5.4 Discussion

This is the first experimental data looking at the biophysical properties of the GPR50 CTD, a region of functional importance (Thomson et al., 2005; Levoye et al., 2006). Circular Dichroism indicates GPR50 is predominantly unstructured with ~20-30% α-helix/-β sheet content. Interestingly, structural content increases in the deletion variant to ~30-60% α-helix/-β sheet.

5.4.1 Structure in the GPR50 CTD

The overall CD data indicates there is more structure to the GPR50 CTD than predicted. The deletion variant of Sample B is even indicated to be 51% α-helical. A 51% α-helical content is surprising given the consensus among structure predictors (Figs 5.2-5.3), the presence of numerous 'helix-breaking' proline residues, and is thus almost certainly incorrect for GPR50 CTD. One explanation is that the results were obtained on a degraded sample that retained only its structured regions, as indicated by mass spectrometry and observed on Western blots. Western blotting in Fig 5.9 suggests that Sample A is perhaps N-terminally and Sample B C-terminally degraded. The C terminus of the CTD is predicted to be more disordered (Fig 5.2-5.3), with possible β-sheet and α-helical sections (Fig 5.2) providing some structure to the N-terminal part of the CTD. The loss of the C-terminal region may be the reason why Sample B is more structured. The combined data in this chapter may thus suggest that Sample A and B are different regions of the GPR50 CTD. If the above is the case the difference in DLS data (Fig 5.10-5.11) suggests that the N-terminal region is more prone to multimerising or extension, resulting in a large particle size. This may however also be due to the His-tag that appears to be more abundant in Sample B (Fig 5.9). Future studies with untagged GPR50 CTD may provide clues.

Although the samples A and B have very different characteristics by DLS and CD, the CD spectra show the same pattern of increased helical content in the deletion variant. As the deletion lies within a region predicted to be of high disorder it is not surprising that removing it will result in an increase in α-helical content (Fig 5.2-5.3

and 5.14-5.15). It is likely that an overrepresentation in α-helical content overall is caused by a loss of unstructured regions. The unstructured regions are more susceptible to proteolysis *in vitro* (Dyson and Wright, 2005) and are lost from the rest of the protein, leaving behind only the residual structured regions in the sample. This property makes it difficult to obtain 'structural' data from unstructured proteins or regions. These technical limitations may thus be more problematic when investigating intrinsically unstructured proteins.

5.4.2 Functional consequences

Unstructured regions in proteins facilitate protein-protein interactions and are highly advantageous for functions such as signal transduction, regulation, cytoskelletal organization and protein-DNA recognition (Dyson and Wright, 2005; Li and Song, 2007). An increase in secondary structure in the deletion could mean a reduction in the binding capacity of interaction partners. Intrinsically unstructured or disordered proteins are known to undergo a structural transition into a folded form upon binding of a target ligand (Fink, 2005). The ESI MS data showed the presence of a nonionic surfactant in the solution. Although the effects of nonionic surfactants on protein structure are minimal compared to ionic surfactants (Colonna et al., 1978) it is also possible that the increase in α-helical content is caused by this.
It would be interesting to test GPR50 CTD under different conditions for instance in the presence of micelles or ionic detergents, as this has been shown to increase the structural propensity of membrane (anchored) proteins (Grimaldi et al.; Vasudevan et al.), or in the presence of interacting molecules. The CTD of RNA polymerase II can adopt a left-handed polyproline type II helix (PPII) under increasing hydrogen bond-promoting solvent trifluoroethanol (TFE) concentrations (Bienkiewicz et al., 2000). One has to be cautious however with deriving conclusions from CD data obtained from solvent media such as TFE, as these are known to be helix-inducing and may cause non-native conformations of the protein, distinct from when using aqueous solutions (Wallace, 2009). Because of the time constraints of this project comparisons between the effects of different solvents or surfactants on structure was not possible.

5.4.3 Methodological constraints

Structure content prediction success with CD is heavily dependent on the presence of representative proteins in the database (Janes, 2005). At the moment all databases (and most structure identification methods) are biased towards α-helical proteins (Dyson and Wright, 2005). The empirical methods in use to date are most accurate at defining helical structures from CD spectra because of the dominance of the characteristic peaks from helices (they are much larger than the ß-sheet contributions) and because the structural nature of helices mean their φ/ψ angles fall in a much narrower range than those of other types of secondary structures, and as a result they are much more well defined (Wallace, 2000). Problems with detecting β-sheet content and disordered content let alone rarer structures like the 3^{10}-helix and polyproline II helix will not be resolved unless more of those proteins are added to the database. Being able to measure protein spectra down to lower wavelengths will increase the accuracy of the predictions (Lees et al., 2006b).

One of the recent developments in CD is synchrotron radiation circular dichroism spectroscopy, whereby spectra down to 165 nm can be obtained (Keller et al., 2009), making is easier to distinguish between structures with similar spectra such as unstructured and polyproline II structures (Miles and Wallace, 2006). Two Dichroweb databases that use synchrotron low-wavelength CD data are databases 2 and 5. However there was little consensus between the two databases used as to how much of the content was structured. Using database 5 resulted in a higher structured content, much higher than would be expected from looking at the spectra, whereas database 2 appeared more accurate. As discussed in the results, this is likely caused by the difference in the way the structure content was attributed by the methods used. Generally it is considered to be better to use a large dataset, and SP175 is the largest available on Dichroweb. Unfortunately, this does not contain information on polyproline II helices, although according to (Lees et al., 2006a) this could be made available.

Other methodological constraints concern the buffering systems for biophysical characterisation. Many common components (for instance NaCl is problematic) absorb strongly in the far UV spectrum, interfering with the CD signal. NaF is one of the few possibilities for maintaining ionic strength (Kelly et al., 2005), in the hope that proteins maintain some of their native fold. In previous experiments, solvents (Bienkiewicz et al., 2000) or detergents (Grimaldi et al.; Vasudevan et al.) were added to the media in order to induce polyproline II structures. This introduces many questions about the physiological relevance of these experiments.

5.4.4 Summary

From this preliminary study we conclude that the GPR50 CTD is predominantly unstructured with increased structured content in the deletion variant. Overall, structured content may however be overpredicted due to degradation of unstructured regions and/or multimerisation of specific regions of the GPR50 CTD. However the experiment needs to be repeated and CD and NMR with shorter fragments of the CTD may be necessary to provide a clearer and more conclusive picture. The structure content of different subregions (regions corresponding to predicted eighth membrane parallel helix, or heptapeptide region, or C terminus) and the effects of proteolytic degradation or multimerisation on the various fragments could then be investigated.

5.4.5 Acknowledgements

I would like to thank Dinesh Soares for his initial report of the structure of the GPR50 CTD; Dinesh, Nick Bradshaw, Martin Wear for help with protein purification; Janice Bramham for help with Circular Dichroism; Liz Blackburn for help with Dynamic Light Scattering and ESI Mass Spectrometry and Andy Cronshaw for help with MALDI-TOF (all at University of Edinburgh). I thank Dinesh Soares and Janice Bramham for critical reading of this chapter. Use of the CTCB Facilities was supported by The Wellcome Trust, the Scottish University Life Sciences Alliance (SULSA) and the BBSRC.

Chapter 6
Concluding remarks

6 Chapter six: Concluding remarks

6.1 Investigating the function of GPR50

Research into the function of GPR50 is very much at its early stages and in the absence of a ligand many questions remain. Since the cloning of the receptor in 1996 (Reppert et al., 1996) several studies have reported its expression in the brain, most notably in the hypothalamus and pituitary, suggesting a role in neuroendocrine signaling. Only one loss-of-function study was published, describing a *GPR50* knockout mouse, and suggesting a metabolic role (Ivanova, 2008). A function in lipid metabolism was supported by a genetic study (Bhattacharrya et al., 2006). One study reported the interaction with the melatonin receptors and its negative effect on melatonin signaling (Levoye et al., 2006). The work described in this thesis was initiated after the discovery of an association of variants in the GPR50 C-terminal domain (CTD) with psychiatric illness in women (Thomson et al., 2005). A sex-specific association of GPR50 with mental illness has since been reported in other studies (Macintyre et al., 2011; Delavest et al., 2011).

Since it was thought at the time that deorphanisation strategies would be initiated by others, it was decided to look for interactors with the GPR50 CTD in order to elucidate its function. GPCRs are known to interact with non-G-proteins via their CTD, resulting in modulation of their function (Ritter and Hall, 2009). The hypothesis was that the interactors would also give insight into the way GPR50 and its variants are associated with mental illness. The putative interactors that were identified by yeast-two-hybrid could be grouped into two classes, neuronal development and lipid metabolism, and key proteins from these broad classes were selected for follow-up.

To recap, key results from each of the previous chapters will be summarised and integrated with other results from this thesis, and past research, into a general conclusion. I will end by mentioning some key questions that arise from this study and suggesting experiments for future research.

6.2 Confirmation of the interactions

In Chapter 2, I showed that GPR50 interacts with Nogo-A, Nogo-C, RTN3, CDH8 and ABCA2 under overexpressed conditions in mammalian cells. Endogenous Gpr50 was shown to colocalise with Nogo-A, Cdh8 and Abca2 in cultured mouse neurons. The exogenous and endogenous expression of these proteins was in agreement with reports in the literature. When investigating the effects of the GPR50$^{\Delta 502\text{-}505/T532A}$ variant associated with mood disorders, overexpressed GPR50 and GPR50$^{\Delta 502\text{-}505/T532A}$ showed a similar subcellular localization in mammalian cells. In addition, overexpressed GPR50 and GPR50$^{\Delta 502\text{-}505/T532A}$ both colocalise and/or co-immunoprecipitate with Nogo-A, Nogo-C, RTN3, CDH8 and ABCA2 in a similar fashion. Co-transfection of GPR50$^{\Delta 502\text{-}505/T532A}$ (and GPR50 to a lesser extent) with RTN3, Nogo-C and Nogo-A was shown to alter its cellular localization, decreasing GPR50 plasma membrane expression and increasing its expression in the ER.

6.3 Developmental expression in mouse brain

In Chapter 3, I showed that Gpr50, Nogo-A and Cdh8 protein expression is enriched in the postsynaptic density and Gpr50, Nogo-A, Cdh8 and Abca2 are all present in the light membrane fraction and crude synaptosome in adult mouse brain. These findings are in agreement with results in Chapter 2 and earlier studies. In addition, I reported for the first time the early developmental expression of Gpr50. *Gpr50* mRNA expression was detected from embryonic day E13, is highest at embryonic stage E18 and was shown to correlate with *Abca2* expression over several developmental stages, and with *Nogo-C*, *Cdh8* and *Abca2* at E18 only. This suggests that E18 is an important timepoint for GPR50 functioning. In addition to confirming several sites reported earlier (Drew et al., 2001; Sidibe et al., 2010), Gpr50 protein was found to be expressed in serotonergic, dopaminergic and noradrenergic nuclei in the adult mouse brain. In addition, Gpr50 was shown to colocalise with Nogo-A, Cdh8 and Abca2 in the amygdala, cortex, hypothalamus and specific brain stem nuclei at E18 and in the adult mouse brain. All three proteins were found to be expressed in the amygdala in the adult.

6.4 Functional studies of GPR50

In Chapter 4, I showed that GPR50 overexpression induces neurite outgrowth in NS-1 cells, a PC12 cell line, in which a neuronal phenotype can be induced in response to NGF. In these cells GPR50 overexpression also appears to attenuate the outgrowth inhibiting characteristics of Nogo-A. Additionally, GPR50$^{\Delta 502\text{-}505/T532A}$ overexpression further increases neurite outgrowth compared to GPR50. Moreover, GPR50 and GPR50$^{\Delta 502\text{-}505/T532A}$ overexpression induces filopodia formation in NS-1 cells and cultured neurons. Reticulon proteins RTN3 and Nogo-C are known to reduce BACE1 activity. In a second assay in HEK293 cells I showed that, GPR50, but not GPR50$^{\Delta 502\text{-}505/T532A}$, overexpression increases *in vitro* BACE1 activity.

6.5 Structural studies of the GPR50 CTD

In Chapter 5, I showed that the GPR50 C-terminal domain (CTD) could be succesfully purified, although its stability in various buffering systems calls for optimisation. Preliminary data that indicate GPR50 CTD is predominantly unstructured and that the GPR50 CTD$^{\Delta 502\text{-}505/T532A}$ is more structured than GPR50. The increased structure content of GPR50$^{\Delta 502\text{-}505/T532A}$ may affect the binding of GPR50 with some of its interaction partners.

6.6 Synthesis

From this, I conclude that GPR50 has interesting interaction partners and potential interaction partners, with links to several disease mechanisms and functions. Taken together the results indicate a role for GPR50 in neurite outgrowth, BACE1 activity and synapse formation and function.

GPR50 is enriched in the postsynaptic density and shows a peak in expression at E18, a key stage in synapse development (Hinds and Hinds, 1976; Matsuki et al., 2005). In addition, GPR50 increases neurite outgrowth and induces the formation of filopodia, which may be precursors of synaptic spines (Mattila and Lappalainen, 2008). Moreover, interactors Nogo-A and Cdh8 are reported to regulate synaptic

plasticity (Aloy et al., 2006; Delekate et al., 2011, Suzuki et al., 2007), a mechanism that is thought to be important for learning and memory processes (Kandel, 2001).

Expression of GPR50 in noradrenergic, serotonergic and dopaminergic nuclei perhaps suggests a role in neurotransmitter signaling and the maintenance of synaptic connections (Verhage et al., 2000), although this clearly needs to further investigation. One of the strongest paradigms in psychiatric illness is the disturbance of neurotransmitter signaling and synaptic functioning, as reflected by the mechanisms of action of antidepressants and antipsychotics (Nutt, 2006).

If GPR50 increases BACE1 activity it may be involved in the processing of BACE1 substrates, such as APP and Neuregulin-1, linking GPR50 to Alzheimer's disease and schizophrenia. The mechanism of BACE1 activity increase and whether GPR50 acts in a substrate-specific manner however needs to be investigated. GPR50 and several of its interactors were found to be expressed in the cortex, in areas where BACE1 activity is correlated with Alzheimer's disease severity (Fukumoto et al., 2002), indicating possible functional sites.

GPR50 affects both neurite outgrowth and BACE1 activity and these processes may be linked. There is emerging evidence for a role of BACE1 and its substrates in neurite outgrowth. Overexpression of BACE1 increased neurite length but decreased the number of filopodia-like protrusions in Neuro2A cells, through processing of one of its substrates, the voltage-gated sodium channel subunit β4 (Miyazaki et al., 2007). Substantial evidence has been generated implying a function of APP in neurite outgrowth (Leyssen et al., 2005; Hoe et al., 2009), neuronal proliferation and survival and cell adhesion (Hughes et al., 2010), synaptic development (Ashley et al., 2005) and interestingly G-protein-coupled receptor signaling (via G_0), (Nishimoto et al., 1993), under non-pathological conditions (Reinhard et al., 2005). Full length APP can either have neurite outgrowth promoting or –inhibiting effects, depending for instance on the developmental timepoint investigated (Perez et al., 1997). Soluble APP, the product of α-secretase and β-secretase cleavage, stimulates neurite

outgrowth, perhaps through interfering with the interaction of integrins with cell surface APP (Young-Pearse et al., 2008).

In addition, aberrant sprouting of neurites is a common feature in the pathology of AD and GPR50 expression was reported to be increased in cells showing degenerative changes (Hamouda et al., 2007). Also, Nogo can negatively regulate this outgrowth in AD mouse models (Masliah et al., 2010). Perhaps GPR50 induces (aberrant) outgrowth in these cells.

What can be said about the effect of the GPR50$^{\Delta 502\text{-}505/T532A}$ variant associated with mood disorders? Preliminary structural analysis indicates an increase in structure in the deletion variant, which may be less favourable to protein-protein interactions (Dyson and Wright, 2005). Although the ability to bind the proteins investigated is not affected (Chapter 2) there are perhaps subtle differences in kinetics that are not detected by the techniques used. In the functional assays GPR50$^{\Delta 502\text{-}505/T532A}$ further increased neurite outgrowth compared to GPR50, which may result in abnormal 'wiring' in the brain, which may be linked to the exessive sprouting in AD pathology (Hashimoto and Masliah, 2003; Masliah et al., 2003). There is however no indication of an increased risk of AD in psychiatric patients. The increase in BACE1 activity that is observed after GPR50 overexpression is not seen with GPR50$^{\Delta 502\text{-}505/T532A}$. This may indicate differences in the processing of the substrates, for instance decreased Aβ load and decreased processing of Neuregulin-1 in GPR50$^{\Delta 502\text{-}505/T532A}$. This turn may lead to a decreased risk in Alzheimer's disease but increase in abnormal myelination and schizophrenia (Savonenko et al., 2008). These hypotheses are however highly speculative and detailed research is needed to substantiate these claims. A schematic of possible GPR50 functioning is presented in Figure 6.1.

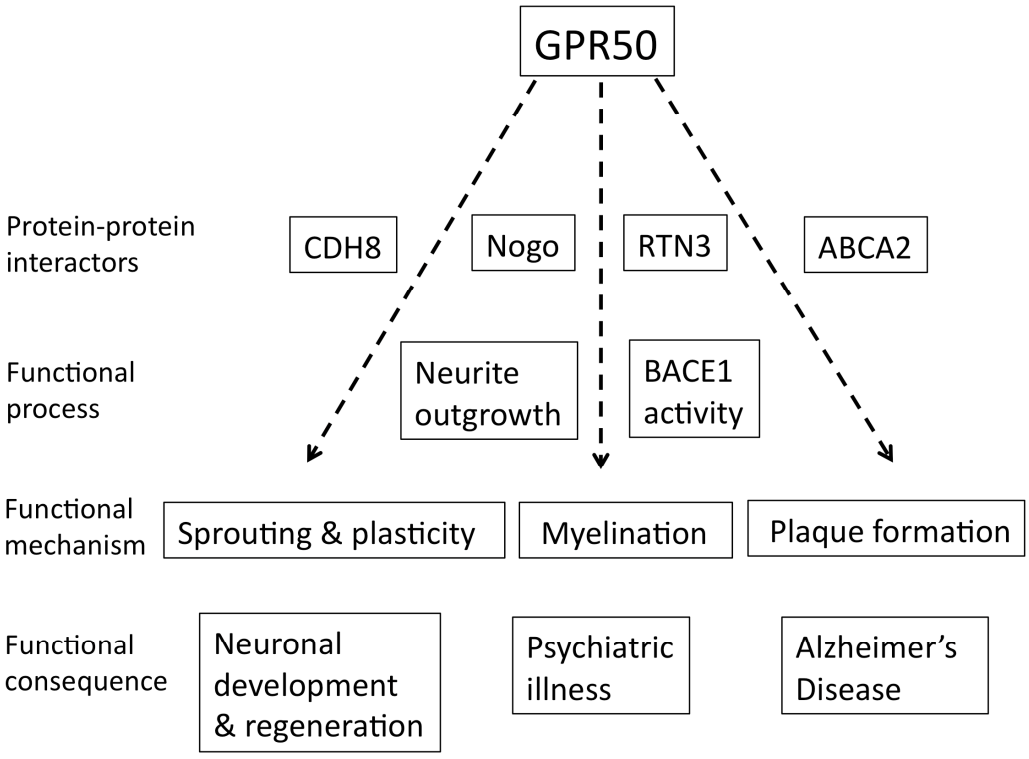

Figure 6.1 *Schematic of GPR50 functioning. Hypothesis based on previous findings results in this thesis. GPR50 can interact with CDH8, Nogo, RTN3, ABCA2 and can increase neurite ourgrowth and BACE1 activity. GPR50 and interactors have been implicated in neuronal development, psychiatric illness and neurodegenerative disorders such as Alzheimer's disease. Further research is needed to elucidate these mechanisms and to establish the role of GPR50 and its interaction partners.*

6.7 Future work

As always, the results in this thesis are limited and lead to more questions than answers. Here follow some of the key remaining questions and suggestions for future research.

1. Are GPR50s interactions direct and are the proteins part of a complex? Results in this thesis indicate GPR50 and interactors are expressed in the same brain regions and subcellular locations. It is therefore possible they interact in a complex. Detailed *in-vitro* binding studies with endogenous and overexpressed proteins are necessary in order to fine map the interaction sites.

2. Does GPR50$^{\Delta 502\text{-}505/T532A}$ affect the stochiometry of its interactions? Although there isn't a clear difference between binding of GPR50 and GPR50$^{\Delta 502\text{-}505/T532A}$ the effects may be subtle.

3. What is the effect of GPR50 knockout/knockdown on its function and the expression and function of the protein-protein interactors? In this thesis no loss-of-function models were used, which are necessary in order to determine the function of GPR50. GPR50 knockout mice are viable, at least in one model (Ivanova et al., 2008), which suggests no major brain or developmental abnormalities in the absence of GPR50. These mice have however not been characterized beyond a metabolic phenotype or in relation to mental illness. Other GPR50 knockout mouse models or stem cells for deriving knockout lines exist (Organon/Schering Plough/Merck and KOMP), neither of which have been characterised to my knowledge. We did try to obtain these mice from Organon but unfortunately were not successful. Knockdown can also be achieved by siRNA in neurons or cell lines.

4. How does GPR50 increase neurite outgrowth and BACE1 activity and is it dependent on the interaction with reticulon proteins? The activity of Rho GTPases and other modulators of the actin cytoskeleton could be measured in response to

GPR50 overexpression and knockout/knockdown. The experiments should be performed in the absence of Nogo/RTN3 to determine if the effects are mediated by these interactors. As for the effect of GPR50 overexpression on BACE1 activity, many questions remain. The possibility of a direct interaction with BACE1 should be investigated as well as the effects of GPR50 overexpression or knockdown on the processing of APP, Neuregulin-1 and other substrates of BACE1.

5. Are there sex-specific effects on expression and function of GPR50? To this end males and females need to be studied separately in order to address sex-specific effects as suggested by genetic studies (Delavest et al., 2011; MacIntyre et al., 2010; Thomson et al., 2005).

6. Is GPR50 involved in neurotransmitter signaling? Given that deorphanisation attempts have been undertaken it is not likely that they would have missed out classic neurotransmitters (although this depends on the point at which the assays have failed). It may however be possible to detect binding or noradrenaline, serotonin and dopamine to GPR50 in a novel assay. Perhaps GPR50 does not signal via these transmitters but modulates its signaling. The possibility of cross-talk between GPR50 and noradrenergic, dopaminergic and serotonergic receptors should also be investigated.

7. What parts of the GPR50 CTD are structured and is its structure altered by its protein-protein interactions? Smaller regions of the CTD need to be examined as necessary for NMR. Purification of GPR50 in the presence of its interactors is expected to alter its confirmation. Structural studies with the GPR50 CTD may however be very difficult or impossible due to the apparent absence of structural elements.

8. What is the role of melatonin or the melatonin receptor-GPR50 heterodimer in GPR50 expression and functioning? Although overexpressed GPR50 and MT1/MT2 have been found to heterodimerise, endogenous dimerisation has not been detected, perhaps due to the difficulty in obtaining specific melatonin receptor antobodies

(Jockers et al., 2008). Perhaps GPR50 can be studied in Melatonin receptor (MT1) knockout mouse, which shows depressive-like behaviour and impaired sensorimotor gating (Weil et al., 2006).

7 References

Acevedo L, Yu J, Erdjument-Bromage H, Miao RQ, Kim JE, Fulton D, Tempst P, Strittmatter SM, Sessa WC (2004) A new role for Nogo as a regulator of vascular remodeling. Nature medicine 10:382-388.

Adolphs R, Baron-Cohen S, Tranel D (2002) Impaired recognition of social emotions following amygdala damage. J Cogn Neurosci 14:1264-1274.

Adolphs R, Tranel D, Damasio H, Damasio AR (1995) Fear and the human amygdala. J Neurosci 15:5879-5891.

Aguirre A, Gallo V (2004) Postnatal neurogenesis and gliogenesis in the olfactory bulb from NG2-expressing progenitors of the subventricular zone. J Neurosci 24:10530-10541.

AHRQ/NIMH (2006) In: (Services UDoHaH, ed): Agency for Healthcare Research and Quality/National Institute of Mental Health.

Akbik F, Cafferty WB, Strittmatter SM (2011) Myelin associated inhibitors: A link between injury-induced and experience-dependent plasticity. Exp Neurol.

Akins MR, Benson DL, Greer CA (2007) Cadherin expression in the developing mouse olfactory system. The Journal of comparative neurology 501:483-497.

Alaerts M, Venken T, Lenaerts AS, De Zutter S, Norrback KF, Adolfsson R, Del-Favero J (2006) Lack of association of an insertion/deletion polymorphism in the G protein-coupled receptor 50 with bipolar disorder in a Northern Swedish population. Psychiatric genetics 16:235-236.

Alexander GE, Crutcher MD (1990) Functional architecture of basal ganglia circuits: neural substrates of parallel processing. Trends in neurosciences 13:266-271.

Allen JA, Halverson-Tamboli RA, Rasenick MM (2007) Lipid raft microdomains and neurotransmitter signalling. Nat Rev Neurosci 8:128-140.

Aloy EM, Weinmann O, Pot C, Kasper H, Dodd DA, Rulicke T, Rossi F, Schwab ME (2006) Synaptic destabilization by neuronal Nogo-A. Brain cell biology 35:137-156.

Alzheimer (1907) Über eine eigenartige Erkrankung der Hirnrinde. Allgemeine Z Psych Psychisch-Gerichtliche Med 64:146–148.

Anderson DJ, Hetzer MW (2008) Reshaping of the endoplasmic reticulum limits the rate for nuclear envelope formation. The Journal of cell biology 182:911-924.

Andrade MA, Perez-Iratxeta C, Ponting CP (2001) Protein repeats: structures, functions, and evolution. J Struct Biol 134:117-131.

Antonyraj KJ, Karunakaran T, Raj PA (1998) Bactericidal activity and poly-L-proline II conformation of the tandem repeat sequence of human salivary mucin glycoprotein (MG2). Archives of biochemistry and biophysics 356:197-206.

APA (1994) Diagnostic and statistical manual of mental disorders (4th ed)
. Washington, DC: American Psychiatric Association.

APA (2000) Diagnostic and statistical manual of mental disorders (4th ed, text revisions). Washington: American Psychiatric Association.

Arborelius L, Owens MJ, Plotsky PM, Nemeroff CB (1999) The role of corticotropin-releasing factor in depression and anxiety disorders. The Journal of endocrinology 160:1-12.

Arendt J (1998) Melatonin and the pineal gland: influence on mammalian seasonal and circadian physiology. Rev Reprod 3:13-22.

Areschoug T, Linse S, Stalhammar-Carlemalm M, Heden LO, Lindahl G (2002) A proline-rich region with a highly periodic sequence in Streptococcal beta protein adopts the polyproline II structure and is exposed on the bacterial surface. Journal of bacteriology 184:6376-6383.

Ashley J, Packard M, Ataman B, Budnik V (2005) Fasciclin II signals new synapse formation through amyloid precursor protein and the scaffolding protein dX11/Mint. J Neurosci 25:5943-5955.

Aston-Jones G, Ennis M, Pieribone VA, Nickell WT, Shipley MT (1986) The brain nucleus locus coeruleus: restricted afferent control of a broad efferent network. Science (New York, NY 234:734-737.

Atwal JK, Pinkston-Gosse J, Syken J, Stawicki S, Wu Y, Shatz C, Tessier-Lavigne M (2008) PirB is a functional receptor for myelin inhibitors of axonal regeneration. Science 322:967-970.

Bancher C, Brunner C, Lassmann H, Budka H, Jellinger K, Wiche G, Seitelberger F, Grundke-Iqbal I, Iqbal K, Wisniewski HM (1989) Accumulation of abnormally phosphorylated tau precedes the formation of neurofibrillary tangles in Alzheimer's disease. Brain Res 477:90-99.

Barrett P, Ivanova E, Graham ES, Ross AW, Wilson D, Ple H, Mercer JG, Ebling FJ, Schuhler S, Dupre SM, Loudon A, Morgan PJ (2006) Photoperiodic regulation of cellular retinol binding protein, CRBP1 [corrected] and nestin in tanycytes of the third ventricle ependymal layer of the Siberian hamster. The Journal of endocrinology 191:687-698.

Baxter MG, Murray EA (2002) The amygdala and reward. Nat Rev Neurosci 3:563-573.

Behan DP, Grigoriadis DE, Lovenberg T, Chalmers D, Heinrichs S, Liaw C, De Souza EB (1996) Neurobiology of corticotropin releasing factor (CRF) receptors and CRF-binding protein: implications for the treatment of CNS disorders. Molecular psychiatry 1:265-277.

Bekirov IH, Needleman LA, Zhang W, Benson DL (2002) Identification and localization of multiple classic cadherins in developing rat limbic system. Neuroscience 115:213-227.

Bekirov IH, Nagy V, Svoronos A, Huntley GW, Benson DL (2008) Cadherin-8 and N-cadherin differentially regulate pre- and postsynaptic development of the hippocampal mossy fiber pathway. Hippocampus 18:349-363.

Belmonte Mahon P et al. (2011) Genome-wide association analysis of age at onset and psychotic symptoms in bipolar disorder. Am J Med Genet B Neuropsychiatr Genet 156:370-378.

Benes FM, Berretta S (2001) GABAergic interneurons: implications for understanding schizophrenia and bipolar disorder. Neuropsychopharmacology 25:1-27.

Berger TW, Semple-Rowland S, Basset JL (1981) Hippocampal polymorph neurons are the cells of origin for ipsilateral association and commissural afferents to the dentate gyrus. Brain Res 215:329-336.

Berger UV, Hediger MA (2001) Differential distribution of the glutamate transporters GLT-1 and GLAST in tanycytes of the third ventricle. The Journal of comparative neurology 433:101-114.

Beychok S (1966) Circular dichroism of biological macromolecules. Science (New York, NY 154:1288-1299.

Bhattacharyya S, Luan J, Challis B, Keogh J, Montague C, Brennand J, Morten J, Lowenbeim S, Jenkins S, Farooqi IS, Wareham NJ, O'Rahilly S (2006) Sequence variants in the melatonin-related receptor gene (GPR50) associate with circulating triglyceride and HDL levels. J Lipid Res 47:761-766.

Bieche I, Olivi M, Champeme MH, Vidaud D, Lidereau R, Vidaud M (1998) Novel approach to quantitative polymerase chain reaction using real-time detection: application to the detection of gene amplification in breast cancer. International journal of cancer 78:661-666.

Bienkiewicz EA, Moon Woody A, Woody RW (2000) Conformation of the RNA polymerase II C-terminal domain: circular dichroism of long and short fragments. J Mol Biol 297:119-133.

Blom N, Gammeltoft S, Brunak S (1999) Sequence and structure-based prediction of eukaryotic protein phosphorylation sites. J Mol Biol 294:1351-1362.

Bouvier M (2001) Oligomerization of G-protein-coupled transmitter receptors. Nat Rev Neurosci 2:274-286.

Bradshaw NJ, Ogawa F, Antolin-Fontes B, Chubb JE, Carlyle BC, Christie S, Claessens A, Porteous DJ, Millar JK (2008) DISC1, PDE4B, and NDE1 at the centrosome and synapse. Biochem Biophys Res Commun 377:1091-1096.

Brenz Verca MS, Bahi A, Boyer F, Wagner GC, Dreyer JL (2003) Distribution of alpha- and gamma-synucleins in the adult rat brain and their modification by high-dose cocaine treatment. The European journal of neuroscience 18:1923-1938.

Briggs MR, Yokoyama C, Wang X, Brown MS, Goldstein JL (1993) Nuclear protein that binds sterol regulatory element of low density lipoprotein receptor promoter. I. Identification of the protein and delineation of its target nucleotide sequence. The Journal of biological chemistry 268:14490-14496.

Broccardo C, Nieoullon V, Amin R, Masmejean F, Carta S, Tassi S, Pophillat M, Rubartelli A, Pierres M, Rougon G, Nieoullon A, Chazal G, Chimini G (2006) ABCA2 is a marker of neural progenitors and neuronal subsets in the adult rodent brain. Journal of neurochemistry 97:345-355.

Budel S, Padukkavidana T, Liu BP, Feng Z, Hu F, Johnson S, Lauren J, Park JH, McGee AW, Liao J, Stillman A, Kim JE, Yang BZ, Sodi S, Gelernter J, Zhao H, Hisama F, Arnsten AF, Strittmatter SM (2008) Genetic variants of Nogo-66 receptor with possible association to schizophrenia block myelin inhibition of axon growth. J Neurosci 28:13161-13172.

Burkhard P, Stetefeld J, Strelkov SV (2001) Coiled coils: a highly versatile protein folding motif. Trends Cell Biol 11:82-88.

Cafferty WB, Duffy P, Huebner E, Strittmatter SM (2010) MAG and OMgp synergize with Nogo-A to restrict axonal growth and neurological recovery after spinal cord trauma. J Neurosci 30:6825-6837.

Carlin RK, Grab DJ, Cohen RS, Siekevitz P (1980) Isolation and characterization of postsynaptic densities from various brain regions: enrichment of different types of postsynaptic densities. The Journal of cell biology 86:831-845.

Caroni P, Schwab ME (1988) Antibody against myelin-associated inhibitor of neurite growth neutralizes nonpermissive substrate properties of CNS white matter. Neuron 1:85-96.

Cedarbaum JM, Aghajanian GK (1978) Afferent projections to the rat locus coeruleus as determined by a retrograde tracing technique. The Journal of comparative neurology 178:1-16.

Celi FS, Cohen MM, Antonarakis SE, Wertheimer E, Roth J, Shuldiner AR (1994) Determination of gene dosage by a quantitative adaptation of the polymerase chain reaction (gd-PCR): rapid detection of deletions and duplications of gene sequences. Genomics 21:304-310.

Chakrabartty A, Kortemme T, Baldwin RL (1994) Helix propensities of the amino acids measured in alanine-based peptides without helix-stabilizing side-chain interactions. Protein Sci 3:843-852.

Chang K, Seabold GK, Wang CY, Wenthold RJ (2010) Reticulon 3 is an interacting partner of the SALM family of adhesion molecules. J Neurosci Res 88:266-274.

Chaste P et al. (2010) Identification of pathway-biased and deleterious melatonin receptor mutants in autism spectrum disorders and in the general population. PLoS One 5:e11495.

Chauvet N, El-Yandouzi T, Mathieu MN, Schlernitzauer A, Galibert E, Lafont C, Le Tissier P, Robinson IC, Mollard P, Coutry N (2009) Characterization of adherens junction protein expression and localization in pituitary cell networks. The Journal of endocrinology 202:375-387.

Chen MS, Huber AB, van der Haar ME, Frank M, Schnell L, Spillmann AA, Christ F, Schwab ME (2000) Nogo-A is a myelin-associated neurite outgrowth inhibitor and an antigen for monoclonal antibody IN-1. Nature 403:434-439.

Chen Y, Tang X, Cao X, Chen H, Zhang X (2006) Human Nogo-C overexpression induces HEK293 cell apoptosis via a mechanism that involves JNK-c-Jun pathway. Biochem Biophys Res Commun 348:923-928.

Chen YS, Akula N, Detera-Wadleigh SD, Schulze TG, Thomas J, Potash JB, DePaulo JR, McInnis MG, Cox NJ, McMahon FJ (2004a) Findings in an independent sample support an association between bipolar affective disorder and the G72/G30 locus on chromosome 13q33. Molecular psychiatry 9:87-92; image 85.

Chen ZJ, Vulevic B, Ile KE, Soulika A, Davis W, Jr., Reiner PB, Connop BP, Nathwani P, Trojanowski JQ, Tew KD (2004b) Association of ABCA2 expression with determinants of Alzheimer's disease. FASEB J 18:1129-1131.

Chiodera P, Volpi R, Capretti L, Marchesi C, d'Amato L, De Ferri A, Bianconi L, Coiro V (1991) Effect of estrogen or insulin-induced hypoglycemia on plasma oxytocin levels in bulimia and anorexia nervosa. Metabolism: clinical and experimental 40:1226-1230.

Cho KO, Hunt CA, Kennedy MB (1992) The rat brain postsynaptic density fraction contains a homolog of the Drosophila discs-large tumor suppressor protein. Neuron 9:929-942.

Choi G, Guo J, Makriyannis A (2005) The conformation of the cytoplasmic helix 8 of the CB1 cannabinoid receptor using NMR and circular dichroism. Biochimica et biophysica acta 1668:1-9.

Chyung AS, Greenberg BD, Cook DG, Doms RW, Lee VM (1997) Novel beta-secretase cleavage of beta-amyloid precursor protein in the endoplasmic reticulum/intermediate compartment of NT2N cells. The Journal of cell biology 138:671-680.

Cichon S et al. (2011) Genome-wide Association Study Identifies Genetic Variation in Neurocan as a Susceptibility Factor for Bipolar Disorder. Am J Hum Genet 88:372-381.

Citron M (2010) Alzheimer's disease: strategies for disease modification. Nat Rev Drug Discov 9:387-398.

Clapcote SJ, Lipina TV, Millar JK, Mackie S, Christie S, Ogawa F, Lerch JP, Trimble K, Uchiyama M, Sakuraba Y, Kaneda H, Shiroishi T, Houslay MD, Henkelman RM, Sled JG, Gondo Y, Porteous DJ, Roder JC (2007) Behavioral phenotypes of Disc1 missense mutations in mice. Neuron 54:387-402.

Coelho DJ, Sims DJ, Ruegg PJ, Minn I, Muench AR, Mitchell PJ (2005) Cell type-specific and sexually dimorphic expression of transcription factor AP-2 in the adult mouse brain. Neuroscience 134:907-919.

Coeytaux K, Poupon A (2005) Prediction of unfolded segments in a protein sequence based on amino acid composition. Bioinformatics (Oxford, England) 21:1891-1900.

Colonna G, Alexander SS, Jr., Yamada KM, Pastan I, Edelhoch H (1978) The stability of cell surface protein to surfactants and denaturants. The Journal of biological chemistry 253:7787-7790.

Compton LA, Johnson WC, Jr. (1986) Analysis of protein circular dichroism spectra for secondary structure using a simple matrix multiplication. Analytical biochemistry 155:155-167.

Conner M, Hicks MR, Dafforn T, Knowles TJ, Ludwig C, Staddon S, Overduin M, Gunther UL, Thome J, Wheatley M, Poyner DR, Conner AC (2008) Functional and biophysical analysis of the C-terminus of the CGRP-receptor; a family B GPCR. Biochemistry 47:8434-8444.

Conway S, Canning SJ, Barrett P, Guardiola-Lemaitre B, Delagrange P, Morgan PJ (1997) The roles of valine 208 and histidine 211 in ligand binding and receptor function of the ovine Mel1a beta melatonin receptor. Biochem Biophys Res Commun 239:418-423.

Conway S, Drew JE, Mowat ES, Barrett P, Delagrange P, Morgan PJ (2000) Chimeric melatonin mt1 and melatonin-related receptors. Identification of domains and residues participating in ligand binding and receptor activation of the melatonin mt1 receptor. The Journal of biological chemistry 275:20602-20609.

Cook DG, Forman MS, Sung JC, Leight S, Kolson DL, Iwatsubo T, Lee VM, Doms RW (1997) Alzheimer's A beta(1-42) is generated in the endoplasmic reticulum/intermediate compartment of NT2N cells. Nature medicine 3:1021-1023.

Cook EH, Jr., Scherer SW (2008) Copy-number variations associated with neuropsychiatric conditions. Nature 455:919-923.

Cordy JM, Hussain I, Dingwall C, Hooper NM, Turner AJ (2003) Exclusively targeting beta-secretase to lipid rafts by GPI-anchor addition up-regulates beta-site processing of the amyloid precursor protein. Proceedings of the

National Academy of Sciences of the United States of America 100:11735-11740.
Corfas G, Roy K, Buxbaum JD (2004) Neuregulin 1-erbB signaling and the molecular/cellular basis of schizophrenia. Nature neuroscience 7:575-580.
Coyle JT, Duman RS (2003) Finding the intracellular signaling pathways affected by mood disorder treatments. Neuron 38:157-160.
Craddock N, O'Donovan MC, Owen MJ (2005) The genetics of schizophrenia and bipolar disorder: dissecting psychosis. Journal of medical genetics 42:193-204.
Crow TJ (2007) How and why genetic linkage has not solved the problem of psychosis: review and hypothesis. The American journal of psychiatry 164:13-21.
Cunningham ET, Jr., Sawchenko PE (1988) Anatomical specificity of noradrenergic inputs to the paraventricular and supraoptic nuclei of the rat hypothalamus. The Journal of comparative neurology 274:60-76.
Curtis AL, Bethea T, Valentino RJ (2006) Sexually dimorphic responses of the brain norepinephrine system to stress and corticotropin-releasing factor. Neuropsychopharmacology 31:544-554.
Davis W, Jr. (2011) The ATP-binding cassette transporter-2 (ABCA2) regulates cholesterol homeostasis and low-density lipoprotein receptor metabolism in N2a neuroblastoma cells. Biochim Biophys Acta.
Davis W, Jr., Boyd JT, Ile KE, Tew KD (2004) Human ATP-binding cassette transporter-2 (ABCA2) positively regulates low-density lipoprotein receptor expression and negatively regulates cholesterol esterification in Chinese hamster ovary cells. Biochim Biophys Acta 1683:89-100.
Dawson D, van den Heuvel CJ (1998) Integrating the actions of melatonin on human physiology. Ann Med 30:95-102.
De Luca A, De Falco M, De Luca L, Penta R, Shridhar V, Baldi F, Campioni M, Paggi MG, Baldi A (2004) Pattern of expression of HtrA1 during mouse development. J Histochem Cytochem 52:1609-1617.
del Castillo FJ, Cohen-Salmon M, Charollais A, Caille D, Lampe PD, Chavrier P, Meda P, Petit C (2010) Consortin, a trans-Golgi network cargo receptor for the plasma membrane targeting and recycling of connexins. Hum Mol Genet 19:262-275.
Delavest M, Even C, Benjemaa N, Poirier MF, Jockers R, Krebs MO (2011) Association of the intronic rs2072621 polymorphism of the X-linked GPR50 gene with affective disorder with seasonal pattern. Eur Psychiatry.
Delekate A, Zagrebelsky M, Kramer S, Schwab ME, Korte M (2011) NogoA restricts synaptic plasticity in the adult hippocampus on a fast time scale. Proceedings of the National Academy of Sciences of the United States of America 108:2569-2574.
Di Maria E, Bonvicini C, Bonomini C, Alberici A, Zanetti O, Gennarelli M (2009) Genetic variation in the G720/G30 gene locus (DAOA) influences the occurrence of psychotic symptoms in patients with Alzheimer's disease. J Alzheimers Dis 18:953-960.
Di Scala F, Dupuis L, Gaiddon C, De Tapia M, Jokic N, Gonzalez de Aguilar JL, Raul JS, Ludes B, Loeffler JP (2005) Tissue specificity and regulation of the N-terminal diversity of reticulon 3. The Biochemical journal 385:125-134.

Diekmann S, Henneke M, Burckhardt BC, Gartner J (2010) Pelizaeus-Merzbacher-like disease is caused not only by a loss of connexin47 function but also by a hemichannel dysfunction. Eur J Hum Genet 18:985-992.

Dietschy JM, Turley SD (2001) Cholesterol metabolism in the brain. Curr Opin Lipidol 12:105-112.

Dodd DA, Niederoest B, Bloechlinger S, Dupuis L, Loeffler JP, Schwab ME (2005) Nogo-A, -B, and -C are found on the cell surface and interact together in many different cell types. The Journal of biological chemistry 280:12494-12502.

Doherty P, Ashton SV, Moore SE, Walsh FS (1991) Morphoregulatory activities of NCAM and N-cadherin can be accounted for by G protein-dependent activation of L- and N-type neuronal Ca2+ channels. Cell 67:21-33.

Donoghue JP, Herkenham M (1986) Neostriatal projections from individual cortical fields conform to histochemically distinct striatal compartments in the rat. Brain Res 365:397-403.

Drew JE, Williams LM, Hannah LT, Barrett P, Abramovich DR (1998) Melatonin receptors in the human fetal kidney: 2-[125I]iodomelatonin binding sites correlated with expression of Mel1a and Mel1b receptor genes. The Journal of endocrinology 156:261-267.

Drew JE, Barrett P, Mercer JG, Moar KM, Canet E, Delagrange P, Morgan PJ (2001) Localization of the melatonin-related receptor in the rodent brain and peripheral tissues. Journal of neuroendocrinology 13:453-458.

Duan X, Chang JH, Ge S, Faulkner RL, Kim JY, Kitabatake Y, Liu XB, Yang CH, Jordan JD, Ma DK, Liu CY, Ganesan S, Cheng HJ, Ming GL, Lu B, Song H (2007) Disrupted-In-Schizophrenia 1 regulates integration of newly generated neurons in the adult brain. Cell 130:1146-1158.

Duerr RH et al. (2006) A genome-wide association study identifies IL23R as an inflammatory bowel disease gene. Science (New York, NY 314:1461-1463.

Dufourny L, Levasseur A, Migaud M, Callebaut I, Pontarotti P, Malpaux B, Monget P (2008) GPR50 is the mammalian ortholog of Mel1c: evidence of rapid evolution in mammals. BMC evolutionary biology 8:105.

Duncan MJ, Takahashi JS, Dubocovich ML (1988) 2-[125I]iodomelatonin binding sites in hamster brain membranes: pharmacological characteristics and regional distribution. Endocrinology 122:1825-1833.

Dunner DL, Fieve RR (1974) Clinical factors in lithium carbonate prophylaxis failure. Arch Gen Psychiatry 30:229-233.

Dwork AJ, Mancevski B, Rosoklija G (2007) White matter and cognitive function in schizophrenia. The international journal of neuropsychopharmacology / official scientific journal of the Collegium Internationale Neuropsychopharmacologicum (CINP) 10:513-536.

Dyson HJ, Wright PE (2005) Intrinsically unstructured proteins and their functions. Nature reviews 6:197-208.

Eastwood SL, Law AJ, Everall IP, Harrison PJ (2003) The axonal chemorepellant semaphorin 3A is increased in the cerebellum in schizophrenia and may contribute to its synaptic pathology. Molecular psychiatry 8:148-155.

Ebisawa T, Karne S, Lerner MR, Reppert SM (1994) Expression cloning of a high-affinity melatonin receptor from Xenopus dermal melanophores. Proceedings

of the National Academy of Sciences of the United States of America 91:6133-6137.
Eglen RM, Bosse R, Reisine T (2007) Emerging concepts of guanine nucleotide-binding protein-coupled receptor (GPCR) function and implications for high throughput screening. Assay Drug Dev Technol 5:425-451.
Ehehalt R, Keller P, Haass C, Thiele C, Simons K (2003) Amyloidogenic processing of the Alzheimer beta-amyloid precursor protein depends on lipid rafts. The Journal of cell biology 160:113-123.
Falls DL (2003) Neuregulins: functions, forms, and signaling strategies. Experimental cell research 284:14-30.
Feng LR, Federoff HJ, Vicini S, Maguire-Zeiss KA (2010) Alpha-synuclein mediates alterations in membrane conductance: a potential role for alpha-synuclein oligomers in cell vulnerability. The European journal of neuroscience 32:10-17.
Feng Y, Wigg K, King N, Vetro A, Kiss E, Kapornai K, Mayer L, Gadoros J, Kennedy JL, Kovacs M, Barr CL (2007) GPR50 is not associated with childhood-onset mood disorders in a large sample of Hungarian families. Psychiatric genetics 17:347-350.
Fernandez A, Llacuna L, Fernandez-Checa JC, Colell A (2009) Mitochondrial cholesterol loading exacerbates amyloid beta peptide-induced inflammation and neurotoxicity. J Neurosci 29:6394-6405.
Ferreira MA et al. (2008) Collaborative genome-wide association analysis supports a role for ANK3 and CACNA1C in bipolar disorder. Nature genetics 40:1056-1058.
Fink AL (2005) Natively unfolded proteins. Curr Opin Struct Biol 15:35-41.
Flower DR (1999) Modelling G-protein-coupled receptors for drug design. Biochimica et biophysica acta 1422:207-234.
Fournier AE, GrandPre T, Strittmatter SM (2001) Identification of a receptor mediating Nogo-66 inhibition of axonal regeneration. Nature 409:341-346.
Fournier AE, Takizawa BT, Strittmatter SM (2003) Rho kinase inhibition enhances axonal regeneration in the injured CNS. J Neurosci 23:1416-1423.
Frayling TM et al. (2007) A common variant in the FTO gene is associated with body mass index and predisposes to childhood and adult obesity. Science (New York, NY 316:889-894.
Frenzel KE, Falls DL (2001) Neuregulin-1 proteins in rat brain and transfected cells are localized to lipid rafts. Journal of neurochemistry 77:1-12.
Fukumoto H, Cheung BS, Hyman BT, Irizarry MC (2002) Beta-secretase protein and activity are increased in the neocortex in Alzheimer disease. Arch Neurol 59:1381-1389.
Garcia MA, Millan C, Balmaceda-Aguilera C, Castro T, Pastor P, Montecinos H, Reinicke K, Zuniga F, Vera JC, Onate SA, Nualart F (2003) Hypothalamic ependymal-glial cells express the glucose transporter GLUT2, a protein involved in glucose sensing. Journal of neurochemistry 86:709-724.
Garel S, Garcia-Dominguez M, Charnay P (2000) Control of the migratory pathway of facial branchiomotor neurones. Development 127:5297-5307.
Geller B, Luby J (1997) Child and adolescent bipolar disorder: a review of the past 10 years. J Am Acad Child Adolesc Psychiatry 36:1168-1176.

Geller B, Badner JA, Tillman R, Christian SL, Bolhofner K, Cook EH, Jr. (2004) Linkage disequilibrium of the brain-derived neurotrophic factor Val66Met polymorphism in children with a prepubertal and early adolescent bipolar disorder phenotype. The American journal of psychiatry 161:1698-1700.

Gerfen CR (1984) The neostriatal mosaic: compartmentalization of corticostriatal input and striatonigral output systems. Nature 311:461-464.

Gerfen CR (1992) The neostriatal mosaic: multiple levels of compartmental organization. Trends in neurosciences 15:133-139.

Gershon ES, Alliey-Rodriguez N, Liu C (2011) After GWAS: searching for genetic risk for schizophrenia and bipolar disorder. The American journal of psychiatry 168:253-256.

Gershon S, Soares JC (1997) Current therapeutic profile of lithium. Arch Gen Psychiatry 54:16-20.

Gil OD, Needleman L, Huntley GW (2002) Developmental patterns of cadherin expression and localization in relation to compartmentalized thalamocortical terminations in rat barrel cortex. The Journal of comparative neurology 453:372-388.

Gil V, Nicolas O, Mingorance A, Urena JM, Tang BL, Hirata T, Saez-Valero J, Ferrer I, Soriano E, del Rio JA (2006) Nogo-A expression in the human hippocampus in normal aging and in Alzheimer disease. Journal of neuropathology and experimental neurology 65:433-444.

Goldstein JL, DeBose-Boyd RA, Brown MS (2006) Protein sensors for membrane sterols. Cell 124:35-46.

Gonzenbach RR, Gasser P, Zorner B, Hochreutener E, Dietz V, Schwab ME (2010) Nogo-A antibodies and training reduce muscle spasms in spinal cord-injured rats. Ann Neurol 68:48-57.

GrandPre T, Nakamura F, Vartanian T, Strittmatter SM (2000) Identification of the Nogo inhibitor of axon regeneration as a Reticulon protein. Nature 403:439-444.

Greene LA, Tischler AS (1976) Establishment of a noradrenergic clonal line of rat adrenal pheochromocytoma cells which respond to nerve growth factor. Proceedings of the National Academy of Sciences of the United States of America 73:2424-2428.

Grimaldi M, Scrima M, Esposito C, Vitiello G, Ramunno A, Limongelli V, D'Errico G, Novellino E, D'Ursi AM (2010) Membrane charge dependent states of the beta-amyloid fragment Abeta (16-35) with differently charged micelle aggregates. Biochimica et biophysica acta 1798:660-671.

Grünewald E, Kinnell HL, Porteous DJ, Thomson PA (2009) GPR50 interacts with neuronal NOGO-A and affects neurite outgrowth. Molecular and Cellular Neuroscience 42:363-371.

Gubitz AK, Reppert SM (1999) Assignment of the melatonin-related receptor to human chromosome X (GPR50) and mouse chromosome X (Gpr50). Genomics 55:248-251.

Gubitz AK, Reppert SM (2000) Chimeric and point-mutated receptors reveal that a single glycine residue in transmembrane domain 6 is critical for high affinity melatonin binding. Endocrinology 141:1236-1244.

Guirland C, Suzuki S, Kojima M, Lu B, Zheng JQ (2004) Lipid rafts mediate chemotropic guidance of nerve growth cones. Neuron 42:51-62.

Gutierrez JA, Solenberg PJ, Perkins DR, Willency JA, Knierman MD, Jin Z, Witcher DR, Luo S, Onyia JE, Hale JE (2008) Ghrelin octanoylation mediated by an orphan lipid transferase. Proceedings of the National Academy of Sciences of the United States of America 105:6320-6325.

Hall J, Whalley HC, Job DE, Baig BJ, McIntosh AM, Evans KL, Thomson PA, Porteous DJ, Cunningham-Owens DG, Johnstone EC, Lawrie SM (2006) A neuregulin 1 variant associated with abnormal cortical function and psychotic symptoms. Nature neuroscience 9:1477-1478.

Hamouda HO, Chen P, Levoye A, Sozer-Topcular N, Daulat AM, Guillaume JL, Ravid R, Savaskan E, Ferry G, Boutin JA, Delagrange P, Jockers R, Maurice P (2007) Detection of the human GPR50 orphan seven transmembrane protein by polyclonal antibodies mapping different epitopes. Journal of pineal research 43:10-15.

Hardeland R (2009) Melatonin: signaling mechanisms of a pleiotropic agent. Biofactors 35:183-192.

Harmar AJ et al. (2009) IUPHAR-DB: the IUPHAR database of G protein-coupled receptors and ion channels. Nucleic acids research 37:D680-685.

Harris GC, Wimmer M, Aston-Jones G (2005) A role for lateral hypothalamic orexin neurons in reward seeking. Nature 437:556-559.

Hartmann T, Bieger SC, Bruhl B, Tienari PJ, Ida N, Allsop D, Roberts GW, Masters CL, Dotti CG, Unsicker K, Beyreuther K (1997) Distinct sites of intracellular production for Alzheimer's disease A beta40/42 amyloid peptides. Nature medicine 3:1016-1020.

Harwood AJ (2003) Neurodevelopment and mood stabilizers. Curr Mol Med 3:472-482.

Hasegawa T, Ohno K, Sano M, Omura T, Omura K, Nagano A, Sato K (2005) The differential expression patterns of messenger RNAs encoding Nogo-A and Nogo-receptor in the rat central nervous system. Brain research 133:119-130.

Hashimoto M, Masliah E (2003) Cycles of aberrant synaptic sprouting and neurodegeneration in Alzheimer's and dementia with Lewy bodies. Neurochem Res 28:1743-1756.

Hattori E, Liu C, Badner JA, Bonner TI, Christian SL, Maheshwari M, Detera-Wadleigh SD, Gibbs RA, Gershon ES (2003) Polymorphisms at the G72/G30 gene locus, on 13q33, are associated with bipolar disorder in two independent pedigree series. Am J Hum Genet 72:1131-1140.

He W, Shi Q, Hu X, Yan R (2007) The membrane topology of RTN3 and its effect on binding of RTN3 to BACE1. The Journal of biological chemistry 282:29144-29151.

He W, Lu Y, Qahwash I, Hu XY, Chang A, Yan R (2004) Reticulon family members modulate BACE1 activity and amyloid-beta peptide generation. Nature medicine 10:959-965.

He W, Hu X, Shi Q, Zhou X, Lu Y, Fisher C, Yan R (2006) Mapping of interaction domains mediating binding between BACE1 and RTN/Nogo proteins. J Mol Biol 363:625-634.

Head BP, Hu Y, Finley JC, Saldana MD, Bonds JA, Miyanohara A, Niesman IR, Ali SS, Murray F, Insel PA, Roth DM, Patel HH, Patel PM (2011) Neuron-targeted caveolin-1 enhances signaling and promotes arborization of primary neurons. The Journal of biological chemistry.

Heath JE, Siedlak SL, Zhu X, Lee HG, Thakur A, Yan R, Perry G, Smith MA, Castellani RJ (2010) Widespread distribution of reticulon-3 in various neurodegenerative diseases. Neuropathology 30:574-579.
Hefner K, Holmes A (2007) Ontogeny of fear-, anxiety- and depression-related behavior across adolescence in C57BL/6J mice. Behav Brain Res 176:210-215.
Hemming ML, Elias JE, Gygi SP, Selkoe DJ (2009) Identification of beta-secretase (BACE1) substrates using quantitative proteomics. PLoS One 4:e8477.
Hennah W et al. (2009) DISC1 association, heterogeneity and interplay in schizophrenia and bipolar disorder. Molecular psychiatry 14:865-873.
Henstridge CM, Balenga NA, Ford LA, Ross RA, Waldhoer M, Irving AJ (2009) The GPR55 ligand L-alpha-lysophosphatidylinositol promotes RhoA-dependent Ca2+ signaling and NFAT activation. Faseb J 23:183-193.
Hering H, Lin CC, Sheng M (2003) Lipid rafts in the maintenance of synapses, dendritic spines, and surface AMPA receptor stability. J Neurosci 23:3262-3271.
Herman JP, Cullinan WE (1997) Neurocircuitry of stress: central control of the hypothalamo-pituitary-adrenocortical axis. Trends in neurosciences 20:78-84.
Hinds JW, Hinds PL (1976) Synapse formation in the mouse olfactory bulb. II. Morphogenesis. The Journal of comparative neurology 169:41-61.
Hoe HS, Lee KJ, Carney RS, Lee J, Markova A, Lee JY, Howell BW, Hyman BT, Pak DT, Bu G, Rebeck GW (2009) Interaction of reelin with amyloid precursor protein promotes neurite outgrowth. J Neurosci 29:7459-7473.
Hong Z, Yang Y, Zhang C, Niu Y, Li K, Zhao X, Liu JJ (2009) The retromer component SNX6 interacts with dynactin p150(Glued) and mediates endosome-to-TGN transport. Cell Res 19:1334-1349.
Hopkins AL, Groom CR (2002) The druggable genome. Nat Rev Drug Discov 1:727-730.
Hu X, Hicks CW, He W, Wong P, Macklin WB, Trapp BD, Yan R (2006) Bace1 modulates myelination in the central and peripheral nervous system. Nature neuroscience 9:1520-1525.
Hu X, He W, Diaconu C, Tang X, Kidd GJ, Macklin WB, Trapp BD, Yan R (2008) Genetic deletion of BACE1 in mice affects remyelination of sciatic nerves. FASEB J 22:2970-2980.
Hu X, Shi Q, Zhou X, He W, Yi H, Yin X, Gearing M, Levey A, Yan R (2007) Transgenic mice overexpressing reticulon 3 develop neuritic abnormalities. EMBO J 26:2755-2767.
Huber AB, Weinmann O, Brosamle C, Oertle T, Schwab ME (2002) Patterns of Nogo mRNA and protein expression in the developing and adult rat and after CNS lesions. J Neurosci 22:3553-3567.
Hubmacher D, El-Hallous EI, Nelea V, Kaartinen MT, Lee ER, Reinhardt DP (2008) Biogenesis of extracellular microfibrils: Multimerization of the fibrillin-1 C terminus into bead-like structures enables self-assembly. Proceedings of the National Academy of Sciences of the United States of America 105:6548-6553.
Hughes M, Snetkov V, Rose RS, Trousil S, Mermoud JE, Dingwall C (2010) Neurite-like structures induced by mevalonate pathway blockade are due to

the stability of cell adhesion foci and are enhanced by the presence of APP. Journal of neurochemistry 114:832-842.
Hyman SE (2007) Can neuroscience be integrated into the DSM-V? Nat Rev Neurosci 8:725-732.
Im YJ, Raychaudhuri S, Prinz WA, Hurley JH (2005) Structural mechanism for sterol sensing and transport by OSBP-related proteins. Nature 437:154-158.
Inoue T, Tanaka T, Takeichi M, Chisaka O, Nakamura S, Osumi N (2001) Role of cadherins in maintaining the compartment boundary between the cortex and striatum during development. Development 128:561-569.
Insel TR (2008) Assessing the economic costs of serious mental illness. The American journal of psychiatry 165:663-665.
Ivanova EA, Bechtold DA, Dupre SM, Brennand J, Barrett P, Luckman SM, Loudon AS (2008) Altered metabolism in the melatonin-related receptor (GPR50) knockout mouse. Am J Physiol Endocrinol Metab 294:E176-182.
Izzo G, Francesco A, Ferrara D, Campitiello MR, Serino I, Minucci S, d'Istria M (2010) Expression of melatonin (MT1, MT2) and melatonin-related receptors in the adult rat testes and during development. Zygote 18:257-264.
Janes RW (2005) Bioinformatics analyses of circular dichroism protein reference databases. Bioinformatics (Oxford, England) 21:4230-4238.
Jick H, Zornberg GL, Jick SS, Seshadri S, Drachman DA (2000) Statins and the risk of dementia. Lancet 356:1627-1631.
Jockers R, Maurice P, Boutin JA, Delagrange P (2008) Melatonin receptors, heterodimerization, signal transduction and binding sites: what's new? Br J Pharmacol 154:1182-1195.
Johnson WC (1999) Analyzing protein circular dichroism spectra for accurate secondary structures. Proteins 35:307-312.
Jones AR, Overly CC, Sunkin SM (2009) The Allen Brain Atlas: 5 years and beyond. Nat Rev Neurosci 10:821-828.
Jones DT (1999) Protein secondary structure prediction based on position-specific scoring matrices. J Mol Biol 292:195-202.
Jonsson L, Ljunggren E, Bremer A, Pedersen C, Landen M, Thuresson K, Giacobini M, Melke J (2010) Mutation screening of melatonin-related genes in patients with autism spectrum disorders. BMC Med Genomics 3:10.
Joyce PR (1984) Age of onset in bipolar affective disorder and misdiagnosis as schizophrenia. Psychol Med 14:145-149.
Kabsch W, Sander C (1983) Dictionary of protein secondary structure: pattern recognition of hydrogen-bonded and geometrical features. Biopolymers 22:2577-2637.
Kaibuchi K, Kuroda S, Fukata M, Nakagawa M (1999) Regulation of cadherin-mediated cell-cell adhesion by the Rho family GTPases. Curr Opin Cell Biol 11:591-596.
Kameda Y, Arai Y, Nishimaki T (2003) Ultrastructural localization of vimentin immunoreactivity and gene expression in tanycytes and their alterations in hamsters kept under different photoperiods. Cell and tissue research 314:251-262.
Kaminski WE, Piehler A, Pullmann K, Porsch-Ozcurumez M, Duong C, Bared GM, Buchler C, Schmitz G (2001) Complete coding sequence, promoter region, and genomic structure of the human ABCA2 gene and evidence for sterol-

dependent regulation in macrophages. Biochem Biophys Res Commun 281:249-258.
Kandel ER (2001) The molecular biology of memory storage: a dialogue between genes and synapses. Science 294:1030-1038.
Kay BK, Williamson MP, Sudol M (2000) The importance of being proline: the interaction of proline-rich motifs in signaling proteins with their cognate domains. Faseb J 14:231-241.
Keefe RS, Fenton WS (2007) How should DSM-V criteria for schizophrenia include cognitive impairment? Schizophr Bull 33:912-920.
Keller LC, Geimer S, Romijn E, Yates J, 3rd, Zamora I, Marshall WF (2009) Molecular architecture of the centriole proteome: the conserved WD40 domain protein POC1 is required for centriole duplication and length control. Mol Biol Cell 20:1150-1166.
Kelly SM, Jess TJ, Price NC (2005) How to study proteins by circular dichroism. Biochimica et biophysica acta 1751:119-139.
Kenny AV, Cousins SL, Pinho L, Stephenson FA (2009) The integrity of the glycine co-agonist binding site of N-methyl-D-aspartate receptors is a functional quality control checkpoint for cell surface delivery. The Journal of biological chemistry 284:324-333.
Kent WJ, Sugnet CW, Furey TS, Roskin KM, Pringle TH, Zahler AM, Haussler D (2002) The human genome browser at UCSC. Genome research 12:996-1006.
Kessler RC, Chiu WT, Demler O, Merikangas KR, Walters EE (2005) Prevalence, severity, and comorbidity of 12-month DSM-IV disorders in the National Comorbidity Survey Replication. Arch Gen Psychiatry 62:617-627.
Kessler RC, Heeringa S, Lakoma MD, Petukhova M, Rupp AE, Schoenbaum M, Wang PS, Zaslavsky AM (2008) Individual and societal effects of mental disorders on earnings in the United States: results from the national comorbidity survey replication. The American journal of psychiatry 165:703-711.
Kessler RC, Berglund P, Demler O, Jin R, Koretz D, Merikangas KR, Rush AJ, Walters EE, Wang PS (2003) The epidemiology of major depressive disorder: results from the National Comorbidity Survey Replication (NCS-R). JAMA 289:3095-3105.
Kido M, Obata S, Tanihara H, Rochelle JM, Seldin MF, Taketani S, Suzuki ST (1998) Molecular properties and chromosomal location of cadherin-8. Genomics 48:186-194.
Kikuno R, Nagase T, Ishikawa K, Hirosawa M, Miyajima N, Tanaka A, Kotani H, Nomura N, Ohara O (1999) Prediction of the coding sequences of unidentified human genes. XIV. The complete sequences of 100 new cDNA clones from brain which code for large proteins in vitro. DNA Res 6:197-205.
Kilpinen H, Ylisaukko-Oja T, Hennah W, Palo OM, Varilo T, Vanhala R, Nieminen-von Wendt T, von Wendt L, Paunio T, Peltonen L (2008) Association of DISC1 with autism and Asperger syndrome. Molecular psychiatry 13:187-196.
Kim DY, Carey BW, Wang H, Ingano LA, Binshtok AM, Wertz MH, Pettingell WH, He P, Lee VM, Woolf CJ, Kovacs DM (2007) BACE1 regulates voltage-gated sodium channels and neuronal activity. Nat Cell Biol 9:755-764.

Kim JE, Li S, GrandPre T, Qiu D, Strittmatter SM (2003) Axon regeneration in young adult mice lacking Nogo-A/B. Neuron 38:187-199.

Kim JH, Ong WY (2009) Localization of the transcription factor, sterol regulatory element binding protein-2 (SREBP-2) in the normal rat brain and changes after kainate-induced excitotoxic injury. Journal of chemical neuroanatomy 37:71-77.

Kim S, Swaminathan S, Shen L, Risacher SL, Nho K, Foroud T, Shaw LM, Trojanowski JQ, Potkin SG, Huentelman MJ, Craig DW, DeChairo BM, Aisen PS, Petersen RC, Weiner MW, Saykin AJ (2011) Genome-wide association study of CSF biomarkers Abeta1-42, t-tau, and p-tau181p in the ADNI cohort. Neurology 76:69-79.

Kim SH, Kook MC, Shin YK, Park SH, Song HG (2004) Evaluation of antigen retrieval buffer systems. Journal of molecular histology 35:409-416.

Kim Y, Nam YJ, Lee C (2005) Analysis of the SREBF2 gene as a genetic risk factor for vascular dementia. Am J Med Genet B Neuropsychiatr Genet 139B:19-22.

Kinney DK, Matthysse S (1978) Genetic transmission of schizophrenia. Annu Rev Med 29:459-473.

Kinoshita A, Fukumoto H, Shah T, Whelan CM, Irizarry MC, Hyman BT (2003) Demonstration by FRET of BACE interaction with the amyloid precursor protein at the cell surface and in early endosomes. Journal of cell science 116:3339-3346.

Kirkland SC, Ying H (2008) Alpha2beta1 integrin regulates lineage commitment in multipotent human colorectal cancer cells. The Journal of biological chemistry 283:27612-27619.

Kivipelto M, Helkala EL, Laakso MP, Hanninen T, Hallikainen M, Alhainen K, Soininen H, Tuomilehto J, Nissinen A (2001) Midlife vascular risk factors and Alzheimer's disease in later life: longitudinal, population based study. BMJ 322:1447-1451.

Kokkola T, Watson MA, White J, Dowell S, Foord SM, Laitinen JT (1998) Mutagenesis of human Mel1a melatonin receptor expressed in yeast reveals domains important for receptor function. Biochem Biophys Res Commun 249:531-536.

Korematsu K, Redies C (1997) Restricted expression of cadherin-8 in segmental and functional subdivisions of the embryonic mouse brain. Dev Dyn 208:178-189.

Korematsu K, Goto S, Okamura A, Ushio Y (1998a) Heterogeneity of cadherin-8 expression in the neonatal rat striatum: comparison with striatal compartments. Experimental neurology 154:531-536.

Korematsu K, Nishi T, Okamura A, Goto S, Morioka M, Hamada J, Ushio Y (1998b) Cadherin-8 protein expression in gray matter structures and nerve fibers of the neonatal and adult mouse brain. Neuroscience 87:303-315.

Kosloff M, Elia N, Joel-Almagor T, Timberg R, Zars TD, Hyde DR, Minke B, Selinger Z (2003) Regulation of light-dependent Gqalpha translocation and morphological changes in fly photoreceptors. EMBO J 22:459-468.

Krishna KK, Hertel N, Redies C (2011) Cadherin expression in the somatosensory cortex: evidence for a combinatorial molecular code at the single-cell level. Neuroscience 175:37-48.

Kruglyak L, Daly MJ, Reeve-Daly MP, Lander ES (1996) Parametric and nonparametric linkage analysis: a unified multipoint approach. Am J Hum Genet 58:1347-1363.

Kruijshaar ME, Barendregt J, Vos T, de Graaf R, Spijker J, Andrews G (2005) Lifetime prevalence estimates of major depression: an indirect estimation method and a quantification of recall bias. Eur J Epidemiol 20:103-111.

Kuang E, Wan Q, Li X, Xu H, Liu Q, Qi Y (2005) ER Ca2+ depletion triggers apoptotic signals for endoplasmic reticulum (ER) overload response induced by overexpressed reticulon 3 (RTN3/HAP). J Cell Physiol 204:549-559.

Kuehner C (2003) Gender differences in unipolar depression: an update of epidemiological findings and possible explanations. Acta psychiatrica Scandinavica 108:163-174.

Kuentzel SL, Ali SM, Altman RA, Greenberg BD, Raub TJ (1993) The Alzheimer beta-amyloid protein precursor/protease nexin-II is cleaved by secretase in a trans-Golgi secretory compartment in human neuroglioma cells. The Biochemical journal 295 (Pt 2):367-378.

Kume H, Murayama KS, Araki W (2009) The two-hydrophobic domain tertiary structure of reticulon proteins is critical for modulation of beta-secretase BACE1. J Neurosci Res 87:2963-2972.

Kuo YM, Emmerling MR, Bisgaier CL, Essenburg AD, Lampert HC, Drumm D, Roher AE (1998) Elevated low-density lipoprotein in Alzheimer's disease correlates with brain abeta 1-42 levels. Biochem Biophys Res Commun 252:711-715.

Kuroda S, Fukata M, Nakagawa M, Kaibuchi K (1999) Cdc42, Rac1, and their effector IQGAP1 as molecular switches for cadherin-mediated cell-cell adhesion. Biochem Biophys Res Commun 262:1-6.

Laird FM, Cai H, Savonenko AV, Farah MH, He K, Melnikova T, Wen H, Chiang HC, Xu G, Koliatsos VE, Borchelt DR, Price DL, Lee HK, Wong PC (2005) BACE1, a major determinant of selective vulnerability of the brain to amyloid-beta amyloidogenesis, is essential for cognitive, emotional, and synaptic functions. J Neurosci 25:11693-11709.

Lanctot PM, Leclerc PC, Clement M, Auger-Messier M, Escher E, Leduc R, Guillemette G (2005) Importance of N-glycosylation positioning for cell-surface expression, targeting, affinity and quality control of the human AT1 receptor. The Biochemical journal 390:367-376.

Laviola G, Macri S, Morley-Fletcher S, Adriani W (2003) Risk-taking behavior in adolescent mice: psychobiological determinants and early epigenetic influence. Neurosci Biobehav Rev 27:19-31.

Le Hellard S, Theisen FM, Haberhausen M, Raeder MB, Ferno J, Gebhardt S, Hinney A, Remschmidt H, Krieg JC, Mehler-Wex C, Nothen MM, Hebebrand J, Steen VM (2009) Association between the insulin-induced gene 2 (INSIG2) and weight gain in a German sample of antipsychotic-treated schizophrenic patients: perturbation of SREBP-controlled lipogenesis in drug-related metabolic adverse effects? Molecular psychiatry 14:308-317.

Le Hellard S et al. (2008) Polymorphisms in SREBF1 and SREBF2, two antipsychotic-activated transcription factors controlling cellular lipogenesis, are associated with schizophrenia in German and Scandinavian samples. Molecular psychiatry.

Lechan RM, Fekete C (2007) Infundibular tanycytes as modulators of neuroendocrine function: hypothetical role in the regulation of the thyroid and gonadal axis. Acta Biomed 78 Suppl 1:84-98.

LeDoux JE (1993) Emotional memory systems in the brain. Behav Brain Res 58:69-79.

Lee CW, Rivera R, Gardell S, Dubin AE, Chun J (2006) GPR92 as a new G12/13- and Gq-coupled lysophosphatidic acid receptor that increases cAMP, LPA5. The Journal of biological chemistry 281:23589-23597.

Lee H, Raiker SJ, Venkatesh K, Geary R, Robak LA, Zhang Y, Yeh HH, Shrager P, Giger RJ (2008) Synaptic function for the Nogo-66 receptor NgR1: regulation of dendritic spine morphology and activity-dependent synaptic strength. J Neurosci 28:2753-2765.

Lee JK, Geoffroy CG, Chan AF, Tolentino KE, Crawford MJ, Leal MA, Kang B, Zheng B (2010) Assessing spinal axon regeneration and sprouting in Nogo-, MAG-, and OMgp-deficient mice. Neuron 66:663-670.

Lee JT, Lee TJ, Kim CH, Kim NS, Kwon TK (2009) Over-expression of Reticulon 3 (RTN3) enhances TRAIL-mediated apoptosis via up-regulation of death receptor 5 (DR5) and down-regulation of c-FLIP. Cancer Lett 279:185-192.

Lee TM, Chan CC (1998) Vulnerability by sex to seasonal affective disorder. Percept Mot Skills 87:1120-1122.

Lees JG, Miles AJ, Wien F, Wallace BA (2006a) A reference database for circular dichroism spectroscopy covering fold and secondary structure space. Bioinformatics (Oxford, England) 22:1955-1962.

Lees JG, Miles AJ, Janes RW, Wallace BA (2006b) Novel methods for secondary structure determination using low wavelength (VUV) circular dichroism spectroscopic data. BMC bioinformatics 7:507.

Lein ES et al. (2007) Genome-wide atlas of gene expression in the adult mouse brain. Nature 445:168-176.

Leung A, Chue P (2000) Sex differences in schizophrenia, a review of the literature. Acta Psychiatr Scand Suppl 401:3-38.

Leung KM, van Horck FP, Lin AC, Allison R, Standart N, Holt CE (2006) Asymmetrical beta-actin mRNA translation in growth cones mediates attractive turning to netrin-1. Nature neuroscience 9:1247-1256.

Levoye A, Dam J, Ayoub MA, Guillaume JL, Couturier C, Delagrange P, Jockers R (2006) The orphan GPR50 receptor specifically inhibits MT1 melatonin receptor function through heterodimerization. EMBO J 25:3012-3023.

Leyssen M, Ayaz D, Hebert SS, Reeve S, De Strooper B, Hassan BA (2005) Amyloid precursor protein promotes post-developmental neurite arborization in the Drosophila brain. EMBO J 24:2944-2955.

Li M, Song J (2007) The N- and C-termini of the human Nogo molecules are intrinsically unstructured: bioinformatics, CD, NMR characterization, and functional implications. Proteins 68:100-108.

Li Q, Lau A, Morris TJ, Guo L, Fordyce CB, Stanley EF (2004) A syntaxin 1, Galpha(o), and N-type calcium channel complex at a presynaptic nerve terminal: analysis by quantitative immunocolocalization. J Neurosci 24:4070-4081.

Lichtenberg D, Goni FM, Heerklotz H (2005) Detergent-resistant membranes should not be identified with membrane rafts. Trends in biochemical sciences 30:430-436.

Lichtenthaler SF, Dominguez DI, Westmeyer GG, Reiss K, Haass C, Saftig P, De Strooper B, Seed B (2003) The cell adhesion protein P-selectin glycoprotein ligand-1 is a substrate for the aspartyl protease BACE1. The Journal of biological chemistry 278:48713-48719.

Linding R, Jensen LJ, Diella F, Bork P, Gibson TJ, Russell RB (2003) Protein disorder prediction: implications for structural proteomics. Structure 11:1453-1459.

Liu BP, Fournier A, GrandPre T, Strittmatter SM (2002) Myelin-associated glycoprotein as a functional ligand for the Nogo-66 receptor. Science (New York, NY 297:1190-1193.

Lohmueller KE, Pearce CL, Pike M, Lander ES, Hirschhorn JN (2003) Meta-analysis of genetic association studies supports a contribution of common variants to susceptibility to common disease. Nature genetics 33:177-182.

Loranger AW (1984) Sex difference in age at onset of schizophrenia. Arch Gen Psychiatry 41:157-161.

Loughlin SE, Foote SL, Bloom FE (1986) Efferent projections of nucleus locus coeruleus: topographic organization of cells of origin demonstrated by three-dimensional reconstruction. Neuroscience 18:291-306.

Luchetti F, Canonico B, Betti M, Arcangeletti M, Pilolli F, Piroddi M, Canesi L, Papa S, Galli F (2010) Melatonin signaling and cell protection function. FASEB J 24:3603-3624.

Luciani MF, Denizot F, Savary S, Mattei MG, Chimini G (1994) Cloning of two novel ABC transporters mapping on human chromosome 9. Genomics 21:150-159.

Lundstrom K (2006) Latest development in drug discovery on G protein-coupled receptors. Curr Protein Pept Sci 7:465-470.

Lupas A, Van Dyke M, Stock J (1991) Predicting coiled coils from protein sequences. Science (New York, NY 252:1162-1164.

Luque JM, de Blas MR, Segovia S, Guillamon A (1992) Sexual dimorphism of the dopamine-beta-hydroxylase-immunoreactive neurons in the rat locus ceruleus. Brain Res Dev Brain Res 67:211-215.

Ma K, Kan L, Wang K (2001) Polyproline II helix is a key structural motif of the elastic PEVK segment of titin. Biochemistry 40:3427-3438.

Ma'ayan A, Jenkins SL, Barash A, Iyengar R (2009) Neuro2A differentiation by Galphai/o pathway. Sci Signal 2:cm1.

MacIntyre DJ, Blackwood DH, Porteous DJ, Pickard BS, Muir WJ (2003) Chromosomal abnormalities and mental illness. Molecular psychiatry 8:275-287.

Macintyre DJ, McGhee KA, Maclean AW, Afzal M, Briffa K, Henry B, Thomson PA, Muir WJ, Blackwood DH (2010) Association of GPR50, an X-linked orphan G protein-coupled receptor, and affective disorder in an independent sample of the Scottish population. Neuroscience letters 475:169-173.

Mack JT, Helke KL, Normand G, Green C, Townsend DM, Tew KD (2011) ABCA2 transporter deficiency reduces incidence of TRAMP prostate tumor metastasis and cellular chemotactic migration. Cancer Lett 300:154-161.

Mack JT, Beljanski V, Soulika AM, Townsend DM, Brown CB, Davis W, Tew KD (2007) "Skittish" Abca2 knockout mice display tremor, hyperactivity, and abnormal myelin ultrastructure in the central nervous system. Molecular and cellular biology 27:44-53.

Mackin P, Young AH (2004) Rapid cycling bipolar disorder: historical overview and focus on emerging treatments. Bipolar disorders 6:523-529.

Magdaleno S, Jensen P, Brumwell CL, Seal A, Lehman K, Asbury A, Cheung T, Cornelius T, Batten DM, Eden C, Norland SM, Rice DS, Dosooye N, Shakya S, Mehta P, Curran T (2006) BGEM: an in situ hybridization database of gene expression in the embryonic and adult mouse nervous system. PLoS Biol 4:e86.

Maher B (2008) Personal genomes: The case of the missing heritability. Nature 456:18-21.

Manavalan P, Johnson WC, Jr. (1987) Variable selection method improves the prediction of protein secondary structure from circular dichroism spectra. Analytical biochemistry 167:76-85.

Manders EEM, Verbeek, F.J., & Aten, J. A. (1993) Measurement of co-localization of objects in dual-colour confocal images

. Journal of Microscopy 169:375-382.

Manji HK, Lenox RH (2000) Signaling: cellular insights into the pathophysiology of bipolar disorder. Biological psychiatry 48:518-530.

Manolio TA (2010) Genomewide association studies and assessment of the risk of disease. N Engl J Med 363:166-176.

Mao Y, Ge X, Frank CL, Madison JM, Koehler AN, Doud MK, Tassa C, Berry EM, Soda T, Singh KK, Biechele T, Petryshen TL, Moon RT, Haggarty SJ, Tsai LH (2009) Disrupted in schizophrenia 1 regulates neuronal progenitor proliferation via modulation of GSK3beta/beta-catenin signaling. Cell 136:1017-1031.

Marchand ER, Riley JN, Moore RY (1980) Interpeduncular nucleus afferents in the rat. Brain Res 193:339-352.

Marinissen MJ, Gutkind JS (2001) G-protein-coupled receptors and signaling networks: emerging paradigms. Trends in pharmacological sciences 22:368-376.

Markakis EA, Palmer TD, Randolph-Moore L, Rakic P, Gage FH (2004) Novel neuronal phenotypes from neural progenitor cells. J Neurosci 24:2886-2897.

Masliah E, Alford M, Adame A, Rockenstein E, Galasko D, Salmon D, Hansen LA, Thal LJ (2003) Abeta1-42 promotes cholinergic sprouting in patients with AD and Lewy body variant of AD. Neurology 61:206-211.

Masliah E, Xie F, Dayan S, Rockenstein E, Mante M, Adame A, Patrick CM, Chan AF, Zheng B (2010) Genetic deletion of Nogo/Rtn4 ameliorates behavioral and neuropathological outcomes in amyloid precursor protein transgenic mice. Neuroscience 169:488-494.

Massat I et al. (2002) Positive association of dopamine D2 receptor polymorphism with bipolar affective disorder in a European Multicenter Association Study of affective disorders. Am J Med Genet 114:177-185.

Matsuki T, Hori G, Furuichi T (2005) Gene expression profiling during the embryonic development of mouse brain using an oligonucleotide-based microarray system. Brain research 136:231-254.

Mattila PK, Lappalainen P (2008) Filopodia: molecular architecture and cellular functions. Nature reviews 9:446-454.

Mazna P, Obsilova V, Jelinkova I, Balik A, Berka K, Sovova Z, Ettrich R, Svoboda P, Obsil T, Teisinger J (2004) Molecular modeling of human MT2 melatonin receptor: the role of Val204, Leu272 and Tyr298 in ligand binding. Journal of neurochemistry 91:836-842.

McAllister-Williams RH, Ferrier IN, Young AH (1998) Mood and neuropsychological function in depression: the role of corticosteroids and serotonin. Psychol Med 28:573-584.

McGee AW, Yang Y, Fischer QS, Daw NW, Strittmatter SM (2005) Experience-driven plasticity of visual cortex limited by myelin and Nogo receptor. Science 309:2222-2226.

McGuffin LJ, Bryson K, Jones DT (2000) The PSIPRED protein structure prediction server. Bioinformatics (Oxford, England) 16:404-405.

McGuffin P, Rijsdijk F, Andrew M, Sham P, Katz R, Cardno A (2003) The heritability of bipolar affective disorder and the genetic relationship to unipolar depression. Arch Gen Psychiatry 60:497-502.

Medina L, Legaz I, Gonzalez G, De Castro F, Rubenstein JL, Puelles L (2004) Expression of Dbx1, Neurogenin 2, Semaphorin 5A, Cadherin 8, and Emx1 distinguish ventral and lateral pallial histogenetic divisions in the developing mouse claustroamygdaloid complex. The Journal of comparative neurology 474:504-523.

Meier S, Brauer AU, Heimrich B, Schwab ME, Nitsch R, Savaskan NE (2003) Molecular analysis of Nogo expression in the hippocampus during development and following lesion and seizure. Faseb J 17:1153-1155.

Meinhart A, Kamenski T, Hoeppner S, Baumli S, Cramer P (2005) A structural perspective of CTD function. Genes & development 19:1401-1415.

Miao RQ, Gao Y, Harrison KD, Prendergast J, Acevedo LM, Yu J, Hu F, Strittmatter SM, Sessa WC (2006) Identification of a receptor necessary for Nogo-B stimulated chemotaxis and morphogenesis of endothelial cells. Proceedings of the National Academy of Sciences of the United States of America 103:10997-11002.

Michailov GV, Sereda MW, Brinkmann BG, Fischer TM, Haug B, Birchmeier C, Role L, Lai C, Schwab MH, Nave KA (2004) Axonal neuregulin-1 regulates myelin sheath thickness. Science (New York, NY 304:700-703.

Miles AJ, Wallace BA (2006) Synchrotron radiation circular dichroism spectroscopy of proteins and applications in structural and functional genomics. Chem Soc Rev 35:39-51.

Millar JK, Wilson-Annan JC, Anderson S, Christie S, Taylor MS, Semple CA, Devon RS, Clair DM, Muir WJ, Blackwood DH, Porteous DJ (2000) Disruption of two novel genes by a translocation co-segregating with schizophrenia. Hum Mol Genet 9:1415-1423.

Millar JK, Pickard BS, Mackie S, James R, Christie S, Buchanan SR, Malloy MP, Chubb JE, Huston E, Baillie GS, Thomson PA, Hill EV, Brandon NJ, Rain JC, Camargo LM, Whiting PJ, Houslay MD, Blackwood DH, Muir WJ, Porteous DJ (2005) DISC1 and PDE4B are interacting genetic factors in schizophrenia that regulate cAMP signaling. Science (New York, NY 310:1187-1191.

Milligan G (2004) G protein-coupled receptor dimerization: function and ligand pharmacology. Mol Pharmacol 66:1-7.

Mingorance A, Fontana X, Sole M, Burgaya F, Urena JM, Teng FY, Tang BL, Hunt D, Anderson PN, Bethea JR, Schwab ME, Soriano E, del Rio JA (2004) Regulation of Nogo and Nogo receptor during the development of the entorhino-hippocampal pathway and after adult hippocampal lesions. Molecular and cellular neurosciences 26:34-49.

Mingorance-Le Meur A, Zheng B, Soriano E, del Rio JA (2007) Involvement of the myelin-associated inhibitor Nogo-A in early cortical development and neuronal maturation. Cereb Cortex 17:2375-2386.

Miyazaki H, Oyama F, Wong HK, Kaneko K, Sakurai T, Tamaoka A, Nukina N (2007) BACE1 modulates filopodia-like protrusions induced by sodium channel beta4 subunit. Biochem Biophys Res Commun 361:43-48.

Molinari EJ, North PC, Dubocovich ML (1996) 2-[125I]iodo-5-methoxycarbonylamino-N-acetyltryptamine: a selective radioligand for the characterization of melatonin ML2 binding sites. Eur J Pharmacol 301:159-168.

Montani L, Gerrits B, Gehrig P, Kempf A, Dimou L, Wollscheid B, Schwab ME (2009) Neuronal Nogo-A Modulates Growth Cone Motility via Rho-GTP/LIMK1/Cofilin in the Unlesioned Adult Nervous System. The Journal of biological chemistry 284:10793-10807.

Morgan AR, Hamilton G, Turic D, Jehu L, Harold D, Abraham R, Hollingworth P, Moskvina V, Brayne C, Rubinsztein DC, Lynch A, Lawlor B, Gill M, O'Donovan M, Powell J, Lovestone S, Williams J, Owen MJ (2008) Association analysis of 528 intra-genic SNPs in a region of chromosome 10 linked to late onset Alzheimer's disease. Am J Med Genet B Neuropsychiatr Genet 147B:727-731.

Morgan L, Arendt J, Owens D, Folkard S, Hampton S, Deacon S, English J, Ribeiro D, Taylor K (1998) Effects of the endogenous clock and sleep time on melatonin, insulin, glucose and lipid metabolism. The Journal of endocrinology 157:443-451.

Morris R (1991) Immunoperoxidase Staining of Gene Products in Cultured Cells Using Monoclonal Antibodies. In, pp 339-359.

Murayama KS, Kametani F, Saito S, Kume H, Akiyama H, Araki W (2006) Reticulons RTN3 and RTN4-B/C interact with BACE1 and inhibit its ability to produce amyloid beta-protein. The European journal of neuroscience 24:1237-1244.

Muresan V, Varvel NH, Lamb BT, Muresan Z (2009) The cleavage products of amyloid-beta precursor protein are sorted to distinct carrier vesicles that are independently transported within neurites. J Neurosci 29:3565-3578.

Muresan Z, Muresan V (2006) Neuritic deposits of amyloid-beta peptide in a subpopulation of central nervous system-derived neuronal cells. Molecular and cellular biology 26:4982-4997.

Nakamura Y, Wood CL, Patton AP, Jaafari N, Henley JM, Mellor JR, Hanley JG (2011) PICK1 inhibition of the Arp2/3 complex controls dendritic spine size and synaptic plasticity. EMBO J 30:719-730.

Nemeroff CB, Evans DL, Gyulai L, Sachs GS, Bowden CL, Gergel IP, Oakes R, Pitts CD (2001) Double-blind, placebo-controlled comparison of imipramine

and paroxetine in the treatment of bipolar depression. The American journal of psychiatry 158:906-912.
Neudert F, Nuernberger KK, Redies C (2008) Comparative analysis of cadherin expression and connectivity patterns in the cerebellar system of ferret and mouse. The Journal of comparative neurology 511:736-752.
Neves-Pereira M, Mundo E, Muglia P, King N, Macciardi F, Kennedy JL (2002) The brain-derived neurotrophic factor gene confers susceptibility to bipolar disorder: evidence from a family-based association study. Am J Hum Genet 71:651-655.
Niederost B, Oertle T, Fritsche J, McKinney RA, Bandtlow CE (2002) Nogo-A and myelin-associated glycoprotein mediate neurite growth inhibition by antagonistic regulation of RhoA and Rac1. J Neurosci 22:10368-10376.
Niethammer M, Smith DS, Ayala R, Peng J, Ko J, Lee MS, Morabito M, Tsai LH (2000) NUDEL is a novel Cdk5 substrate that associates with LIS1 and cytoplasmic dynein. Neuron 28:697-711.
Nishimoto I, Okamoto T, Matsuura Y, Takahashi S, Murayama Y, Ogata E (1993) Alzheimer amyloid protein precursor complexes with brain GTP-binding protein G(o). Nature 362:75-79.
Nobes CD, Hall A (1995) Rho, rac, and cdc42 GTPases regulate the assembly of multimolecular focal complexes associated with actin stress fibers, lamellipodia, and filopodia. Cell 81:53-62.
Novak G, Tallerico T (2006) Nogo A, B and C expression in schizophrenia, depression and bipolar frontal cortex, and correlation of Nogo expression with CAA/TATC polymorphism in 3'-UTR. Brain Res 1120:161-171.
Novak G, Kim D, Seeman P, Tallerico T (2002) Schizophrenia and Nogo: elevated mRNA in cortex, and high prevalence of a homozygous CAA insert. Brain research 107:183-189.
Nutt DJ (2006) The role of dopamine and norepinephrine in depression and antidepressant treatment. J Clin Psychiatry 67 Suppl 6:3-8.
O'Dowd BF, Ji X, Alijaniaram M, Rajaram RD, Kong MM, Rashid A, Nguyen T, George SR (2005) Dopamine receptor oligomerization visualized in living cells. The Journal of biological chemistry 280:37225-37235.
Obradovic Z, Peng K, Vucetic S, Radivojac P, Dunker AK (2005) Exploiting heterogeneous sequence properties improves prediction of protein disorder. Proteins 61 Suppl 7:176-182.
Oertle T, Schwab ME (2003) Nogo and its paRTNers. Trends Cell Biol 13:187-194.
Oertle T, Huber C, van der Putten H, Schwab ME (2003a) Genomic structure and functional characterisation of the promoters of human and mouse nogo/rtn4. J Mol Biol 325:299-323.
Oertle T, van der Haar ME, Bandtlow CE, Robeva A, Burfeind P, Buss A, Huber AB, Simonen M, Schnell L, Brosamle C, Kaupmann K, Vallon R, Schwab ME (2003b) Nogo-A inhibits neurite outgrowth and cell spreading with three discrete regions. J Neurosci 23:5393-5406.
Okabe T, Nakamura T, Nishimura YN, Kohu K, Ohwada S, Morishita Y, Akiyama T (2003) RICS, a novel GTPase-activating protein for Cdc42 and Rac1, is involved in the beta-catenin-N-cadherin and N-methyl-D-aspartate receptor signaling. The Journal of biological chemistry 278:9920-9927.

Okada H, Zhang W, Peterhoff C, Hwang JC, Nixon RA, Ryu SH, Kim TW (2010) Proteomic identification of sorting nexin 6 as a negative regulator of BACE1-mediated APP processing. FASEB J 24:2783-2794.

Pagnamenta AT, Khan H, Walker S, Gerrelli D, Wing K, Bonaglia MC, Giorda R, Berney T, Mani E, Molteni M, Pinto D, Le Couteur A, Hallmayer J, Sutcliffe JS, Szatmari P, Paterson AD, Scherer SW, Vieland VJ, Monaco AP (2011) Rare familial 16q21 microdeletions under a linkage peak implicate cadherin 8 (CDH8) in susceptibility to autism and learning disability. Journal of medical genetics 48:48-54.

Palczewski K, Kumasaka T, Hori T, Behnke CA, Motoshima H, Fox BA, Le Trong I, Teller DC, Okada T, Stenkamp RE, Yamamoto M, Miyano M (2000) Crystal structure of rhodopsin: A G protein-coupled receptor. Science (New York, NY 289:739-745.

Palkovits M (1999) Interconnections between the neuroendocrine hypothalamus and the central autonomic system. Geoffrey Harris Memorial Lecture, Kitakyushu, Japan, October 1998. Frontiers in neuroendocrinology 20:270-295.

Parisiadou L, Fassa A, Fotinopoulou A, Bethani I, Efthimiopoulos S (2004) Presenilin 1 and cadherins: stabilization of cell-cell adhesion and proteolysis-dependent regulation of transcription. Neurodegener Dis 1:184-191.

Park YU, Jeong J, Lee H, Mun JY, Kim JH, Lee JS, Nguyen MD, Han SS, Suh PG, Park SK (2010) Disrupted-in-schizophrenia 1 (DISC1) plays essential roles in mitochondria in collaboration with Mitofilin. Proceedings of the National Academy of Sciences of the United States of America 107:17785-17790.

Peng K, Radivojac P, Vucetic S, Dunker AK, Obradovic Z (2006) Length-dependent prediction of protein intrinsic disorder. BMC bioinformatics 7:208.

Perala J, Suvisaari J, Saarni SI, Kuoppasalmi K, Isometsa E, Pirkola S, Partonen T, Tuulio-Henriksson A, Hintikka J, Kieseppa T, Harkanen T, Koskinen S, Lonnqvist J (2007) Lifetime prevalence of psychotic and bipolar I disorders in a general population. Arch Gen Psychiatry 64:19-28.

Peranen J, Rikkonen M, Kaariainen L (1993) A method for exposing hidden antigenic sites in paraformaldehyde-fixed cultured cells, applied to initially unreactive antibodies. J Histochem Cytochem 41:447-454.

Perez RG, Zheng H, Van der Ploeg LH, Koo EH (1997) The beta-amyloid precursor protein of Alzheimer's disease enhances neuron viability and modulates neuronal polarity. J Neurosci 17:9407-9414.

Peruzzo B, Pastor FE, Blazquez JL, Schobitz K, Pelaez B, Amat P, Rodriguez EM (2000) A second look at the barriers of the medial basal hypothalamus. Exp Brain Res 132:10-26.

Phatnani HP, Greenleaf AL (2006) Phosphorylation and functions of the RNA polymerase II CTD. Genes & development 20:2922-2936.

Pike LJ (2006) Rafts defined: a report on the Keystone Symposium on Lipid Rafts and Cell Function. J Lipid Res 47:1597-1598.

Pinos H, Collado P, Rodriguez-Zafra M, Rodriguez C, Segovia S, Guillamon A (2001) The development of sex differences in the locus coeruleus of the rat. Brain research bulletin 56:73-78.

Prilusky J, Felder CE, Zeev-Ben-Mordehai T, Rydberg EH, Man O, Beckmann JS, Silman I, Sussman JL (2005) FoldIndex: a simple tool to predict whether a

given protein sequence is intrinsically unfolded. Bioinformatics (Oxford, England) 21:3435-3438.
Prior M, Shi Q, Hu X, He W, Levey A, Yan R (2010) RTN/Nogo in forming Alzheimer's neuritic plaques. Neurosci Biobehav Rev 34:1201-1206.
Puglielli L, Tanzi RE, Kovacs DM (2003) Alzheimer's disease: the cholesterol connection. Nature neuroscience 6:345-351.
Qi Y, Wang JK, McMillian M, Chikaraishi DM (1997) Characterization of a CNS cell line, CAD, in which morphological differentiation is initiated by serum deprivation. J Neurosci 17:1217-1225.
Qu X, Qi Y, Lan P, Li Q (2002) The novel endoplasmic reticulum (ER)-targeted protein HAP induces cell apoptosis by the depletion of the ER Ca(2+) stores. FEBS Lett 529:325-331.
Raiker SJ, Lee H, Baldwin KT, Duan Y, Shrager P, Giger RJ (2010) Oligodendrocyte-myelin glycoprotein and Nogo negatively regulate activity-dependent synaptic plasticity. J Neurosci 30:12432-12445.
Rajendran L, Honsho M, Zahn TR, Keller P, Geiger KD, Verkade P, Simons K (2006) Alzheimer's disease beta-amyloid peptides are released in association with exosomes. Proceedings of the National Academy of Sciences of the United States of America 103:11172-11177.
Ranscht B (2000) Cadherins: molecular codes for axon guidance and synapse formation. Int J Dev Neurosci 18:643-651.
Reich DE, Lander ES (2001) On the allelic spectrum of human disease. Trends Genet 17:502-510.
Reinhard C, Hebert SS, De Strooper B (2005) The amyloid-beta precursor protein: integrating structure with biological function. EMBO J 24:3996-4006.
Reiter E, Lefkowitz RJ (2006) GRKs and beta-arrestins: roles in receptor silencing, trafficking and signaling. Trends Endocrinol Metab 17:159-165.
Ren H, Yu D, Ge B, Cook B, Xu Z, Zhang S (2009) High-level production, solubilization and purification of synthetic human GPCR chemokine receptors CCR5, CCR3, CXCR4 and CX3CR1. PLoS One 4:e4509.
Reppert SM, Weaver DR, Ebisawa T (1994) Cloning and characterization of a mammalian melatonin receptor that mediates reproductive and circadian responses. Neuron 13:1177-1185.
Reppert SM, Weaver DR, Cassone VM, Godson C, Kolakowski LF, Jr. (1995a) Melatonin receptors are for the birds: molecular analysis of two receptor subtypes differentially expressed in chick brain. Neuron 15:1003-1015.
Reppert SM, Weaver DR, Ebisawa T, Mahle CD, Kolakowski LF, Jr. (1996) Cloning of a melatonin-related receptor from human pituitary. FEBS Lett 386:219-224.
Reppert SM, Godson C, Mahle CD, Weaver DR, Slaugenhaupt SA, Gusella JF (1995b) Molecular characterization of a second melatonin receptor expressed in human retina and brain: the Mel1b melatonin receptor. Proceedings of the National Academy of Sciences of the United States of America 92:8734-8738.
Reppert SM, Perlow MJ, Ungerleider LG, Mishkin M, Tamarkin L, Orloff DG, Hoffman HJ, Klein DC (1981) Effects of damage to the suprachiasmatic area of the anterior hypothalamus on the daily melatonin and cortisol rhythms in the rhesus monkey. J Neurosci 1:1414-1425.

Reyes BA, Drolet G, Van Bockstaele EJ (2008) Dynorphin and stress-related peptides in rat locus coeruleus: contribution of amygdalar efferents. The Journal of comparative neurology 508:663-675.

Reyes BA, Valentino RJ, Xu G, Van Bockstaele EJ (2005) Hypothalamic projections to locus coeruleus neurons in rat brain. The European journal of neuroscience 22:93-106.

Reyes BA, Glaser JD, Magtoto R, Van Bockstaele EJ (2006) Pro-opiomelanocortin colocalizes with corticotropin- releasing factor in axon terminals of the noradrenergic nucleus locus coeruleus. The European journal of neuroscience 23:2067-2077.

Rhoades KL, Singh N, Simon I, Glidden B, Cedar H, Chess A (2000) Allele-specific expression patterns of interleukin-2 and Pax-5 revealed by a sensitive single-cell RT-PCR analysis. Curr Biol 10:789-792.

Richard D, Huang Q, Timofeeva E (2000) The corticotropin-releasing hormone system in the regulation of energy balance in obesity. Int J Obes Relat Metab Disord 24 Suppl 2:S36-39.

Richard M, Giannetti N, Saucier D, Sacquet J, Jourdan F, Pellier-Monnin V (2005) Neuronal expression of Nogo-A mRNA and protein during neurite outgrowth in the developing rat olfactory system. The European journal of neuroscience 22:2145-2158.

Riddell DR, Christie G, Hussain I, Dingwall C (2001) Compartmentalization of beta-secretase (Asp2) into low-buoyant density, noncaveolar lipid rafts. Curr Biol 11:1288-1293.

Ritter SL, Hall RA (2009) Fine-tuning of GPCR activity by receptor-interacting proteins. Nat Rev Mol Cell Biol 10:819-830.

Rocca DL, Martin S, Jenkins EL, Hanley JG (2008) Inhibition of Arp2/3-mediated actin polymerization by PICK1 regulates neuronal morphology and AMPA receptor endocytosis. Nat Cell Biol 10:259-271.

Romero P, Obradovic Z, Li X, Garner EC, Brown CJ, Dunker AK (2001) Sequence complexity of disordered protein. Proteins 42:38-48.

Rozen S, Skaletsky HJ (2000) Primer3 on the WWW for general users and for biologist programmers. In: Bioinformatics Methods and Protocols: Methods in Molecular Biology. (Krawetz S, Misener S, eds), pp 365-386. Totowa, NJ: Humana Press.

Rump TJ, Muneer PM, Szlachetka AM, Lamb A, Haorei C, Alikunju S, Xiong H, Keblesh J, Liu J, Zimmerman MC, Jones J, Donohue TM, Jr., Persidsky Y, Haorah J (2010) Acetyl-L-carnitine protects neuronal function from alcohol-induced oxidative damage in the brain. Free Radic Biol Med 49:1494-1504.

Saarimaki-Vire J, Alitalo A, Partanen J (2011) Analysis of Cdh22 expression and function in the developing mouse brain. Dev Dyn 240:1989-2001.

Sachs GS (1996) Treatment-resistant bipolar depression. Psychiatr Clin North Am 19:215-236.

Sachs GS, Nierenberg AA, Calabrese JR, Marangell LB, Wisniewski SR, Gyulai L, Friedman ES, Bowden CL, Fossey MD, Ostacher MJ, Ketter TA, Patel J, Hauser P, Rapport D, Martinez JM, Allen MH, Miklowitz DJ, Otto MW, Dennehy EB, Thase ME (2007) Effectiveness of adjunctive antidepressant treatment for bipolar depression. N Engl J Med 356:1711-1722.

Saha S, Chant D, Welham J, McGrath J (2005) A systematic review of the prevalence of schizophrenia. PLoS Med 2:e141.

Saito T, Yamada K, Wang Y, Tanaka Y, Ohtomo K, Ishikawa K, Inagaki N (2007) Expression of ABCA2 protein in both non-myelin-forming and myelin-forming Schwann cells in the rodent peripheral nerve. Neurosci Lett 414:35-40.

Sakai H, Tanaka Y, Tanaka M, Ban N, Yamada K, Matsumura Y, Watanabe D, Sasaki M, Kita T, Inagaki N (2007) ABCA2 deficiency results in abnormal sphingolipid metabolism in mouse brain. The Journal of biological chemistry 282:19692-19699.

Sakata T (1995) Histamine receptor and its regulation of energy metabolism. Obes Res 3 Suppl 4:541S-548S.

Sakata T, Yoshimatsu H, Kurokawa M (1997) Hypothalamic neuronal histamine: implications of its homeostatic control of energy metabolism. Nutrition 13:403-411.

Sakurai T et al. (1998) Orexins and orexin receptors: a family of hypothalamic neuropeptides and G protein-coupled receptors that regulate feeding behavior. Cell 92:1 page following 696.

Satoh J, Onoue H, Arima K, Yamamura T (2005) Nogo-A and nogo receptor expression in demyelinating lesions of multiple sclerosis. Journal of neuropathology and experimental neurology 64:129-138.

Savaskan E, Ayoub MA, Ravid R, Angeloni D, Fraschini F, Meier F, Eckert A, Muller-Spahn F, Jockers R (2005) Reduced hippocampal MT2 melatonin receptor expression in Alzheimer's disease. Journal of pineal research 38:10-16.

Savaskan E, Jockers R, Ayoub M, Angeloni D, Fraschini F, Flammer J, Eckert A, Muller-Spahn F, Meyer P (2007) The MT2 melatonin receptor subtype is present in human retina and decreases in Alzheimer's disease. Current Alzheimer research 4:47-51.

Savonenko AV, Melnikova T, Laird FM, Stewart KA, Price DL, Wong PC (2008) Alteration of BACE1-dependent NRG1/ErbB4 signaling and schizophrenia-like phenotypes in BACE1-null mice. Proceedings of the National Academy of Sciences of the United States of America 105:5585-5590.

Schnitzer J, Franke WW, Schachner M (1981) Immunocytochemical demonstration of vimentin in astrocytes and ependymal cells of developing and adult mouse nervous system. The Journal of cell biology 90:435-447.

Schwab ME (2004) Nogo and axon regeneration. Current opinion in neurobiology 14:118-124.

Schwab ME (2010) Functions of Nogo proteins and their receptors in the nervous system. Nat Rev Neurosci 11:799-811.

Schwartz MW, Woods SC, Porte D, Jr., Seeley RJ, Baskin DG (2000) Central nervous system control of food intake. Nature 404:661-671.

Scott LJ et al. (2007) A genome-wide association study of type 2 diabetes in Finns detects multiple susceptibility variants. Science (New York, NY 316:1341-1345.

Sebat J et al. (2004) Large-scale copy number polymorphism in the human genome. Science (New York, NY 305:525-528.

Sebat J et al. (2007) Strong association of de novo copy number mutations with autism. Science (New York, NY 316:445-449.

Selkoe DJ (2002) Deciphering the genesis and fate of amyloid beta-protein yields novel therapies for Alzheimer disease. The Journal of clinical investigation 110:1375-1381.

Shapiro L, Colman DR (1999) The diversity of cadherins and implications for a synaptic adhesive code in the CNS. Neuron 23:427-430.

Sharma V, Mazmanian D (2003) Sleep loss and postpartum psychosis. Bipolar disorders 5:98-105.

Sherman DL, Brophy PJ (2005) Mechanisms of axon ensheathment and myelin growth. Nat Rev Neurosci 6:683-690.

Shi Q, Prior M, He W, Tang X, Hu X, Yan R (2009) Reduced amyloid deposition in mice overexpressing RTN3 is adversely affected by preformed dystrophic neurites. J Neurosci 29:9163-9173.

Shimada T, Toriyama M, Uemura K, Kamiguchi H, Sugiura T, Watanabe N, Inagaki N (2008) Shootin1 interacts with actin retrograde flow and L1-CAM to promote axon outgrowth. The Journal of cell biology 181:817-829.

Shin JW, Shim ES, Hwang GH, Jung HS, Park JH, Sohn NW (2006) Cell size-dependent Nogo-A expression in layer V pyramidal neurons of the rat primary somatosensory cortex. Neuroscience letters 394:117-120.

Sidibe A, Mullier A, Chen P, Baroncini M, Boutin JA, Delagrange P, Prevot V, Jockers R (2010) Expression of the orphan GPR50 protein in rodent and human dorsomedial hypothalamus, tanycytes and median eminence. Journal of pineal research 48:263-269.

Siehler S (2009) Regulation of RhoGEF proteins by G12/13-coupled receptors. Br J Pharmacol 158:41-49.

Sim LJ, Joseph SA (1991) Arcuate nucleus projections to brainstem regions which modulate nociception. Journal of chemical neuroanatomy 4:97-109.

Simonen M, Pedersen V, Weinmann O, Schnell L, Buss A, Ledermann B, Christ F, Sansig G, van der Putten H, Schwab ME (2003) Systemic deletion of the myelin-associated outgrowth inhibitor Nogo-A improves regenerative and plastic responses after spinal cord injury. Neuron 38:201-211.

Simons K, Toomre D (2000) Lipid rafts and signal transduction. Nature reviews 1:31-39.

Singh A, Boyer JL, Der CJ, Zohn IE (2010) Transformation by a nucleotide-activated P2Y receptor is mediated by activation of Galphai, Galphaq and Rho-dependent signaling pathways. J Mol Signal 5:11.

Skaper SD, Moore SE, Walsh FS (2001) Cell signalling cascades regulating neuronal growth-promoting and inhibitory cues. Prog Neurobiol 65:593-608.

Sklar P, Gabriel SB, McInnis MG, Bennett P, Lim YM, Tsan G, Schaffner S, Kirov G, Jones I, Owen M, Craddock N, DePaulo JR, Lander ES (2002) Family-based association study of 76 candidate genes in bipolar disorder: BDNF is a potential risk locus. Brain-derived neutrophic factor. Molecular psychiatry 7:579-593.

Small SA, Gandy S (2006) Sorting through the cell biology of Alzheimer's disease: intracellular pathways to pathogenesis. Neuron 52:15-31.

Smith EN et al. (2009) Genome-wide association study of bipolar disorder in European American and African American individuals. Molecular psychiatry 14:755-763.

Solomon DA, Keitner GI, Ryan CE, Miller IW (1998) Lithium plus valproate as maintenance polypharmacy for patients with bipolar I disorder: a review. J Clin Psychopharmacol 18:38-49.

Speert DB, SJ MC, Seasholtz AF (2002) Sexually dimorphic expression of corticotropin-releasing hormone-binding protein in the mouse pituitary. Endocrinology 143:4730-4741.

Sperry RW (1963) Chemoaffinity in the Orderly Growth of Nerve Fiber Patterns and Connections. Proceedings of the National Academy of Sciences of the United States of America 50:703-710.

Sreerama N, Woody RW (1994) Poly(pro)II helices in globular proteins: identification and circular dichroic analysis. Biochemistry 33:10022-10025.

Sreerama N, Venyaminov SY, Woody RW (2000) Estimation of protein secondary structure from circular dichroism spectra: inclusion of denatured proteins with native proteins in the analysis. Analytical biochemistry 287:243-251.

Stefansson H, Steinthorsdottir V, Thorgeirsson TE, Gulcher JR, Stefansson K (2004) Neuregulin 1 and schizophrenia. Ann Med 36:62-71.

Stefansson H et al. (2002) Neuregulin 1 and susceptibility to schizophrenia. Am J Hum Genet 71:877-892.

Stevens JR (1992) Abnormal reinnervation as a basis for schizophrenia: a hypothesis. Arch Gen Psychiatry 49:238-243.

Straub RE, Jiang Y, MacLean CJ, Ma Y, Webb BT, Myakishev MV, Harris-Kerr C, Wormley B, Sadek H, Kadambi B, Cesare AJ, Gibberman A, Wang X, O'Neill FA, Walsh D, Kendler KS (2002) Genetic variation in the 6p22.3 gene DTNBP1, the human ortholog of the mouse dysbindin gene, is associated with schizophrenia. Am J Hum Genet 71:337-348.

Sullivan PF (2005) The genetics of schizophrenia. PLoS Med 2:e212.

Sullivan PF, Lin D, Tzeng JY, van den Oord E, Perkins D, Stroup TS, Wagner M, Lee S, Wright FA, Zou F, Liu W, Downing AM, Lieberman J, Close SL (2008) Genomewide association for schizophrenia in the CATIE study: results of stage 1. Molecular psychiatry 13:570-584.

Suzuki S, Sano K, Tanihara H (1991) Diversity of the cadherin family: evidence for eight new cadherins in nervous tissue. Cell regulation 2:261-270.

Suzuki SC, Inoue T, Kimura Y, Tanaka T, Takeichi M (1997) Neuronal circuits are subdivided by differential expression of type-II classic cadherins in postnatal mouse brains. Molecular and cellular neurosciences 9:433-447.

Suzuki SC, Furue H, Koga K, Jiang N, Nohmi M, Shimazaki Y, Katoh-Fukui Y, Yokoyama M, Yoshimura M, Takeichi M (2007) Cadherin-8 is required for the first relay synapses to receive functional inputs from primary sensory afferents for cold sensation. J Neurosci 27:3466-3476.

Swaab DF, Bao AM, Lucassen PJ (2005) The stress system in the human brain in depression and neurodegeneration. Ageing research reviews 4:141-194.

Swanson LW, Sawchenko PE (1980) Paraventricular nucleus: a site for the integration of neuroendocrine and autonomic mechanisms. Neuroendocrinology 31:410-417.

Tachikawa M, Watanabe M, Hori S, Fukaya M, Ohtsuki S, Asashima T, Terasaki T (2005) Distinct spatio-temporal expression of ABCA and ABCG transporters in the developing and adult mouse brain. Journal of neurochemistry 95:294-304.

Takata A, Kim SH, Ozaki N, Iwata N, Kunugi H, Inada T, Ujike H, Nakamura K, Mori N, Ahn YM, Joo EJ, Song JY, Kanba S, Yoshikawa T, Kim YS, Kato T (2011) Association of ANK3 with bipolar disorder confirmed in East Asia. Am J Med Genet B Neuropsychiatr Genet 156:312-315.

Tan EC, Chong SA, Wang H, Chew-Ping Lim E, Teo YY (2005) Gender-specific association of insertion/deletion polymorphisms in the nogo gene and chronic schizophrenia. Brain research 139:212-216.

Tanaka S, Ishii K, Kasai K, Yoon SO, Saeki Y (2007) Neural expression of G protein-coupled receptors GPR3, GPR6, and GPR12 up-regulates cyclic AMP levels and promotes neurite outgrowth. The Journal of biological chemistry 282:10506-10515.

Taniguchi H, Kawauchi D, Nishida K, Murakami F (2006) Classic cadherins regulate tangential migration of precerebellar neurons in the caudal hindbrain. Development 133:1923-1931.

Tanzi RE, Bertram L (2005) Twenty years of the Alzheimer's disease amyloid hypothesis: a genetic perspective. Cell 120:545-555.

Teng FY, Tang BL (2008) Cell autonomous function of Nogo and reticulons: The emerging story at the endoplasmic reticulum. J Cell Physiol 216:303-308.

Ter Horst GJ, Copray JC, Liem RS, Van Willigen JD (1991) Projections from the rostral parvocellular reticular formation to pontine and medullary nuclei in the rat: involvement in autonomic regulation and orofacial motor control. Neuroscience 40:735-758.

Thomson PA, Wray NR, Thomson AM, Dunbar DR, Grassie MA, Condie A, Walker MT, Smith DJ, Pulford DJ, Muir W, Blackwood DH, Porteous DJ (2005) Sex-specific association between bipolar affective disorder in women and GPR50, an X-linked orphan G protein-coupled receptor. Molecular psychiatry 10:470-478.

Togashi H, Abe K, Mizoguchi A, Takaoka K, Chisaka O, Takeichi M (2002) Cadherin regulates dendritic spine morphogenesis. Neuron 35:77-89.

Tompa P (2002) Intrinsically unstructured proteins. Trends in biochemical sciences 27:527-533.

Toriyama M, Shimada T, Kim KB, Mitsuba M, Nomura E, Katsuta K, Sakumura Y, Roepstorff P, Inagaki N (2006) Shootin1: A protein involved in the organization of an asymmetric signal for neuronal polarization. The Journal of cell biology 175:147-157.

Tran PV, Akana SF, Malkovska I, Dallman MF, Parada LF, Ingraham HA (2006) Diminished hypothalamic bdnf expression and impaired VMH function are associated with reduced SF-1 gene dosage. The Journal of comparative neurology 498:637-648.

Vacic V et al. (2011) Duplications of the neuropeptide receptor gene VIPR2 confer significant risk for schizophrenia. Nature 471:499-503.

Vale W, Spiess J, Rivier C, Rivier J (1981) Characterization of a 41-residue ovine hypothalamic peptide that stimulates secretion of corticotropin and beta-endorphin. Science (New York, NY 213:1394-1397.

Valentino RJ, Foote SL, Page ME (1993) The locus coeruleus as a site for integrating corticotropin-releasing factor and noradrenergic mediation of stress responses. Annals of the New York Academy of Sciences 697:173-188.

Van Bockstaele EJ, Branchereau P, Pickel VM (1995) Morphologically heterogeneous met-enkephalin terminals form synapses with tyrosine hydroxylase-containing dendrites in the rat nucleus locus coeruleus. The Journal of comparative neurology 363:423-438.

Van Bockstaele EJ, Colago EE, Valentino RJ (1996) Corticotropin-releasing factor-containing axon terminals synapse onto catecholamine dendrites and may presynaptically modulate other afferents in the rostral pole of the nucleus locus coeruleus in the rat brain. The Journal of comparative neurology 364:523-534.

van Coevorden A, Mockel J, Laurent E, Kerkhofs M, L'Hermite-Baleriaux M, Decoster C, Neve P, Van Cauter E (1991) Neuroendocrine rhythms and sleep in aging men. Am J Physiol 260:E651-661.

Vandesompele J, De Preter K, Pattyn F, Poppe B, Van Roy N, De Paepe A, Speleman F (2002) Accurate normalization of real-time quantitative RT-PCR data by geometric averaging of multiple internal control genes. Genome biology 3:RESEARCH0034.

Vassar R, Kovacs DM, Yan R, Wong PC (2009) The beta-secretase enzyme BACE in health and Alzheimer's disease: regulation, cell biology, function, and therapeutic potential. J Neurosci 29:12787-12794.

Vassar R et al. (1999) Beta-secretase cleavage of Alzheimer's amyloid precursor protein by the transmembrane aspartic protease BACE. Science (New York, NY 286:735-741.

Vassilatis DK, Hohmann JG, Zeng H, Li F, Ranchalis JE, Mortrud MT, Brown A, Rodriguez SS, Weller JR, Wright AC, Bergmann JE, Gaitanaris GA (2003) The G protein-coupled receptor repertoires of human and mouse. Proceedings of the National Academy of Sciences of the United States of America 100:4903-4908.

Vasudevan SV, Schulz J, Zhou C, Cocco MJ (2010) Protein folding at the membrane interface, the structure of Nogo-66 requires interactions with a phosphocholine surface. Proceedings of the National Academy of Sciences of the United States of America 107:6847-6851.

Vaudry D, Stork PJ, Lazarovici P, Eiden LE (2002) Signaling pathways for PC12 cell differentiation: making the right connections. Science (New York, NY 296:1648-1649.

Verhage M, Maia AS, Plomp JJ, Brussaard AB, Heeroma JH, Vermeer H, Toonen RF, Hammer RE, van den Berg TK, Missler M, Geuze HJ, Sudhof TC (2000) Synaptic assembly of the brain in the absence of neurotransmitter secretion. Science (New York, NY 287:864-869.

Vetrivel KS, Thinakaran G (2010) Membrane rafts in Alzheimer's disease beta-amyloid production. Biochimica et biophysica acta 1801:860-867.

Vetrivel KS, Meckler X, Chen Y, Nguyen PD, Seidah NG, Vassar R, Wong PC, Fukata M, Kounnas MZ, Thinakaran G (2009) Alzheimer disease Abeta production in the absence of S-palmitoylation-dependent targeting of BACE1 to lipid rafts. The Journal of biological chemistry 284:3793-3803.

Vlasov PK, Vlasova AV, Tumanyan VG, Esipova NG (2005) A tetrapeptide-based method for polyproline II-type secondary structure prediction. Proteins 61:763-768.

Voeltz GK, Prinz WA, Shibata Y, Rist JM, Rapoport TA (2006) A class of membrane proteins shaping the tubular endoplasmic reticulum. Cell 124:573-586.

Voineskos AN, Lerch JP, Felsky D, Shaikh S, Rajji TK, Miranda D, Lobaugh NJ, Mulsant BH, Pollock BG, Kennedy JL (2011) The brain-derived neurotrophic factor Val66Met polymorphism and prediction of neural risk for Alzheimer disease. Arch Gen Psychiatry 68:198-206.

Vulevic B, Chen Z, Boyd JT, Davis W, Jr., Walsh ES, Belinsky MG, Tew KD (2001) Cloning and characterization of human adenosine 5'-triphosphate-binding cassette, sub-family A, transporter 2 (ABCA2). Cancer research 61:3339-3347.

Wakana Y, Koyama S, Nakajima K, Hatsuzawa K, Nagahama M, Tani K, Hauri HP, Melancon P, Tagaya M (2005) Reticulon 3 is involved in membrane trafficking between the endoplasmic reticulum and Golgi. Biochem Biophys Res Commun 334:1198-1205.

Wald C, Wu C (2010) Biomedical research. Of mice and women: the bias in animal models. Science (New York, NY 327:1571-1572.

Wallace BA (2000) Synchrotron radiation circular-dichroism spectroscopy as a tool for investigating protein structures. Journal of synchrotron radiation 7:289-295.

Wallace BA (2009) Protein characterisation by synchrotron radiation circular dichroism spectroscopy. Q Rev Biophys 42:317-370.

Wallrabe H, Periasamy A (2005) Imaging protein molecules using FRET and FLIM microscopy. Curr Opin Biotechnol 16:19-27.

Wang H, Song L, Laird F, Wong PC, Lee HK (2008) BACE1 knock-outs display deficits in activity-dependent potentiation of synaptic transmission at mossy fiber to CA3 synapses in the hippocampus. J Neurosci 28:8677-8681.

Wang X, Chun SJ, Treloar H, Vartanian T, Greer CA, Strittmatter SM (2002) Localization of Nogo-A and Nogo-66 receptor proteins at sites of axon-myelin and synaptic contact. J Neurosci 22:5505-5515.

Ward JJ, Sodhi JS, McGuffin LJ, Buxton BF, Jones DT (2004) Prediction and functional analysis of native disorder in proteins from the three kingdoms of life. J Mol Biol 337:635-645.

Warren MS, Zerangue N, Woodford K, Roberts LM, Tate EH, Feng B, Li C, Feuerstein TJ, Gibbs J, Smith B, de Morais SM, Dower WJ, Koller KJ (2009) Comparative gene expression profiles of ABC transporters in brain microvessel endothelial cells and brain in five species including human. Pharmacol Res 59:404-413.

Wehrman TS, Casipit CL, Gewertz NM, Blau HM (2005) Enzymatic detection of protein translocation. Nat Methods 2:521-527.

Westphal NJ, Seasholtz AF (2006) CRH-BP: the regulation and function of a phylogenetically conserved binding protein. Front Biosci 11:1878-1891.

Wheelock MJ, Johnson KR (2003) Cadherins as modulators of cellular phenotype. Annu Rev Cell Dev Biol 19:207-235.

Whitmore L, Wallace BA (2004) DICHROWEB, an online server for protein secondary structure analyses from circular dichroism spectroscopic data. Nucleic acids research 32:W668-673.

Whitmore L, Wallace BA (2008) Protein secondary structure analyses from circular dichroism spectroscopy: methods and reference databases. Biopolymers 89:392-400.

WHO (1992) ICD-10 : The ICD-10 Classification of Mental and Behavioural Disorders : Clinical Descriptions and Diagnostic Guidelines. Geneva: World Health Organisation.

WHO (2001
) The World Health Report 2001- Mental Health: New Understanding, New Hope. In, pp 24-29: World Health Organisation.

Willem M, Garratt AN, Novak B, Citron M, Kaufmann S, Rittger A, DeStrooper B, Saftig P, Birchmeier C, Haass C (2006) Control of peripheral nerve myelination by the beta-secretase BACE1. Science (New York, NY 314:664-666.

Willi R, Aloy EM, Yee BK, Feldon J, Schwab ME (2009) Behavioral characterization of mice lacking the neurite outgrowth inhibitor Nogo-A. Genes Brain Behav 8:181-192.

Willi R, Weinmann O, Winter C, Klein J, Sohr R, Schnell L, Yee BK, Feldon J, Schwab ME (2010) Constitutive genetic deletion of the growth regulator Nogo-A induces schizophrenia-related endophenotypes. J Neurosci 30:556-567.

Williams EJ, Walsh FS, Doherty P (1994) The production of arachidonic acid can account for calcium channel activation in the second messenger pathway underlying neurite outgrowth stimulated by NCAM, N-cadherin, and L1. Journal of neurochemistry 62:1231-1234.

Wojcik S, Engel WK, Yan R, McFerrin J, Askanas V (2007) NOGO is increased and binds to BACE1 in sporadic inclusion-body myositis and in A beta PP-overexpressing cultured human muscle fibers. Acta neuropathologica 114:517-526.

Wonders CP, Anderson SA (2006) The origin and specification of cortical interneurons. Nat Rev Neurosci 7:687-696.

Wong J, Quinn CM, Brown AJ (2006) SREBP-2 positively regulates transcription of the cholesterol efflux gene, ABCA1, by generating oxysterol ligands for LXR. The Biochemical journal 400:485-491.

Woolf CJ (2003) No Nogo: now where to go? Neuron 38:153-156.

WTCCC (2007) Genome-wide association study of 14,000 cases of seven common diseases and 3,000 shared controls. Nature 447:661-678.

Wu YH, Zhou JN, Van Heerikhuize J, Jockers R, Swaab DF (2007) Decreased MT1 melatonin receptor expression in the suprachiasmatic nucleus in aging and Alzheimer's disease. Neurobiol Aging 28:1239-1247.

Wu YH, Zhou JN, Balesar R, Unmehopa U, Bao A, Jockers R, Van Heerikhuize J, Swaab DF (2006) Distribution of MT1 melatonin receptor immunoreactivity in the human hypothalamus and pituitary gland: colocalization of MT1 with vasopressin, oxytocin, and corticotropin-releasing hormone. J Comp Neurol 499:897-910.

Xiang R, Liu Y, Zhu L, Dong W, Qi Y (2006) Adaptor FADD is recruited by RTN3/HAP in ER-bound signaling complexes. Apoptosis 11:1923-1932.

Xiao R, Boehnke M (2009) Quantifying and correcting for the winner's curse in genetic association studies. Genet Epidemiol 33:453-462.

Yamashita S (2007) Heat-induced antigen retrieval: mechanisms and application to histochemistry. Progress in histochemistry and cytochemistry 41:141-200.

Yan R, Bienkowski MJ, Shuck ME, Miao H, Tory MC, Pauley AM, Brashier JR, Stratman NC, Mathews WR, Buhl AE, Carter DB, Tomasselli AG, Parodi LA, Heinrikson RL, Gurney ME (1999) Membrane-anchored aspartyl protease with Alzheimer's disease beta-secretase activity. Nature 402:533-537.

Yang XJ, Kow LM, Funabashi T, Mobbs CV (1999) Hypothalamic glucose sensor: similarities to and differences from pancreatic beta-cell mechanisms. Diabetes 48:1763-1772.

Yokota T, Mishra M, Akatsu H, Tani Y, Miyauchi T, Yamamoto T, Kosaka K, Nagai Y, Sawada T, Heese K (2006) Brain site-specific gene expression analysis in Alzheimer's disease patients. Eur J Clin Invest 36:820-830.

Yokoyama Y, Fukazawa Y, Ito T, Sato H (2002) Identification of unknown surfactants using electrospray mass spectrometry and NMR spectroscopy preceded by liquid ionization mass spectrometry. Spectrochimica acta 58:1453-1460.

Young-Pearse TL, Chen AC, Chang R, Marquez C, Selkoe DJ (2008) Secreted APP regulates the function of full-length APP in neurite outgrowth through interaction with integrin beta1. Neural Dev 3:15.

Zawilska JB, Skene DJ, Arendt J (2009) Physiology and pharmacology of melatonin in relation to biological rhythms. Pharmacol Rep 61:383-410.

Zhang B, Schmoyer D, Kirov S, Snoddy J (2004) GOTree Machine (GOTM): a web-based platform for interpreting sets of interesting genes using Gene Ontology hierarchies. BMC bioinformatics 5:16.

Zhao LX, Zhou CJ, Tanaka A, Nakata M, Hirabayashi T, Amachi T, Shioda S, Ueda K, Inagaki N (2000) Cloning, characterization and tissue distribution of the rat ATP-binding cassette (ABC) transporter ABC2/ABCA2. The Biochemical journal 350 Pt 3:865-872.

Zheng B, Ho C, Li S, Keirstead H, Steward O, Tessier-Lavigne M (2003) Lack of enhanced spinal regeneration in Nogo-deficient mice. Neuron 38:213-224.

Zhou CJ, Inagaki N, Pleasure SJ, Zhao LX, Kikuyama S, Shioda S (2002) ATP-binding cassette transporter ABCA2 (ABC2) expression in the developing spinal cord and PNS during myelination
. The Journal of comparative neurology 451:334-345.

Zhou X, Hu X, He W, Tang X, Shi Q, Zhang Z, Yan R (2011) Interaction between amyloid precursor protein and Nogo receptors regulates amyloid deposition. FASEB J 25:3146-3156.

Zhu HY, Guo HF, Hou HL, Liu YJ, Sheng SL, Zhou JN (2007) Increased expression of the Nogo receptor in the hippocampus and its relation to the neuropathology in Alzheimer's disease. Hum Pathol 38:426-434.

Zollner S, Pritchard JK (2007) Overcoming the winner's curse: estimating penetrance parameters from case-control data. Am J Hum Genet 80:605-615.

Supplementary figures 1-6: Allen Brain Atlas of adult mouse brain
http://mouse.brain-map.org/atlas/index.html
Images of the sections isolated and studied in Chapter 3.

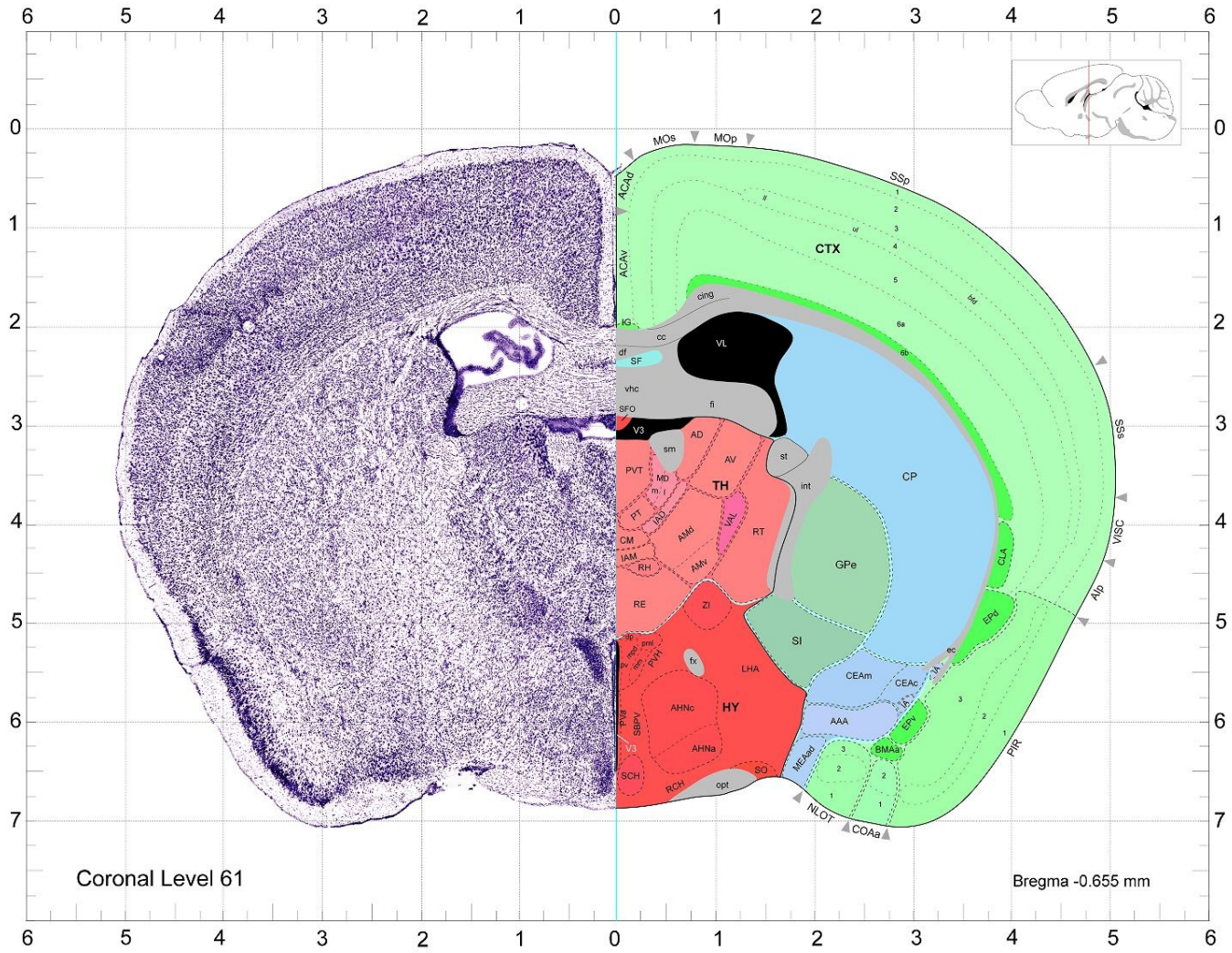

Supplementary Figure 1

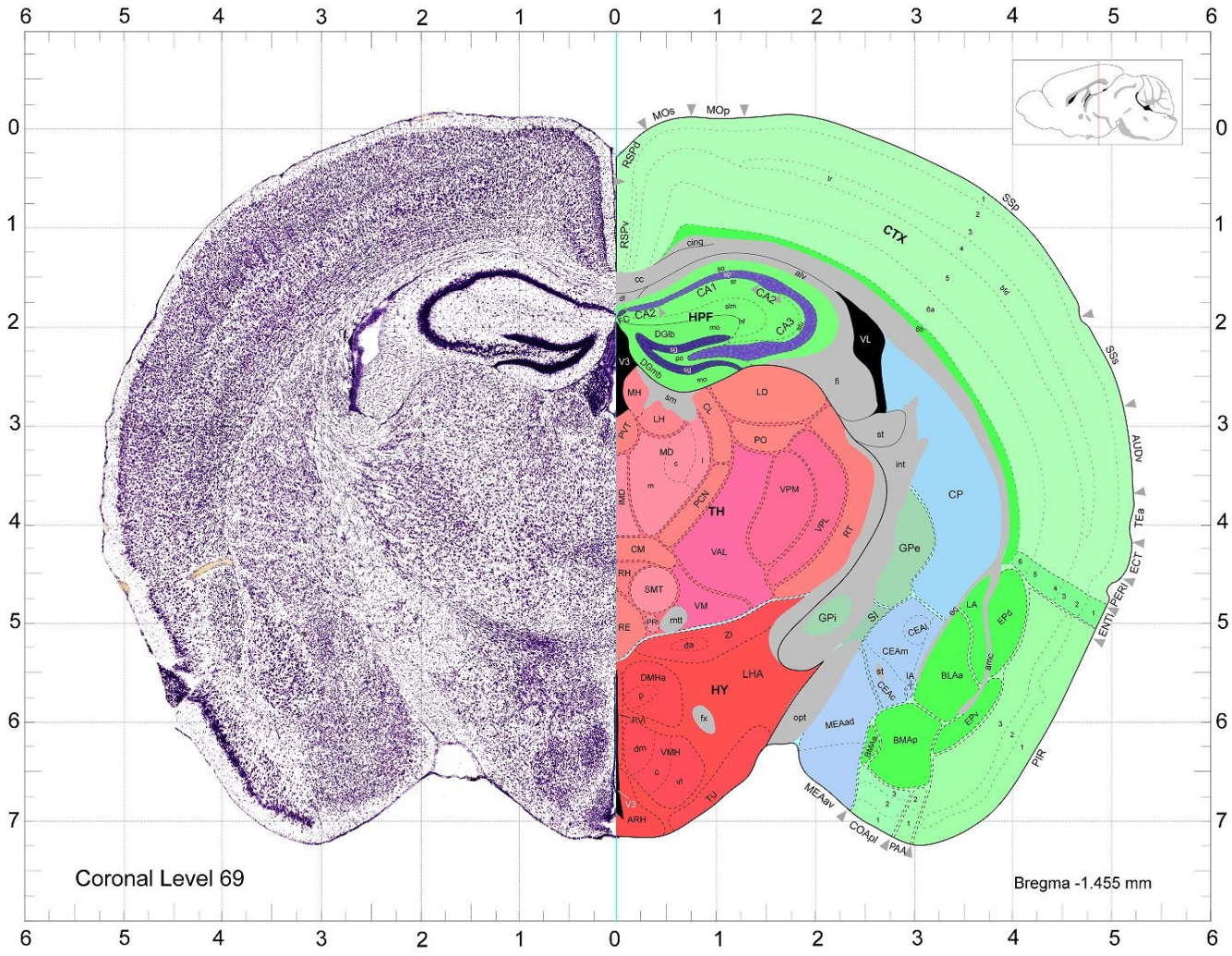

Supplementary Figure 2

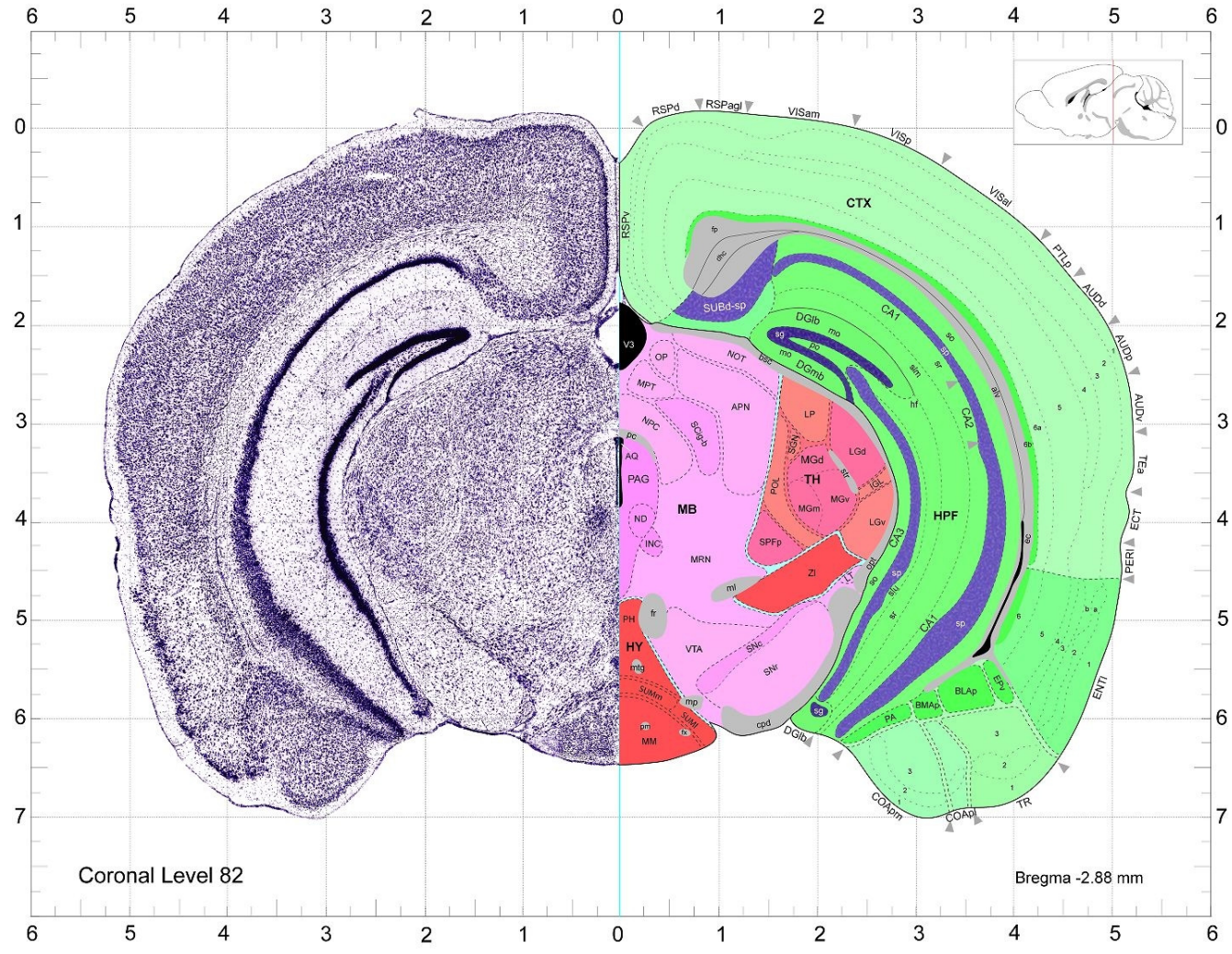

Supplementary Figure 3

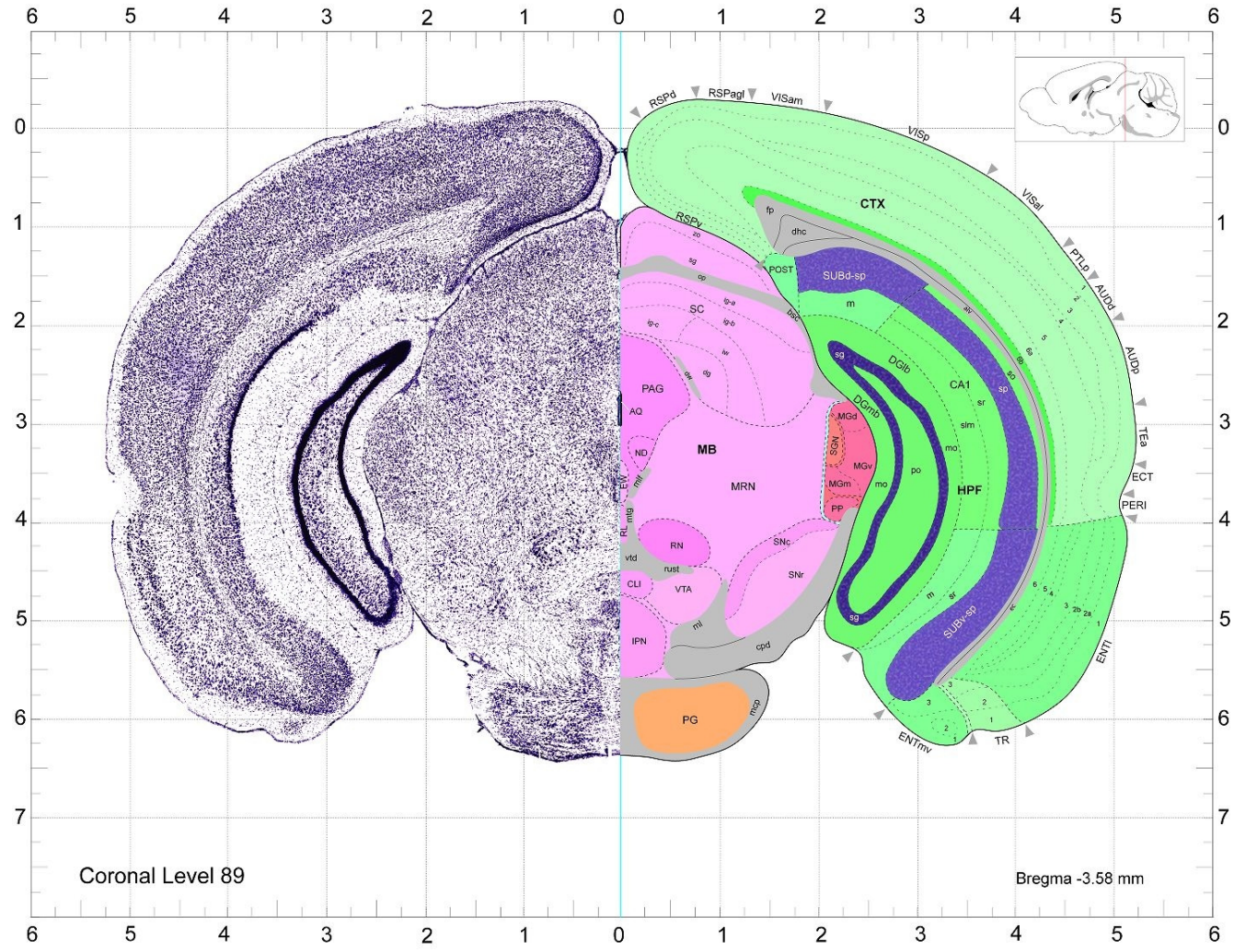

Supplementary Figure 4

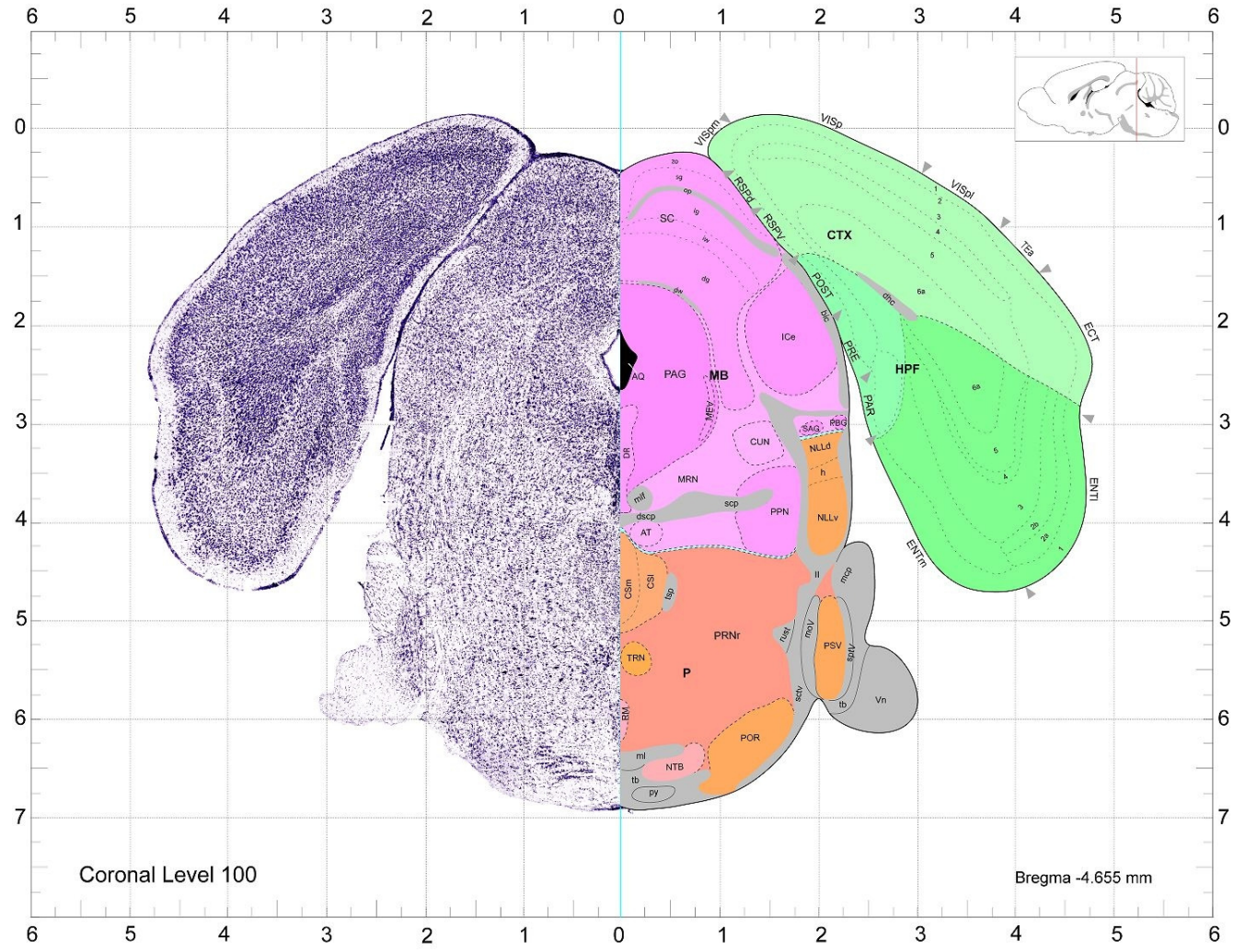

Supplementary Figure 5

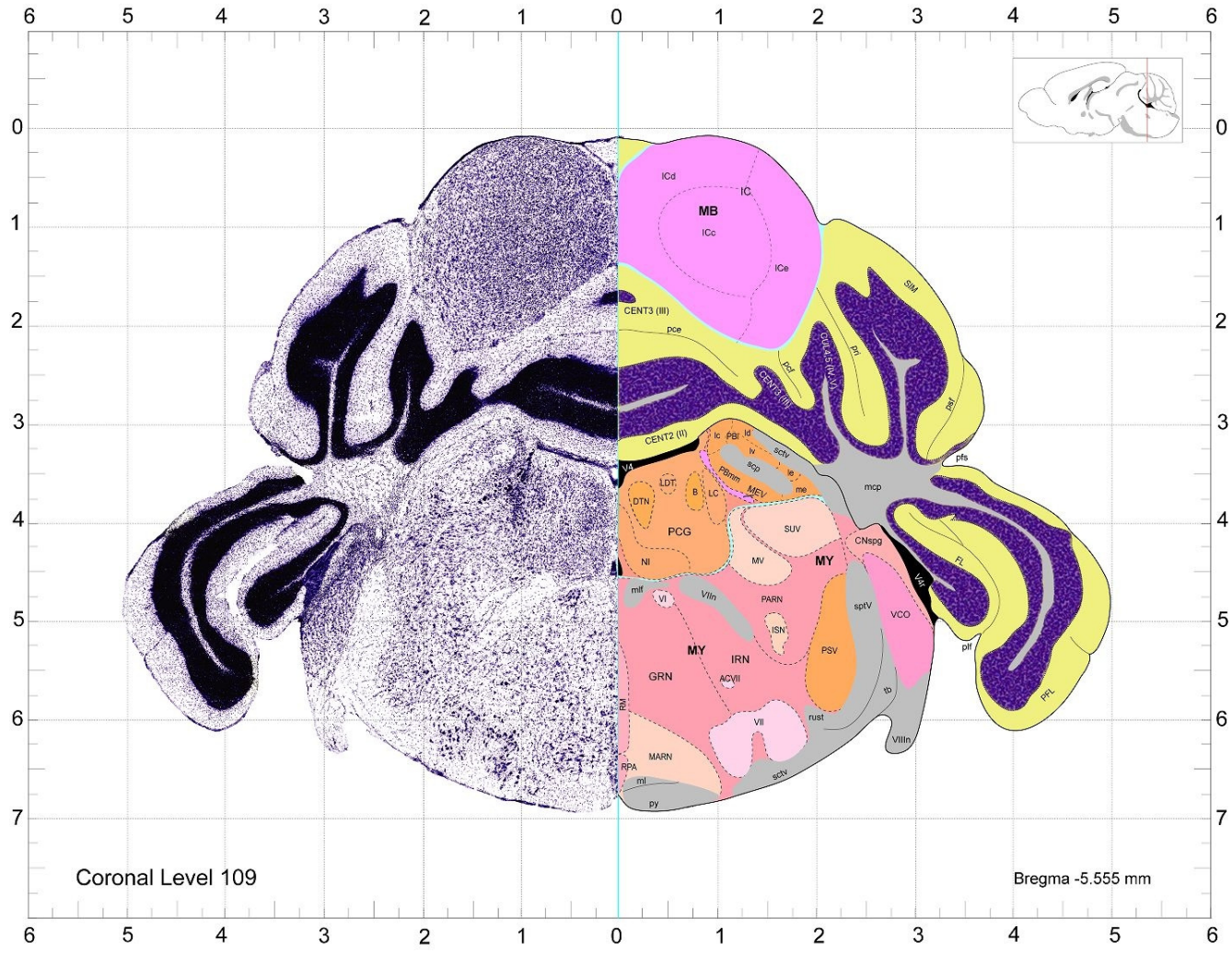

Supplementary Figure 6

8 Publications from this thesis

Grünewald E, Kinnell HL, Porteous DJ, Thomson PA (2009) GPR50 interacts with neuronal NOGO-A and affects neurite outgrowth. Molecular and Cellular Neuroscience 42:363-371.